DOCTOR OF PHILOSOPHY

Novel Multifunctional Laser Diagnostics

Stewart, Neil

Award date:
2013

Awarding institution:
University of Dundee

DOCTOR OF PHILOSOPHY

Novel Multifunctional Laser Diagnostics

Neil Andrew Stewart

2013

University of Dundee

NOVEL MULTIFUNCTIONAL LASER DIAGNOSTICS

A Thesis presented for the degree of
Doctor of Philosophy
to the University of Dundee by

Neil Andrew Stewart B.Sc. MBA

College of Medicine Dentistry and Nursing
School of Medicine
Academic Section of Urology
Clinical Academic Practice
Ninewells Hospital, Dundee

and

Photonics and Nanoscience Group
School of Engineering, Physics and Mathematics
University of Dundee

December 2013

Acknowledgements

A considerable number of people have been instrumental in supporting the work reported is this thesis. Undertaking to complete this work at 50 years young is somewhat unusual and the greatest acknowledgement must be for my loving wife Hazel, who supported unreservedly the on-going juvenile behaviour of her husband and tolerated the many very late nights and lost weekend's necessary to complete this endeavour. Also, to my son Duncan and daughter Heather go my thanks for not complaining too much about their too often absent father.

To my original supervisor Professor Edik Rafailov who 7 years ago prompted my interest in photons, lasers and Biophotonics, despite his failure to answer my often asked question, "what is a photon?", in all other respects his support has been crucial, from deciding to embark upon this work to its completion. Dr Ghulam Nabi for his support in composing this thesis. Within the Photonics and Nanoscience group I have had the pleasure of making many friends, two of whom stand out for special mention.

Dr Andrey Dunaev (meaning River Dun, the same as Dundee) who has provided enormous technical support with the LAKK-M and done a great deal of the leg work to aid data collection and been there to discuss and debate the meaning and analysis of results and the next steps; I hope your English improved more than my Russian. Dr Ksenia Fedorova who has offered encouragement throughout this work and whose detailed critical feedback on this document deserves credit for any quality to be found within these pages.

Finally, to my mother and deceased father for their unending enthusiasm and unquestioning support for whatever path I have chosen to wander down over the last 50 years.

Declarations

I, Neil Andrew Stewart, hereby certify that this thesis has been written by me, that it is a record of work carried out by me, that it has not been submitted in any previous application for a higher degree and that all references cited have been consulted by myself.

Signature of candidate..... Date 20/11/13

I confirm that Neil Stewart has completed the minimum duration period of registration for part-time study at the University of Dundee, and has fulfilled the conditions of the University of Dundee, thereby qualifying him to submit this thesis in application for the degree of Doctor of Philosophy.

Signed ..... Date 29/11/13

Contents

1 List of Abbreviations

AODC – Analogue Optical Dynamic Channel

AOSC – Analogue Optical Static Channel

ADC – Analogue Digital Conversion

ALA - 5-aminolevulinic acid

AU – Arbitrary Units

AVA – Arteriovenous Anastomoses

BI – Bypass Index

BO – Biological Object

CARS – Coherent Anti-Stokes Raman Scattering

CCD – Charge Coupled Device

CFC – Coefficient of Fluorescence Contrast

DCT – Dense Connective Tissue

DMSO – Dimethyl Sulfoxide

FAD – Flavin adenine dinucleotide

FNM - Flavomononucleotide

FRR – Fluorescence Redox Ratio

GSTP - Glutathione S-transferase pi

IA – Interpretive Algorithm

IC – Internal Controller

IFOS – Irradiation Formation Optical Scheme

IR – Infra-Red

IROS – Irradiation Registration Optical Scheme

IS – Irradiation Source

KO – Knock-out

LDF – Laser Doppler Flowmetry

LDPM – Laser Doppler Perfusion Monitoring

LED – light emitting diode

LFD - Laser Fluorescence Diagnostics

MBS Medical Biotechnology System

MCCU – Main Control Computing Unit

MNLDS – Multi-functional Non-invasive Laser Diagnostics System

MSI – Multispectral Imaging

MTR – Medical Technical Requirements

NADH – Nicotinamide adenine dinucleotide

NADPH - Nicotinamide adenine dinucleotide phosphate

NB - Nutritional Bloodflow

NMS – Non-invasive Medical Spectrophotometry

NRBC - Number of Red Blood Cells

OC – Oxygen Consumption

OCT – Optical Coherence Tomography

OD – Optical Density

OE – Oxygen Extraction

OME - Oxygen Metabolism Efficiency

OS – Oxygen Saturation

PDT – Photodynamic Therapy

PpIX – Protoporphyrin IX

PS-OCT - Polarisation Sensitive OCT

PU – Perfusion Units

RSD – Coefficient of Variation

SCI/P – Specialised Control Units

SD – Standard Deviation

SFM – Structural Functional Model

SHG – Second Harmonic Generation

SRS – Stimulate Raman Scattering

StO_2 – Oxygen Saturation

TD-OCT – Time Domain OCT

THG – Third Harmonic Generation

TPEF - Two-photon excitation microscopy

TRO- Tissue Reflectance Oximetry

UV – Ultra-Violet

WT – Wild Type

2 Publications in Peer-reviewed Journals

1. INVESTIGATING TISSUE RESPIRATION AND SKIN MICROHAEMOCIRCULATION UNDER ADAPTIVE CHANGES AND THE SYNCHRONIZATION OF BLOOD FLOW AND OXYGEN SATURATION RHYTHMS. Dunaev A.V., Sidorov V.V., Krupatkin A.I., Rafailov I.E., Palmer S.G., Stewart N.A., Sokolovski S.G., Rafailov E.U. , Physiological Measurement, 2014 (accepted 11.02.2014).

2. SUBSTANTIATION OF MEDICAL AND TECHNICAL REQUIREMENTS FOR NON-INVASIVE SPECTROPHOTOMETRIC DIAGNOSTIC DEVICES Dunaev, A.V., Zherebtsov E.A., Rogatkin, D.A., Stewart, N.A., Sokolovski, S.G., Rafailov, E.U., J. Biomed. Opt. 18(10), 107009 (Oct 28, 2013).

3. ANAEROBIC DIGESTION OF MUNICIPAL SOLID WASTES CONTAINING VARIABLE PROPORTIONS OF WASTE TYPES. Akunna, J. C.; Abdullahi, Y. A.; Stewart, N.A. "Water Science and Technology" Volume: 56 Issue: 8 Pages: 143-149, 2007

3 Contributions to Peer-reviewed Conferences

1. BASIC PRINCIPLES OF DESIGN AND FUNCTIONING OF MULTIFUNCTIONAL LASER DIAGNOSTIC SYSTEM FOR NON-INVASIVE MEDICAL SPECTROPHOTOMETRY Rogatkin, DA; Sokolovski, SG; Fedorova, KA; Stewart, NA ; Sidorov, VV; Rafailov, EU SPIE Conference on Advanced Biomedical and Clinical Diagnostic Systems IX: San Francisco, CA: JAN 23-25, 2011 ADVANCED BIOMEDICAL AND CLINICAL DIAGNOSTIC SYSTEMS IX Book Series: Proceedings of SPIE Volume: 7890 Article Number: 78901H DOI: 10.1117/12.874258 Published: 2011

2. MULTI-PARAMETER ANALYSIS IN BLOOD CIRCULATIONAND PERFUSION BASED DIAGNOSTICS Stewart N.A., Dunaev A.V., Sokolovski S.G., Sidorov V.V., Rafailov E.U. 15th International Conference on Laser Optics, St. Petersburg, Russia, Jun 25-29, 2012. (Presented by N.A. Stewart)

3. LASER REFLECTANCE OXIMETRY AND DOPPLER FLOWMETRY IN ASSESSMENT OF COMPLEX PHYSIOLOGICAL PARAMETERS OF CUTANEOUS BLOOD MICROCIRCULATION, Andrey V. Dunaev ; Victor V. Sidorov ; Neil A. Stewart ; Sergei G. Sokolovski and Edik U. Rafailov, Proc. SPIE 8572, Advanced Biomedical and Clinical Diagnostic Systems XI, 857205 (March 22, 2013); doi:10.1117/12.2001797

4. THE STUDY OF INTERRELATION BETWEEN THE RHYTHMS OF TISSUE OXYGEN SATURATION AND MICROVASCULAR BLOOD FLOW I.E. Rafailov, A.V. Dunaev, V.V. Sidorov, A.I. Krupatkin, S.G. Palmer, N.A. Stewart, S.G. Sokolovski, G. Nabi, E.U. Rafailov. Conference on Photonic technologies 4th-6th September 2013, Aston University, Birmingham UK

5. THE STUDY OF SYNCHRONISATION OF RHYTHMS OF MICROVASCULAR BLOOD FLOW AND OXYGEN SATURATION DURING ADAPTIVE CHANGES. A.V. Dunaev, V.V. Sidorov, A.I. Krupatkin, S.G. Palmer, I.E. Rafailov, N.A. Stewart, S.G. Sokolovski, E.U. Rafailov, Proc. SPIE 8935, Advanced Biomedical and Clinical Diagnostic Systems XII, 89350A (February 27, 2014); doi:10.1117/12.2035748; (presented by N.A. Stewart)

6. NOVEL MEASURE FOR THE CALIBRATION OF LASER DOPPLER FLOWMETRY DEVICES. Dunaev A.V. , Zherebtsov E.A., Rogatkin D.A., Sokolovski S.G. , Stewart N.A. , Rafailov E.U. *Proc. SPIE* 8936, Design and Quality for Biomedical Technologies VII, 89360D (March 4, 2014); doi:10.1117/12.2035651

4 Other dissemination

1. LASER SPECTROSCOPIC IN VIVO MEASUREMENT OF CARDIOVASCULAR DISEASE BIOMARKERS IN A MURINE MODEL OF THE CONDITION. Stewart N.A., Akbar N., Dunaev A., Sokolovski S., Rafailov E.U., Khan F. Poster presentation at photonics meets biology summer school 2013, Crete.

5 Summary

The research presented in this thesis set out to contribute to knowledge seeking to advance the state-of-the-art in laser based, multi-functional, non-invasive diagnostic systems. The results of the work have contributed to the development of methodological generic approaches to the development of devices using light to detect and analyse biomarkers relevant to human health and disease conditions. Following the development of methodologies the research then progresses to examine *in-vivo* the potential of the integrated spectroscopic technologies to detect changes and rhythms in the micro-vasculature of the skin relevant to the response of the subjects to emotional and physical stress. The results uncover myogenic rhythm synchronisation as a potential marker of adaptive response. The complexity of monitoring and interpreting key biomarkers of metabolism, NADH and FAD and the derived redox ratio is addressed in detail. Analysis of results of around 3,000 functional scans, including tissue oxygen saturation and laser Doppler flowmetry, provides new insights into bio-technological issues. The challenges identified with biological characteristics include sampling zones and physiological features of the skin. Technological, photonics, electronics and computing challenges emerge from the results. These should be considered in advancing the integration of bio-photonic technologies toward realising meaningful diagnostic poly-bio-markers relevant to developing algorithms capable of delivering consistent, reliable and meaningful diagnostic information with utility in clinical practice for early diagnosis of disease conditions such as cancers and cardio-vascular diseases in individuals from the global population. The results have been published in peer-reviewed international journals and presented at major international conferences in the field.

6 Aims and Objectives

This aims of this work which has its origin in a collaboration between the University of Dundee Photonics and Nanoscience Group (PNG) and the SPE Lasma of Moscow, RF and is set out below

a) **Develop a laser diagnostics device in the spectral band from 365nm to 1300nm.**
b) **Develop and test of a series of diagnostic algorithms.**
c) **Explore applications for the examination of functional conditions of human soft tissues as well as their system of blood microcirculation.**

These objectives were developed around the need to firstly understand the performance and underlying design characteristics of the Lasma multi-functional laser diagnostics device, this led me to explore the design principles and compare with other available mono-functional devices available in Europe and the USA.

The next challenge was to define understand and define the benefits of multi-functional diagnostics and which parameters could be developed based on the data available from an integrated multi-functional device. This would involve me in algorithm development, while the software coding was necessarily performed by programmers in Russia.

Finally, in order to explore the utility of the algorithms and parameters developed I progressed a series of experiments with human volunteers, in collaboration with the PNG research group, and animal models to generate and analyses data from the systems.

This journey aimed to progress the state of the art both in terms of the design and function of laser diagnostics principles and technology and in our understanding of the interaction of light with biological materials. The contrast between highly defined and well known principles in the laser physics domain with the much less charted and understood biological and physiological aspects of medical diagnostics and biomarker discovery was notable.

Challenges in translating, for example, published data on spectroscopic data collected in-vitro into the in vivo systems were tackled with interest and generated novel results.

Chapter 1 – BASIC PRINCIPLES OF LIGHT INTERACTION WITH BIOLOGICAL MATERIALS

1.1 Introduction

Light, or more specifically, electromagnetic radiation, from infrared through visible to ultraviolet interacts with living materials in many different ways. This field of research is termed biophotonics. It involves the exposition of biological materials to light followed by the detection and analysis of any resulting reflected or transmitted light.

Biophotonics includes the study of all organisms from prokaryotes to eukaryotes and indeed *ex-vivo* and *in-vitro* study of all organisms and biomaterials may be performed. It can be described as the "development and application of optical techniques, particularly imaging, to the study of biological molecules, cells and tissue" (KCL, 2013), and biophotonic techniques generally provide the distinct advantage of being non-destructive in that they preserve the integrity of the biological cells being examined.

In 1923 Alexander Gurwitsch discovered "ultra-weak" photon emission suggested a type of connection between photon emission and cell division rate, which was detected and discovered by his observations and discovery of a photon emission from things such as onions and yeast. This photo emission was later published and referred to in his terms as "mitogenetic radiation" (Gurvich & Frenkel, 1943).

Fritz-Albert Popp first referred to the phenomenon of "Biophotons" (Popp, 1973), as a single Quanta transmitted by living organisms in continuous and repeating cycle. Scientists and experts in the area referred to the emissions as biophotons and to the field as "BIOPHOTONICS".

The 1960's and 70's also saw the first laser construction by Theodore Maiman in 1960 (National_Laser, 2013) followed by rapid developments in laser science and technology including the first gallium-arsenide semiconductor lasers in 1962 (National_Laser, 2013). Lasers play an increasingly important role in Biophotonics. By the 1970's the first medical use of lasers for surgery was being pioneered in the USA and in the USSR. Their unique intrinsic properties such as precise wavelength selection, broad wavelength coverage, high spectral resolution and strong power densities make them the most universal light source for a growing number of applications.

1.2 Biomedical Optics

An important field of application of lasers is biomedical optics. Here, they offer great utility for diagnosis, therapy and surgery. For the development of novel methods of laser-based biomedical diagnostics careful study of light propagation in biological tissues is necessary to enhance our understanding of the optical measurements undertaken, increase research and development capacity and the diagnostic reliability of optical technologies. Ultimately, fulfilling these requirements will increase uptake in clinical applications of laser based diagnostics and therapeutics. To address these challenges informative biomarkers relevant to the biological and physiological function or disease state of the organism must be selected. These indicators are the results of the analysis of tissues and cells, such as blood. For non-invasive diagnostics peripheral blood, cells and tissue can potentially provide comprehensive information on the condition of the human organism. A detailed study of the light scattering and absorption characteristics can quickly detect physiological and morphological changes in the cells due to thermal, chemical, antibiotic treatments, etc. (Jacques, 2013), (Koenig & Schneckenburger, 1994), (Leahy & Nilsson, 2010), (Krupatkin & Sidorov, 2005), (Lister, Wright, & Chappell, 2012), (Tuchin, Tissue Optics - Light Scattering Methods and Instruments for Medical

Diagnosis, 2000) The selection of a laser source to study the structure of biological particles also benefits from the fact that gross pathological changes are not induced and diagnostics make effective use of the monochromatic directional coherence properties of laser radiation,.

1.3 Autofluorescence

The natural emission of light by endogenous biological structures such as mitochondria and lysosomes after they have absorbed light is termed autofluorescence, and it is thus differentiated from light originating from artificially added exogenous fluorescent markers or fluorophores (Monici, 2005). The phenomenon of autofluorescence was originally observed in quinine sulphate illuminated by prismatically dispersed sunlight (Stokes G.G., 1852) which led to the term Stokes Shift to describe fluorescence displacement to a longer wavelength than the exciting light.

Molecules have various electronic orbital states, referred to as energy levels. Fluorescence spectroscopy is fundamentally connected with these electronic and vibrational states. Generally, the examined species has a low energy electronic state (a ground state) and a higher energy excited state. Within these electronic states there exist various vibrational states.

In fluorescence spectroscopy, the molecule is excited, by the absorption of a photon, from its ground electronic state to a vibration state in one of the excited electronic states. Molecular collisions, with other molecules, then cause the excited molecule to lose vibrational energy until it reaches the lowest vibrational state of the excited electronic state. This process is most easily visualized with a Jablonski diagram, Figure 1.

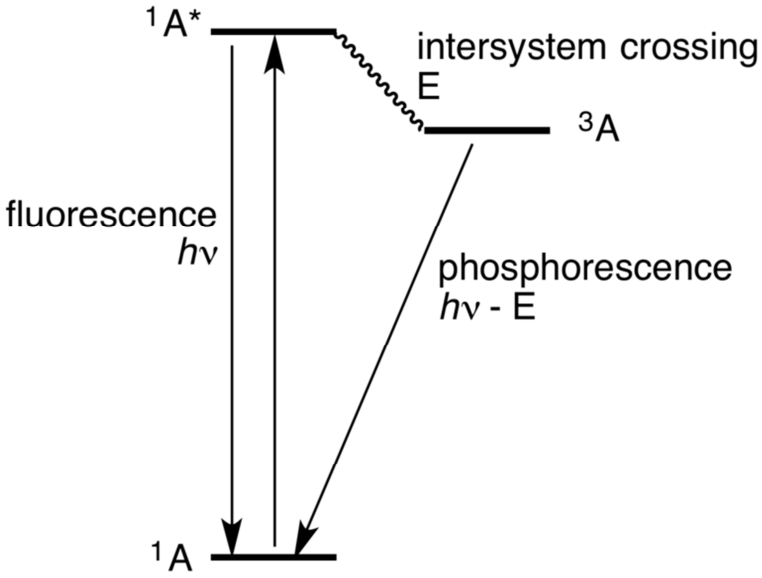

Figure 1- Jablonski diagram showing the excitation of a molecule A to its singlet excited state (1A*) followed by intersystem crossing to the triplet state (3A) which relaxes to the ground state by phosphorescence ©CreativeCommons (Smokefoot)

The molecule then emits a photon as it drops down or returns to one of the vibrational levels of the ground electronic state. Species can drop down into several different ground state vibrational levels. The photons emitted will therefore have different energies, and thus frequencies. By frequency analysis of the light emitted in fluorescence spectroscopy, along with their relative intensities, the structure of the different vibrational levels can be defined.

Cells contain molecules, which become fluorescent when excited by UV and or visible radiation of suitable wavelength. This fluorescence emission, arising from endogenous fluorophores, is an intrinsic property of cells and is called auto-fluorescence, to be distinguished from fluorescent signals obtained by adding exogenous markers.

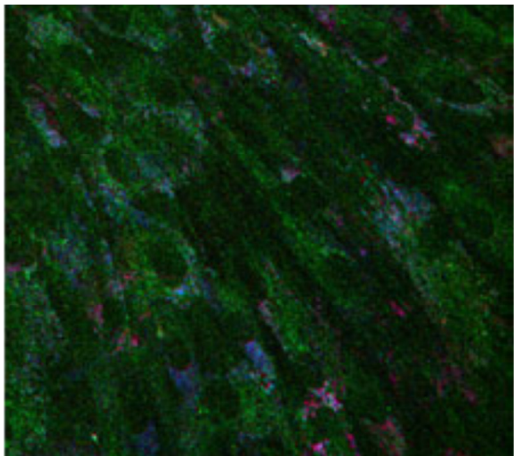

Figure 2 - NADH (green), FAD (blue) and lipofuscin (red) fluorescence among propagating mesenchymal cells, reproduced from **(Georgakoudi, 2013)**

Cell auto-fluorescence predominantly originates from liposomes and mitochondria. Generally, proteins containing an increased amount of the amino acids tryptophan, tyrosine and phenylalanine show some degree of auto-fluorescence (Lohmann & Paul, 1989). The most important endogenous fluorophores are aromatic amino acids, lipo-pigments and pyridine (NADPH) and flavin enzyme cofactors. It has been reported that NADPH and flavins are the most commonly observed auto-fluorescing molecules and that the extracellular matrix will also contribute to auto-fluorescence because of the intrinsic properties of collagen and elastin (Shadzad, Edetsberger, & Koehler, 2010).

Due to high levels of the endogenous fluorophores collagen and elastin the extracellular matrix frequently contributes more to tissue auto-fluorescence emission than cellular components. This is because collagen and elastin have a relatively high quantum yield. Changes in the amount and distribution of endogenous fluorophores indicate variations occurring in the cell and tissue state during physiological and/or pathological processes and chemical-physical properties of their microenvironment (Monici, 2005). Bio-analytical methods based on auto-fluorescence monitoring can therefore be utilised to obtain information about the morphological and physiological state of cells and tissues. Furthermore, because auto-fluorescence analysis does not require any treatment of

fixing or staining of the specimens it can be performed in real time. Recent progress in spectroscopic and imaging techniques has led to the development of many different applications both in basic research and diagnostics.

1.4 The Structure and Optical Properties of Biological Tissues

Unlike other forms of radiation light suffers from the disadvantage of being highly absorbed by most biological materials, with the exception of the eye where the cornea lens and vitreous gel for obvious reasons have low absorption, enabling analysis and imaging by various photonic techniques several centimetres deep into the body to reach the retina. Thus, for photonics based non-invasive diagnostics and therapy, studies are limited principally to penetration of a few millimetres into the epithelium and endothelium of amniotic organisms.

In terms of optical parameters the tissues of most interest are the fibrous tissues. Collagen type I is the main component of dense connective tissue (DCT). Amongst the collagen fibres are rows of fibre-forming cells, fibroblasts, which manufacture the fibres. DCT forms rope-like structures, such as tendons and ligaments. DCT also forms the lower layers of the dermis, in multiple strata. In dense irregular tissues fibroblasts and matrix fibres predominantly collagen, are oriented differently, i.e. not in a parallel orientation. This type of tissue is also present in the dermis layer and papillary region of skin.

Despite of considerable morphological differences all fibrous tissues conform to certain general descriptions. They comprise a larger than normal relative volume of intracellular materials and the number of individual cells is lower than that in most other tissues. Their structure is characterised by the presence of fibrous materials including collagen, elastin and reticular fibres, which are the main

structural elements of the fibrous tissue, and bounded by chemically complex intercellular substances (Kulikov, 2014).

The major component of functional elements of the human body such as tendons, cartilage and the skin dermis are collagen fibre. Collagen has a specific protein structure and discernible three-dimensional location of polypeptide chains. Collagen comprises a larger number of the amino acids glycine, proline, hydroxyproline, alanine and lysine, than other proteins. Collagen molecules form a triple-helix of polypeptide macromolecules, two identical chains and an additional one with slightly different chemical composition (Shoulders, 2009). The length of the collagen molecule is reported as 280 nm with a diameter of 1.5 nm (Weinstein, 1960).Collagen makes up 25–30% of the total protein in an adult or 6% of total body weight (Sikorski, 2001).

1.5 The Structure and Optical Properties of the Skin

Human skin is a turbid multicomponent biological medium and it is challenging to develop models to adequately describe its structure. The optical qualities of such a complex environment depend on many factors. In order to devise a model relevant to the optical properties of the dermis an understanding in the biological features and structure of skin is necessary (See Figure 3).

The dermis (skin) comprises two main layers. The external keratinized epithelium-epidermis layer is flat and multi-layered. The average thickness of the epidermis, which has relatively constant thickness, is approximately 100 μm (Jacques, 1991). The epidermis has two discreet layers of cells: an external, corneal (stratum corneum) layer of dry keratinocyte or corneocytes and inner cellular layers. Epidermal stem cells reside in the lower part of the epidermis (basal cell layer). Epidermal stem cells divide in a stochastic manner yielding either more stem cells or transit amplifying cells (Houben, De

Paepe, & Rogiers, 2007). Some of the transits amplifying cells continue to proliferate then commit to differentiate and migrate towards the surface of the epidermis. Those stem cells and their differentiated progeny are organized into columns named epidermal proliferation units. (Allen & Potten, 1974). The epidermal cells in the epithelium are often called keratinocytes because fibrous proteins family they bulky produce is keratins. The epidermis brings together a migrating subpopulation of melanocytes and melanosomes which are cellular sites of synthesis, storage and transport of melanin, the light-absorbing pigment which makes melanosomes responsible for the colour and photo-protection of skin tissues. Melanosomes have a diameter of about 400nm and melanin polymers are 30–400nm in diameter (Kollias, 1991).

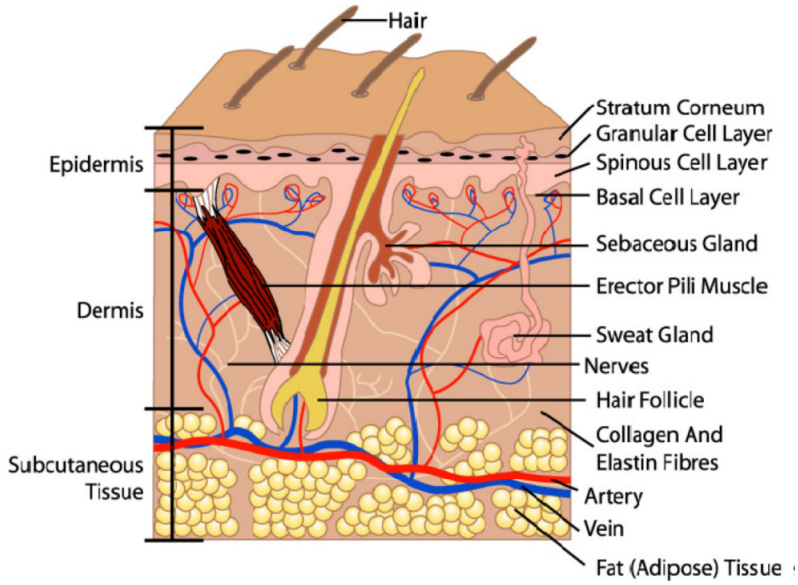

Figure 3 - Human Skin Diagram, reproduced from (Health_Advisors, 2013)

Beneath the epidermis the dermis is composed of dense fibrous, elastic tissue which forms the largest volume of the skin. The average dermis thickness is around 1.5–2.0 mm (Meglinski, 2001). It is in this layer that the outermost vascular and nervous system elements appear. Under the dermis the

hypodermis is formed of a fatty and connective tissue based subcutaneous tissue, which has a more variable thickness.

The DCT in the dermis includes collagen and elastin fibres with an approximate diameter of 60 nm, packed in bundles of dermal lamellae interspersed with and an amorphous salt and water substance called inter-fibrillar gel.

The dermis is normally considers to have two discreet layers, the stratum papillary and reticular dermis (Goldsmith & Odland, 1991). The papillary dermis is the outer part of the dermal connective tissue that is formed under the epidermis and contains more free distribution of elastin and collagen fibres than the reticular layer. The reticular dermal layer is where the clearly divided vascular structure skin is present. The two systems are a system of micro-vessels that deliver nourishment to the derma and second deeper subcutaneous layer of veins and arteries which enable heat exchange from blood to the external environment.

1.6 Structure and Optical Properties of Blood

Blood is a crucial and complex biological fluid comprising 57% (of blood volume) liquid plasma and 43% cellular (enzymatic) materials. Blood plasma is 90–91% water and between 6.5–8.0% is protein with the remainder (2%) of low molecular weight substances. Blood cells, or platelets, are 99% red and 1% white cells and platelets in a normal healthy human.

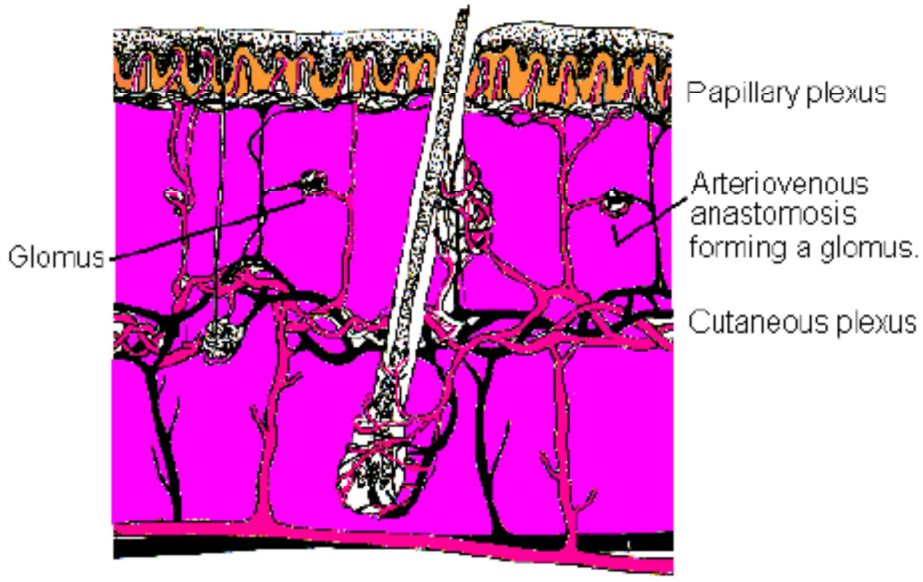

Figure 4 - Dermal blood flow black arterial and red venous blood; produced from **(TeleAnatomy, 2013)**

Red blood cells are disk shaped with a thickness of between 2-4 µm and diameter around 7µm. Haemoglobin or oxy-haemoglobin, dependent on the oxygenation state is carried in these red blood cells. The oxy-haemoglobin will predominate in arterial blood while the red (deoxygenated) haemoglobin will predominate in venous blood (Figure 4). The ratio of oxygenated haemoglobin to total haemoglobin is known as oxygen saturation (OS) which is a parameter with obvious diagnostic utility which is routinely monitored during surgery. Blood absorption is influenced primarily by absorption of water, haemoglobin and oxy-haemoglobin. The absorption spectra of these blood elements are charted in Figure 5.

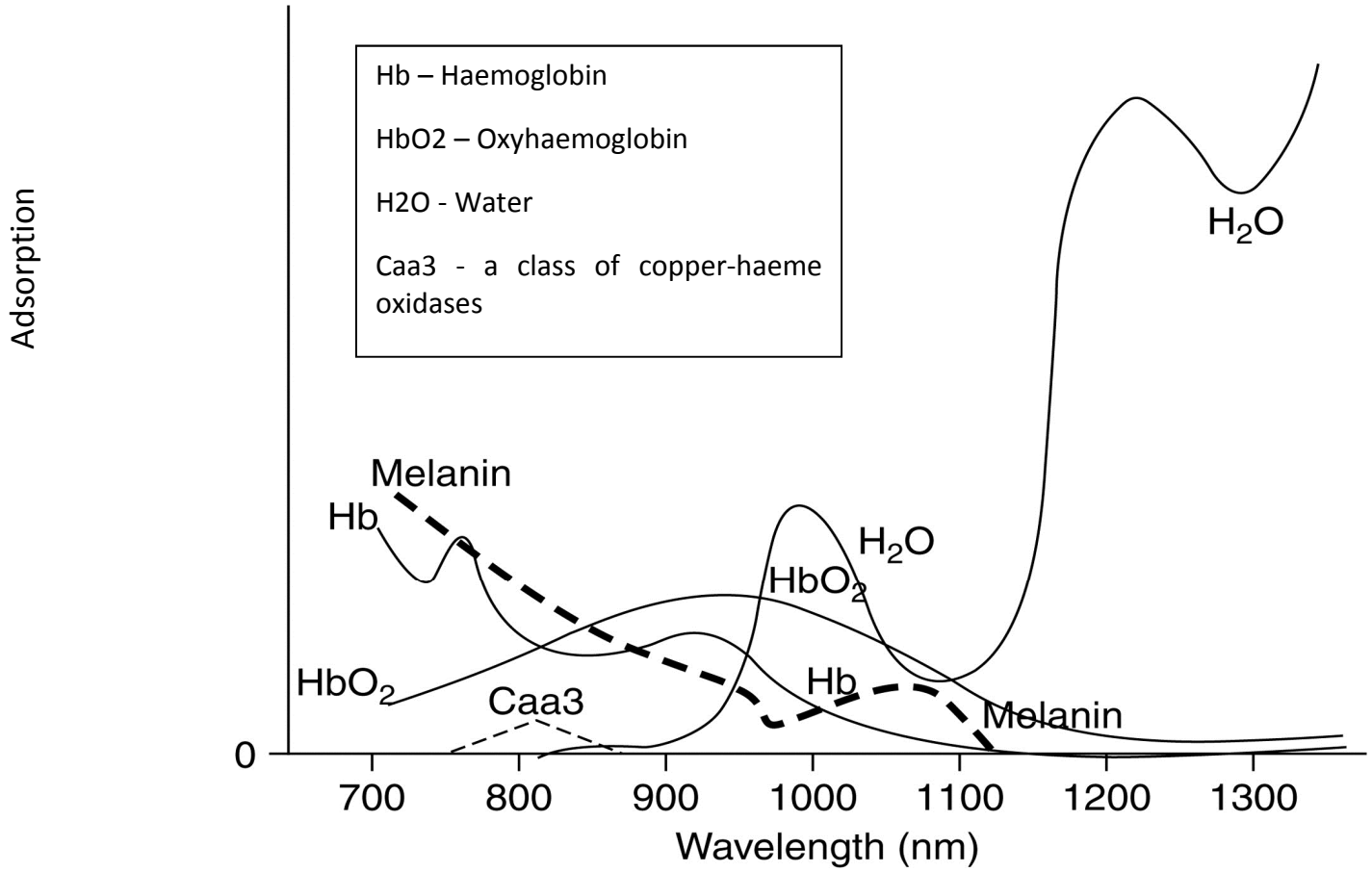

Figure 5 - Relative absorbance curves for light absorbing molecules in tissue, reproduced from (SensorInc, 2013)

If the haematocrit increases, then the number of red blood cells is increased with a resultant increase in light scattering and absorption. At haematocrit or red blood cell volume greater than 0.5 the erythrocytes adhere to each other, creating a homogeneous mass absorbed by haemoglobin causing light scattering in the blood plasma cavity between the masses of red blood cells. It is clear then that blood is a highly complex and dynamic material for study by spectroscopic means and it must also be noted that the optical characteristics of tissues and their components are temperature dependent and will change with increased or reduced temperature which is of course more likely close to the skin surface.

1.7 Reflection and Scattering

At the boundary between air and biological tissues, such as the skin surface radiation will be reflected (Fresnel reflection) due to the higher refractive index of tissue. Tissue is an inhomogeneous optical absorber which will absorb the non-reflected radiation which penetrates the tissue.

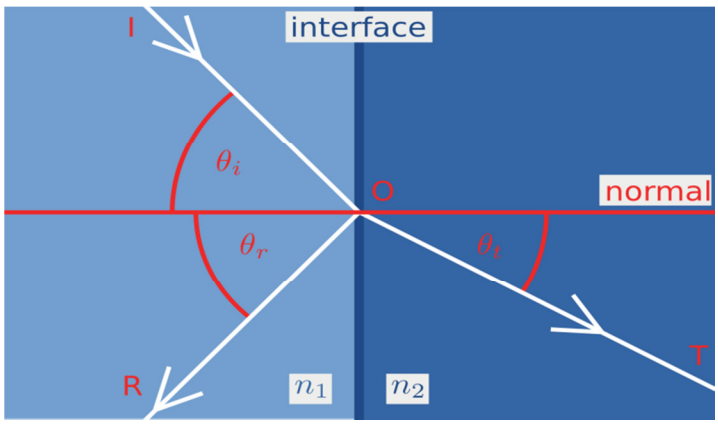

Figure 6 - Refraction of light at the interface between two media with different refractive indexes ($n_2>n_1$) © Creative Commons

In Figure 6, a light ray **I** travelling through material with refractive index n_1 is incident on **O** where it arrives at the interface between the two media. Part of the radiation is reflected along **OR** and part is

refracted along **OT**. The angles that the rays make to the normal of the interface will be θ_i, θ_r and θ_t, respectively. The fraction of the radiation **I** that is reflected will be the reflectance **R** and the fraction that is refracted will be the transmittance **T**.

The skin light interaction is typified by high levels of light scattering it is highly scattering turbid medium, due to the large number of scattering centres randomly distributed in the volume (Cheong, Prahl, & Welch, 1990). The wavelength of the energy and the optical characteristics of the biological materials will determine the degree of scattering.

Light scattering happens because of fluctuations in the density of tissue and refractive index fluctuations in the volume of tissue. The sort of light scattering depends on the correlation of the size of the light scattering particles the wavelength of the scattered radiation, and the refractive index ratio of the particle causing the scattering and its surroundings (Bohren & Huffman, 1986). Light scattering in tissue consisting of a large number of particles is very different from light scattering caused by individual particles. This difference if due firstly to interference of the individual scattered waves with each other and the incident wave, and secondly, very often, compound scattering effects (re-radiation) are important. Thirdly, particle interactions do prevent independent movement. During propagation in the skin multiple laser scattering and absorption of the beam leads to both broadening and attenuation. A large proportion of the radiation will be backscattered, that is, propagated in the reverse direction. Cell nuclei, membranes and organelles are the predominant sources of scattering in most biological tissues. Absorbed light is also converted into heat or can be re-radiated as fluorescence, phosphorescence or consumed in photo-biochemical reactions.

1.8 Absorption

Absorption of light is characterised by energy loss when light passes through a biological structure (Tuchin, Light scattering study of tissues, 1997). The absorbed light energy is transferred into heat, used in photochemical reactions or re-radiated as luminescence. The absorption spectra of the skin, or any tissue, are regulated by molecules with double bonds (chromophores of skin) in the biological tissues. In the epidermis amino acid and nucleic acid chromophores absorb light in the ultraviolet wavelength range. The predominant biological chromophore of skin in the visible spectrum is melanin. The absorption spectrum of the melanin pigment has no pronounced absorption bands, rather, it absorbs across a broad spectral region between 300 and 1200 nm. In the near UV and visible spectral regions, with the exception of melanin, the main dermal chromophores are flavins, carotenoids, bilirubin, phycobilins and vitamins, plus elastin and collagen fibres (Utz, Barth, Knuschke, & Sinichkin, 1993). The skin also has blood vessels containing haemoglobin which significantly affects the skin's absorption spectrum. Higher levels of blood in the dermis will produce greater levels of radiation absorption in the spectral regions corresponding to blood. In calculating optimum radiation parameters it is important to consider the volume of blood in the studied tissue volume. In living tissue haemoglobin binds oxygen in the blood. The absorption spectra of the two forms of haemoglobin are distinctive (Figure 6). Oxy-haemoglobin has an absorption band near 405 nm (Soret band) and the characteristic double peak absorption in the area of 545–575 nm while Deoxy-haemoglobin strongly absorbs near 430 nm and is weak close to 550nm (Andersen & Bjerring, 1990) (Anderson, Parrish, & Jaenicke, 1982). The spectra haemoglobin in both oxygenated states is emphatically different with a cross-over in the near infra-red region (Figure 8)

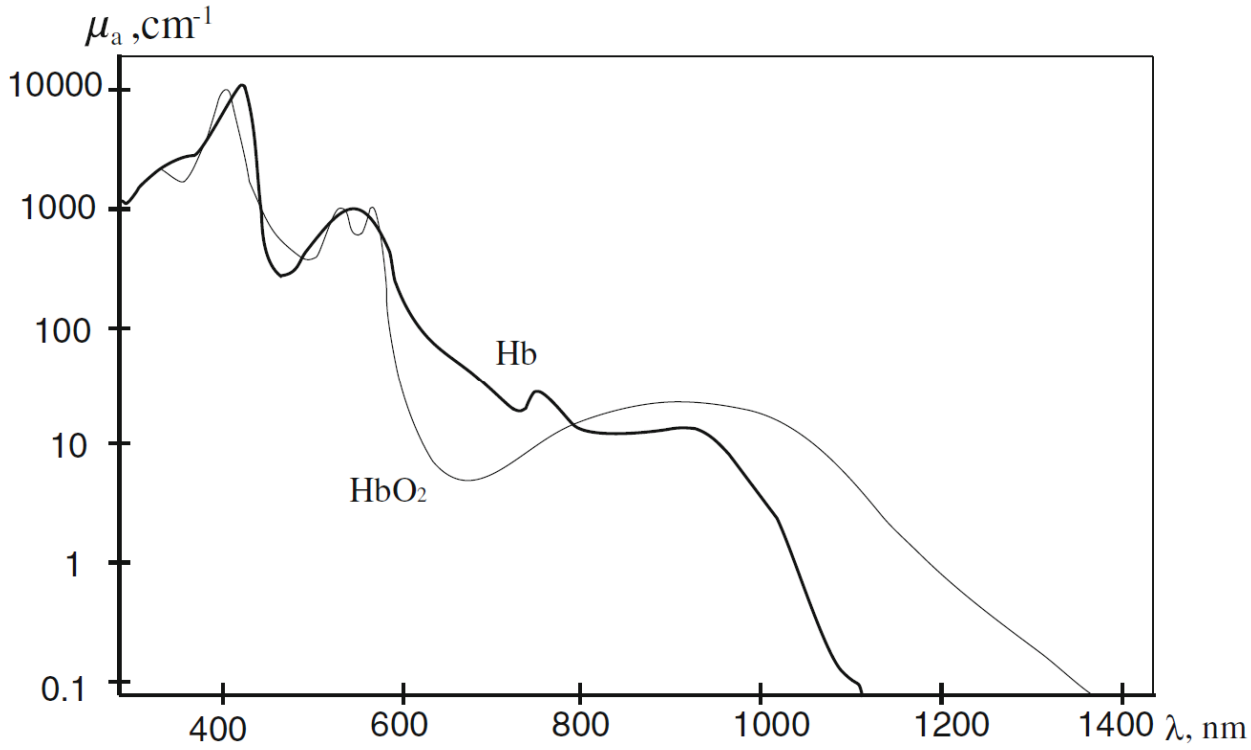

Figure 7- The absorption spectra of haemoglobin and oxyhaemoglobin Reproduced from **(Kulikov, Laser Interaction with Biological Material, 2014)**.

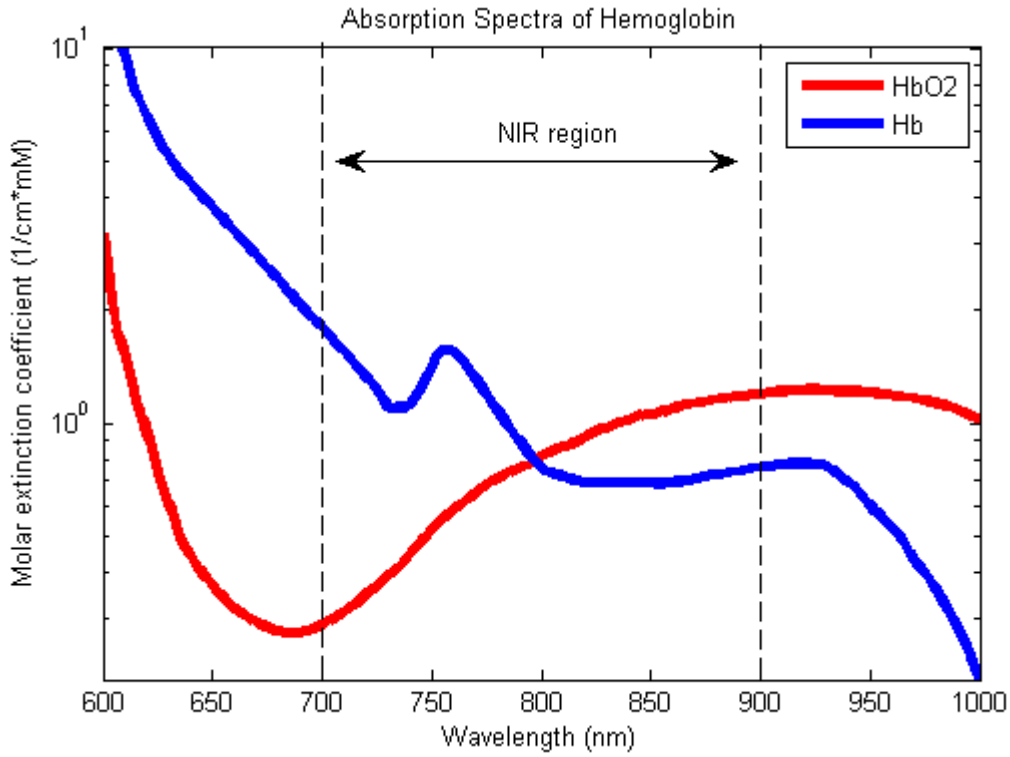

Figure 8 - NIR spectra of oxy and deoxy haemoglobin; compiled from http://omlc.ogi.edu/spectra/hemoglobin/summary.html © Creative Commons Adrian Curtin

In the IR region of the spectrum (λ = 700nm – 1000nm) all biomolecules have relatively intense absorption bands. The spectral absorption of water largely determines skin absorption from λ = 1400nm and above.

The major absorption band of fatty tissue is in the ultraviolet and infrared region of the spectrum. Subcutaneous fatty tissue light absorption is defined by the absorption bands of lipids, water, and β-carotene.

For biological tissue, the absorption spectrum is governed by the dominant absorption centres and water level in the tissue. To determine the power of laser radiation appropriate for investigation of biological tissue study of the subject's composition and knowledge of the relevant absorption coefficient at the radiation wavelength is required. The ultraviolet and infrared (λ >2 μm) regions are the predominant absorption and scattering wavelengths.

Light in the visible spectrum, 400-700 nm, penetrates only to the depth of a few cell layers into the biological tissue, typically the penetration depth of tissue is 500–2,500μm. Absorption and scattering thus predominates in the radiation reflected from the skin, affecting from one-tenth to half of the incident radiation. At wavelengths between 0.6 to 1.5μm scattering predominates with less absorption and the depth of penetration increases markedly to 8,000–10,000μm.

The wavelength of the reflection coefficient will vary significantly depending on the type of tissue. Thus, the major variable affecting the optical properties tissues are structure, physiological condition, hydration level, homogeneity, and the type of measurements performed (*in-vivo-in-vitro)*. Laser light in biological tissue is attenuated exponentially. The intensity of the collimated radiation is estimated using Beer-Lambert law which states that there is a logarithmic relationship between the

transmission, **T**, of light through a substance and the product of the absorption coefficient of the substance, **α** and the path length **ℓ**. The absorption coefficient is written as a product of the molar absorptivity, **ε** and the molar concentration c of the absorbing species in the tissue.

Equation 1-1

$$T = \frac{I}{I_0} = 10^{-\alpha \ell} = 10^{-\varepsilon \ell c}$$

Where, I_0 and I are the intensity (or power per unit area) of the incident light and the transmitted light, respectively; σ is cross section of light absorption by a single particle

The transmission, or transmissivity, can be described in terms of an absorbance which, for liquids, is;

Equation 1-2

$$A = -\log_{10}\left(\frac{I}{I_0}\right)$$

This means that the absorbance becomes linear with the concentration according to;

Equation 1-3

$$A = \varepsilon \ell c = \alpha \ell$$

A very important optical characteristic of tissue is the optical depth penetration. The significant value of the scattering anisotropy of biological tissues and multiple scattering is described by the Beer-Lambert law, above. In deriving the effects that occur in tissues under the influence of radiation the absorption of water is crucial as it is the major component of almost all tissues. The human body contains about 55–65% water. An adult weighing 100 kg contains an average of 60 litres of water, of which about 37 l is intracellular and 22 l are the extracellular fluids.

Water is the medium in which almost all bio-chemical reactions take place as well as the physio-chemical processes such as osmosis, diffusion, transport and others which are critical for life. Nowhere does life exist without water. In the UV, visible and NIR wavelengths the absorption

coefficient of water is very low. In these areas, the absorption of tissue is largely determined by the absorption of pigments, especially for the skin—the absorption spectra of melanin and blood haemoglobin and oxy-haemoglobin. Absorption by melanin is the most substantial component of the total absorption of the skins outermost layers, the epidermis and corneal layer.

To calculate the optical density (OD) of the epidermis, we can use the following calculation:

Equation 1-4

$$OD = \mu^{melanin} * h$$

Where, $\mu^{melanin}$ is the absorption coefficient of melanin, h is the thickness of the epidermis.

Optical density depends on the level of melanin in the epidermis, which is a consequence of many factors of which the main one is the skin type. Note: The dermis is very different from the epidermis in both structure and composition. The scattering coefficient of the dermis is weaker at longer wavelengths and scattering plays a crucial role in defining the depth of radiation penetration at all wavelengths in the dermis. Thus, longer wavelengths penetrate deeper. This is mostly explained by the occurrence of melanin, which absorbs less at longer wavelengths. According to Cheong, Prahl, & Welch, 1990, for a skin sample, the penetration depth is 150−200μm at λ = 633 nm and increases to 210 - 400μm at λ = 675 nm, almost doubling for an increase in wavelength of only 42nm.

1.9 Laser Doppler Flowmetry (LDF)

Laser Doppler Flowmetry (LDF) uses the laser beam's Doppler shift to determine particle velocity in fluid flows in transparent or semi-transparent media. The fundamental setup for LDF is to cross two collimated, monochromatic and coherent laser beams in the flow being measured, usually obtained

by splitting a single beam to ensure coherence. Beams are focussed to an intersection through optics, where they interfere to generate a set of straight fringes. Particles pass through the fringes reflecting light which is collected by the receiving optics and focused on a photodetector.

Fluctuations in reflected light intensity are detected, the frequency of which represents the Doppler shift between the incident and scattered light and is proportional to the particle velocity of the red blood cells. If the sensor is arranged so that the fringes from the light source are at 90 degrees to the fluid flow direction the signal from the photodetector will be directly proportional to the particle velocity (Figure 9 - Illustration of Laser Doppler Flowmetry).

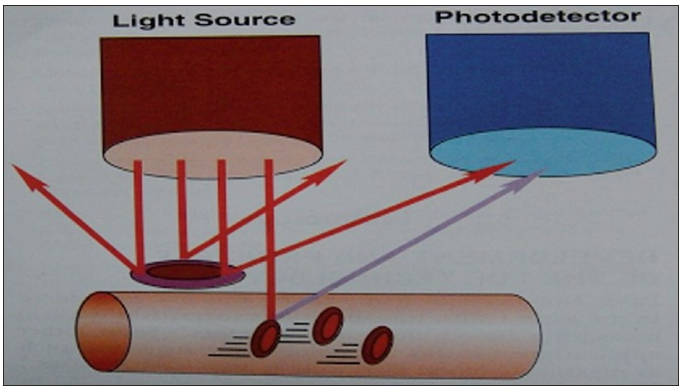

Figure 9 - Illustration of Laser Doppler Flowmetry © Creative Commons

LDF is used in haemodynamics to measure blood flow in human tissues and organs such as skin. A low-power laser beam achieves adequate penetration into the skin to backscatter and Doppler shifted light from erythrocytes. The data generated can be used to monitor and extrapolate the effects of exercise, drugs, environmental, or physical influences on examined micro-vascular areas (Stern, 1985)

In addition to direct measurement, LDF can also be used for imaging blood flow (Figure 10 - Illustration of LDF imaging set-up and image. This area is now finding direct application in medical practice. (Moor_Inst, 2013)

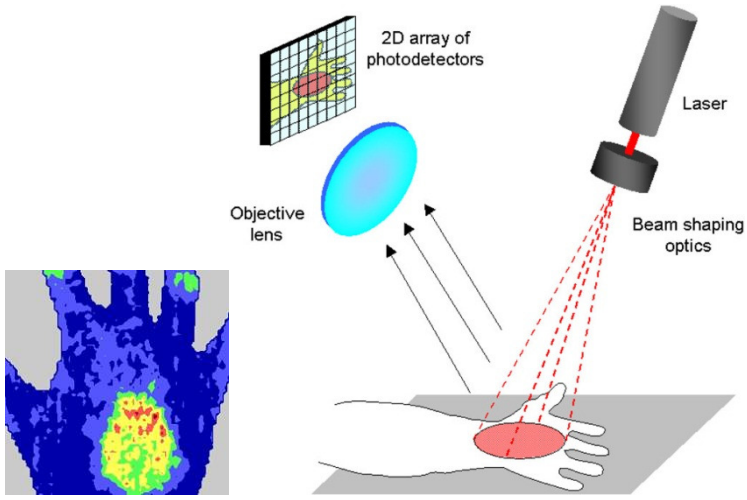

Figure 10 - Illustration of LDF imaging set-up and image © Creative Commons

1.10 Pulse Oximetry

Pulse oximetry is a non-invasive LED or laser based measurement method. Generally it uses two small LEDs of different wavelengths emitting in the direction of a photodiode through a semi-transparent part of the subject's body, normally a fingertip or earlobe. One LED emits at a red wavelength of 660 nm, and the other is infra-red at 905 to 940 nm. At these wavelengths absorption of oxy-haemoglobin and its deoxygenated form differs significantly (See Figure 7- The absorption spectra of haemoglobin and oxyhaemoglobin Figure 11, below); therefore, the oxy/deoxy-haemoglobin ratio can be calculated from the absorption ratio of red and infrared light.

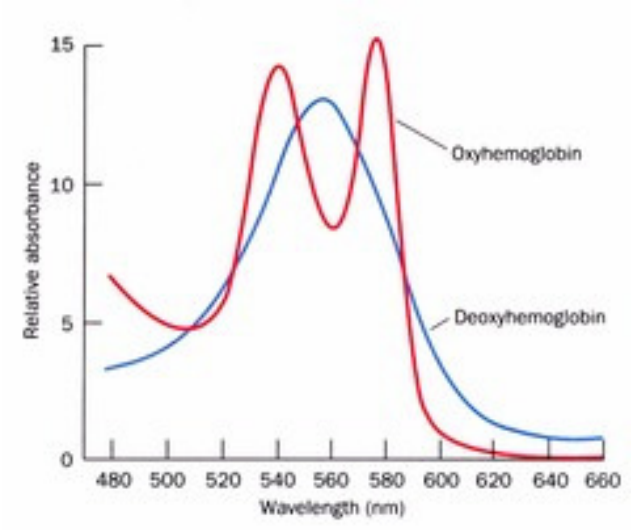

Figure 11 - Haemoglobin and Oxy-haemoglobin absorption at 450-660nm Reproduced from **(Quizlet, 2013)**

The measured signal oscillates with enlargement and contraction of arterial blood vessels in response to the heart beating. Therefore, examining only the difference between minimum and maximum absorption will thus determine only the arterial blood absorption. Detecting a pulse is, therefore, essential to the operation of a pulse-oximeter.

iData Research reported the U.S. market for pulse oximetry equipment and sensors as more than $700Mn in 2011. (iData, 2012) In 2008, the majority of major medical equipment manufacturers in China were also producers of pulse oximeters. (ResearchInChina, 2008)

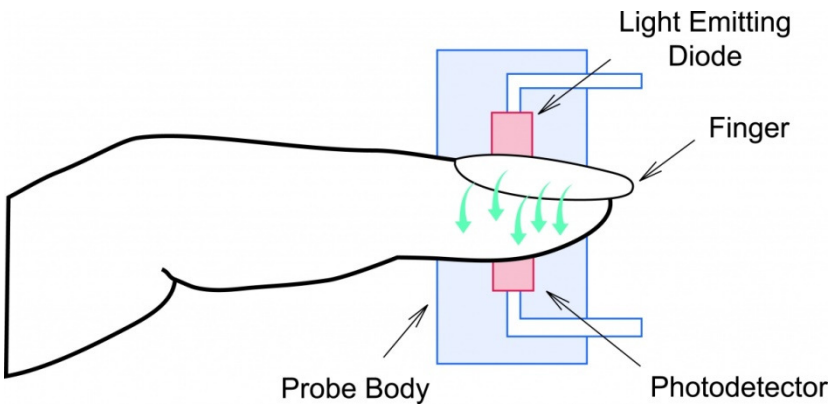

Figure 12 - Typical pulse oximetry set-up (homecaremag.com)

Despite its enormous commercial success pulse oximetry does suffer some limitations in its use. The technique measures only haemoglobin saturation, not ventilation and is not a complete measure of respiratory sufficiency. Because pulse oximetry cannot indicate base oxygen deficit, carbon dioxide levels, blood pH, or bicarbonate concentration it is not an alternative to performing blood gas checks, StO_2 figures cannot provide data on the content of oxygen in the blood. As blood oxygen is mostly carried by haemoglobin; in severe anaemia, the blood has less total oxygen, although the haemoglobin may be fully saturated.

Neither is pulse-oximetry a comprehensive indicator of vaso-circulatory adequacy. In circumstances of insufficient blood flow or anaemia tissues may be hypoxic although oxygen saturation may be high in the limited volume of blood analysed. Pulse-oximetry can measure only the ratio of bound haemoglobin (the source of the monitored absorption), it is therefore possible for errors in the interpretation to occur when haemoglobin binds to substances different to oxygen. For example, haemoglobins affinity to carbon monoxide is higher than to oxygen, thus a satisfactory StO_2 reading can be reported even though the patient may be hypoxemic. This inaccuracy can delay the diagnosis of hypoxia caused by carbon monoxide poisoning

1.11 Laser Doppler Flowmetry and Tissue Reflectance Oximetry

The above techniques can be combined to calculate an index of blood microcirculation (Perfusion) by measuring changes in oxygenation relative to the blood volume.

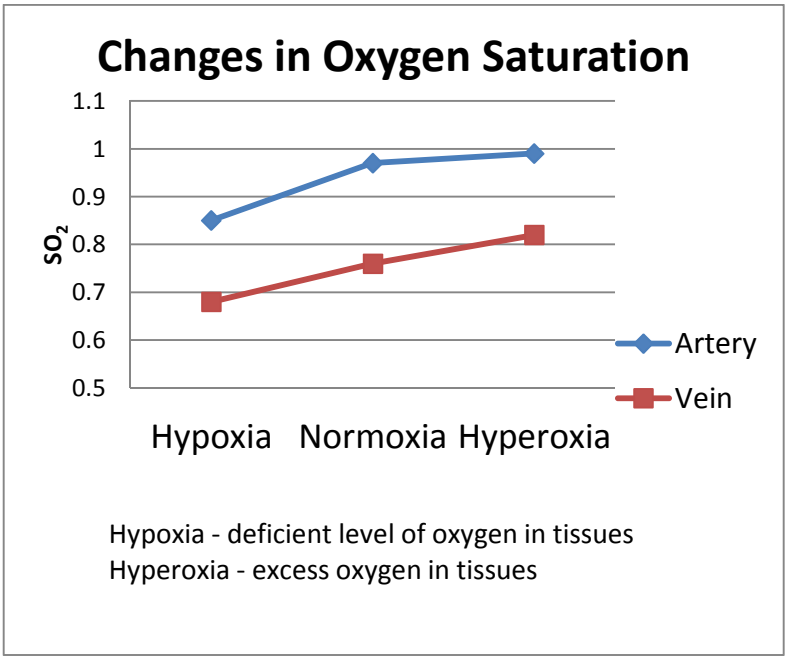

Figure 13 - Changes in arterial to venus blood oxygenation

The perfusion index, the ratio of the pulsatile blood flow to non-pulsatile flow in peripheral tissue is calculated as:

Equation 1-5

$$I_m = k \cdot N_{RBC} \cdot V_{RBC}$$

Where,

K = proportional coefficient,
N_{RBC} = number of red blood cells (erythrocytes),
V_{RBC} = velocity average of red blood cells (erythrocytes) in the measured tissue.

The TRO method allows for the calculation of the parameters S_tO_2 and V_b according to the following methodology. Tissue oxygen saturation is defined as the percentage composition of oxyhaemoglobin

in the sum of only two haemoglobin fractions – oxyhaemoglobin and deoxyhaemoglobin (Krupatkin A., 2007):

Equation 1-6

$$SO_2 = \frac{C_{HbO_2}}{C_{HbO_2} + C_{Hb}}$$

where, if the molar concentration of H_bO_2 in the blood is designated as C_{HbO2} and the overall molar concentration of all the fractions of haemoglobin in the blood, including H_bO_2, is designated as the sum of C_{HbO2} and C_{Hb}, then the parameter V_b can be calculated as follows:

Equation 1-7

$$V_b = \frac{C_{blood}}{C_{blood} + C_{other}}$$

Where, C_{other} is the molar concentration of all secondary cellular structures in the examined volume of tissue.

1.12 Laser Based Diagnostic Spectroscopy

Biophotonics have recently focussed substantial energies to develop and design of non-invasive spectroscopic techniques for the diagnosis of malignant tumours (Wagnieres, Star, & Wilson, 1998), (Scott & al, 2000), (Hewett, et al., 2000). Laser diagnostics methods are founded on the assertion that the optical properties of biological tissues signify their physiological and functional states. Technological advances now mean that assessment of tissues optical properties of absorbance, scattering, reflectance, fluorescence, as has being done for decades by conventional laboratory spectroscopy in histological tests, can now be performed *in vivo* using a non- or minimally invasive procedures. Physicians may thus make conclusive decisions in real time regarding a patient's

condition. Most minimally-invasive optical and laser medical diagnostic methods and techniques can be termed as a "minimally-invasive clinical spectrophotometry".

Laser Fluorescence Diagnostics (LFD) is a non-invasive medical diagnostic approach based on the autofluorescence of biomolecules containing endogenous fluorophores such as porphyrins and the coenzymes NADH, NADPH, and FAD. These fluoresce between 400-600nm and are indicators of metabolic function. Blue-green autofluorescence is therefore an appropriate measure of the function of metabolism and cell or tissue disruptions. Autofluorescence in the yellow/red spectral region is based mainly on endogenous porphyrins. Pathological micro-organisms such as *pseudomonas aerugenosa* can be located and quantified by the presence and intensity of fluorophores they synthesise. This permits fluorescence based detection of a variety of skin diseases, including acne and squamous cell carcinoma. The sensitivity of non-invasive laser based autofluorescence diagnostics can be enhanced by time-gated fluorescence measurements using an appropriate time delay between ultra-short laser excitation and detection. (Koenig & Schneckenburger, 1994)

Autofluorescence is often enhanced by the topical application of the porphyrin precursor 5-aminole-vulinic acid (ALA) creams which rouse increased endothelial synthesis of protoporphyrin (PPIX). PPIX is a photolabile fluorophores, the *in vivo* irradiation of which initiates a cytotoxic reaction. Therefore, real-time autofluorescence measurement and imaging during phototherapy can inform on the efficiency and improve the efficacy of ALA based PDT.

Table 1 - Absorption and fluorescence peaks of common biological chromophores adapted from data in (Koenig & Schneckenburger, 1994)

Chromophore	Solvent	Absorption (nm)	Fluoresence (nm)
Tryptophan	H2O	220,280,288	320-350 (1)
Thyrosin	H2O	220,275	305 (2)
Collagen	-	300-340	420-460
Elastin	-	340-340	420-460
NADH	H2O	260-340	470
NADPH	H2O	260-340	470
Flavins	H2O	260,370,450	530
Uroporphyrin	DMSO	404,501,533,568,622	624
Coproporphyrin	DMSO	398,497,531,565,620	622
Protoporphyrin	DMSO	406,505,540,575,630	633

The skin can be considered as an absorbing medium with strong scattering and fluorescent properties which absorbs 95% of irradiated light and allows a wavelength dependant depth penetration of between 100 to 6,000 µm (1981) (Anderson & Parrish, 1981).

Extensive efforts have recently been made to optimise the design of fibre-optic probes and develop algorithms to distinguish spectroscopic “signatures” of the tissue in healthy and disease conditions. However, most of these devices are designed to determine single physiological parameter like blood oxygenation and perfusion rate, or the abundance of fluorescent component/s, commonly, NADH, FAD, porphyrins or exogenous photosensitisers. To date, there are few biophotonic diagnostic devices capable of monitoring, in real-time, multiple skin optical characteristics in concert. Together with laser Doppler flowmetry (LDF) and tissue reflectance oximetry (TRO) autofluorescence can potentially provide a highly sensitive approach for identification of tumour-related metabolomics changes and changes in connective proteins as well as disorders related to respiratory system activity and the blood microcirculation system (Andersson-Engels & Wilson, 1992). There is growing testimony that

the physiological characteristics of skin tissue autofluorescence and blood oxygenation/perfusion are radically altered when cancer incursion and metastasis take place (Arifler, Pavlova, Gillenwater, & Richards-Kortum, 2008), (Müller & al., 2003). This provides impetus to the idea of developing multi-channel non-invasive spectrophotometry. Extremely intriguing in this respect is that neoplastic progression in the transformation from normal to cancer tissue is associated with cessation of normal collagen-elastin proteolysis regulation by matrix-vitiating proteinases (Mueller & Fusenig, 2002). This process which results in structural changes to the stromal collagen matrix and decomposition of collagen fibres should lead to variations from normal in stromal light scattering.

Therefore, study of the scattering qualities of collagen fibres may be an imperative action to advance a more complete representation of changes in optical properties associated with neoplasia. Pathological changes that occur in the cell itself may also be determined by means of analysis of changes in fluorescence intensity of amino acids as by-products of collagen and elastin degradation

1.13 State-of-The-Art in Optical Technology

Multispectral imaging (MSI). Here, light from a LED is relayed through a fibre to the tissue. Reflected light and induced (auto) fluorescence is spectrally resolved on a CCD camera, giving a spectral vision enhanced in spectral range and sensitivity. With 'Enhanced Spectral Vision' the physician will be capable to observe suspected diseased tissue and/or (abnormal) physiology (e.g. blood perfusion) with maximum contrast. This technique records high-resolution hyper-spectral images of the examined tissue area continuously with high frame rate. Using fast GPU processing and special algorithms, the spectral images are converted in real time into intuitive image presentations.

Depending on the specific diagnostic application, the operating parameters of the vision system can be set to achieve optimal sensitivity and selectivity.

This imaging method can be used as navigation and guidance towards diseased areas on a macroscopic level. When suspected areas are identified, microscopic techniques like nonlinear autofluorescence/harmonic imaging and OCT can be used to obtain an ***optical biopsy*** in vivo to confirm the disease with high specificity.

Optical Coherence Tomography (OCT) can produce micrometre-resolution, three-dimensional images from media with high levels of optical scattering like biological tissue. Optical coherence tomography involves interferometry normally using near-infrared light. The use of these relatively long wavelengths enables penetration of several millimetres into the tissue. (Fercher, Mengedoht, & Werner, 1988) (Huang, et al., 1991) The principle of OCT is analogous to ultrasound, where the time delay of scattered waves is measured to determine the location of scattering structures in tissue. In OCT, a broadband light source (i.e., a source with a short coherence length) is coupled into a Michelson interferometer. Light reflected from the sample and reference arm interferes in the detection arm. Only light that has travelled the same path length in the sample and reference arm to within the coherence length of the source produces interference (coherence gating). OCT creates 2Dimensional cross sectional images of tissue up to a depth of 2 mm and with a resolution of 7-30 micron. The predominant enactment of OCT is Time Domain OCT (TD-OCT), in which a reference arm length is rapidly scanned. Each depth scan (A-line) produces a single depth profile in a cross-sectional image. Multiple scattered light is rejected by a combination of confocal detection and coherence gating. OCT is ideally suited for fibre-optic implementation, since only a single spatial mode of the reflected sample light is detected. Just as different stains can be used to enhance the contrast in histology (the examination of thin tissue slices by a pathologist), various extensions of OCT allow the

visualization of features not readily apparent in traditional OCT. Polarization Sensitive OCT (PS-OCT) (de Boer, Milner, van Gemert, & Nelson, 1997), measures the depth resolved changes in the polarization state reflected from tissue. Many biological structures such as nerve, muscle and collagen change the polarization state due to birefringence associated with their linear structure. In Doppler OCT two sequential A-lines are acquired at the same location. Phase resolved detection of the interference fringes permits the determination of small phase shifts between the interferograms. The phase difference $\Delta\varphi$ divided by the time lapse ΔT between the sequential A-lines gives a Doppler shift $\Delta\omega = \Delta\varphi / \Delta T$, associated with the motion of the scattering particle. (Zhao, Shen, Xiang, de Boer, & Nelson, 2000), (Zhao & al, 2000). Doppler OCT permits an accurate mapping of the vasculature (White & al, 2003), (Makita & al, 2006). Both reduction of tissue birefringence due to destruction of the extra-cellular collagen and elastin matrix and increased vascularization are associated with abnormal tissue growth and carcinoma. PS-OCT will be able to measure the depth resolved collagen and elastin density and provide much more detailed information. Vascular networks with increased vessel growth and complex networks of tortuous vessels of various sizes are associated with dysplasia. Increased vascularisation around tumours can be visualized with Doppler OCT as contrast mechanism for tissue characterization.

Nonlinear imaging. This technique achieves penetration depth of around 0.5mm, high resolution and intrinsic tissue contrast. Nonlinear microscopy, where a signal photon is generated by an interaction of two or more photons, has improved the penetration depth in tissue to hundreds of micrometres by using longer wavelengths, due to the lower sensitivity of longer wavelength light (>700 nm) to scattering. It offers advantages over other modes of fluorescence, particularly in thick biological specimens (Denk & al, 1990): the long wavelength light is less destructive than shorter wavelength light sources, minimizing photo-toxicity associated with prolonged exposure to light, and the

requirement for a high photon flux limits the fluorescent excitation volume to the point of focus of the microscope objective permitting optical sectioning without de-scanning the emitted light. This allows for placement of sensitive detectors near the scanned specimen thereby optimising the light collection efficiency. Multi-photon fluorescence microscopy achieves spatial resolution on the order of 1 μm, enabling the identification of intrinsic indicators within tissue, such as nicotinamide adenine dinucleotide, retinol and indoleamines, at a cellular level (Zipfel & al, 2003), (Bacskai & al, 2002). Other non-linear mechanisms can deliver fundamental, label-free image contrast in non-linear microscopy; second-harmonic generation (SHG), third-harmonic generation (THG), coherent anti-Stokes Raman scattering (CARS), and stimulated Raman scattering (SRS). THG microscopy has been shown to be a powerful and adaptable instrument for label-free brain imaging at video rates and volumes of ~250x250x600 μm^3, with 1 μm^3 resolution (Witte, et al., 2011). THG is now a firmly established nonlinear imaging technique (Barad, Eisenberg, Horowitz, & Silberberg, 1997) which has the remarkable property that the phase-matching conditions required can be improved by the presence of breaks in the laser focal volume. Brain tissue lipids generate THG images very efficiently. THG has demonstrated utility in label-free imaging of axons, neurons, blood vessels and even single blood cells. Multicolour nonlinear fluorescence microscopy combined SHG and THG fluorescence has produced images with the resolution and detail of standard histology without the use of exogenous stains. The imaging of intrinsic tissue markers such as nicotinamide adenine dinucleotide, retinol, indoleamines, collagen and membranes has the potential to provide crucial facts for physiology and pathology. For the experiments two laser systems are available: a mode-locked Ti:sapphire oscillator equipped with an optical parametric oscillator (Mira-OPO, APE Berlin, and Coherent Chameleon Ultra II) and a similar laser system equipped with a commercial two-photon laser-scanning microscope (LaVisionBiotech), modified for SHG/THG imaging.

Nonlinear imaging techniques (TPEF-SHG-THG) have been developed for the investigation of cellular and sub-cellular activities. Recently, non-linear optical techniques used in combination with microscopy have provided opportunities for renewed technological advances in the fields of medicine and biology. (Tserevelakis & al, 2011) Due to their inherent advantages (high lateral and axial resolution, increased penetration depth, elimination of photo-damage and photo-bleaching phenomena, intrinsic 3-D imaging capability) in comparison with conventional and confocal microscopy, non-linear microscopy techniques comprise a unique and extremely powerful tool for the extraction of valuable information from biological samples. Cell tracking, embryogenesis and neuro-degeneration phenomena as well as the functional *in vivo* imaging of various biological samples such as HeLa cells, C. elegans, and mouse embryos have been extensively studied (Kyvelidou & al, 2011).

Multispectral Optical Tomography: In the field of biomedical imaging, 3D tomographic devices have been designed and realised for the study of a wide range of biological processes *in vivo* in laboratory animals and in pre-clinical and clinical protocols involving tissue samples, such as biopsies. (Zacharakis & al, 2011). These methodologies have been based both in intrinsic contrast provided by auto-fluorescence, absorption and scattering of native tissue components and in externally administered fluorescence agents. In addition, the appropriate theoretical models for light propagation in diffusive media, such as tissue have been developed along with the incorporation of reconstruction techniques for the production of quantitative 3D images of optical contrast. Cancer progression and metabolism, immunological disorders, cell population dynamics and tissue oxygenation have been successfully imaged volumetrically in small animals using Fluorescence Tomography. Furthermore, polarization sensitive Diffused Optical Computed Tomography has been used for the pre-histological assessment

of pigmented skin biopsy samples, providing sample differentiation, spatial extension and depth of invasion of melanocytic lesions. (Papadakis & al, 2010).

1.14 Summary of Chapter 1

Trends in both modern medical diagnostics and treatment are towards those which minimise invasiveness, pharmaceutical (chemical) and other ecologically and physiologically undesirable effects on the human organism.

Growth of the human population, combined with its rapid ageing in developed nations is leading to an enormous increased demand on medical resources. Medical technologies that produce a maximum effect with the minimum expenditure of time are therefore urgently required. These requirements are met by the latest optical (laser) clinical non-invasive diagnostic methods that began to appear in many leading countries all over the World, including the EU and Russia.

Laser diagnostics techniques are founded on a simple obvious basis that the optical properties of biological tissues are a function of the condition and physiology of the investigated tissues and organs. The spectroscopic properties of tissues and fluids exhibit differences between their normal healthy and their disease state. Therefore, it argued that it is possible to determine clinical diseases by measuring and interpreting the *in vivo* spectral characteristics of absorbance, scattering, reflectance, fluorescence. Essentially, the same fundamental functional principles as non-invasive optical diagnostics are used in established pathology laboratories, the advantage is that non-invasive diagnostics are performed *in vivo* and in a *real-time* . With the exception of laser tomography most non-invasive optical and laser medical diagnostic techniques can be regarded as “non-invasive clinical spectrophotometry techniques”.

Chapter 2 – BASIC PRINCIPLES OF DESIGN AND FUNCTIONING OF MULTIFUNCTIONAL LASER DIAGNOSTIC SYSTEM FOR NON-INVASIVE MEDICAL SPECTROPHOTOMETRY

Based on the developed knowledge and understanding described in Chapter 1, I now moved on to address the first aim of the work*, **to develop a laser diagnostics device in the spectral band from 365nm to 1300nm***. The work described here is based on the hypothesis that ***the underlying design principles of laser diagnostics can be described in a comprehensive systematic theory***.

This Chapter, therefore, presents a review of Laser Diagnostic Systems as related to Multifunctional Laser Diagnostics and their development with an analysis of the major components to provide a framework for modular development and modelling of systems at the concept and design stage.

2.1 Introduction

Optical properties of *in vivo* biological tissues with normal and d i s e a s e pathology have become the subject of mainstream intensive research study at a global level over the past few decades. Specific biophotonic diagnostic techniques have the capability to gather enormous amounts of information on biological tissues non-invasively, *in vivo* and in real-time as described in Chapter 1. These technologies allow us to confidently conceive and investigate a new area of multifunctional diagnostics and to develop optical non-invasive diagnostic devices and systems (Rogatkin, 1998), (Tuchin, 2002) , (Rogatkin & Lapaeva, 2003). It is already common medical and surgical practice to use commercial instruments for optical pulse oximetry and laser Doppler flowmetry (LDF) or laser Doppler perfusion monitoring (LDPM)

(Fredriksson, Fors, & Johansson, 2007) as well as fluorescence diagnostics (Loschenov & al, 1998), optical coherence and diffusion tomography (Tuchin, 2002), (Bouama & Tearney, 2002), tissue fat detectors, blood glucose, haemoglobin and oxyhaemoglobin analysers (Anderson & Parrish, 1981). The most commonly implemented of this array of optical technologies is non-invasive medical spectrophotometry (**NMS**) (Tuchin, 2002), without bio-sampling the patient's body (skin, oral mucosa, blood, etc.) the levels and accumulation dynamics of various biochemical markers: oxyhaemoglobin, flavin respiratory enzymes, porphyrins, lipofuscin, NADH, etc. can be estimated. It is further proposed that the most promising direction for NMS device development is multifunctional (universal) laser non-invasive diagnostic systems (**MLNDS**) which in a single system combines various NMS methods, such as fluorescence and absorption spectroscopy, laser Doppler flowmetry, etc. (Gorenkov, Rogatkin, & al, 2002). This allows therapists and clinicians not only to receive the arithmetic sum of the diagnostic information that could be collected by each of individual method but also to conduct multifunctional patient examination measurements to identify subtle individual characteristics of blood flow and tissue metabolism using simultaneous and comprehensive data from different diagnostic techniques (Tchernyi & al., 2006).

Until recently, single and at the best dual function diagnostic instruments have been designed empirically in the absence of any consideration of a systemic theory. However, there is a clear case for a common theoretical framework for the development and operation of medical optoelectronic devices applicable generally and also specifically to MLNDS. Any new diagnostic device has its own specificities which in varying degrees affect the entire process of development and validation starting from the common stages of concept and technical design

through to integration of the entire system. The primary step is to define the problem and formalise the features of the system followed by the development of a generalised structural and functional design and physical and mathematical model of the envisaged device. The specific features of the system will arise at this formulation stage including the general function of the device, its architectural layout, metrological and data processing requirements, software and methodological provisions.

These issues have not been fully addressed with respect to MLNDS leaving a gap for a formalised theoretical framework for the development of such systems. The following work seeks to make some progress towards filling this gap and through investigation to uncover the main systemic and methodological principles underlying the design of MLNDS. It offers a formal description of the objectives, formulate the main functions and provide a generalised model for the structure and function of MLNDS. General modular construction principles for MLNDS hardware are developed and the critical role of algorithms and software in the overall design and synthesis of MLNDS is validated.

2.2 Formal description of detailed sub-system representation

Consistent with the latest developments in instruments for NMS (Rogatkin D. and L.Lapaeva, 2003) in the context of this work we consider MLNDS as any implementation of a diagnostic device in this class, regardless of individual optical techniques and radiation source or laser (if using lasers as a source of radiation) NMS. According to (Ahutin, 1981), any medical diagnostic device is an open medical biotechnology system (MBS), a combination of biological and technical elements jointed into a uniform functional system where all elements are linked into a control loop (open-loop in this case). There are two biological

objects in this open-loop system: a patient and a clinician-physician controlling the system analysing information outputs from the device and then deciding what medical treatments shall be prescribed to the patient.

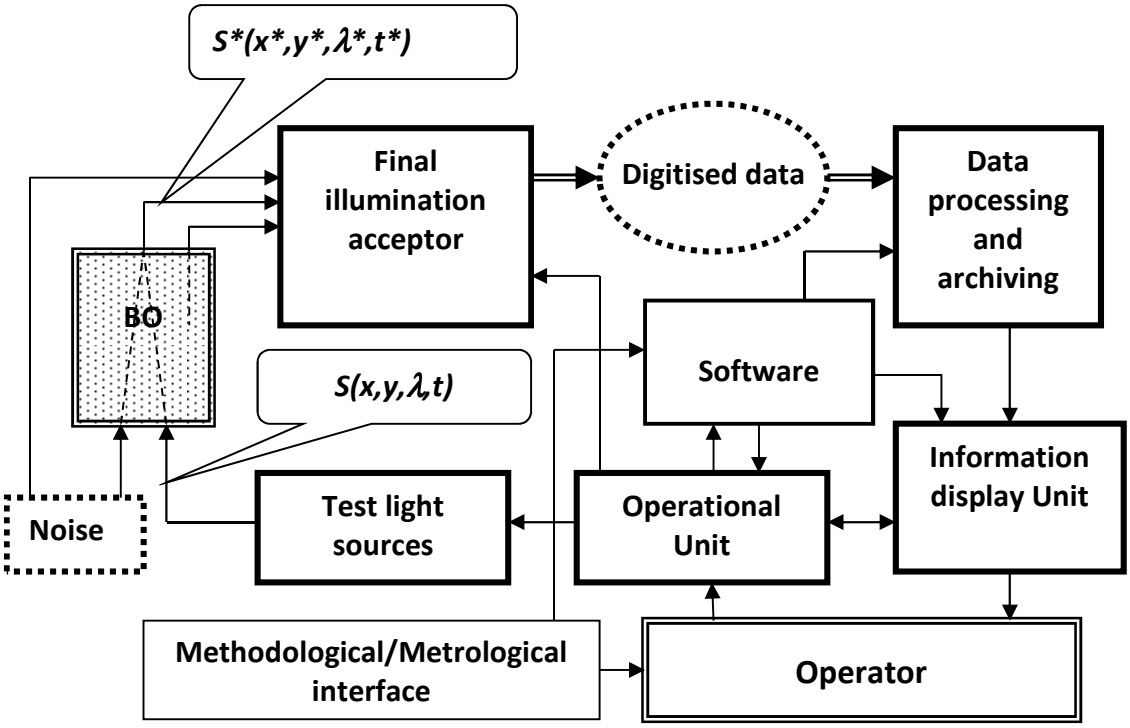

Figure 14 - Schematic representation of the open systems architecture of MLNDS

Therefore the main aim of this study is to describe a multi-functional diagnostic system (MLNDS) for obtaining comprehensive information from BO by optical spectral sensing. The MLNDS contains light sources illuminating BO which generate output analogue information called initial analogue optical signal *S(x, y, λ, t)*, where *x* and *y*, the spatial coordinates on the surface of the BO, λ - wavelength, *t* - time. BOs due to their individual optical properties associated with anatomical, morphological and biochemical properties of tissue, encode the initial optical signal *S(x, y, λ, t)* changing its basic parameters: spectral power density, shape,

repetition rate and pulse duration, depth by amplitude/frequency modulation into the final optical signal *S*(x*, y*, λ*, t*)*. MLNDS will aim to collect as full as possible a final encoded signal *S*(x*, y*, λ*, t*)* filter out external interference signals and noise comparing against information on the initial signal *S(x, y, λ, t),* calculate the necessary optical and physical BO parameters. In the final stage of data processing the optical and physical data should be converted by a MLNDS into meaningful medical and biological parameters interpreted in medical terms (Rogatkin, 2004).

Since the final optical signal coming from BO is an analogue signal MLNDS should process discretise and digitise *S*(x*, y*, λ*, t*)* sampled signals for all the basic parameters of amplitude, wavelength, time intervals (the basic principle of extracting information from analogue signals (Oppenheim & Schafer, 1975) (Mosyagin, Nemtinov, & Lebedev, 1990). The final optical-physical and biomedical information from the subject BO should then be processed in a MLNDS by computer processing and/or interpretive algorithms and procedures implemented in the software (Rogatkin, 2004), (Bessonov, Kolbas, & Rogatkin, 2007). The MLNDS clinician should be able to adopt this information in a familiar form and store it in a database and/or medical record documentation.

A generalised formal description of system and task representation is illustrated in Figure 14 - Schematic representation of the open systems architecture of MLNDS. Thus a MLNDS appears to be a complex parameter-measuring system in which more than two-thirds of the functional characteristics and efficacy are determined by the capacity of its computing resources and

software methodology (Rogatkin, 2004). Consequently, the most important step in creating any MLNDS is the development of data processing algorithms and software implementation, particularly during the development of general the ideology of the computational process in terms of diagnostic data processing and analysis.

No standardised data processing algorithms for MLNDS have been published to date, nor any general mathematical models for calculation of the irradiation field distributed in randomly inhomogeneous medium such as biological tissues which (models) which offer precise analytical solutions for irradiation fluxes emerging from bio-tissue like light scattering and absorbing. Therefore, a large amount of theoretical research in NMS is aimed at the development of models and algorithms suitable for particular systems (Rogatkin, 2007), (Rogatkin, 1998), (Tuchin, 2002) including the creation of virtual physical and mathematical models of BO in terms of the theory of light propagation and scattering in turbid media (Ishimaru, 1981). Since these models are the basis of modern methods of analysis and data processing in NMS the choice of model in the design phase will hugely influence the clinical efficacy and diagnostic potential of MLNDS. Since the available models and algorithms only solve specific cases at particular wavelengths for defined irradiation schemes and geometry for the detection of the final optical signal $S^*(x^*, y^*, \lambda^*, t^*)$ then the selected methods and data processing algorithms "dictate" to the developer the entire architecture of the MLNDS transmitter-receiver unit, as illustrated in Figure 14 - Schematic representation of the open systems architecture of MLNDS. This fact is secondary to the MLNDS software and as they influence only the physical elements for generation, registration and translation of the optical and electronic signals necessary for the close-looped work of computing, processing and interpretive algorithms of MLNDS software.

2.3 Structural and functional model of MLNDS and its main function

One of the first and fundamental tasks in designing any new optic-electronic equipment, including medical devices, is the creation of an adequate structural-functional model (**SFM**) for the new device and determination of its general functional objectives (Rogatkin, Lapaeva, Petritskaya, & Sidorov, 2009). We will consider one of possible SFM (Figure 15 - Structural-Functional Model (SFM) of a generalised MLNDS) of generalized MLNDS based on (Gorenkov, Rogatkin, & al, 2002) (Rogatkin, Siderov, & Schumsky, 2008).

In developing the SFM the ideology of a modular-unit system with a discrete set of irradiation sources (**IS**) corresponding with a discrete set of detecting wavelengths is used. This means that the IS in the MLNDS generates a discrete set of optical probing signals (the first level of signal definition by spectrum and exposure time)

Equation 2-1

$$W_i = W_i(\Delta\lambda_i, \Delta t_i)$$

where:

W_i - the irradiation power of *i*-th source;

$\Delta\lambda_i$ - spectral range of W_i;

Δt_i - time interval of *i*-th source.

The Irradiation Formation Optical Scheme (**IFOS**) generates a focused light beam with surface (illumination) power density P at BO:

Equation 2-2

$$P = f(x, y, \lambda, t, Wi)$$

The analysed BO acts as a spectral nonlinear optical filter and converts the IS power density P into power density P* of the exiting irradiation from BO which is equivalent to an encoding function of the initial optical signal.

Equation 2-3

$$P^* = f^*(x^*, y^*, \lambda^*, t, W_i, W_{f1}) = B(x \to x^*, y \to y^*, \lambda \to \lambda^*, t, \{m_j(t)\}) \cdot (P + P_{f1})$$

where:

B - encoding dimensionless function of irradiation by BO;

$\{m_j(t)\}$ - an array of biomedical, optical-physical parameters of the BO that affects the coding function;

W_{f1} and P_{f1} - power and power density of the background irradiation (noise) passing through the BO.

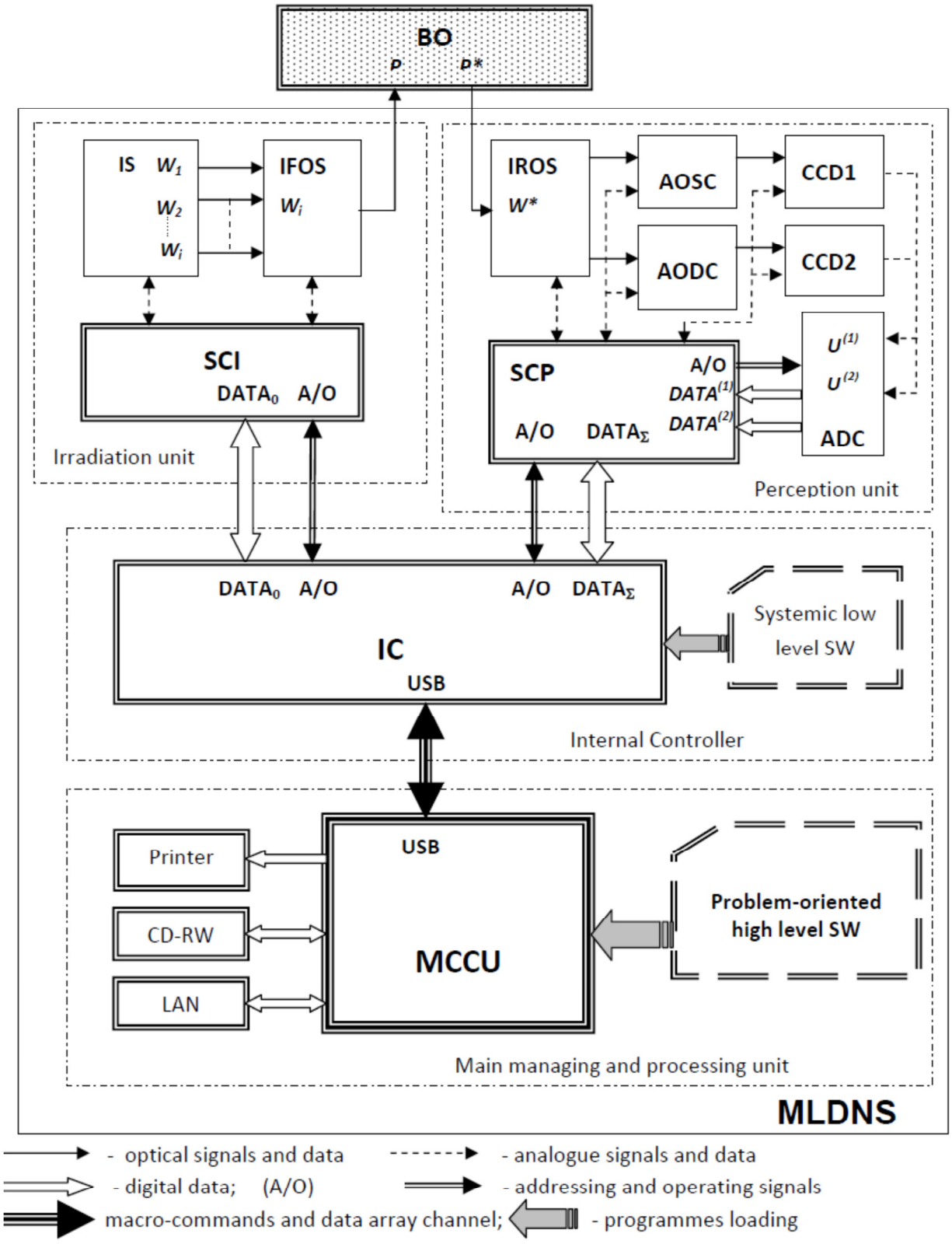

Figure 15 - Structural-Functional Model (SFM) of a generalised MLNDS

The Irradiation Registration Optical Scheme (**IROS**) of the MLNDS collects at aperture angle ω* the final irradiation *P** returned from BO distributed over its surface and delivers it to the MLNDS. The IROS also collects some of the initial background irradiation (W_{f2}) not originating from BO. Thus, the total MLNDS radiation power of *W** may be represented as:

Equation 2-4

$$W^*(\lambda^*,t,\{m_j(t)\},\ldots)=\int_0^{\omega^*}P^*(x^*,y^*,\lambda^*,t,\{m_j(t)\},\ldots)d\omega+W_{f2}(\lambda^*,t)$$

This allows us to formulate a general function of MLNDS as determining the array *{mj (t)}* of measured *W** values as a function of signal amplitude, wavelength range and the BO investigation time as known functions:

Equation 2-5

$$P=f(x,y,\lambda,t,W_i)$$

In general to determine the unknown elements in j $\{m_j(t)\}$ array as a function of time it is necessary to have k ≥ j measurements as function of time. It is necessary for MLNDS, as shown in (Gorenkov, Rogatkin, & al, 2002), to deliver the key function of detecting and separating different weak (in amplitude but static during short time intervals) BO signals of fluorescence (in a fluorescent diagnostics channel) or a dynamic in the main spectrum range Δλi (for scattering and absorption spectroscopy and Doppler flowmetry channels). In the present SFM this requirement is taken into account by introducing two analogue optical channels – a static one (AOSC) and dynamic one (AODC). By designing the channel as a polychromator with simultaneous recording of full spectrum by sensitive detectors such as

CCD comparison and discretisation of the signals against a registered optical spectrum (λ^*) in AOSC is performed.

Signal discretisation in the dynamic channel (AODC) is performed on the basis of initial discretisation of the spectrum ($\Delta\lambda_i$) of emitting sources by choosing a suitable set of lasers, and general discretisation of the signal time in AOSC and AODC is performed by choosing different sampling time and sampling frequency of the CCD for each channel: CCD1 and CCD2.

The amplitude signal discretisation can be carried out using a standard analogue-digital conversion (ADC) of electrical signals from CCD of perception unit which transmits data arrays for temporary storage, sorting and further processing into the memory of the internal controller (**IC**). The same controller provides MLNDS with low-level distribution of control commands and data between perception unit and illumination unit. Low-level electronic control of units and modules perception and illumination units is covered by specialized control units (**SCI** and **SCP**). The final high-level data processing and communication of MLNDS with operator is made by the main control and computing system (**MCCU**) on the basis of modern high-speed computer. Thus the system signal processing *W** in MLNDS leads to creation of two main sets of stresses {*U(n)*} from CCD and two full digital data sets {DATA (n)} storing information about amplitude, optical spectrum, and dynamic parameters of the signals:

Equation 2-6

$$W^* \rightarrow \left\{ \begin{array}{l} \{U^{(1)}_{\Delta\lambda_i,\lambda^*}\} \rightarrow \{DATA^{(1)}_{\Delta\lambda_i,\lambda^*,t_1}\} \\ \{U^{(2)}_{\Delta\lambda_i,t_2}\} \rightarrow \{DATA^{(2)}_{\Delta\lambda_i,t_2,t_1}\} \end{array} \right\}$$

where: $t_2 << t_1$ and t_1 is the time scales of signal discretisation at short time intervals (≤ seconds) and a relatively long time intervals (minutes, hours, days), correspondently. The high-level algorithms and computational tasks of the MCCU are predominantly reduced to two main functions:

- restoration on the basis of the actual optical-physical measurements and,
- medical, and biological properties of the BO:

Equation 2-7

$$\{m_j(t)\} = CA\left\{ \begin{array}{l} \{DATA^{(1)}_{\Delta\lambda_i,\lambda^*,t_1}\} \\ \{DATA^{(2)}_{\Delta\lambda_i,t_2,t_1}\} \end{array} \right\}$$

Where *CA* is a computational algorithm and the interpretation of the computed data array $\{m_j(t)\}$ in terms of biological condition with the probabilistic clinical classification of the situation:

Equation 2-8

$$\{CS\} = IA[\{m_j(t)\}]$$

Where: *IA* is an interpretive algorithm and {*CS*} is a text information array of the clinical situation of BO observed for that particular survey.

This representation of a SFM of MLNDS enables design stages to be isolated into explicit subtasks to be solved: computational algorithms, parametric synthesis of the units and blocks of the MLNDS, etc. in addition to creating virtual simulative mathematical MLNDS models for use at the initial stages of ideological and technical design.

2.4 Principles for the design MLNDS modules

The SFM elaborated above for MLNDS informs the MLNDS developer of a logical simple and optimal framework methodology to consider design and structural development of a MLNDS. This offers a framework for the creation of an integrated modular system from individual structural-functional elements which are highly typical for many optic-electronic diagnostic devices.

This work was inspired when reviewing and analysing recent publication containing description and technical specification of various optic-electronic units, their technical schematics and technological solutions (Spectrum Medical) (Oxford_Optronix, 2013) (Woodley Lab Diagnostics) (Life Technologies) (SPE LAZMA). General trends in global instrument development were investigated through the advertising publications in magazines such as Opto & Laser Europe, Photonics Spectra and Europhotonics. Finally, this analysis indicates that in contrast to the traditional manufacturers of individual components (chips, lenses, etc.) and final products (full scale equipment) a new class of the manufacturer has appeared since the mid 1970-80's, which produces individual universal optic-electronic

subunits and functional blocks. For example, "Point Source Ltd." and "Photonics Products" (USA) offers finished laser modules with electronic drivers for different wavelengths with standard interfaces and control systems for direct embedding of these modules into a fully integrated system. "Piezosystem Jena GmbH" also produces a sub-system for positioning and alignment of optical elements for use in complex photonics systems. "Andor Technology Co." produces CCD detectors and sensors for "OEM" technology which can be directly coupled to signals from a standard Personal Computer via a normal USB connection. "Acton Research Corp." produces spectrophotometry modules with various sensitivity and spectral resolution from tiny on board with "PCI" connectors for PC installation to highly sensitive monochromators and polychromators with built-in electronic alignment, CCD, analogue amplifier, and Analogue Digital Converter (ADC) Modules capable of working with any PC.

Thus, for the manufacturer of medical diagnostic equipment such as MLNDS, there is no longer a need to develop from scratch all the basic components and units of the device. It is simply a matter of choosing the module (unit) with most suitable technical characteristics on the market and adapting it to the input and output parameters required for the new system. This allows reduces the main design work for individual MLNDS elements to the engineering of the main optic-electronic and laser elements.

Consequently the scientific concept of MLNDS design has the following basic principles:

a) maximum standardisation of individual units and modules of the MLNDS
b) maximum functional specialisation of units and modules of the MLNDS
c) structural-functional hierarchy of the units and modules within MLNDS
d) optimal sharing of hardware and software functions between MLNDS units and modules

e) compatibility of these modules and systems to a higher hierarchy controller (PCs)
f) consideration to up-grading the system with more efficient elements.

2.5 Medical and technical requirements for non-invasive spectrophotometric diagnostics

Here we proposes a scientific approach to the formulation of medical and technical requirements for non-invasive spectrophotometric diagnostic devices using optical technologies such as laser Doppler flowmetry and absorption spectroscopy. The theoretical modeling framework, metrological certification and testing of these devices are still in the early stages of development. The estimation of the received signal levels for wavelengths between 514-940 nm is highly dependent on the blood volume level in the subject tissue (Dunaev, Zherebtsov, Rogatkin, Stewart, Sokolovski, & Rafailov, 2013). Here we aim to develop and describe an approach which allows, in particular, the calculation of the technical and metrological performance constraints of the instruments, such as the ranges of the sensitivity and power related signal-to-noise ratios for different spectral channels and different biomedical (biochemical and physiological) parameters. The hypothesis is that the specialised medical and technical requirements for the non-invasive spectrophotometric diagnostic devices can be defined, thus enabling them to develop in due course to the level of a standardised measurement technique.

Substantial progress in photonics and biophotonics has been made in bringing the development of novel and non-invasive optical diagnostic devices to biomedicine (Liu, Kohl-

Bareis, & Huang, 2011), (Rogatkin, Sokolovski, Fedorova, Stewart, Sidorov, & Rafailov, 2011), (Oxford_Optronix, 2013), (Leahy & Nilsson, 2010), (Kramme, Hoffmann, & Pozos, 2011), (Kraitl, Timm, & Ewald, 2010). Though there are a great variety of devices in this class, the largest group of equipment implements the principle of non-invasive medical spectrophotometry (NMS) (Rogatkin D. and L.Lapaeva, 2003). These optical systems can report the levels of various biochemical components such as de/oxyhaemoglobins, collagen/elastin, porphyrins, lipofuscin, NADH, flavins etc. in tissues. They can thus measure the dynamics of metabolism and examine the major regulatory processes of blood flow without the need to take biopsies. A promising direction in the development of NMS devices is the creation of multifunctional non-invasive diagnostic systems, which can allow acquisition of comprehensive real time biomedical information from the site examined.

These diagnostic systems are generally empirically designed in the absence of any well-developed and systematised theory. The theoretical modelling framework, metrological certification and testing of these devices are still in the earliest stages of development. There are virtually no evidence-based approaches and techniques to intelligently formulate specialised medical and technical requirements (MTRs) for diagnostic device parameters. For example, there are few recommendations and rationales in the literature for selecting the accuracy class required for NMS devices (Rogatkin, Dunaev, & Lapaeva, 2010). More recently, the theoretical issues of formalising diagnostic tasks for NMS have been examined, with structural and functional model circuits developed and physical-mathematical theory generalised for NMS (Rogatkin, Sokolovski, Fedorova, Stewart, Sidorov, & Rafailov, 2011), (Cysewska-Sobusiak, 2000), (Tchernyi, Rogatkin, Bychenkov, & Polyakov, 2005). These apply to the general phases of the ideological and technical design and realisation of such

equipment. These authors considered some key features of metrology of the NMS for *in vivo* measurements (Rogatkin, Dunaev, & Lapaeva, 2010). For instance, they proposed an investigation into the diagnostic volume in NMS, alongside a theoretical and experimental study of the impact of diagnostic volume on the metrological parameters of such devices. In addition, it has been proposed to develop reproducible and standard methods of tuning, calibration and verification of NMS devices without the use of human subjects by using optical phantoms as test-objects.

The work here aims to contribute to the further development of the scientific approaches to substantiate the medical and technical requirements for non-invasive spectrophotometric diagnostic devices. The work is primarily based on study of the influence of tissue blood volume on registered signal levels and the sensitivity of such devices.

2.6 Methods and functional scheme of measurements by NMS

In NMS the most sensitive method known for recording the dynamic processes in the blood microcirculatory system is LDF. This is based on the measurement of Doppler frequency shifts, which occur after the backscattering of radiation from red blood cells moving at different speeds in small vessels – arterioles, capillaries and venules (Leahy & Nilsson, 2010) (see page 18, Laser Doppler Flowmetry (LDF)). This is represented as a microcirculation index I_m in arbitrary perfusion units. Perfusion fluctuations are recorded as a complex non-periodic process. The variable component provides valuable information on the modulation of blood flow. Spectral signal processing algorithms used for decoding and analysis provide information about the vascular tone in terms of contribution of the different regulatory

mechanisms of endothelial, neurogenic, myogenic, breath, pulse micro-haemodynamics (Krupatkin & Sidorov, 2005), (see page 76 Measurement of Blood Flow Oscillations:)

Tissue reflectance oximetry (TRO) is based on the principles of absorption spectroscopy and allows non-invasive (*in vivo*, transcutaneous) monitoring of micro-haemodynamics and oxygen transport and utilisation within the entire blood microcirculation system (Colquhoun, Tucker-Schwartz, Durieux, & Thiele, 2012), (Amzina, Micheev, Rogatkin, & Sidorov, 2005). TRO determines the relative volume of all fractions of haemoglobin (total haemoglobin) in a tissue volume, the average level of blood volume – V_b and oxygen saturation of the microvasculature, generally containing arterioles with oxyhaemoglobin and venules with deoxyhaemoglobin, the average level of tissue oxygen saturation – S_tO_2 (Rogatkin, Sokolovski, Fedorova, Stewart, Sidorov, & Rafailov, 2011).

By following an integrated biotechnical approach, we can formulate discreet measurement tasks for the methods incorporated in the NMS and consider the general functional scheme of the measurements made in NMS (Figure 16). In the diagnostic device, light with a wavelength λ and with a power $P_s(\lambda)$ from the radiation source *1* is delivered by optical lighting system *2* to the examined biological object (BO) *3*. Depending on the diagnostic method, the light source may be either a monochromatic (laser) or a set of variable light sources with different emission spectra.

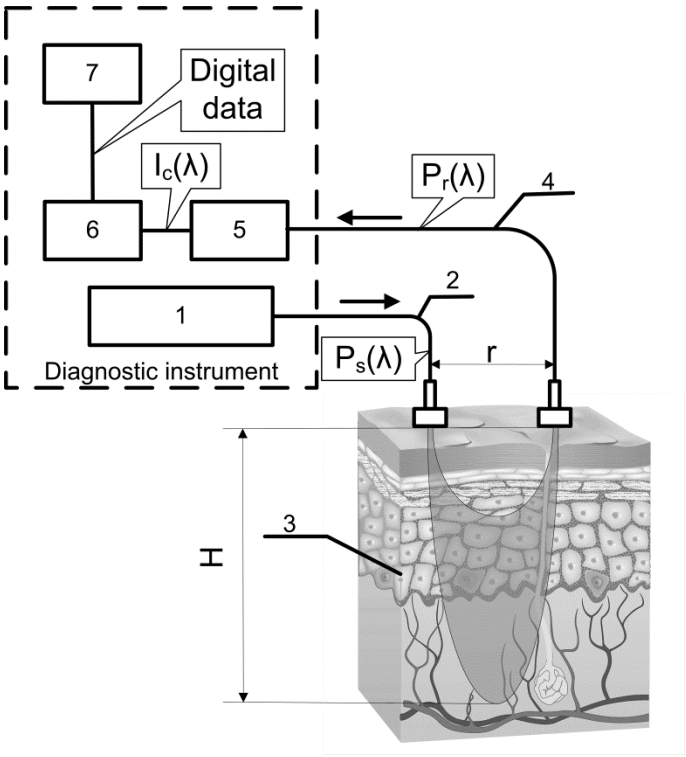

Figure 16 - Generalised functional scheme of optical measurement by NMS: 1 - radiation source, 2 - optical lighting scheme, 3 - biological object, 4 - irradiation transport system, 5 - photodetector, 6 - electronics, 7 computer.

Ps(λ)—power from the radiation source, Pr(λ)—received power (backscattered radiation), Ic (λ)—photocurrent on photodetector, H—measurement depth, r—separation distance between the source and detector fibers.

In tissue, radiation is extensively scattered at the boundaries of morphological irregularities and is partially absorbed by substances like water, melanin, haemoglobin, etc. before the re-emergence of the attenuated radiation (see page 12 - Reflection and). Due to multiple scattering events, part of the radiation exiting the BO forms a flux of backscattered light. This irradiation with power $P_r(\lambda) < P_s(\lambda)$ is delivered to the device by the irradiation transporting system *4* to the recording unit of the diagnostic device. In a simplified case it is sent to the photodetector *5* that performs a linear transformation of the optical power $P_r(\lambda)$ to the photocurrent $I_c(\lambda)$. The produced electrical signal is processed in analogue mode

(photocurrent $I_c(\lambda)$ to voltage $U(\lambda)$ conversion, amplification, filtering, etc.) in the electronics block *6*, digitised and transmitted to the computer *7* for further computation. As a result, biomedical parameters such as I_m, S_tO_2 and V_b are calculated. Thus, generally NMS implements indirect measurement methodology (Bronzino, 2000), (Czichos, Saito, & Smith, 2011).

Changes in blood microcirculation can be registered by the diagnostic NMS following changes in the optical properties of bio-tissue. Thus, changes in the optical properties of biological tissues have a major impact on signal levels recorded by the NMS and must be included in developing the medical and technical requirements of optical diagnostic devices.

2.7 Theoretical estimation of the levels of the received signals

Theoretical estimation of the signal variability measured by a NMS device operating in a backscattering mode using different spectral channels leads to the challenge of quantitative metrology using such measurements. It should be noted that attempts have been made to estimate the measurement depth (parameter *H* in the schematic Figure 16) and diagnostic volume for some methods of NMS (for example, LDF (Fredriksson & Larsson, 2009)). However, they use numerical simulation methods which do not deal with the relationship of estimated signal levels or medical and technical requirements for the optical diagnostic devices. Depending on the types of tissues studied (with different absorption, scattering and others properties), the measurement depth can range from 1-8 mm (Rogatkin, Dunaev, & Lapaeva, Metrological Support of Methods and Devices for Noninvasive Medical Spectrophotometry, 2010).

A biological object considered in the functional schematic (Figure 16) can be represented as we have done before as a non-linear spectral-optical filter, which converts the power of initial $P_s(\lambda)$ to the power of secondary radiation $P_r(\lambda)$. Such a representation is mathematically equivalent to the multiplication of the original optical signal by a dimensionless coding function $B(\lambda)$ which is dependent on the optical and physical, medical and biological parameters of the object, as well as the lighting conditions and delivered irradiation. The well-known expression obtained for the diffusion approximation of a semi-infinite medium can be cited as an example of the $B(\lambda)$ function (Tuchin, Handbook of optical biomedical diagnostics, 2002):

Equation 2-9

$$B(\lambda) = \frac{z_0 A}{2\pi} \cdot \left[\frac{\mu_d}{r^2 + z_0^2} + \frac{1}{(r^2 + z_0^2)^{3/2}} \right] \cdot \exp\left[-\mu_d (r^2 + z_0^2)^{1/2} \right]$$

Where,

$z_0 = 1/\mu_s'$ representing the effective path length of the light;

A is the detector area;

r is the separation distance between the source and detector fibres in Figure 16; $\mu_d = [3\mu_a(\mu_a + \mu_s')]^{1/2}$, $\mu_s' = (1-g)\mu_s$ is the reduced scattering coefficient;

$g = g(\lambda)$ the anisotropy factor;

$\mu_s = \mu_s(\lambda)$ the scattering coefficient;

$\mu_a = \mu_a(\lambda)$ the absorption coefficient.

For most non-transparent biological tissues, the anisotropy factor value is in the range of 0.7-0.95 and the $g(\lambda)$ for skin (both the dermis and epidermis) can be determined by the following empirical equation (Jacques, 1996):

Equation 2-10

$$g(\lambda) = 0.7645 + 0.2355 \cdot (1 - \exp(-\frac{\lambda - 500nm}{729.1nm})) \ ,$$

For the theoretical estimation of the parameters for the received signals it is possible to calculate values of the *B(λ)* function according to equation (2.1) for commonly used wavelengths at different levels of blood volume:

Equation 2-11

$$\mu_s(V_b) = V_b \cdot \mu_{sb}(\lambda) + (1 - V_b) \cdot \mu_{st}(\lambda)$$

$$\mu_a(V_b) = V_b \cdot \mu_{ab}(\lambda) + (1 - V_b) \cdot \mu_{at}(\lambda) \ ,$$

Where, V_b is the blood volume in tissue,

μ_{sb}, μ_{ab} are scattering and absorption coefficients of blood;

μ_{st}, μ_{at} are scattering and absorption coefficients of bloodless tissue (bloodless dermis/papillary dermis).

Absorption spectroscopy (TRO/NIRS) commonly uses wavelengths in the visible (most often – green, yellow, red) and/or infrared ranges, while in LDF – red/infrared ranges are used (Liu, Kohl-Bareis, & Huang, 2011), (Rogatkin, Sokolovski, Fedorova, Stewart, Sidorov, & Rafailov, 2011), (Leahy & Nilsson, 2010). Considering, as an example, the "LAKK-M" system (Rogatkin, Sokolovski, Fedorova, Stewart, Sidorov, & Rafailov, 2011) or other NMS devices using LDF and absorption spectroscopy technology (Liu, Kohl-Bareis, & Huang, 2011), (Kramme, Hoffmann, & Pozos, 2011), (Timm, Kraitl, Schnurstein, & Ewald, 2013), for

calculations in this work we therefore used 514-940 nm range of wavelengths (specifically for green – 514 nm, for yellow – 584 nm, for red – 633 nm and for infrared – 800 and 940 nm).

There are a number of articles in existing literature which offer data regarding the impact of blood volume on tissues optical characteristics (Jacques, 1996), (Jacques, 2013), (Lister, Wright, & Chappell, 2012). From these publications it is possible to assess the approximate range of blood volume of different skin surfaces. Meglinski & Matcher (Meglinski & Matcher, 2002), (Meglinski & Matcher, 2003) provide data on the blood volume of skin layers, for example papillary dermis = 4% and upper blood net dermis = 30%. Lister *et al* (Lister, Wright, & Chappell, 2012) report a range of 0.2-2% for epidermal and dermal blood volume fractions. Reported data on the blood volume in the skin of the forearm is 5.03% (Matcher, Cope, & Delpy, 1997), and at a tissue depth of 100-300 μm the blood volume is 2-5% (Jacques, 1996) and, from our own experience, blood volume of the palmar surface of middle finger is 10-20% (Dunaev, Sidorov, Stewart, Sokolovski, & Rafailov, 2013). Taking all of these into account, this study uses 0-20% as the range of the tissue blood volume, and in some cases up to 50% to assess the changes in functions.

Taking the value of the spacing r = 1 mm (Fredriksson & Larsson, 2009), (Liebert, Leahy, & Maniewski, 1998), which can be up to 3 mm (Takatani, 1989), the area of the detector (an optical multimode fibre with about NA=0.22) A=0.003 mm^2 and using the appropriate scattering and absorption coefficients (Kienle, Lilge, Patterson, Wilson, Hibst, & Steiner, 1995), (Tuchin, 2000) (Table 2), B(λ) can be plotted against tissue blood volume V_b (Figure 17). Figure 18 shows B(λ) with V_b=1; 5; 10 and 15% for the 514-940 nm range of

wavelengths respectively. It should be noted that these graphs are constructed using 5 points, as it is difficult to find the complete range of values of the necessary scattering and absorption coefficients for blood and bloodless dermis for all the same wavelengths. It is shown in Figure 19 that B(λ) is dependent on the value of the source-detector spacing r=0.5-2.0 mm when V_b=10%.

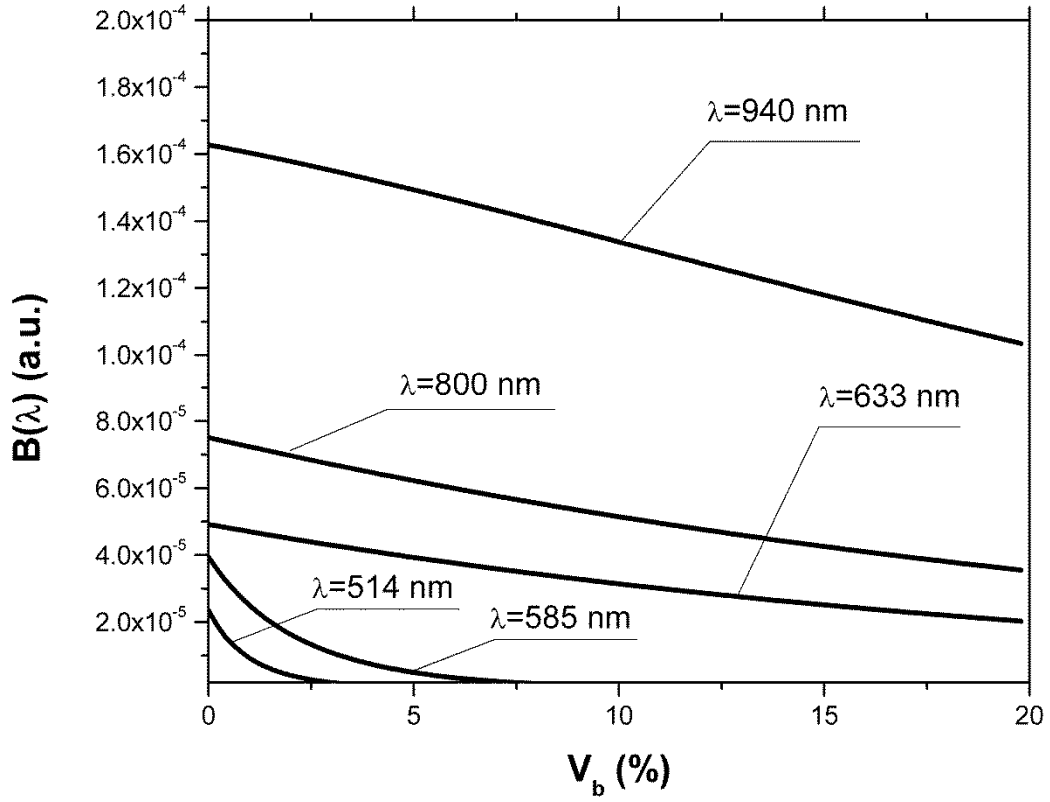

Figure 17 - The dependence of B(λ) on the level of the tissue blood volume V_b. Here and in the following graphs, calculations for the 514- and 800- nm curves used the optical properties of blood for a wavelength of 517 and 810 nm, respectively (from Table 2**).**

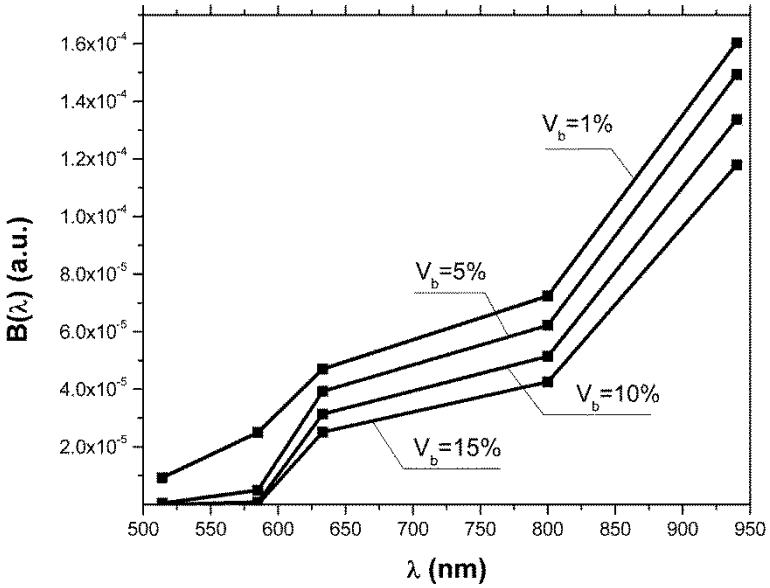

Figure 18 - The dependence of B(λ) on the range of the wavelengths from 514 to 940 nm for different levels of the tissue blood volume (V_b = 1%, 5%, 10%, 15%).

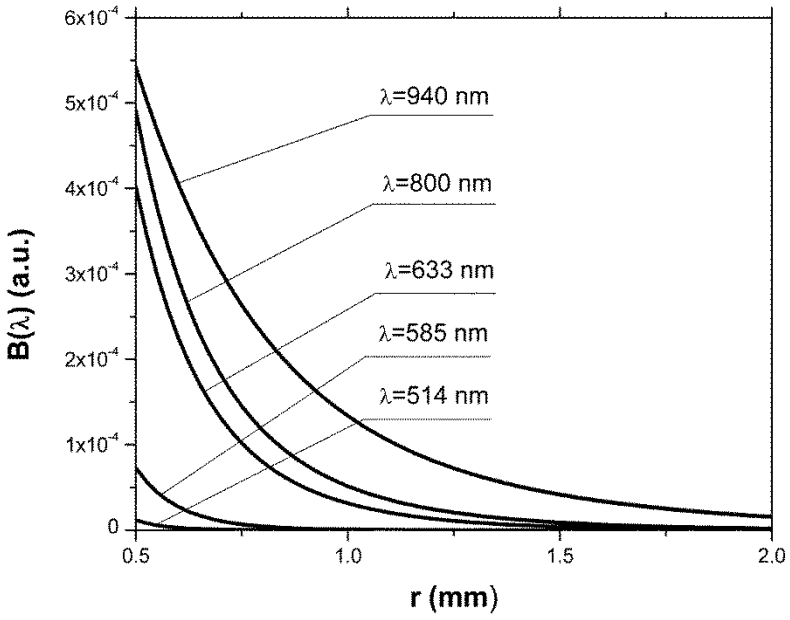

Figure 19 - The dependence of B(λ) on the value of the source–detector spacing r = 0.5 to 2.0 mm for the tissue blood volume V_b = 10%.

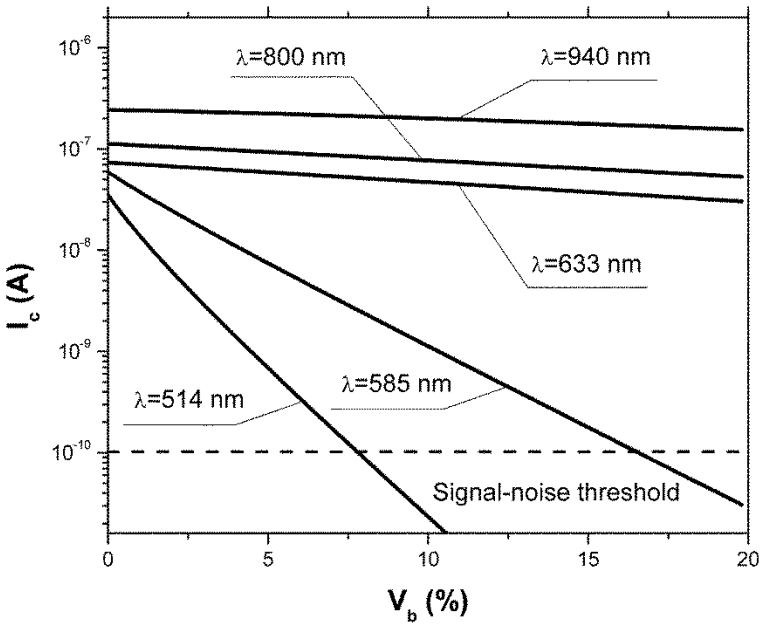

Figure 20 - The dependence of the photocurrent I_c upon the level of the tissue blood volume V_b.

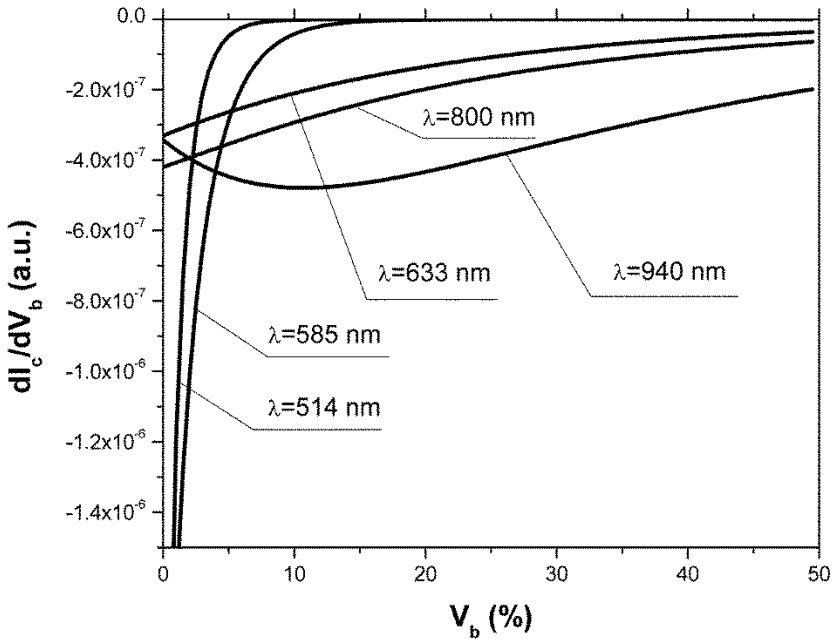

Figure 21 – The dependence of the derivative of photocurrent I_c with respect to blood volume upon the level of the tissue blood volume V_b.

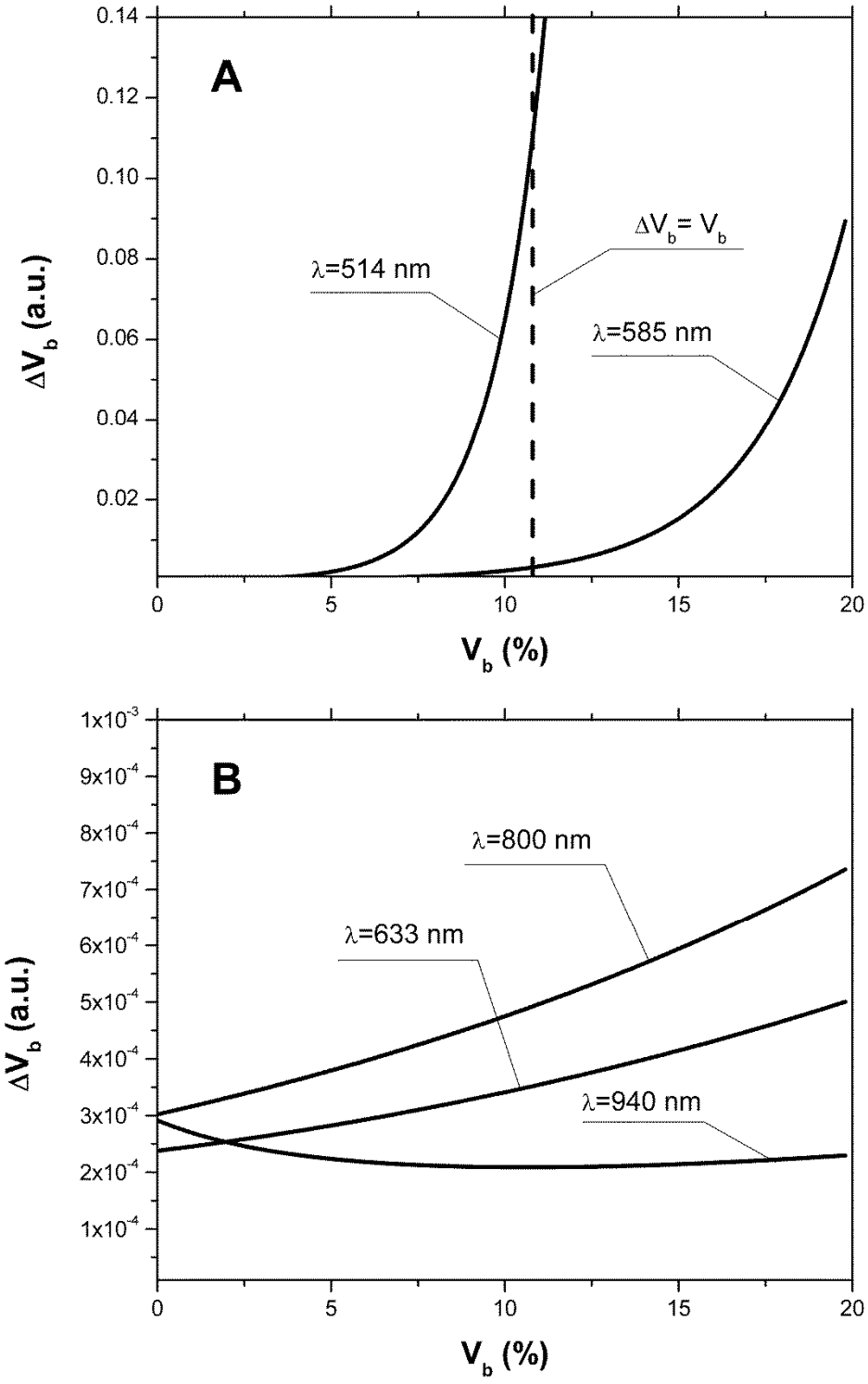

Figure 22 – The dependence of the change of the blood/tissue ratio ΔV_b, which corresponds to the change of the photocurrent in 0.1 nA, on the tissue blood volume V_b: for λ = 514 and 585 nm (a) and for λ = 633, 800, and 940 nm (b).

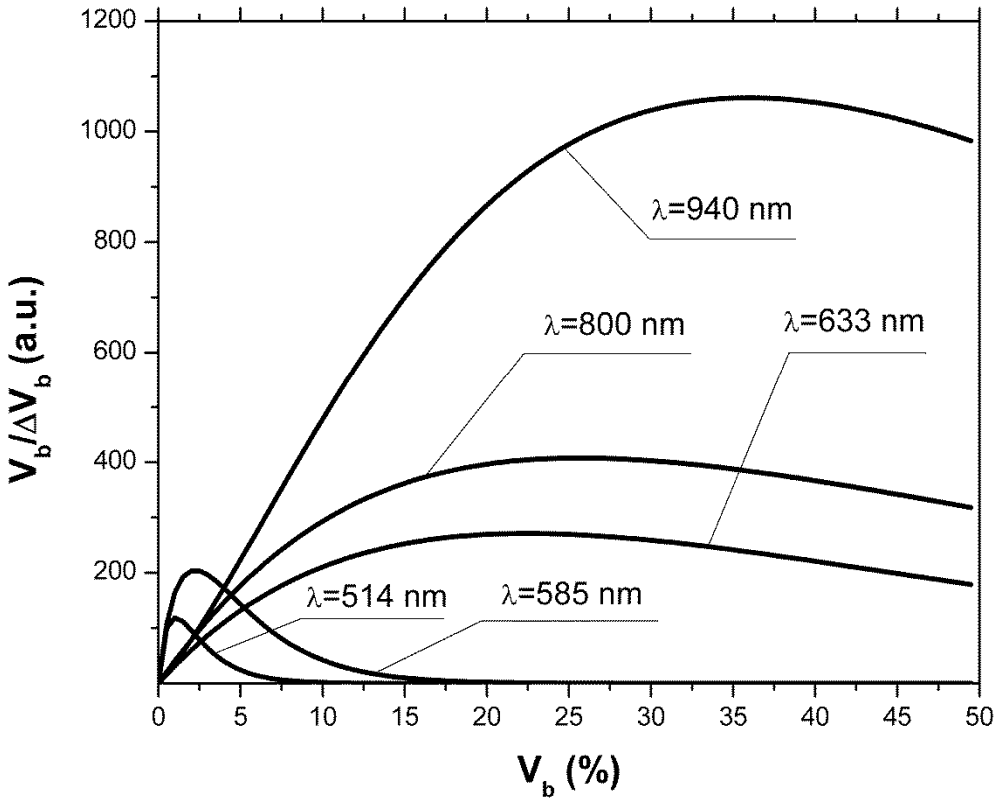

Figure 23 – The dependence of the signal-to-noise ratio of the signal on the level of the tissue blood volume V_b.

Table 2 - Optical properties of blood and bloodless tissue (adapted from (Jacques, Skin Optics, 1998) μ_{sb} *– blood scattering coefficient;* μ_{ab} *– blood absorption coefficient;* g – anisotropy factor; μ_{st} *– tissue scattering coefficient;* μ_{at} *– tissue absorption coefficient*

λ, nm	Blood			Tissue		
	μ_{sb}, cm^{-1}	μ_{ab}, cm^{-1}	g	μ_{st}, cm^{-1}	μ_{at}, cm^{-1}	g
514	-	-	-	250	3	0.77
517	468	354	0.995	-	-	-
585	467	191	0.995	196	3	0.79
633	644.7	15.5	0.982	187.5	2.7	0.80
800	-	-	-	175	2.3	0.85
810	690	6.5	0.989	-	-	-
940	458.58	6.79	0.990	105.57	0.24	0.91

Thus, as shown in Figure 17, the signal attenuation is 4-5 orders of magnitude. Probe power in this type of device generally ranges up to 10 mW (Rogatkin & Lapaeva, 2003), with 3-4 mW being used in the LAKK-M system. At a probe power of 3 mW, and sensor sensitivity of 0.5 A/W (e.g. silicon photodiode literature values are 0.72 A/W (Haus, 2010) and 0.3-0.7 A/W (HAMAMATSU, 2013)), the registered photocurrents will be in the order of several μA.

The dependence of the photocurrent I_c and its derivative with respect to the blood volume of tissue dI_c/dV_b (the differential sensitivity) relative to the level of the blood volume V_b are shown on Figure 20 and Figure 21 respectively. To account for signal noise and instrument errors a signal ambiguity threshold was set to respect the medical and technical requirements for non-invasive spectrophotometric diagnostic devices. A magnitude of 0.1 nA was selected for this threshold, as dark photocurrent is in the range 1 pA (HAMAMATSU, 2013) to 10 nA (Cvijetic, 2004). The minimum registered change in blood volume ΔV_b must be greater than or equal to the volume corresponding to the selected threshold photodetector current change. Figure 22 shows the change in blood volume ΔV_b corresponding to the change of the photocurrent by 0.1 nA against the tissue blood volume V_b.

The ratio $V_b/\Delta V_b$ (Figure 23) can be interpreted as the signal-to-noise ratio (SNR) during blood volume registration by the NMS devices. Hence the relation in Figure 23 is the dependence of SNR upon the level of blood volume at a given wavelength. Figure 23 also shows that in the case of 633 nm and 800 nm (red and infrared) light, the maximum SNR for NMS devices is in the higher tissue blood volume range near 15-20%, and for the 940 nm wavelength this maximum corresponds to 25-30% tissue blood volume.

2.8 Results and interpretation for NMS device capabilities

Theoretical data gained in this work shows that the use of NMS devices for functional diagnostics has specialised medical and technical requirements. The development of a common basis for the engineering design of such systems is necessary. With NMS it is also necessary to create a complete system of metrological support, as for instruments and measurement techniques in general (Rogatkin, Dunaev, & Lapaeva, 2010). However, there are a number of specific features of the technology which add complexity in solving such problems. One of these features is a nonlinear dependence on the physical properties of the biological object (such as light transmission) from its physiological state (e.g. blood volume level) and the wavelength of the probe radiation. A second feature is a wide range of variation of the physiological parameters, e.g. blood volume, which strongly affects the absorption of the radiation in the tissue. All of these problems can be solved by deriving the appropriate relationships which will improve the accuracy of diagnostics of the corresponding methods.

As shown in Figure 17 to Figure 23, analysis of the dimensionless coding function graphs $B(\lambda)$ and the derivative characteristics based on this function (I_c, dI_c/dV_b, ΔV_b, $V_b/\Delta V_b$) highlights three spectral range dependent groups. These groups are related to the changes in optical absorption and scattering coefficients of blood and tissue (see **Table 2 - Optical properties of blood and bloodless tissue**). The first group, at 514 and 585 nm, is defined by the blood's similar and strong absorption curves for the green and yellow light. In the second group the absorption coefficient of blood decreases by an order of magnitude for red and IR wavelengths. In the third group at IR (940 nm) the absorption coefficient of blood remains

at a similar level, but the absorption coefficient of tissue decreases by an order of magnitude.

For example, Figure 17 to Figure 20 show that with linear variation of the blood volume, the light transmission through the tissue will vary nonlinearly, but the logarithm of photocurrent can make the characteristics of MTRs linear. Figure 18 demonstrates that increasing the wavelength of tissue irradiation in the range of 314-940 nm increases the dimensionless coding function *B(λ)* at any fixed tissue blood volume. It is evident that in the spectral range of 633-940 nm, *B(λ)* has an almost linear inverse relationship to tissue blood volume. However, between 514-633 nm, this function exhibits a significant nonlinear decrease with increased tissue blood volume. These dependences are probably due to absorption by blood at 500-585 nm being an order of magnitude higher than at 630-700 nm (Jacques, 2013), (Lister, Wright, & Chappell, 2012), (Roggan, Friebel, Dorschel, Hahn, & Muller, 1999). Figure 17 and Figure 18 demonstrate that optical properties of blood (primarily the absorption coefficient) in the observed spectral range, and consequently the tissue blood volume, have a major impact on *B(λ)*.

Figure 19 confirms the need to consider the parameter *r* using different wavelengths in the NMS devices depending on the tissue of study (absorption and scattering coefficients and the level of tissue blood volume).

It is apparent from the computed data (Figure 20) that the green (when $V_b \approx 8\%$) and yellow (when $V_b \approx 16\%$) irradiation power used in the present case must be increased in order to exceed the signal-noise threshold due to the stronger absorption of these wavelengths by biological tissue.

The analysis of data from Figure 21 and Figure 22 shows that at higher blood volume the discrimination of the changes in the blood volume by NMS devices is reduced and the relationship can be described by nonlinear function. In turn, the sensitivity of the NMS devices to the blood volume is also a non-linear function. Thus, in formulation of MTRs for NMS devices this nonlinearity must be considered. The differential sensitivity (dI_c/dV_b) depicted in Figure 22(a) clearly demonstrates that the detection of lower blood volumes in tissue (under 10%) should preferably be probed with green (514 nm), yellow (585 nm), red (633 nm) and infrared (800 nm) wavelengths. However, to detect tissue blood volumes of greater than 10-20% with a high differential resolution and sensitivity, a wavelength of 940 nm is preferred.

Figure 22 shows the minimum discernible ΔV_b signal and the consequent rapid reduction in signal-noise ratio with increase in blood volume for green and yellow light (Figure 22a). For example, the useful signal becomes indistinguishable against background noise ($\Delta V_b = V_b$) when $V_b \approx 11\%$ at a wavelength of 514 nm. The dependence of ΔV_b upon V_b is much less pronounced for the red and infrared spectra (Figure 22b) compared to the green and yellow light, although these relationships are also non-linear.

Data from Figure 23 justifies the use of different wavelengths for measuring different ranges of tissue blood volumes. Green and yellow light provide greater sensitivity for a low blood volume (up to 5%), while the infrared irradiation is more efficient in terms of sensitivity and SNR even at higher blood volumes. Delivering the necessary light power for each wavelength for a given blood volume is essential, particularly for measurement of the upper levels of blood volume by TRO. In addition, at levels above 5% of tissue blood volume the

blood perfusion and consequently S_tO_2 measurements become unreliable due to SNRs of less than 10 for the green wavelength. In general, the theoretical limit of the measurement scale for TRO is an average tissue blood volume level of 0-30% with the selected input data and geometry of the receiving radiation.

Similar reasoning can be extended to laser Doppler flowmetry (800-940 nm), which is the most sensitive technique for monitoring micro-vascular rhythms. According to the data presented, this approach is not near its limit of sensitivity and should have good resolution over a broad range of V_b. According to Figure 23 for examination of tissue with blood volume level around 10-15% with an acceptable SNR, a wavelength of 800 nm should be applied. In the case of 20-30% (for example, when measuring the internal organs with an endoscopic probe) of tissue blood volume however, the 940 nm wavelength is preferable. Moreover, our data (Figure 21) defines the lowest detection limits of the blood volume for each wavelength.

It should be noted that the function *B(λ)*, based on a homogeneous model, has a number of limitations. It does not account for a number of optical characteristics and properties of biological tissues, for example, the refractive index, as well as layer structures of skin and the so called vessel packaging effect (Fredriksson & Larsson, 2009). Moreover, it is reported that differing levels of melanin and water alter the optical properties of the tissue relevant to the *B(λ)* function (Meglinski & Matcher, 2003), (Petrov, Doronin, Whelan, Meglinski, & Yakovlev, 2012). These factors affect the NMS measurement result and must be taken into account in formulating the medical and technical requirements for devices of this type. It must be emphasized that the measurement accuracy (systematic error) of NMS is

significantly affected by the algorithms used for calculation of biomedical parameters (Rogatkin, Dunaev, & Lapaeva, 2010). Thus, the computational algorithms currently used for calculating S_tO_2 and V_b by TRO have a complex and multistep character; the scatter of the measured results is 2-3 times greater than the measurement errors of the initial physical signals (Rogatkin, Lapaeva, Bychenkov, Tereshchenko, & Shumskii, 2013).

It should also be underlined that in addition to the thermal noise in NMS systems there are other limitations (electrical noise, instability of the radiation source, etc.), which should also be taken into account and normalised in formulating MTRs.

2.9 Conclusions

The application of new non-invasive medical spectrophotometric techniques and instruments for the functional diagnosis and evaluation of therapeutic interventions requires the specification of the medical and technical requirements for the specific type of medical devices. Considering different levels of the tissue blood volume, the approach proposed here allows the calculation of important technical and metrological restrictions of the instruments, such as the sensitivity ranges and power related signal-to-noise ratios for different spectral channels and biomedical parameters. It is clear that the nonlinearity of the measurements carried out with NMS systems depend directly on the characteristics of the examined object. In general, the further successful development of NMS technology will be heavily dependent on the metrological support of these devices and their methods of use. This support will ultimately enable non-invasive spectrophotometric diagnostics to be raised from a research level technology to a standardised technology satisfying the requirements of clinicians and end-users.

2.10 LAKK-M MLNDS

The development of the LAKK-M multifunctional, laser-based non-invasive diagnostic system has followed, more or less, the methodology elaborated in this chapter. The device includes 4 narrow-band LED and semiconductor laser sources at the following wavelengths;

Function	**Wavelength**		
TRO		0.53µm	0.63µm
LFD	0.37 µm	0.53µm	0.63µm
LDF (NIR)			1.064µm

Table 3 – Laser used in LAKK-M by function

	Laser power (mW) and mode(CW/P)				Penetration Depth* (mm)
Channel / λ (nm)	**370**	**530**	**630**	**1064**	
TRO	n/a	~2 P	~2 P	n/a	~1-3
LFD	~3 CW	~4 CW	~4 CW	n/a	~1-3
LDF	n/a	n/a	n/a	~2mW CW	~2-4

*CW = continuous wave P = Average power in pulsed mode (*Figures will vary according to material)*

The system is intended for simultaneous investigation of the characteristics of certain biological activities in a single sampled *in-vivo* tissue volume. An assessment of the condition of the subject tissue with respect to the following important markers of biological vitality is provided.

- Vascular tone condition in arterial and vascular micro-circulation
- Oxygen transport, consumption and saturation in the micro-circulation

- Metabolic condition from spectroscopic analysis of relative concentration of compounds, proteins and enzymes involved in metabolic processes

An image of the device is shown in Figure 24 - The "LAKK-M" MLNDS device, below.

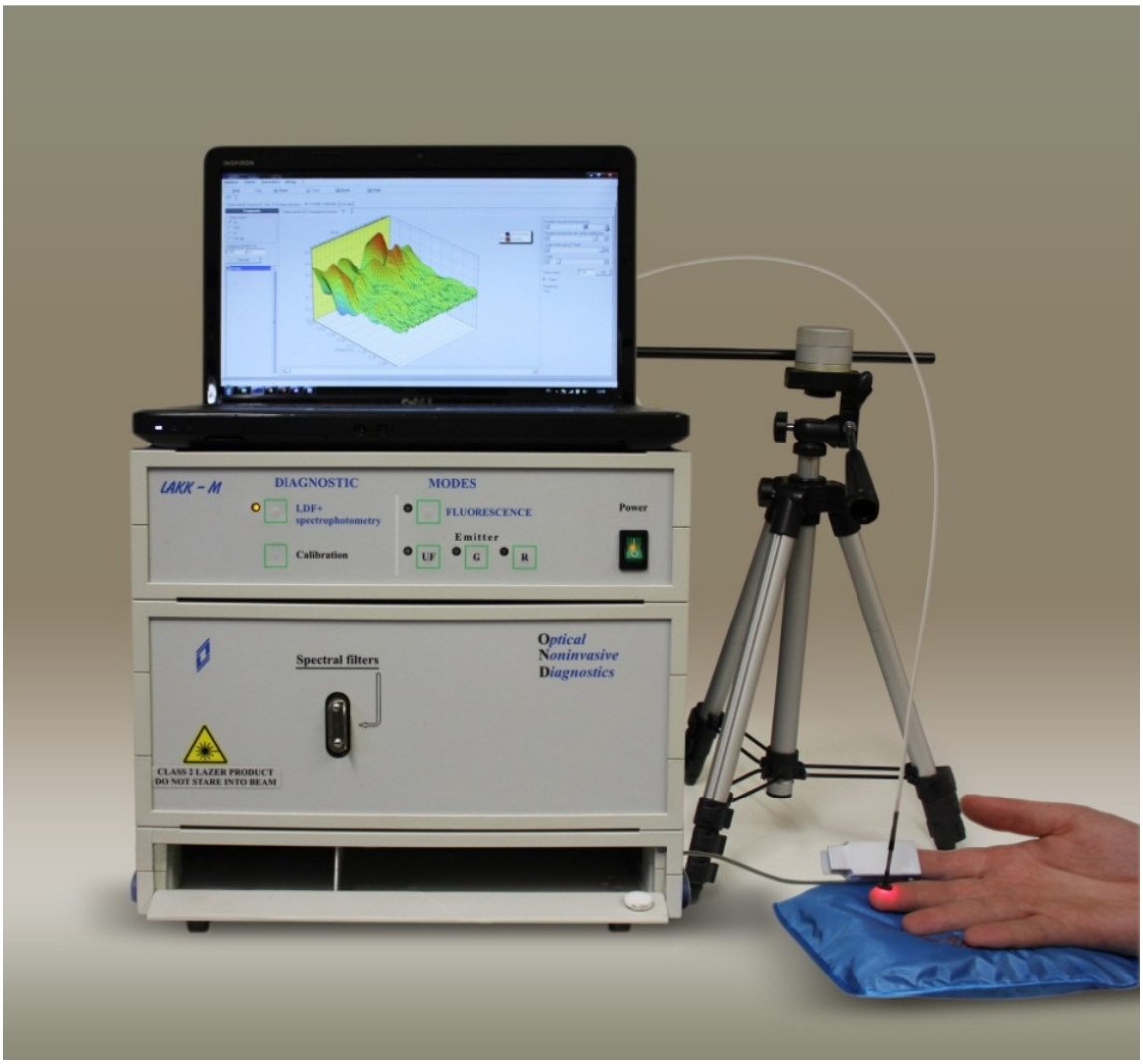

Figure 24 - The "LAKK-M" MLNDS device

The device apparatus includes a fibre-optic system to allow analysis at selected points on the body. An illustration of the laser, detector and spectrophotometer set-up at the fibre-optic tip is shown in Figure 25.

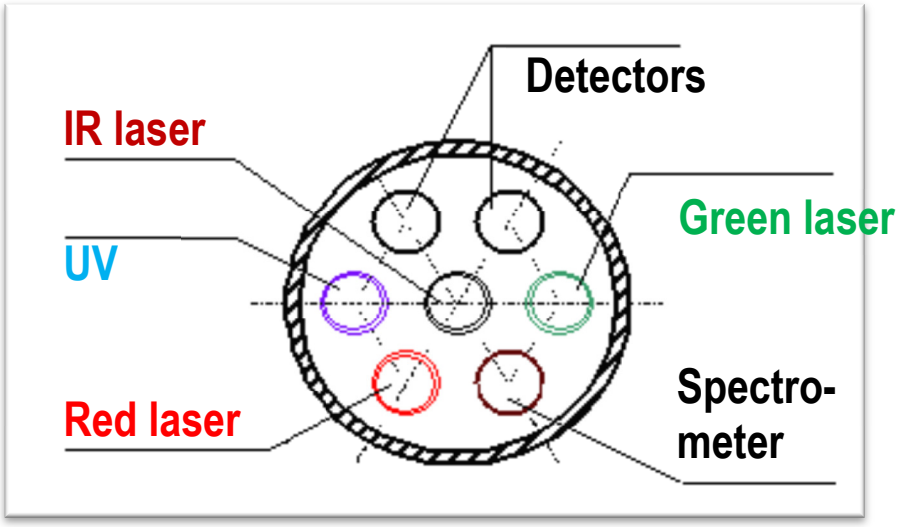

Figure 25 – Fibre-optic tip for flexible placement

Typical readouts from the software algorithms are shown in Figure 26 to Figure 29.

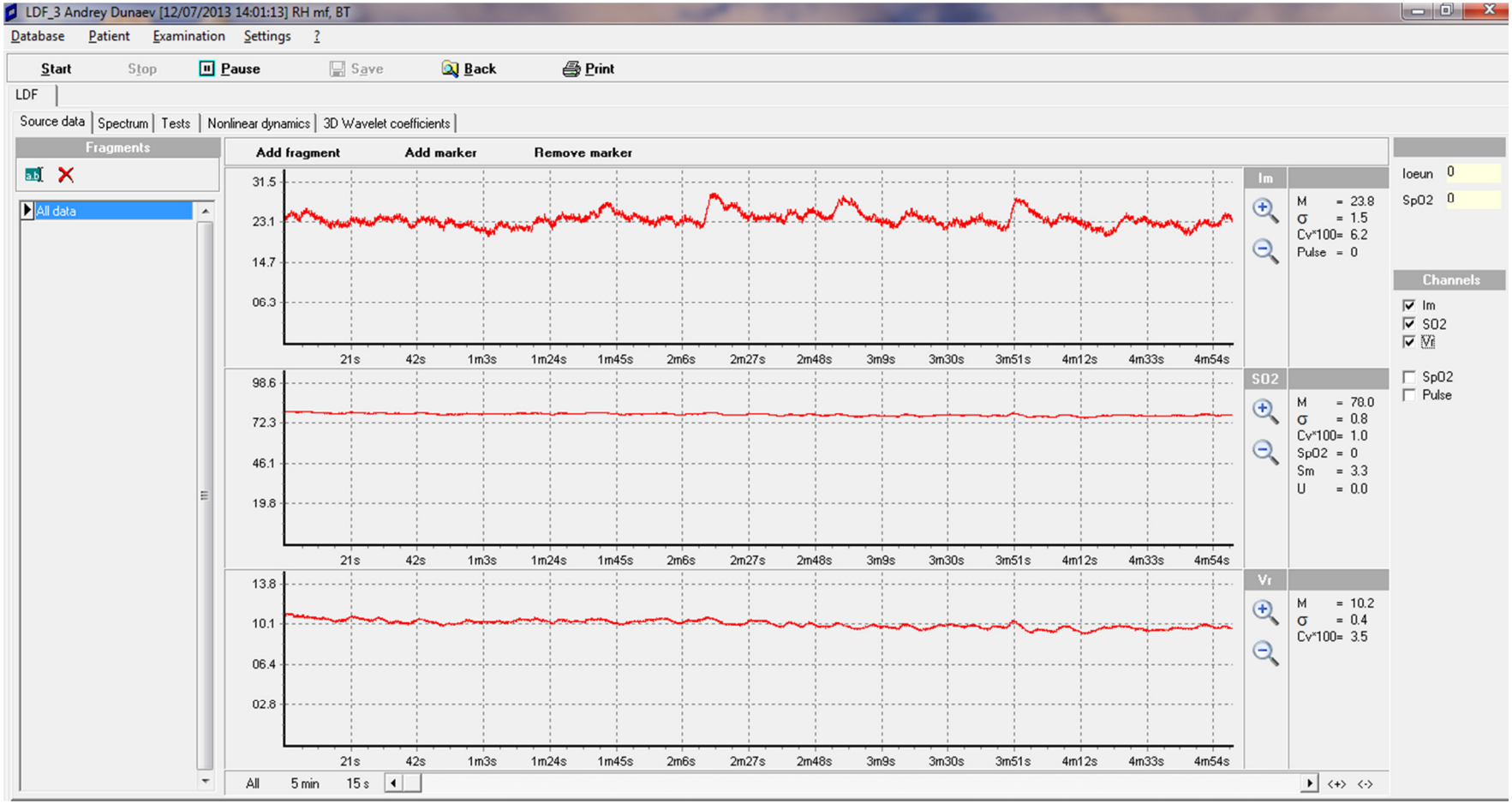

Figure 26 - Example of a typical recording of blood flow and oxygen saturation in skin micro-vessels (LDF- and TRO-channels)

The system is highly sensitive and responsive to real-time events such as breath holding or occlusion tests as can be seen in Figure 27.

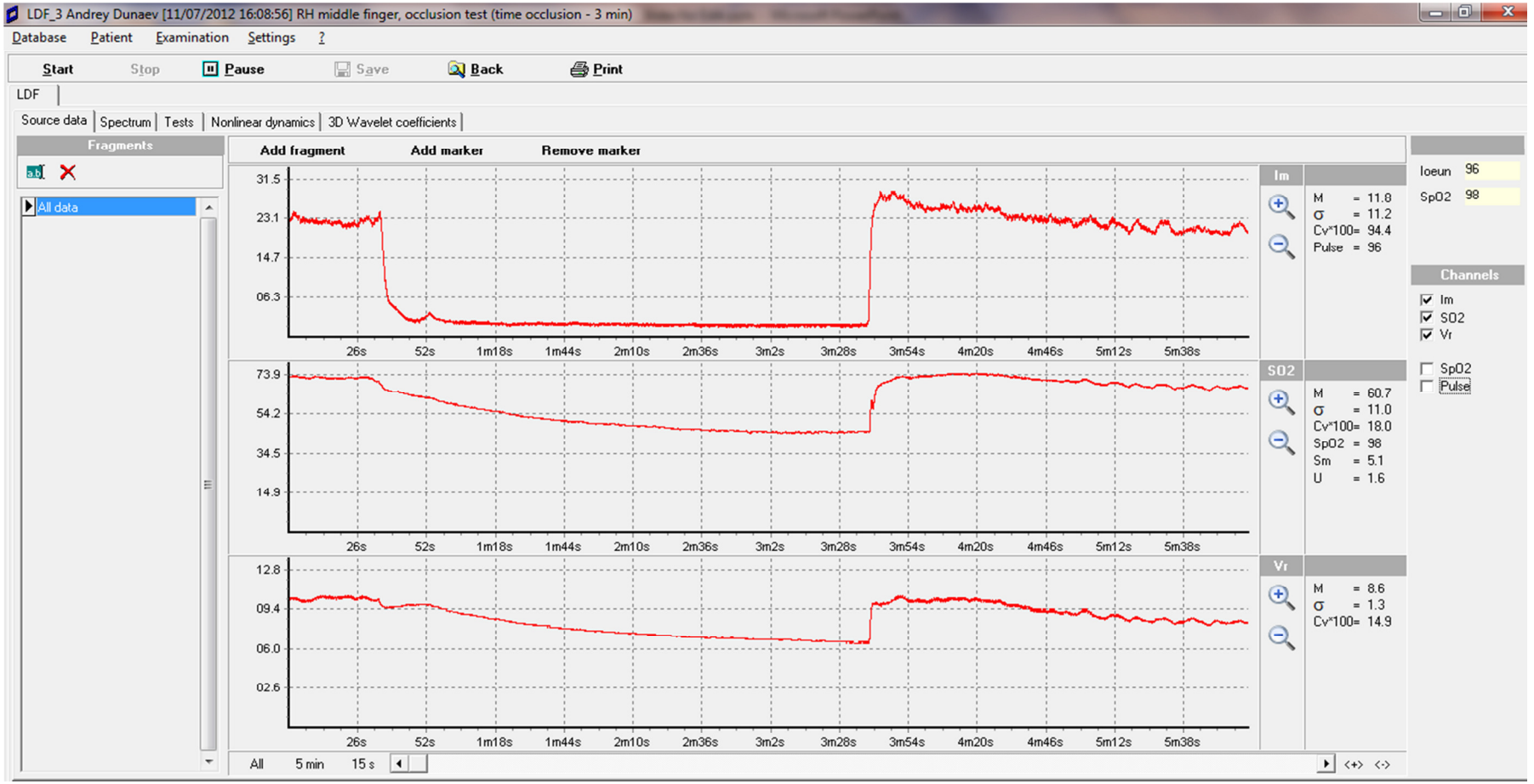

Figure 27 - Example of a typical LDF and TRO recording of occlusion test (time of occlusion 3 min).

Spectral wavelet analysis is fully integrated in the system software allowing oscillations to be calculated and visualised as in Figure 28. The wavelet analysis technique is fully explained in Chapter 3.

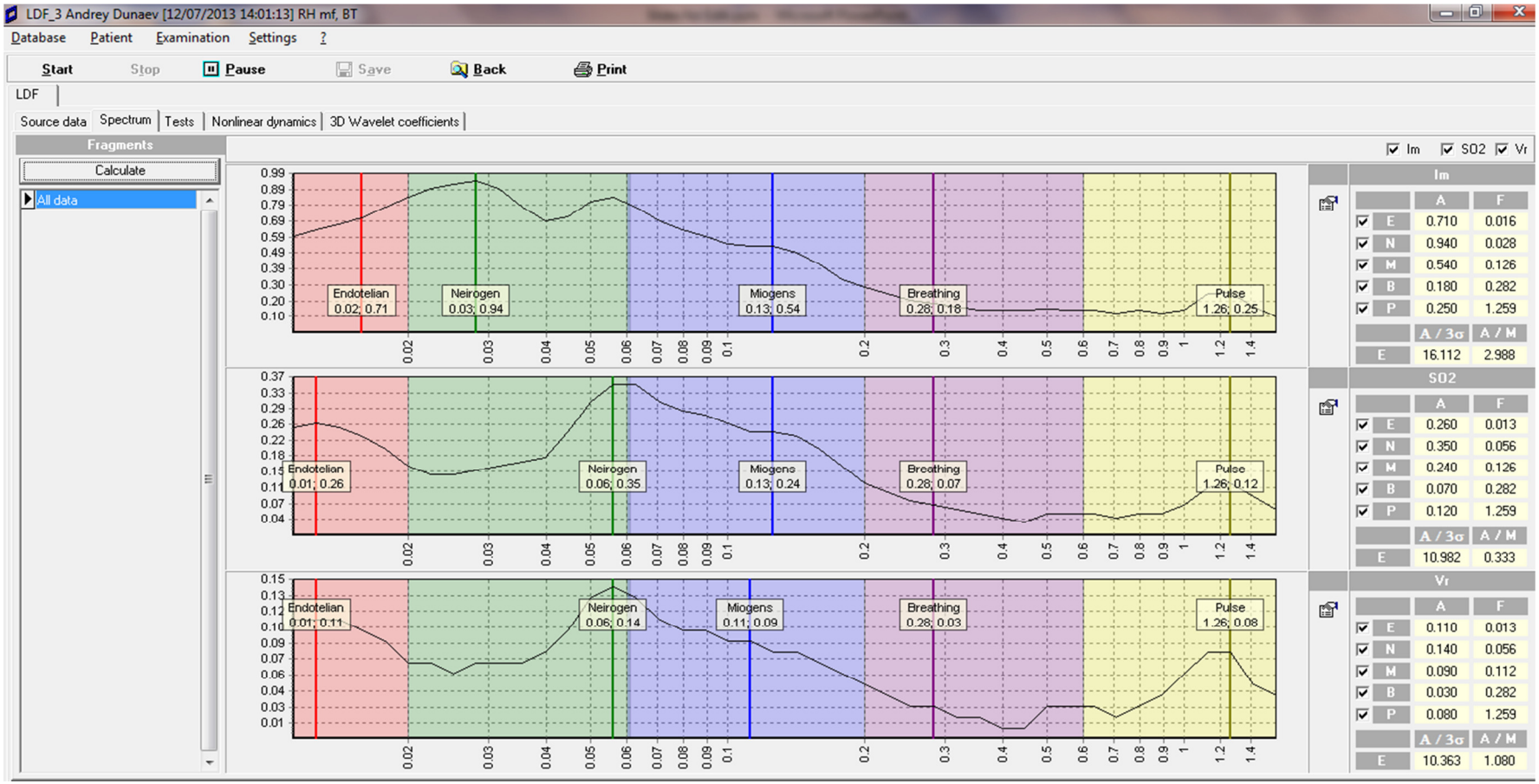

Figure 28 - wavelet-spectrum recorded oscillations

An example of the fluorescence spectrum produced is shown in Figure 29, note the fluorescence peaks for the molecules of interest are shown on the chart and in the selection menu.

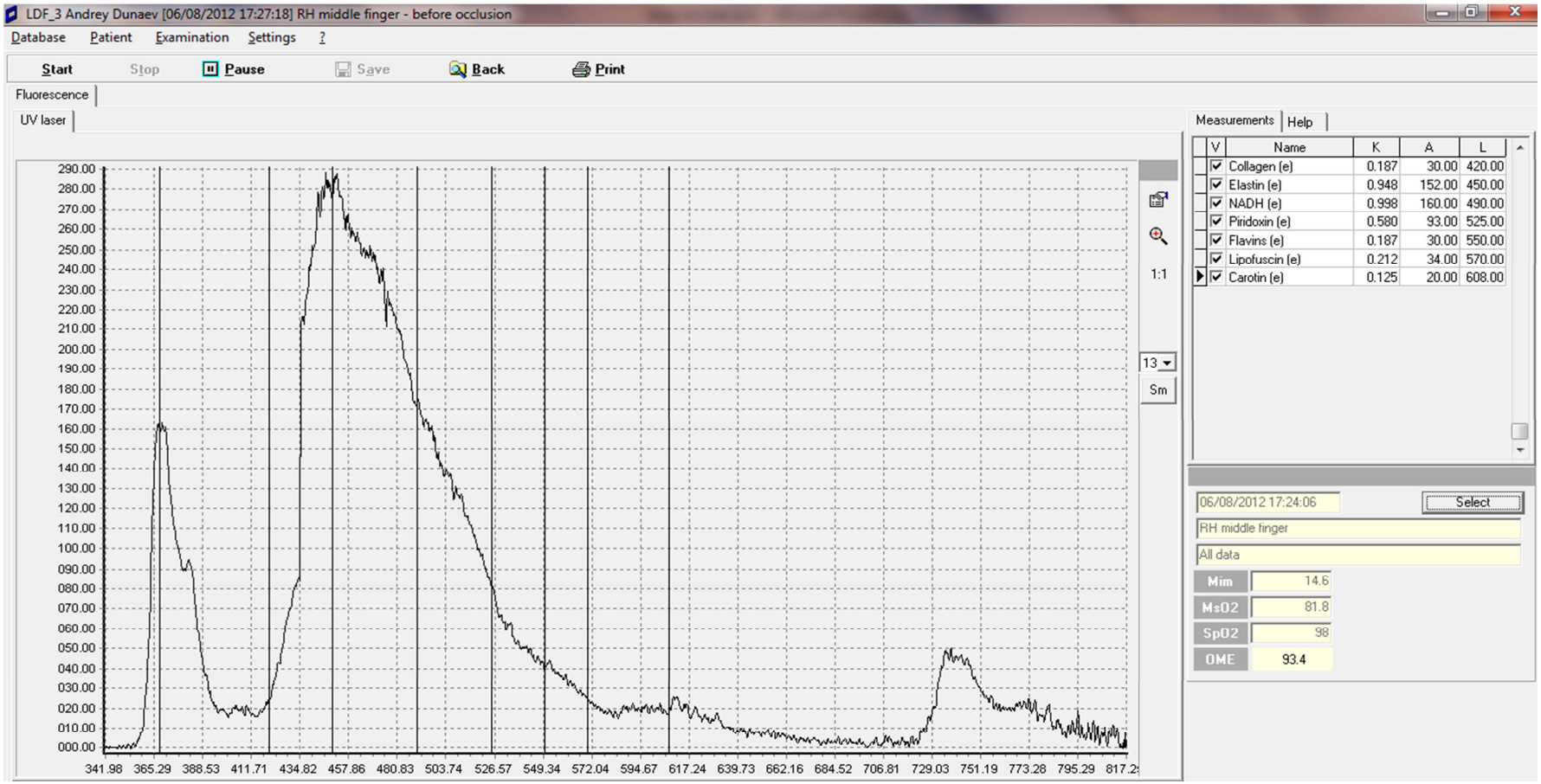

Figure 29 - Representative fluorescence spectrum with UV excitation wavelength

2.11 Summary of Chapter 2

Devising a general engineering theory of multifunctional diagnostic systems for non-invasive medical spectrophotometry is an important and promising problem in modern biomedical engineering. This work studied and aimed to formalise in scientific engineering terms the detailed objectives for the realisation of multifunctional laser non-invasive diagnostic systems (MLNDS). The Structure-Functional Model presented as well as the unified function of a generalised MLNDS has been formulated and developed. The key role of the system software for MLNDS general architecture at steps of ideological-technical designing has been shown and the basic principles of and opportunities for modular design in the area of MLNDS hardware are suggested. We then went on to develop a scientific framework for the formulation of the medical and technical requirements for non-invasive spectroscopic diagnostics based on known empirical data and values from the literate as a step towards the substantiation of the techniques capabilities and ultimately standardisation.

Chapter 3 – MULTI-PARAMETRIC ANALYSIS IN TISSUE METABOLISM, BLOOD CIRCULATION AND PERFUSION BASED DIAGNOSTICS

3.1 Multi-parametric analysis and complex diagnostic parameters

Multi-functional non-invasive laser-based diagnostic systems, single devices integrating various optical diagnostics techniques, represent a promising and progressing area in biomedical spectrophotometry. (Rogatkin, Sokolovski, Fedorova, Stewart, Sidorov, & Rafailov, 2011) These systems typically combine a number of approaches: laser fluorescence diagnostics (LFD), absorption spectroscopy (tissue reflectance oximetry – TRO), laser Doppler flowmetry (LDF) and pulse oximetry. This allows medics and clinicians not only to receive the collective results of the biochemical and physiological parameters which would normally be collected by each individual technique but also, and more importantly, to perform multi-parameter patient examination to identify more subtle individual characteristics of blood flow and tissue metabolism based on the simultaneous use of different diagnostic techniques and comprehensive data analysis. This possibility is realized in the LAKK-M system which allows the following blood microcirculation parameters to be obtained: index of blood microcirculation (Im), tissue oxygen saturation (StO2), relative blood volume (Vb), arterial blood saturation (SaO2). Together with collection and analysis of fluorescence spectra of tissue endogenous biomarkers this device is a unique and comprehensive system for research and diagnostics in various fields of biomedicine (cardiovascular diseases, diabetes, cancer, cosmetic surgery, etc.).

However, numerous experiments have identified unacceptably high variations in LDF and TRO readings (up to 30% of standard deviation from the average value for each parameter)

(Makarov & Rogatkin, 2010). This presents a serious problem for the correct interpretation of data acquired by doctors and seriously limits the prospects for use of this approach in general medical practice. This work aims to overcome this high level of parameter variation and via the use of complex relative parameters reduce the variation and ease integrated analysis and clinical interpretation of blood flow , tissue oxygen utilization and biomarkers fluorescence. Furthermore, improved interpretation at a quantitative level of flow velocity based on LDF is targeted by correlation with representative cardiovascular flow phantoms. It is important that this approach can be used for all four LAKK-M channels resulting in increased and readily interpretable information content. The results of this experiment are presented in Chapter 4, section 4.3, page 128.

3.2 Measurement of Blood Flow Oscillations:

The difficulties in standardising measurement of cutaneous blood micro-dynamics caused by high variability are well known (Stewart, Dunaev, Sokoliovski, Sidorov, & Rafailov, 2012). Furthermore, it is reported that in vivo LDF and TRO measurements have high variability, at least in the range of ± 30% in terms of σ (standard deviation, SD) of the average measured values for each parameter (I_m, S_tO_2, V_b) (Makarov & Rogatkin, 2010). Moreover, these results were obtained during long-term studies in two apparently healthy volunteers to estimate the individual momentary variability in the oscillation of the oxygenation in peripheral tissue and blood microcirculationover a long period of observation. It should be emphasised that this work did not set out to evaluate the variability of the oscillations in a statistically defined group (age, sex, pathology, etc.). The aim was to assess long-term

individual variability of the oscillations in a subject (a healthy volunteer) over one month, as such data does not exist in the literature. Therefore, we hypothesise that multi-parametric analysis, using multiple integrated optical techniques within a single diagnostic device, can demonstrate a closer correlation with peripheral haemodynamics and oxygen utilisation in tissues.

It has been reported that the use of spectral signal processing algorithms (LDF-graphs) for decoding and analysis provides information about the condition of vascular tone in terms of its contribution to the different mechanisms of micro-hemodynamic regulation (myogenic, neurogenic, etc.) (Krupatkin & Sidorov, 2005) 1. The results of LDF measurements, index of blood microcirculation (I_m) or perfusion, assessed in conventional perfusion units (PU), has shown a complex, non-periodic process which must contain information on the modulation of blood flow.

These period processes occurring in the vasculature are termed vasomotion, the spontaneous oscillation in tone of blood vessels, independent of heart beat or respiration. While vasomotion was first observed by Jones in 1852, the complete mechanisms responsible for its generation and its physiological importance remain to be elucidated, however several hypotheses have been put forth (Aalkjaer & Nilsson, 2005) (Linke, Bartoo, & Pollack, 1993).

The TRO method can be used to determines relative microcirculation blood volume (V_b) in the surface layers of the soft tissues (skin, mucous membranes of the organs) and tissue oxygen saturation (S_tO_2) of the microvasculature in the inspected area of biological tissue. There are isolated cases of spectral processing algorithms recorded signals (S_tO_2- and V_b-

graphs), being used to assess vasomotion, and myogenic rhythms, for example (Thorn, Kyte, Slaff, & Shore, 2011). A wavelet is a mathematical function used to divide a given function or continuous-time signal into different scale components. We can assign a frequency range to each scale component, which can then be analysed with a resolution that matches its scale. A wavelet transform is then used to represent blood oxygen saturation and flow as a function by wavelets. The wavelets are scaled and translated copies of a finite-length or fast-decaying oscillating waveform. Wavelet transforms have advantages over traditional Fourier transforms for representing functions that have discontinuities and sharp peaks, and for accurately deconstructing and reconstructing finite, non-periodic and/or non-stationary signals such as those derived in multifunctional laser diagnostics. I propose here that analysis of oscillation signals recorded by TRO according to the frequency ranges, similar to LDF-graphs, may be of practical interest in studying the parameters of microcirculation of blood.

3.3 Classification of blood flow oscillations and variability

Five rhythmic components (oscillations) are considered which can be isolated from LDF recordings using wavelet analysis which are termed in accordance with the modern interpretation of their genesis (Salerud, Tenland, Nilsson, & Oberg, Rhythmical variations in human-skin blood-flow, 1983), (Bracic & Stefanovska, 1998), (Stefanovska, Bracic, & Kvernmo, 1999), (Kvandal, Landsverk, Bernjak, Stefanovska, Kvernmo, & Kirkeboen, 2006):

Table 4 Biological rhythms

Rhythm	Frequency interval (Hz)	Cycles per minute	Source
Endothelial	0.0095-0.02	0.57-1.2	Endothelial cell vaso-constriction/dilation
Neurogenic	0.02-0.06	1.2-3.6	Central nervous system
Myogenic	0.06-0.16	3.6-9.6	Myocyte cell contraction
Breathing	0.16-0.4	9.6-24	In/Exhalation
Pulse	0.4-1.6	24-96	Heartbeat

Possible physiological processes causing fluctuations in blood micro-flow in the frequency range of endothelial rhythms still are currently under discussion. The endothelium is normally considered to follow only diurnal regulation. However, it has been proposed that endothelial rhythms in at frequency of around 1 cycle per minute may be explained by the rhythmic release of the vasodilator nitric oxide into the endothelium (Kvandal, Landsverk, Bernjak, Stefanovska, Kvernmo, & Kirkeboen, 2006)(Stefanovska, Bracic, & Kvernmo, 1999). Although included in the wavelet analysis range confirmation that this frequency is associated with endothelial function is the subject of further research beyond the scope of work here.

It is believed that fluctuations in neurogenic rhythms (at about 0.04 Hz) are relevant to vasomotion of arterioles. An increase in the amplitude of the oscillations may be an indicator of lower neurogenic resistance and possibly increase in blood flow in the arterioles, venular shunt with an increase in myogenic tone (Krupatkin & Sidorov, 2005). It is believed that the source of myogenic oscillations (at approximately 0.1 Hz) is the spontaneous activity of smooth muscle cells (myocytes) in resistance vessels and pre-capillary sphincters, also termed vasomotion and associated the with regulation of blood pressure. Periodic oscillations with a frequency of about 0.3 Hz are synchronised with breathing, respiratory function is often poorly represented in the LDF-signal. Periodic

oscillations with a frequency of about 1 Hz in the skin are synchronised with the heart rate and represent the variations that reflect changes in the diameter of blood vessels induced by the pulsation of the flow due to cardiac cycle.

It is known that the amplitude of the oscillations in these ranges varies considerably for individuals probably due to the high lability (relatively unstable transient nature) of blood flow in the capillaries and other vessels of the microvasculature which are a prerequisite for tissue homeostasis. Deviation of the oscillation amplitude at a fixed test area for a homogeneous group of subjects can be up to 15% (Krasnikov, Matrusov, Piskunova, Sidorov, & Chemeris, 2000), It is also reported that the large number of participants necessary to obtain statistically significant values is a barrier to realising the diagnostic potential of the method, confining it, for the time being, to research use (Tikhonova, Tankanag, & Chemeris, 2013) . Nevertheless, data on the physiological variation in one individual assessed over a period of time was absent in the literature.

3.4 Research Methodology

In this study we used the MLNDS "LAKK-M" (SPE "LAZMA", Russia), which besides of LDF and TRO has pulse oximetry and LFD channels (Fig. 1). This system allows simultaneous recording of the I_m, S_tO_2, V_b parameters in a tissue volume (Rogatkin, Sokolovski, Fedorova, Stewart, Sidorov, & Rafailov, 2011). The study was conducted on an adult male, age 35, with no cardiovascular disease history. The measurements were performed on the skin pad (palmar surface) of the right middle finger. This area was selected because it is rich in arteriolar-venular anastomoses (AVA) and the variability of the LDF signal is less than in tissue with fewer shunts (Salerud, Tenland, Nilsson, & Oberg, 1983). Consequently, it is ideal

for this research aimed at evaluating the proportion of nutritive blood flow from the known formula (see page 22 Laser Doppler Flowmetry and Tissue Reflectance Oximetry, and hence the parameters such as myogenic, neurogenic and endothelial-dependent component tone (Krupatkin & Sidorov, 2005).

All measurements were performed daily during the month at the same time (around 11:00 am) to avoid any influence from circadian rhythms influence on the blood circulation. Measurements duration was 3 minutes over a total of 22 measurements (days). An example of screenshot of the registered parameters is presented in Figure 30 - Screenshot of the LDF and TRO graphs. At the end of the observation time the oscillation rhythms of each measurement were analysed using the built-in wavelet analysis module (Figure 31 - Screenshot of the wavelet analysis). The wavelet analysis determined the maximum amplitude of δI_m, δS_tO_2, δV_b and the corresponding frequency for each of the 5 oscillation types for each of the 3 parameters of I_m, S_tO_2 and V_b.

In addition to variability, the data were assessed for parameters such as: bypass index (BI), index of tissue oxygen use (taking into account nutritional blood flow) (I), index of perfusion oxygen saturation in microvascular blood (S_m) and the index of oxygen consumption rate in tissue (U1 and U2), calculated according to (Stewart, Dunaev, Sokoliovski, Sidorov, & Rafailov, 2012) and (Krupatkin, Rogatkin, & Sidorov, 2007) respectively.

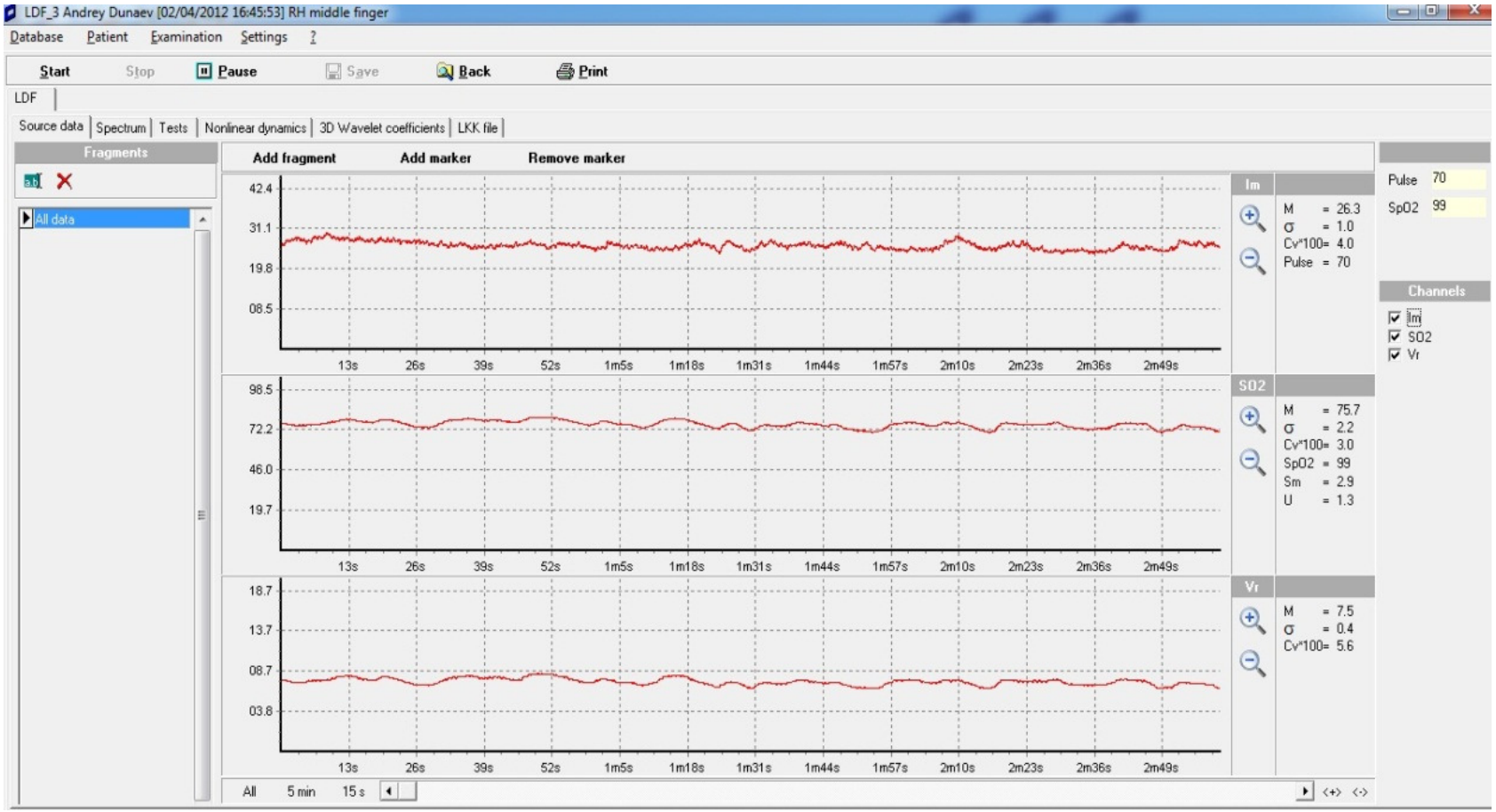

Figure 30 - Screenshot of the LDF and TRO graphs

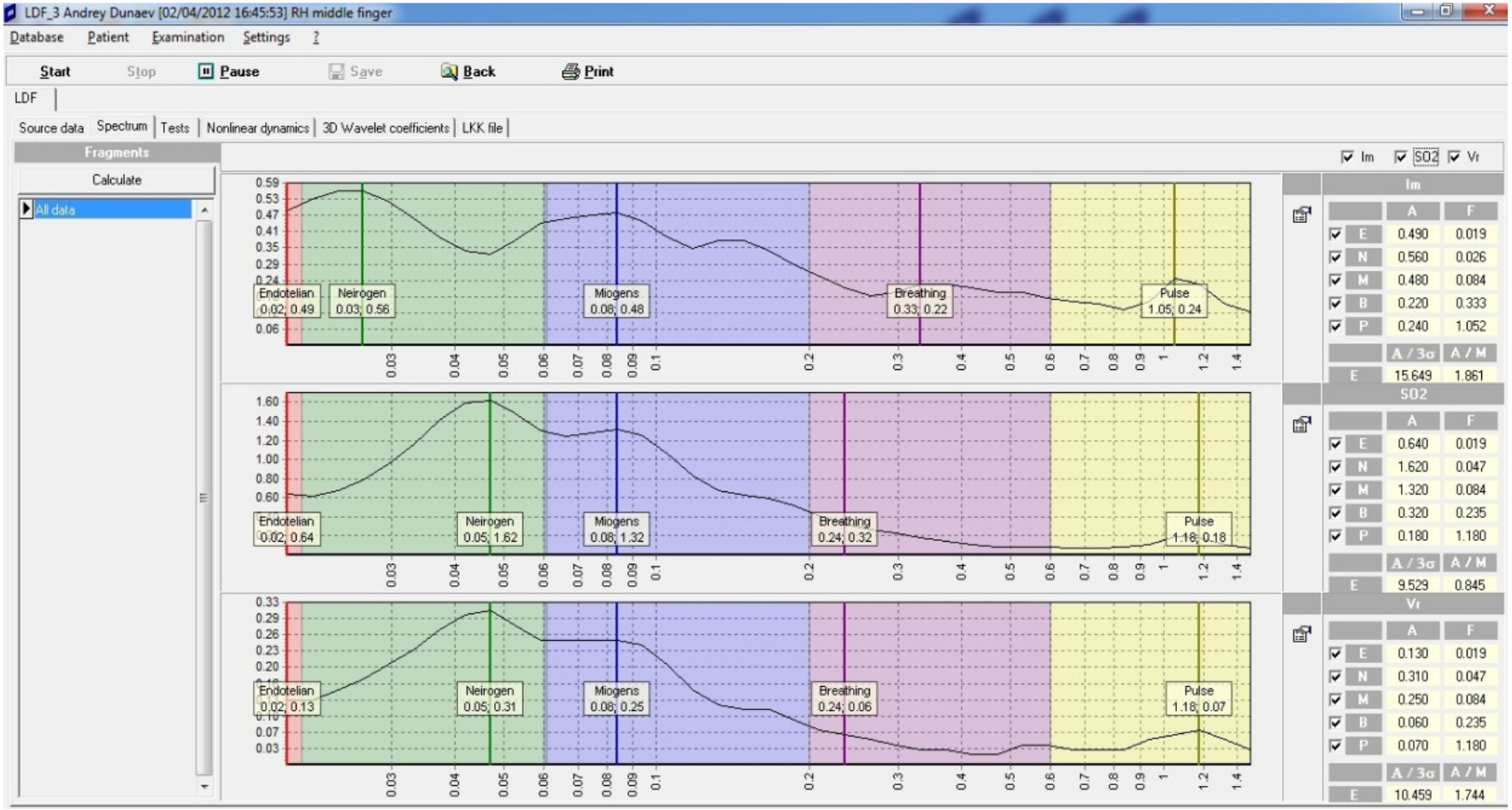

Figure 31 - Screenshot of the wavelet analysis

3.5 Results and discussion

These results are presented below in Table 5 - Statistical evaluation of the measured LDF and TRO parameters and Figure 32 to Figure 37 .

Table 5 shows the statistical evaluation (*M*, is mean value, *SD is* standard deviation, k_v is a coefficient of variation) of the measured LDF and TRO methods for parameters of I_m, S_tO_2, V_b and calculated on the basis of their indicators. Figure 32 shows a diagram of changes in the parameters of I_m, S_tO_2 and V_b for a month in one subject.

Table 5 - Statistical evaluation of the measured LDF and TRO parameters

№	Statistic parameters	Measured parameters			Calculated parameters								
		I_m, PU	S_tO_2, %	V_b, %	*NT*	*MT*	*ET*	*BI*	*NB*, PU	*I*	S_m	U_1	U_2
1	*M*	25.6	62.5	8.7	1.76	2.06	2.00	1.23	11.90	19.36	2.5	1.6	3.9
2	*SD*	3.5	10.2	1.4	0.49	0.54	0.54	0.40	3.10	6.01	0.5	0.3	1.5
3	k_v, %	13.5	16.4	16.3	27.59	26.47	27.17	32.57	25.80	31.02	20.5	16.8	37.7

Analysis of the data shows the greatest variability in the parameters obtained by the TRO (16%), whereas the variability of the microcirculation index (I_m) in our study turned out not more than 14%, less than 50% of the variation in previously reported data (Makarov & Rogatkin, 2010), which was obtained over only 10 days. This may be due to the specific devices used by these authors with different diagnostic volumes and/or differences in the design of the optical probes. Our work was conducted as a longer-term study specifically in order to contrast with the published shorter-term study data previously used to report variation.

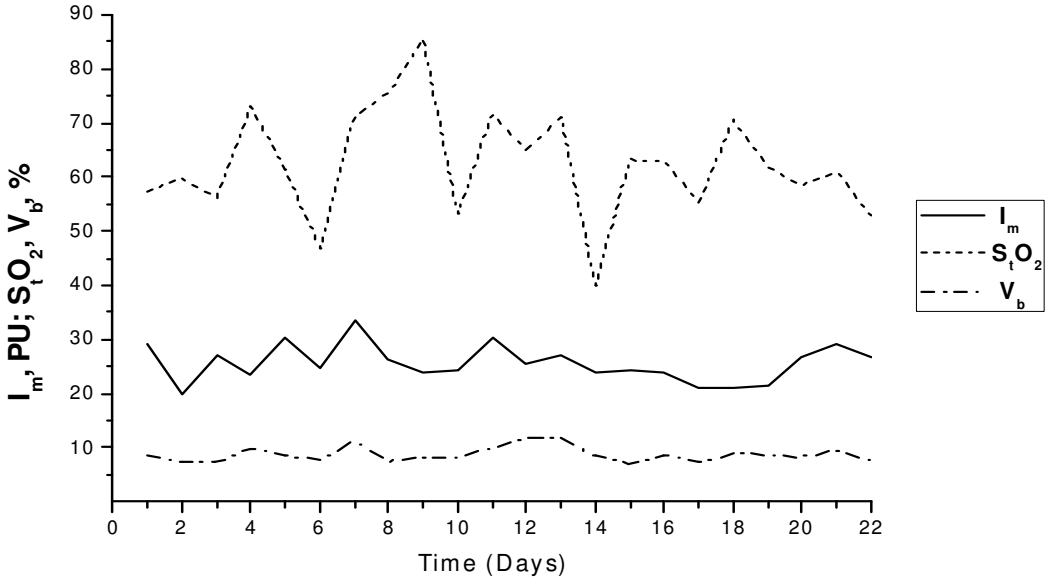

Figure 32 - Representative Im, StO2 and Vb monitored during a month

The calculated values of MT, NT, ET and BI demonstrate a high variability (up to30%) due to the reliance of their calculations, as it will be shown below, of the oscillation amplitudes with high variability. The nutritional blood flow (NB) component was 11.9±3.1 PU, which is about half the mean value of the index of blood microcirculation 25.6±3.5 PU. The Sm index has a variability of about 20%, while the index of oxygen rate of use in tissue (U2) has a variability factor twice that of the alternative (U1), since its calculation is based on two parameters at once with variability of 16%. In aiming to reduce the influence of these variations in the measured parameters it is clearly preferable to use the integrated index calculation U1.

Figure 33, Figure 34 and Figure 35 show the oscillations changes over the course of the month for the LDF-, StO2- and Vb-graphs respectively. Figure 36 shows corresponding histogram of the distributions of mean value and SD for these oscillations.

Analysis of the data in general shows a high variability of the investigated oscillations in all 3 graphs. The smallest variation is the Vb in endothelial (30%), neurogenic (35%) and myogenic components (40%). While pulse rhythms variability turned out about 33%, which is greater than 23% variability in blood perfusion rhythms. The most variable component, in all the 5 rhythms, was StO2-parameter (50%) while the greatest variation is observed in endothelial (44%) and myogenic rhythms (40%) LDF-graphs, in myogenic (54%) and breathing rhythms (55%) StO2-graphs and in myogenic (38%) and pulse rhythms (33%) Vb-graphs.

Rhythm	I_m variation (SD%)	S_tO_2 variation (SD%)	*V_b variation (SD%) in*
Endothelial	44	44	30
Neurogenic	35	50	35
Myogenic	40	54	40
Breathing	25	55	35
Pulse	20	45	33

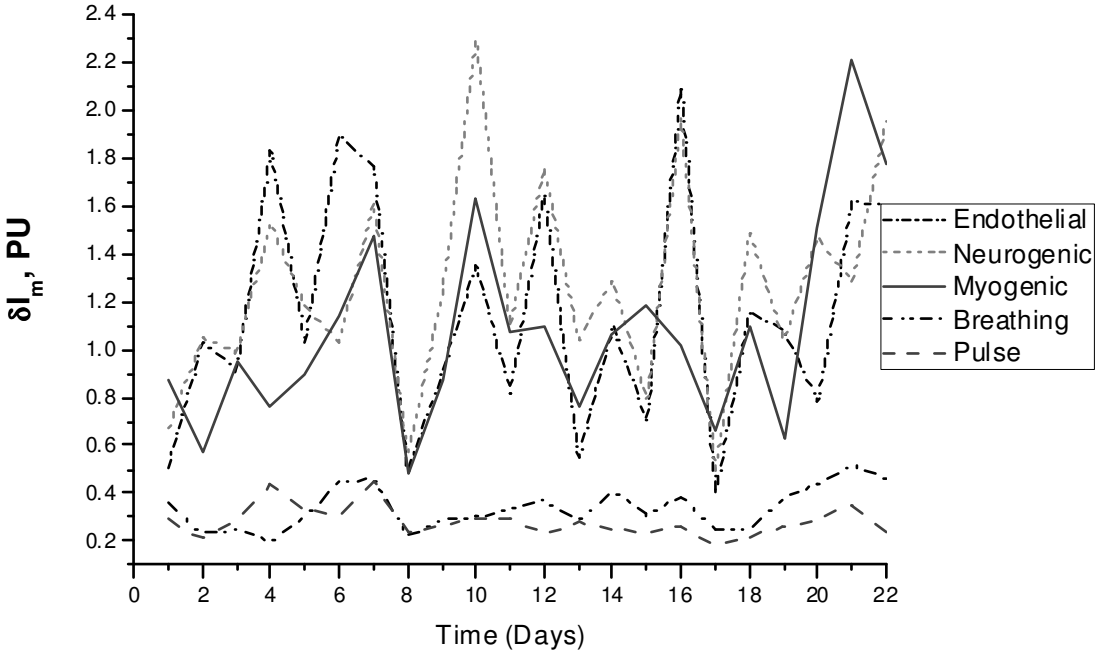

Figure 33 - Changes in blood perfusion

a)

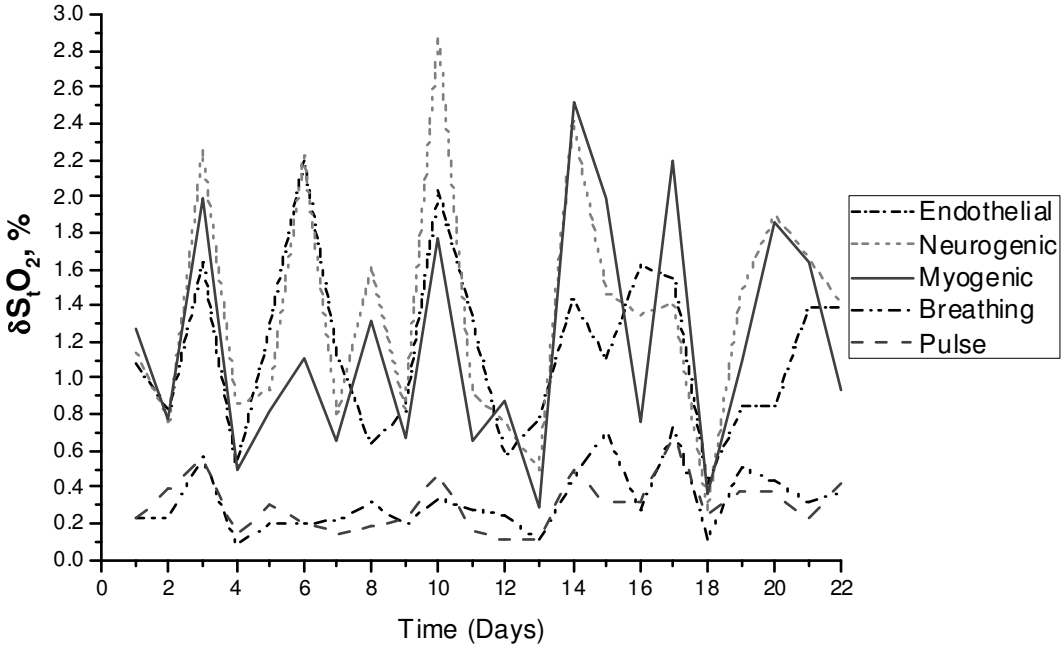

Figure 34 - Changes in Oxygen saturation

b)

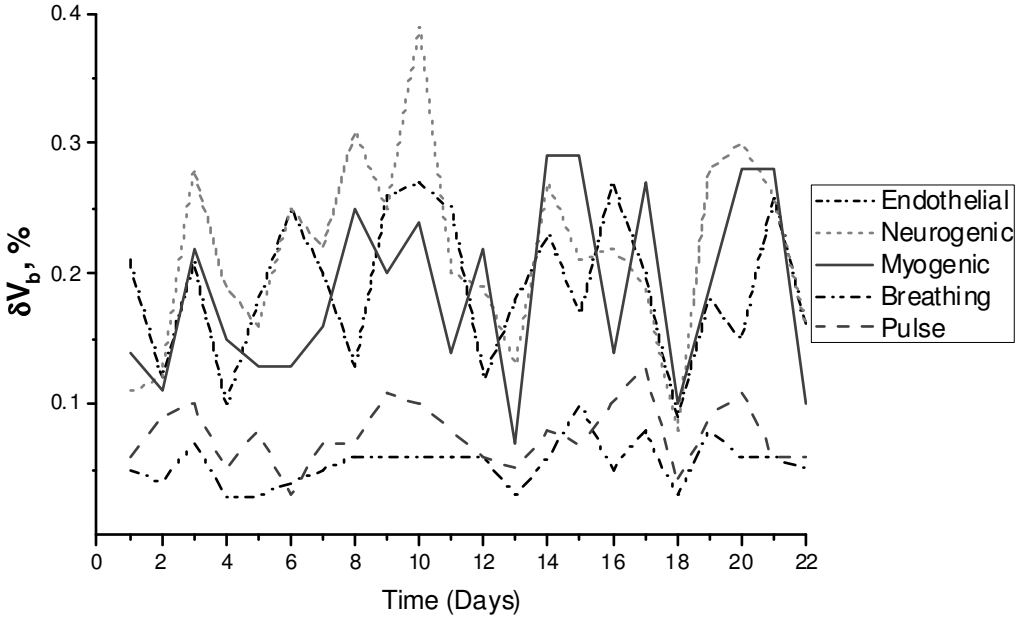

Figure 35 - Changes in blood volume

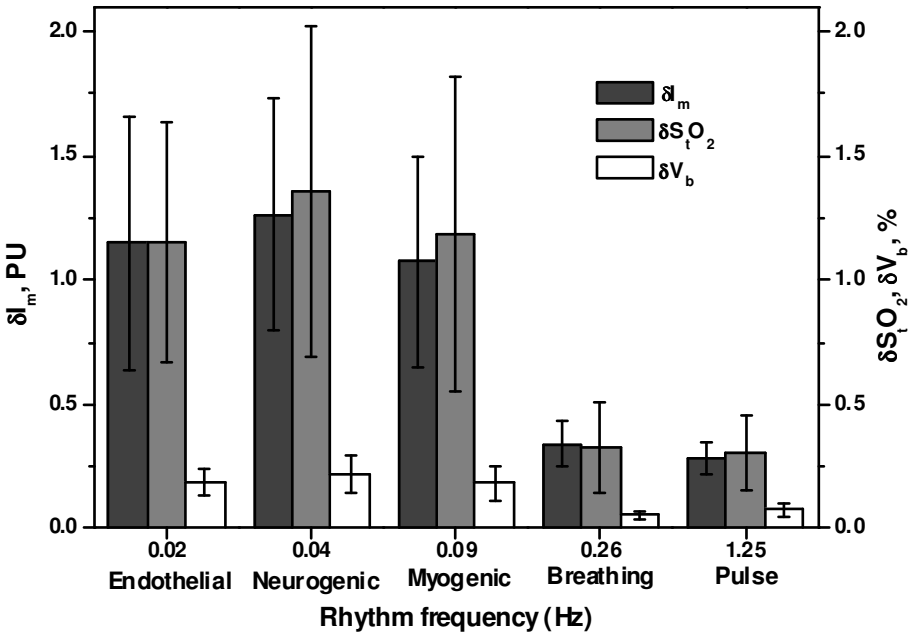

Figure 36 - Blood perfusion, S_tO_2 and V_b average over one month in one individual

Some synchronicity in the 5 components of the fluctuations during the recording period of the study can be seen in the Figure 33, Figure 34 and Figure 35. For example, analysis of

these and Figure 32 shows rising neurogenic rhythm of oscillations with a periodicity of approximately 7 days (3-, 10-, 16- and 22- days), which corresponds precisely to an increase in perfusion (Im) on the same days as the exercise was undertken. This may be considered quite natural due to the more intense work of arteriolar myocytes under conditions of adaptive change. At the same times the subject also showed an increase in tissue oxygen saturation (StO2).

It is interesting to note that the results allow us to assess the relationships between blood perfusion and StO2. For instance, a pattern can be seen manifested three times during the trial (at days 7, 16 and 18) where we observe a decrease in tissue oxygen saturation with increasing amplitude of myogenic oscillations. Thus, the increase in hydrostatic pressure is accompanied by an increase in the diffusion of oxygen in tissues and, consequently, a decrease in tissue oxygen saturation, which corresponds to the data given in (Thorn, Kyte, Slaff, & Shore, 2011).

Figure 36, presents a histograms of oscillations in the LDF-, StO2-and Vb-data amplitudes, except for the amplitudes of pulse rhythms to Vb-graphs, in which the pulse oscillations predominated over breathing. This is most likely due to the physiological source of the parameter Vb being more dependent on pulse than breathing fluctuations.

The gathered data allows us to estimate the long-term variability of 5 rhythms for all 3 parameters. Figure 37 shows the related oscillations of myogenic vasomotion for the blood perfusion, StO2 and Vb. This approach extends the assessment of the contribution of a particular component in each of the 3 graphs.

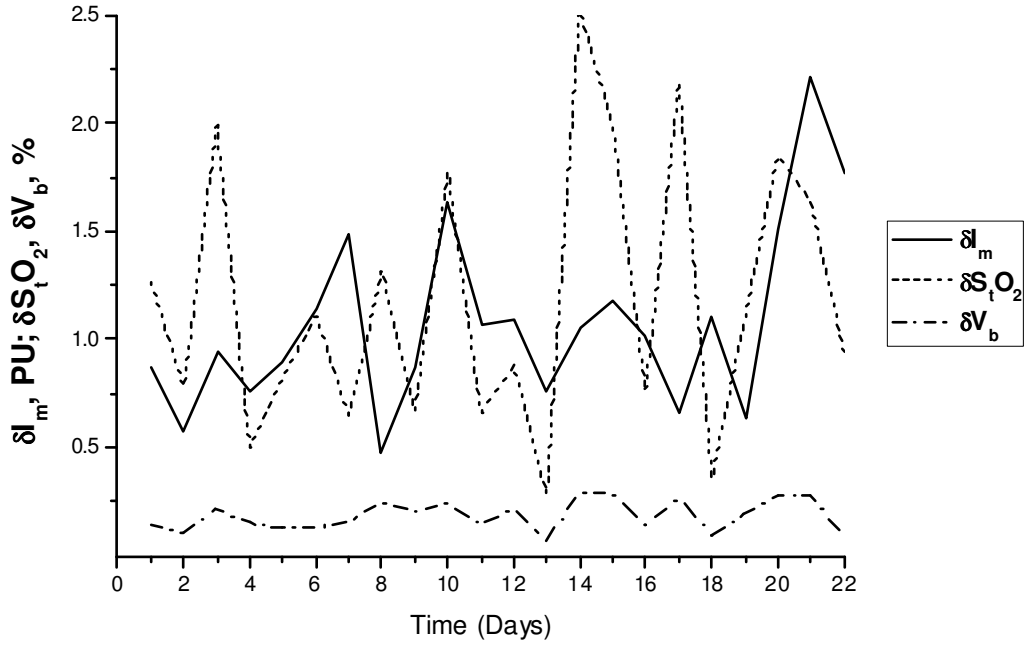

Figure 37 - Representative oscillations for myogenic vasomotion of blood perfusion, S_tO_2 and V_b

3.6 Conclusions

Five rhythmic components: endothelial, neurogenic, myogenic, breath and heart pulses were detected showing high variability of up to 30 – 50%. Rhythmic components were generally synchronous with some latency between Im and StO2 in the myogenic component supporting the hypothesis of strong correlation between peripheral haemo-dynamics and oxygen utilisation in tissues. The results obtained confirm that peripheral blood flow and tissue oxygenation is characterised by high variability and presently unpredictability (lability). This dynamic behaviour is, no doubt, essential for adaptation of the organism to various stresses and biological dynamics. The observed irregularity of oscillations (30-50%) may be partially explained by the peculiarities of the non-invasive optical diagnostic technique applied here, particularly the low diagnostic tissue volume (in this case about

1mm3). Obviously, the blood flow and oxygenation in such a small volume will vary significantly simply due to spatial heterogeneity in biological tissues.

However, this long-term observation and analysis of individual variability in blood rhythm (LDF- and StO2-parameters) has suggested a previously unconsidered correlation between peripheral haemo-dynamics and oxygen utilisation in tissues. This confirmed increase in the information content of the data contemporaneously confirms the requirement to factor these variables into models or algorithms used for non-invasive optical diagnostic techniques. The algorithms developed might include a factor for the specific detected rhythmic oscillations to normalise the calculated blood flow and perfusion data with the objective of reducing the variability of data caused by rhythmic oscillations.

3.7 Synchronisation of micro-vascular blood flow and oxygen saturation rhythms under normal and adaptive change conditions

This research aimed to use MLNDS to investigate micro-vascular blood flow and oxyhaemoglobin saturation to identify relevant biorhythms for the study of human cardiovascular condition.

3.8 Introduction

The evaluation of stress-induced adaptive changes in the tissue respiration and circulatory systems of individuals may provide important information for studies in physiology and clinical medicine. The recent development of multi-functional non-invasive laser based diagnostic systems, such as the “LAKK-M” (SPE "LAZMA" Ltd, Russia) ((Rogatkin, Dunaev, & Lapaeva, 2010), (Rogatkin, Sokolovski, Fedorova, Stewart, Sidorov, & Rafailov, 2011), has made it possible to conduct simultaneous real-time studies on a number of tissue parameters, including microvascular blood flow using laser Doppler flowmetry (LDF) and oxygen saturation of skin tissue using tissue reflectance oximetry (TRO) (Rogatkin D. and L.Lapaeva, 2003), (Stewart, Dunaev, Sokoliovski, Sidorov, & Rafailov, 2012), (Dunaev, Sidorov, Stewart, Sokolovski, & Rafailov, 2013).

The results of LDF measurements, representing “index of blood microcirculation (I_m)” or “perfusion”, assessed in conventional perfusion units (PU), reveal a complex, non-periodic process. This variable component contains information on the modulation of blood flow. Use of spectral signal processing algorithms on LDF-graphs for decoding and analysis provides information about the condition of vascular tone in terms of its contribution to the different mechanisms of micro-hemodynamic regulation (Bracic & Stefanovska, 1998),

(Krupatkin & Sidorov, 2005). Oscillatory processes play an important role in the functioning of the system of tissue microcirculation (Stefanovska, Bracic, & Kvernmo, 1999), (Bernjak, Stefanovska, Urbancic-Rovan, & Azman-Juvan, 2005), (Krupatkin A., 2007), (Krupatkin, 2011). Several frequency ranges of blood flow oscillations in micro-vascular networks have been identified, as defined in section 3.3. Many medical publications are devoted to the study of myogenic oscillations, because they characterise the state of pre-capillary sphincters, which play an important role in the regulation of blood flow (Schmidt-Lucke, Borgstrom, & Schmidt-Lucke, 2002), (Graff, Morales, Smit, De Jong, De Mul, & Rakhorst, 2007), (Schmiedel, Schroeter, & Harvey, 2007), (Newman, Dwyer, St-Pierre, Richards, Clark, & Rattigan, 2009), (Rossi, et al., 2013).

Tissue reflectance oximetry is based on the principles of absorption spectroscopy and allows non-invasive (in vivo, transcutaneous) monitoring of micro-haemodynamics and oxygen transport and utilisation within the entire blood microcirculation system (Amzina, Micheev, Rogatkin, & Sidorov, 2005), (Colquhoun, Tucker-Schwartz, Durieux, & Thiele, 2012), (Quaresima, Ferrari, & Fantini, 2013). TRO determines the relative volume of all fractions of haemoglobin in a tissue volume (average level of blood volume – V_b, in percent) and oxygen saturation of the microvasculature, generally containing arterioles with oxyhaemoglobin and venules with deoxyhaemoglobin (average level of tissue oxygen saturation – S_tO_2, in percent). The changes in tissue oxygen saturation are therefore essentially the increases and decreases of tissue oxygen consumption. There have been a few studies of rhythms (for example, spectral processing algorithms) within these recorded TRO-signals (Coca, Zheng, Mayhew, & Billings, Non-linear analysis of vasomotion oscillations in reflected light measurements, 1998), (Coca, Zheng, Mayhew, & Billings, 2000), (Stefanovska, 2009), (Thorn,

Matcher, Meglinski, & Shore, 2009), and literature reporting the relationships between perfusion, I_m, and S_tO_2-graphs are rare (Tyrrell, Thorn, Shore, Campbell, & Curnow, 2011), (Bernjak, Stefanova, McClintock, Owen-Lynch, & Clarkson, 2012). In isolated cases it has been used to assess vasomotion and myogenic rhythms for perfusion and tissue oxygen saturation, for example (Thorn, Kyte, Slaff, & Shore, 2011). We propose here that analysis of oscillation signals recorded by TRO according to the frequency ranges, similar to LDF plots, is of interest in studying the characteristics of microcirculation of blood.

The aim of this research was to use LDF and TRO data to investigate tissue respiration during the synchronisation of micro-vascular blood flow and oxygen saturation rhythms under normal conditions and during adaptive changes.

3.9 Methods and materials

In this study we used a "LAKK-M" system, which, besides LDF and TRO, contains pulse oximetry and laser fluorescence diagnostic channels (Dunaev, Sidorov, Stewart, Sokolovski, & Rafailov, 2013) (Figure 24). This system includes near-infrared (1064 nm), red (640 nm) and green (532 nm) lasers for LDF- and TRO-channels and allows simultaneous recording of the I_m, S_tO_2 and V_b parameters in a tissue volume about 3-5 mm^3 (with the separation distance between the source and detector fibers of around 1 mm) (Rogatkin, Sokolovski, Fedorova, Stewart, Sidorov, & Rafailov, 2011).

The LDF channel uses traditional methodology, with the results of perfusion in accordance with the following well known equation (Obeid, 1993), (Leahy & Nilsson, 2010):

Equation 3-1

$$I_m = \frac{k\int f \cdot V(f)df}{\int V(f)df},$$

where k is the coefficient of the device (calibration factor), f is the value of the Doppler frequency and the $V(f)$ is the Doppler signal amplitude.

The TRO channel of the "LAKK-M" system calculates the parameters S_tO_2 and V_b according to the following methodology. Tissue oxygen saturation is defined as the percentage composition of oxyhaemoglobin in the sum of two haemoglobin fractions – oxyhaemoglobin and deoxyhaemoglobin (Krupatkin & Sidorov, 2005):

For saturation and blood volume calculation equations see, Chapter 1, Equation 1-6 and Equation 1-7, page 24.

The value of the molar concentration is determined by the absorption by biological tissue of radiation at different wavelengths. On the basis of the well-known Beer-Lambert law and taking into account multicomponent bio-tissue, the absorption coefficient can be calculated using the following formula:

Equation 3-2

$$\mu_a(\lambda) = \sum_i \varepsilon_i(\lambda) \cdot C_i.$$

Where $\varepsilon_i(\lambda)$ is the molar extinction coefficient for the biochemical medium component i, while C_i is the molar concentration of component i in the tested region.

During the implementation of the TRO function of this device, two wavelengths (640 nm and 532 nm) are used. Taking into account certain restrictions, the molar concentrations of haemoglobin fractions vital for the calculation of S_tO_2 and V_b can be calculated using the following equations (Khalil, 2006), (Heusmann, Koelzer, & Mitic, 1996):

Equation 3-3

$$\mu_a(\lambda_1) = \varepsilon_{Hb}(\lambda_1)\cdot C_{Hb} + \varepsilon_{HbO_2}(\lambda_1)\cdot C_{HbO_2} + \varepsilon_{other}(\lambda_1)\cdot C_{other},$$

$$\mu_a(\lambda_2) = \varepsilon_{Hb}(\lambda_2)\cdot C_{Hb} + \varepsilon_{HbO_2}(\lambda_2)\cdot C_{HbO_2} + \varepsilon_{other}(\lambda_2)\cdot C_{other},$$

Where $\varepsilon_{other}(\lambda_j)$ is the sum molar extinction coefficient of light at different wavelengths by all other skin structures.

Studies of different durations were conducted with 8 volunteers with no history of cardiovascular disease, aged 21-49 years, comprising 3 females and 5 males (Table 6).

These studies involved simultaneously recording the parameters of LDF (I_m), TRO (S_tO_2) and pulse oximetry (S_aO_2 - arterial blood saturation with oxygen). In order to assess the I_m and the S_tO_2 oscillatory component, spectral wavelet analysis of oscillations was used (software 3.0.2.384, LAZMA, Russia). This program uses a continuous wavelet transform, with the Morle complex valued wavelet being used as the analysing wavelet (Tankanag & Chemeris, 2008), (Tankanag & Chemeris, 2009). The study was performed at ambient temperature, 21–22°C, in a sitting position after a 30 min rest. The temperature of the volunteers was measured on the tested regions of skin by an infrared clinical thermometer “Medisana” 76120 (FTN). All temperatures recorded were within the range of 34-36°C. The measurements were performed on the inner (palmar) surface of the right middle finger. This

area was chosen because it is rich in arteriovenous anastomoses (AVAs) and variability of the LDF signal is less than in tissue with fewer shunts (Salerud, Tenland, Nilsson, & Oberg, 1983). It should be emphasized that this area is regulated almost exclusively by the autonomic nervous system and is very responsive to adaptive changes. In addition, studies were conducted in an area almost completely devoid of AVAs - the lower forearm's medial surface (the skin without AVAs), characterised by greater nutritive blood flow.

Table 6 - Volunteer and study data.

№ volunteer	Age, years	Sex	Duration of studies, months	Number of basic tests		Number of occlusion tests	Number of studies after sport
				With AVAs	Without AVAs		
1	36	male	6	80	41	-	20
2	29	female	1	19	-	20	-
3	49	male	2	23	5	-	-
4	20	male	1	18	14	-	-
5	23	male	2	27	25	-	-
6	29	female	4	34	31	-	-
7	24	female	2	22	21	-	-
8	23	male	3	25	17	-	-
Total:	29±9.5	-	-	248	154	20	20
							Tests:422

The male participant of 36 years (volunteer №1) was studied over the course of 6 months, totalling 100 records in the skin with AVAs including 20 "before and after" records to monitor the effects of exercise, in this case swimming (500 m), which can be considered a form of stress for the study of adaptive changes. Readings were taken after a rest period of 20-30 minutes after the exercise, with the temperatures being recorded prior to each one falling in the range of 34-35°C. It should be noted that the use of LDF and TRO to investigate the blood microcirculation system was done over duration of 51 days. In addition to basic

test controls recorded prior to swimming, further basic test recordings were produced for an hour after each session (with short 1-2 minute breaks). This led to the experiments based on sports load having 183 basic tests. However, as the adaptive changes under sports load were recorded on a volunteer without prior athletic training, only data from 20 basic tests (n=20) recorded in the first two weeks of training were used for analysis and calculation of oxygen consumption. This volunteer's studies were also conducted in the skin without AVAs (tests=41).

Volunteer №2, a female participant, age 24, was studied over the course of 1 month, totalling 39 studies only in the skin with AVAs: 19 basic tests for 3 minutes plus 20 tests with an occlusion for 1 min followed by a 3 min post occlusion period. The occlusion was used to induce adaptive changes in the volunteer. These occlusion tests were carried out on the same day as the basic tests, after a period of 20-30 minutes rest.

For the remaining volunteers (№3-8), only basic tests were performed on both points of interest (skin with and without AVAs) and they were not subjected to additional stress. Studies of these volunteers were performed by myself and members of the Photonics and Nanoscience Group five times a week (when possible) at around the same time of day, and always followed the methodology described above. It is important to note that all volunteers prior to testing were questioned about their psycho-emotional state and were recorded as either normal or under emotional stress.

Wavelet analysis was performed on 5 rhythmic oscillations of I_m- and S_tO_2-records, namely endothelial (0.0095-0.02 Hz); neurogenic (0.02-0.06 Hz); myogenic (0.06-0.16 Hz); breathing (0.16-0.4 Hz) and pulse (0.4-1.6 Hz) (Stefanovska, Bracic, & Kvernmo, 1999), (Kvandal,

Landsverk, Bernjak, Stefanovska, Kvernmo, & Kirkenboen, Low-frequency oscillations of the laser Doppler perfusion signal in human skin, 2006), (Krupatkin, 2008), (Krupatkin, 2009). For the purposes of this investigation, however, the endothelial component was not required. The typical forms of perfusion and tissue oxygen saturation are shown in Figure 38a and the results of the wavelet analysis for them during the basic test are presented in Figure 38b.

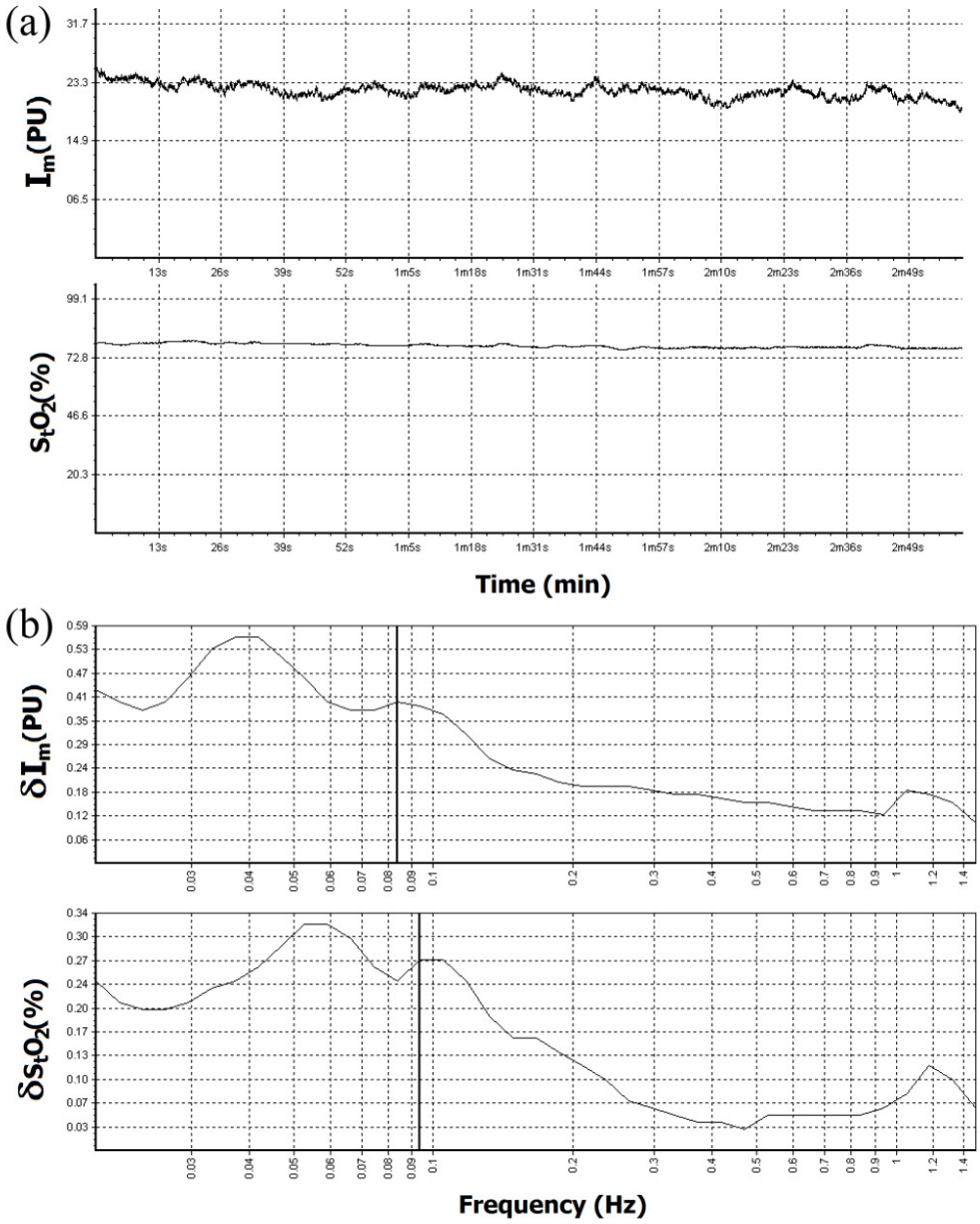

Figure 38- (a) The typical form of perfusion and tissue oxygen saturation graphs, measured using LDF and TRO, respectively and (b) wavelet analysis results following such basic tests, where δI_m – amplitude of perfusion oscillations, δS_tO_2 - amplitude of oxygen saturation oscillations. Furthermore, in (B), a line is used to represent the amplitude oscillation of microvascular blood flow $(\delta I_m)_m$=0.40 PU at a frequency of f_m=0.084 Hz and tissue oxygen saturation $(\delta S_tO_2)_m$=0.27% at a frequency of f_m=0.094 Hz for myogenic rhythms.

Of particular interest is the analysis and comparison of oxygen consumption in tissue under normal conditions and during adaptive changes, accompanied by sympathetic vasomotor reflex (synchronisation and resonance of the myogenic oscillation in perfusion and tissue oxygen saturation). A relationship between the activation of vasomotion and oxygen consumption has been previously identified (Kislukhin, 2004). According to the methodology thoroughly explained in recent literature (Krupatkin, 2012) and using data from the spectral wavelet analysis of I_m- and S_tO_2-graphs, we have calculated the extraction and consumption of oxygen in tissue for all 8 volunteers. It should be noted that what we understand about general oxygen saturation oscillations and in particular concerning myogenic rhythms is as follows. Myogenic oscillations of oxygen saturation I believe primarily result from changes in tissue oxygen consumption. These changes correspond to the oscillations of blood flow in the myogenic range and are therefore directly linked to myogenic response in the vessels to regulate and maintain appropriate blood pressure and flow. In this work the tissue oxygen saturation is monitored by a spectrophotometric technique. The dynamics of the recorded data originate from the modulation of blood flow as a result of the oscillations of perfusion due to the myogenic regulation of micro-vascular tone which maintains blood pressure. Thus, the oxygen saturation value oscillations depend primarily on the blood flow oscillations resulting from changes in the micro-vascular tone.

Oxygen extraction (*OE*), assessed in arbitrary units (AU), was calculated as follows:

Equation 3-4

$$OE = \frac{S_aO_2 - S_vO_2}{S_aO_2},$$

where S_vO_2 - venous blood oxygen saturation, calculated using spectral wavelet analysis of tissue oxygen saturation changes. We also analysed the amplitude of tissue oxygen saturation changes $(\delta S_tO_2)_c$, topographically linked to the arterial blood of the microvasculature (predominantly cardiac rhythms), and the amplitude of tissue oxygen saturation changes $(\delta S_tO_2)_r$, topographically linked to the venous blood of the microvasculature (predominantly respiratory rhythms) (Krupatkin, 2008). If the $(\delta S_tO_2)_c/(\delta S_tO_2)_r$ ratio ≤ 1, then S_vO_2 is taken to be equal to S_tO_2. This variant predominates in most cases of recordings from the skin without AVAs. If the $(\delta S_tO_2)_c/(\delta S_tO_2)_r$ ratio > 1, then:

Equation 3-5

$$S_vO_2 = \frac{S_tO_2}{(\delta S_tO_2)_c/(\delta S_tO_2)_r}.$$

This variant predominates in most cases of recordings from the skin with AVAs. In cases where resonance in oxygen saturation occurs in the active frequency bands (for example, in the myogenic range during adaptive changes), the values for cardiac rhythm, (δStO2)c , and respiratory rhythm,(δStO2)r , may not be expressed in the spectrum, and the venous oxygen saturation, SvO2 , calculation has some specific features. In cases where resonance in oxygen saturation changes within the range of the total myogenic and respiratory bands, SvO2= StO2. In the skin zones with significant AVAs, an additional factor, the bypass index (BI) for StO2, is required:

Equation 3-6

$$S_vO_2 = \frac{S_tO_2}{BI(S_tO_2)},$$

where:

Equation 3-7

$$BI(S_tO_2) = 1 + \frac{(\delta S_tO_2)_n}{(\delta S_tO_2)_m},$$

where $(\delta S_tO_2)_n$ and $(\delta S_tO_2)_m$ are the amplitudes of oxygen saturation changes in neurogenic and myogenic rhythms respectively.

Oxygen consumption (*OC*), assessed in arbitrary units (AU), was calculated as follows:

Equation 3-8

$$OC = I_{mn} \cdot \left(S_aO_2 - S_vO_2\right),$$

where I_{mn} is the nutritive blood flow value was calculated according to the equation:

Equation 3-9

$$I_{mn} = \frac{I_m}{BI(I_m)},$$

Where, $BI(I_m)$ is the bypass index calculated for skin with AVAs similarly to Equation 3-7, but only using perfusion data. For skin zones without AVAs:

Equation 3-10

$$BI(I_m) = \frac{(\delta I_m)_{\max}}{(\delta I_m)_m},$$

where $(\delta I_m)_{max}$ is the maximum amplitude of the dominant oscillations in the active range of frequencies up to 0.15 Hz and $(\delta I_m)_m$ is amplitude of oscillations of myogenic rhythms.

Data collected on oxygen consumption for determination of synchronisation and resonance of myogenic oscillations in perfusion and oxygen saturation changes during periods of adaptive change was processed separately. It should be noted that the OC equation (Equation 3-8) includes the perfusion rate value, due to which the OC value (calculated according to Fick's principle; which proposes that cardiac output can be calculated as the quotient of total oxygen consumption of the body by the variance between oxygen content in arterial blood and venous blood (Medical_Dictionary, 2013)) reflects the oxygen consumption rate.

Furthermore, the normalised amplitude of myogenic rhythms was calculated using the standard deviation of perfusion and of tissue oxygen saturation, respectively:

Equation 3-11

$$(\delta I_m)'_m = \frac{(\delta I_m)_m}{\sigma_{per}}; \qquad (\delta S_t O_2)'_m = \frac{(\delta S_t O_2)_m}{\sigma_{sat}},$$

where σ_{per} and σ_{sat} = standard deviation of perfusion and tissue oxygen saturation during a basic test, respectively.

The data presented is mean averaged ± SD. Statistical analysis was performed using OriginPro 8 SRO version v.8.0724 with data sets tested for normality by the Kolmogorov-Smirnov and Shapiro-Wilk tests. For normally distributed data, group comparisons were made by carrying out a parametric unpaired t-test. For the nonparametric statistics paired test was used (notated [a] and [b] in Table 8). For the non-normally distributed data, the Mann-Whitney test of nonparametric statistics was used to compare the two groups (normal and with adaptive changes conditions).

3.10 Results and discussion

Analysis of the data indicates only one synchronisation and resonance of vasomotion in micro-vascular blood flow and oxygen saturation in the myogenic oscillation range and only during periods of adaptive changes – for example, stressful situations or reaction to sports load. The typical form of perfusion and tissue oxygen saturation, along with the results of wavelet analysis of these parameters during adaptive changes, are presented in Figure 39.

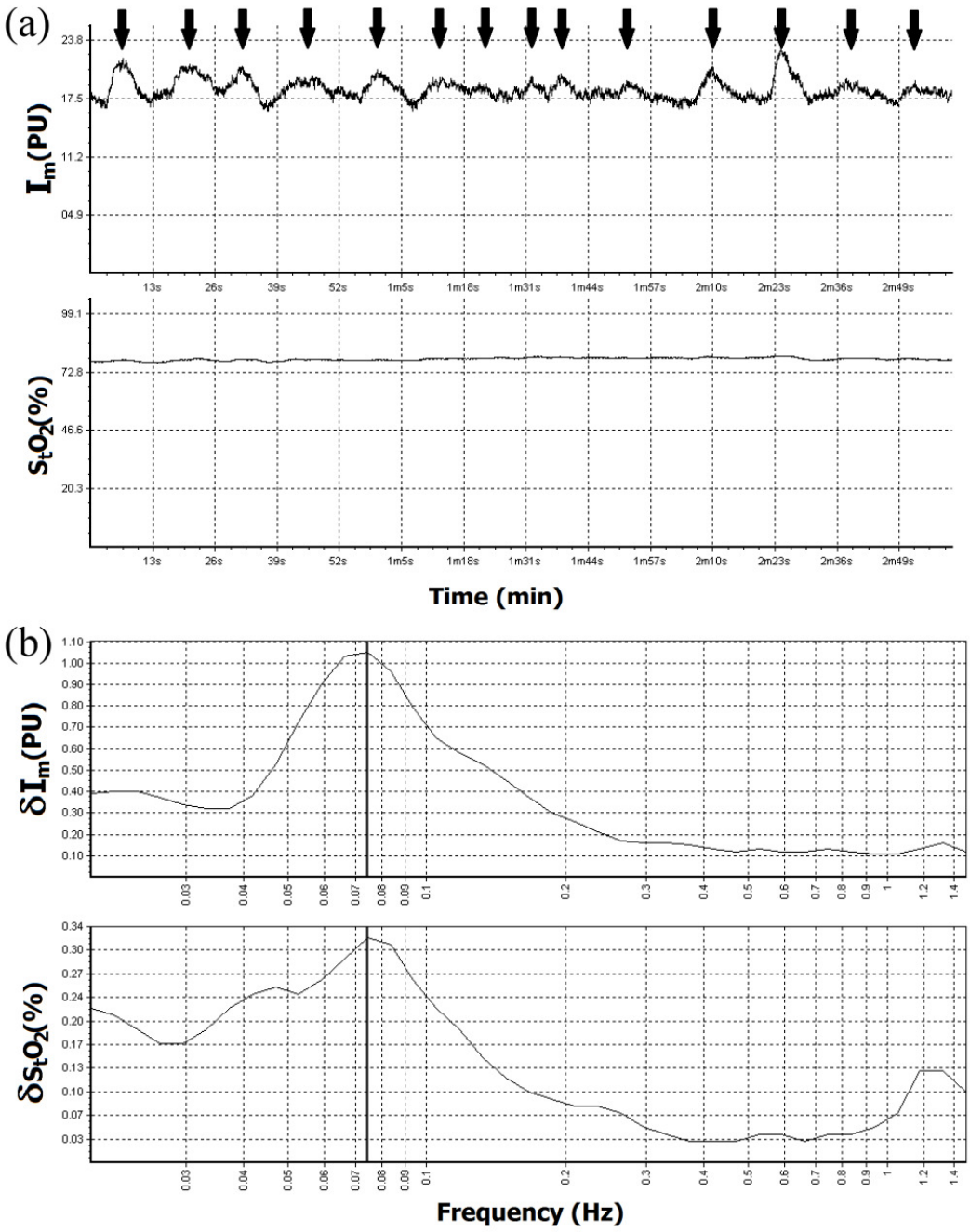

Figure 39 - (a) Perfusion and oxygen saturation graphs in cases of myogenic oscillation, represented on the Im-graph by a ↓ and (b) typical example of resonance and synchronised rhythms (fm=0.074 Hz) of microvascular blood flow (δIm)m=1.05 PU and oxygen saturation (δStO2)m=0.32% within the range of only myogenic oscillation (vasomotion) during adaptive changes.

The parameters for calculating oxygen extraction and consumption for all volunteers were obtained using the approaches detailed in the methods section above. The results of measurements in the skin with AVAs and calculations of the parameters of tissue respiration (oxygen extraction and consumption) for volunteer №1 with the single largest sample of recorded data are shown in Table 2. The results of measurements and calculations for both areas studied (skin with and without AVAs) for all the 8 volunteers are shown in Table 7.

Table 7 - The results of measurements

Table 7a - in the skin with AVAs and calculation of oxygen extraction and consumption for volunteer №1

№	Parameters	State		
		Norm (tests=58)	With adaptive changes - stress (tests=21)	With adaptive changes - sport (tests=20)
1	I_m(total), PU	20.8±2.7	20.3±3.1	20.3±2.4
2	I_{mn}(nutritive), PU	8.4±1.6	10.6±1.9[a]	11.5±1.3[a]
3	S_aO_2, %	98.1±0.5	97.9±0.5	97.7±0.5
4	S_tO_2, %	76.1±2.9	75.2±2.8	76.3±4.2
5	S_vO_2, %	39.8±10.3	41.2±5.5	41.7±5.5
6	V_b, %	9.9±0.9	10.0±0.9	10.4±0.8
7	$(\delta I_m)'_m$, AU	0.44±0.14	0.54±0.15[b]	0.61±0.14[b]
8	$(\delta S_tO_2)'_m$, AU	0.39±0.15	0.44±0.15	0.54±0.21[b]
9	$f_m(\delta I_m)$, Hz	0.071±0.012	0.077±0.019[b]	0.092±0.015[b]
10	$f_m(\delta S_tO_2)$, Hz	0.081±0.026	0.092±0.035	0.092±0.014[b]
11	$BI(I_m)$, AU	2.5±0.4	1.9±0.2[b]	1.8±0.2[b]
12	$BI(S_tO_2)$, AU	2.4±0.7	1.8±0.2[b]	1.9±0.2[b]
13	*OE*, AU	0.59±0.11	0.58±0.06	0.57±0.06
14	*OC*, AU	488.6±131	597±109[b]	641±91[b]

[a] significant difference ($p < 0.05$) observed from normal state, calculated by a *t*-test.

[b] significant difference ($p < 0.05$) observed from normal state, calculated by the Mann-Whitney test.

The results of measurements in the skin with AVAs and calculation of oxygen extraction and

consumption for first volunteer are shown here.

Nutritive perfusion:

As the data of this Table shows, during adaptive changes, a significant increase in the nutritive perfusion is observed in the zones with AVAs: for example, for volunteer №1 – 8.4±1.6 PU vs. 10.6±1.9 PU, $p < 0.05$ (for stress) and 8.4±1.6 PU vs. 11.5±1.3 PU, $p < 0.05$ (for sport).

Oxygen consumption:

Increasing oxygen consumption was therefore due to an increase in perfusion rather than an increase in OE, thus adaptive changes naturally lead to the intensification of oxygen consumption in zones with AVAs: for example, for volunteer №1 – 488.6±131 AU vs. 597±109, $p < 0.05$ (for stress) and 488.6±131 AU vs. 641±91 AU, $p < 0.05$ (for sport).

Frequency of myogenic oscillations in perfusion and tissue oxygen saturation:

Analysis of recorded time fragments under normal conditions, during stress and following exercise presented distinct differences in the frequency of myogenic oscillations in perfusion and tissue oxygen saturation. As the data on this Table shows, the frequency of myogenic oscillations in tissue oxygen saturation rhythms and the vasomotion in perfusion both increase under adaptive changes (heading towards the so-called central frequency of myogenic oscillations – 0.1 Hz). This is particularly expressed in the case of the reaction to sports load for volunteer №1 with perfusion 0.071±0.012 Hz vs. 0.092±0.015 Hz, $p < 0.05$ and tissue oxygen saturation 0.081±0.026 Hz vs. 0.092±0.014 Hz, $p < 0.05$. This is likely the result of higher levels of adaptive change causing more intense and clear synchronisation of vasomotion.

Table 7b - The averaged results of measurements and calculations for all 8 volunteers

№	Parameters	Skin with AVAs		Skin without AVAs	
		Norm (tests=187)	With adaptive changes (tests=60)	Norm (tests=128)	With adaptive changes (tests=26)
1	I_m(total), PU	21.0±3.1	21.4±3.4	2.5±0.8	2.8±0.9
2	I_{mn}(nutritive), PU	8.6±0.5	11.1±2.2[a]	1.7±0.8	2.8±0.8[b]
3	S_aO_2, %	98.1±0.4	97.9±0.4	97.9±0.4	97.8±0.6
4	S_tO_2, %	78.3±4.7	77.7±5.7	66.2±9.3	61.9±7.3
5	S_vO_2, %	41.6±13.7	41.9±6.1	58.2±12.7	61.3±7.3
6	V_b, %	10.2±1.8	9.9±1.5	6.3±1.7	6.0±1.4
7	$(\delta I_m)'_m$, AU	0.44±0.13	0.52±0.13[b]	0.46±0.13	0.67±0.11[b]
8	$(\delta S_tO_2)'_m$, AU	0.33±0.15	0.41±0.17[b]	0.25±0.13	0.77±0.19[b]
9	$f_m(\delta I_m)$, Hz	0.086±0.023	0.084±0.025	0.089±0.018	0.086±0.021
10	$f_m(\delta S_tO_2)$, Hz	0.091±0.029	0.093±0.035	0.090±0.019	0.084±0.021[b]
11	$BI(I_m)$, AU	2.5±0.5	1.9±0.2[b]	1.6±0.6	1.0±0.06[b]
12	$BI(S_tO_2)$, AU	2.7±0.7	1.9±0.2[b]	2.4±1.6	1.0±0.2[b]
13	*OE*, AU	0.58±0.14	0.57±0.06	0.41±0.13	0.37±0.07
14	*OC*, AU	495±170	617±123[b]	69±40	102±38[b]

[a] significant difference ($p < 0.05$) observed from normal state, calculated by a *t*-test.

[b] significant difference ($p < 0.05$) observed from normal state, calculated by the Mann-Whitney test.

The data received for volunteer №1 (Table 7a) presented 41 cases (20 cases of which were after exercise) of synchronisation and resonance of vasomotion in micro-vascular blood flow and oxygen saturation out of a total of 99 recorded measurements of skin containing AVAs. For the total population (Table 7b), 60 out of 247 measurements of AVA containing skin and 26 out of 154 measurements in AVA free skin were observed to have synchronisation.

Nutritive perfusion:

Again, for all volunteers during adaptive changes we can observe a significant increase in the nutritive perfusion in the zones with AVAs: 8.6±0.5 PU vs. 11.1±2.2 PU $p < 0.05$ (for stress). For the zones without AVAs: 1.7±0.8 PU vs. 2.8±0.8 PU $p < 0.05$ (for stress).

Oxygen consumption:

And increasing oxygen consumption in the zones with AVAs: 495±170 AU vs. 617±123 AU, $p < 0.05$ (for stress). For the zones without AVAs: 69±40 AU vs. 102±38 AU, $p < 0.05$ (for stress).

The results from our studies on adaptive changes (stress- or exercise-induced) support our hypothesis that during resonance and synchronization of blood flow and oxygen saturation rhythms via myogenic oscillation there is increased tissue oxygen consumption compared with normal conditions.

Thus, extraction of oxygen remains unchanged (for zones with and without AVAs). Therefore, we suggest that the bypass index may be used as a marker of adaptive changes (during stress conditions), calculated based on perfusion and tissue oxygen saturation.

Normalized perfusion and tissue oxygen saturation vasomotion amplitudes:

The analysis of data presented in this table also shows that normalized perfusion vasomotion amplitudes (for example in the regions with AVA for all volunteers – 0.44±0.13 AU vs. 0.52±0.13, $p < 0.05$) and tissue oxygen saturation (0.33±0.15 AU vs. 0.41±0.17, $p < 0.05$) increase under adaptive changes. This is the result of these amplitudes shifting towards synchronisation at the microcirculatory level to maintain homeostasis in the oxygen

delivery and consumption system. These cases demonstrate increased blood flow and oxygen transport into the nutritive flux, which is reflected in the spectrum as a rise in myogenic oscillation amplitude. The oxygen delivered to the nutritive flux can move into tissues and be consumed in the process of metabolism.

This results in an increasing OC and/or OE. If the tissue exchange is not active, the oxygen may be shunted.

This is particularly visible in areas without AVAs, where the shunting happens via major vessels. In this circumstance, however, OC and/or OE do not rise or fall despite an increase in myogenic amplitudes to a resonance within the spectrum (for example, for the perfusion of all volunteers 0.46±0.13 AU vs. 0.67±0.11 AU, $p < 0.05$ and for the tissue oxygen saturation 0.25±0.13 AU vs. 0.77±0.19 AU, $p < 0.05$).

The human skin contains functionally distinct zones or regions, differing in morphological properties and regulation of micro-vascular blood flow. These can be classified as with and without the presence of AVAs. The zones with AVAs are functionally designed and intended for the implementation of thermoregulatory homeostasis and are almost exclusively regulated by the sympathetic adrenergic nervous system. Additionally, the values of perfusion and intravascular pressure of the skin micro-vessels is generally higher in regions containing AVAs. The zones of skin without AVAs are characterised by lower blood flow in micro-vessels and a higher contribution of the venous component. As the data of Table 7 shows, during adaptive changes a significant increase in the nutritive perfusion (I_{mn}) is observed in the zones with AVAs: for example, for volunteer №1 – 8.4±1.6 PU increased to 10.6±1.9 PU, $p < 0.05$ when under stress and 8.4±1.6 PU rose to 11.5±1.3 PU, $p < 0.05$ during

adaptation to physical (sport) stress, and for all volunteers – 8.6±0.5 PU increased to 11.1±2.2 PU $p < 0.05$ when under stress. There was no change in oxygen extraction in either of the zones, with and without AVAs. Increased oxygen consumption was, therefore, the result of an increase in perfusion rather than an increase in OE, thus the response to adaptive change conditions was an intensification of oxygen consumption in zones with AVAs driven by an increase in perfusion: for example, oxygen consumption results for volunteer №1 increased from 488.6±131 AU to 597±109, $p < 0.05$ as a result of stress and to 641±91 AU, $p < 0.05$ in response to physical stress induced by sport; for the entire group of volunteers OC rose from 495±170 AU to 617±123 AU, $p < 0.05$ under stress conditions. There were more cases observed of synchronisation of myogenic rhythms in micro-vascular blood flow and oxygen saturation in zones with AVAs, this result is most likely due to the larger numbers of autonomic nerves, which are very responsive to adaptive changes. Additionally, adaptive changes caused by sport were manifested more clearly during the early stages of physical training (first 2-3 weeks). This is probably due to a more intense initial adaptation of the microcirculatory system to the physical loads upon the organism.

The results from our studies on adaptive changes (stress- or exercise-induced) support my hypothesis that during resonance and synchronisation of blood flow oscillations and oxygen saturation changes via myogenic oscillation there is increased tissue oxygen consumption compared with normal conditions. Thus, extraction of oxygen remains unchanged. In all cases the bypass index reduced under conditions of stress and exercise, thereby confirming reduced circulatory AVAs as one healthy physiological response to stress. Therefore, I suggest that the bypass index may be used as a marker of adaptive changes (indicating stress conditions), calculated based on perfusion and tissue oxygen saturation.

The increase in amplitude of myogenic rhythm reflects a modulation of the hydrostatic pressure in the capillaries, resulting in an increase in diffusion of oxygen into the tissues, hence the changes in tissue oxygen saturation. Time shifts and frequency characteristics are obviously specific to particular individuals. For example, the number of recorded cases of adaptive changes for each volunteer is presented in Table 8.

Table 8 - Individual cases of adaptive changes per volunteer.

№ Volunteer	With AVAs		Without AVAs	
	Adaptive changes	Total	Adaptive changes	Total
1	41	99	7	41
2	5	39	-	-
3	4	23	1	5
4	4	18	4	14
5	11	27	0	25
6	9	34	9	31
7	2	22	3	21
8	3	25	2	17

Analysis of recorded time fragments under normal conditions, during stress and following exercise presented distinct differences in the frequency of myogenic oscillations in perfusion and tissue oxygen saturation changes. As the data on Table 7 - The results of measurements shows, the frequency of oxygen saturation changes corresponding to the oscillations of blood flow in the myogenic range and the vasomotion in perfusion both increase under adaptive changes (heading towards the so-called central frequency of myogenic oscillations – 0.1 Hz). This is particularly expressed in the case of the reaction to sports load for volunteer №1 with perfusion 0.071±0.012 Hz vs. 0.092±0.015 Hz, $p < 0.05$ and tissue oxygen saturation 0.081±0.026 Hz vs. 0.092±0.014 Hz, $p < 0.05$. This is likely the result of higher

levels of adaptive change causing more intense and clear synchronisation of vasomotion. Occasionally, complete synchronisation will be achieved when the frequency of both myogenic oscillations coincide. For example, this case is presented in Figure 40.

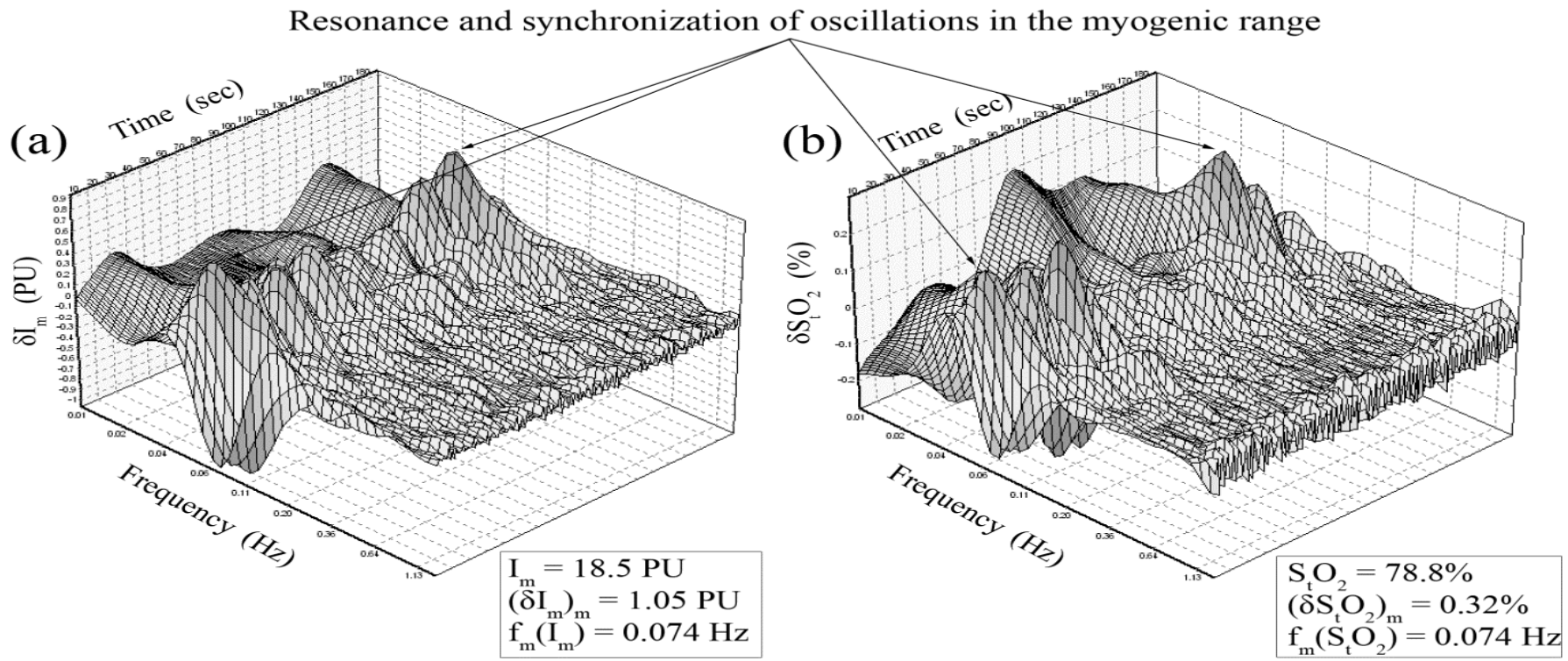

Figure 40 - Typical example of the 3D wavelet analysis of resonating and synchronised myogenic rhythms of micro-vascular blood flow (a) and oxygen saturation changes (b) during adaptive changes.

The analysis of data presented in tables 2-3 also shows that normalised perfusion vasomotion amplitudes (for example in the regions with AVA for all volunteers – 0.44±0.13 AU vs. 0.52±0.13, $p < 0.05$) and tissue oxygen saturation (0.33±0.15 AU vs. 0.41±0.17, $p < 0.05$) increase under adaptive changes. This is the result of these amplitudes shifting towards synchronisation at the micro-circulatory level to maintain homeostasis in the oxygen delivery and consumption system. These cases demonstrate increased blood flow and oxygen into the nutritive flux, which is reflected in the spectrum as a rise in myogenic oscillations amplitude. The oxygen delivered to the nutritive flux can move into tissues and be consumed in the process of metabolism. This results in an increasing OC and/or OE. If the tissue exchange is not active, the oxygen may be shunted. This is particularly visible in areas without AVAs, where the shunting happens via major vessels. In this circumstance, however, neither OC nor OE rise or fall despite an increase in myogenic amplitudes to a resonance within the spectrum. For example, in tissue without AVAs the average change in perfusion oscillation amplitude in the myogenic rhythm frequency range, $(\delta I_m)_m$, for all volunteers increased from 0.46±0.13 AU to 0.67±0.11 AU, $p < 0.05$ in response to adaptive stress and changes in myogenic tissue oxygen saturation, $(\delta S_t O_2)_m$, were even more significant rising from 0.25±0.13 AU to 0.77±0.19 AU, $p < 0.05$) in response to adaptive stress.

Data analysis has demonstrated an increase in resonance and synchronisation of micro-vascular blood flow and oxygen saturation rhythms as an adaptive change in myogenic oscillation (vasomotion) resulting from exercise and potentially from psycho-emotional stress. An explanation for this observed response may be that the synchronisation of myogenic rhythms facilitates maximum oxygen delivery to tissue following or during periods

of physical or emotional stress. The data obtained show differences in myogenic oscillations in both the ordinary state of the body (normality) and during episodes of sympathoadrenal activation (e.g. emotional stress). Normally, all systems of the body (including blood circulation, respiration, metabolism, etc.) work in different phases and frequencies, are exhibiting non-linearity and independence. Synchronisation of myogenic rhythms during adaptive changes may promote increased oxygen consumption resulting from increased micro-vascular blood flow velocity. The data above indicates that adaptive changes lead to the intensification of oxygen consumption in zones with AVAs due to an increased perfusion. Furthermore, as these zones have rich autonomic innervation, they are very sensitive to adaptive change leading to them having a higher incidence of myogenic rhythm synchronisation of micro-vascular blood flow and oxygen saturation. During adaptive changes (under particular emotional stress, etc.), synchronisation increases, reducing the freedom of micro-vascular blood flow regulation.

Ultimately, our suggested approaches for the use of the laser technology in investigating tissue respiration and skin micro-circulation under adaptive changes, through the analysis of the synchronisation of blood flow and oxygen saturation rhythms observed within the data, have shown themselves to be highly informative of the response of the subject's micro-circulation system and offers interesting prospects for further investigation as a potential diagnostic methodology relevant to vascular function. These results example the potential utility of the LAKK-M device and of multifunctional laser diagnostics generally to provide important physiological data using novel methodology and software.

Chapter 4 – METABOLIC ASSESSMENT OF MITOCHONDRIA, LEVELS OF OXYGEN CONSUMPTION AND GLYCOLYSIS

4.1 Introduction

Ultraviolet (UV) radiation can case harmful effects which can be classified as acute or chronic. The acute effects of UV-A (400 – 315 nm) and UV-B (315 – 280 nm) exposure are both short-lived and reversible. These effects include mainly sunburn (or erythema) and tanning (or pigment darkening). The chronic effects of over exposure to both UV-A and UV-B can be much more serious, even life threatening, and include premature aging of the skin, suppression of the immune system, damage to the eyes, and skin cancer. The UV wavelength used in the LAKK-M is 370nm (UV-A), however the power level of the UV-LED is so low, ~1000 W/m^2, that it represents a fraction of the UV-A exposure experienced by a few seconds in daylight at an average of 1367 W/m^2 .

UV-visible light absorbance and fluorescence are very important qualitative and even quantitative tools used in analytical chemistry. We can therefore anticipate their utility in a MLNDS. The data collected could provide information regarding the presence and relative abundance of molecules involved in metabolism and respiration and thus compliment haemodynamic and oxygenation state information gathered using TRO and LDF.

There are many absorptive and fluorescent biological materials present in the skin which will be involved in any spectroscopic analysis. We are mainly interested for the purposes of diagnostics in those involved in metabolic processes and respiratory chains. The compounds of interest will include

- **Nicotinamide adenine dinucleotide (NAD^+) and its reduced form (NADH)**
- **Flavin adenine dinucleotide (FAD) and its reduced form $FADH_2$**

Both of these compounds are redox cofactors and closely involved in respiratory metabolic reactions. FAD has accommodation for two hydrogens while NAD can accept one hydrogen, therefore based on electron transfer $FADH_2$ produces less ATP than by NADH.

At a general level we can consider the oxidation of fuel molecules, also known as catabolism. In these processes, we can consider NADH and $FADH_2$ as shuttles, carrying electrons - in the form of hydride ions -from fuel molecules to oxygen in which NADH and $FADH_2$ are formed from NAD+ and FAD, respectively.

The common theme in all of these reactions is that in each case, NAD+ and FAD have accepted H2 – two high-energy electrons and two protons - from an organic substrate that is being oxidized. NADH and FADH2 then serve as conduits in the transfer of these electrons to molecular oxygen, reducing it to water, **Figure 41** .

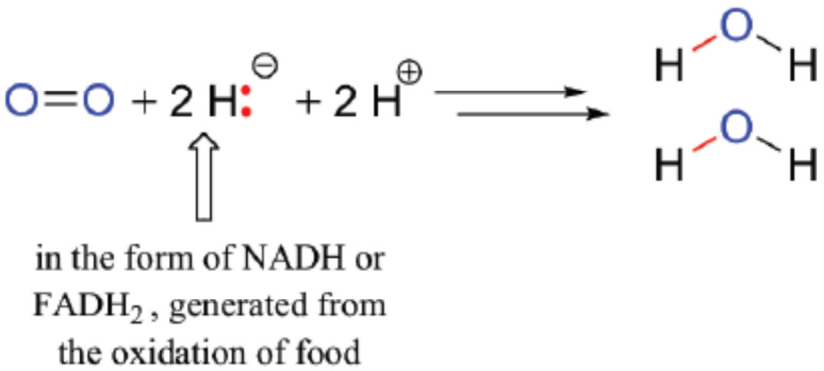

Figure 41 – NADH and $FADH_2$ as carriers of hydrides from fuel molecules to water

The actual process by which electrons flow from NADH and FADH2 to water, and also by which the energy thereby released is converted into ATP, is a long, complicated multi-enzyme pathway called the 'electron- transport chain' of 'oxidative phosphorylation' Figure 42.

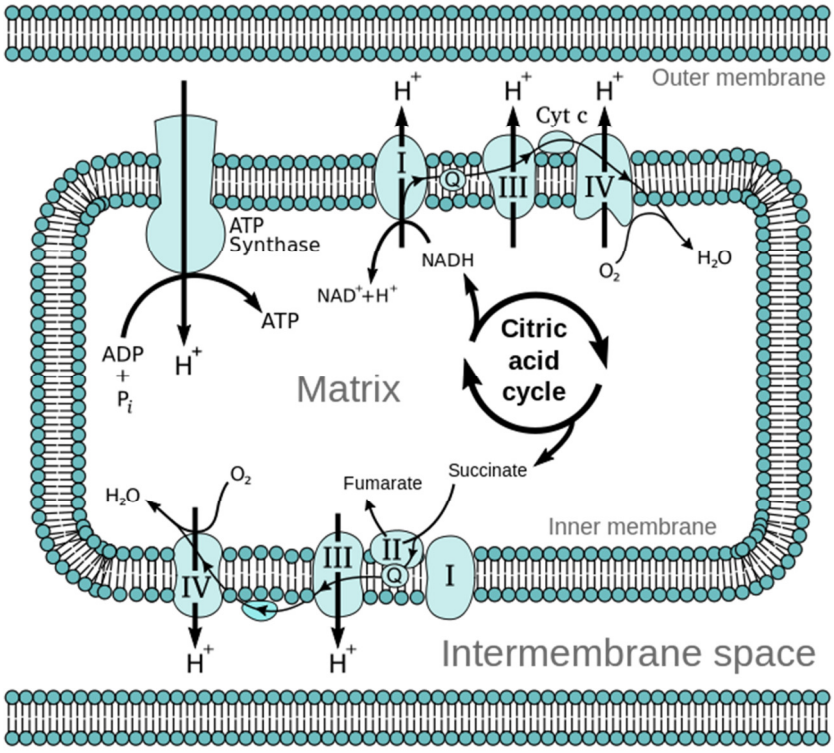

Figure 42 – Mitochondrial electron transport chain (Wikipedia)

The cells of all forms of life require NADPH. It is the primary biological reducing agent used to build large reduced molecules from small, oxidized precursors. Moreover, it has been suggested that depleted levels of the coenzyme nicotinamide adenine dinucleotide phosphate (NADPH), which is the reduced form of NADP+ which differs from NAD+ only by the presence of an additional phosphate group on the ribose with the adenine moiety, may be associated with altering the regulation of certain nuclear transcription factors associated

with for example cancer (Wallace, 2012). Nicotinamide adenine dinucleotide (NAD+), reduced nicotinamide adenine dinucleotide (NADH), nicotinamide adenine dinucleotide phosphate (NADP+) and reduced nicotinamide adenine dinucleotide phosphate (NADPH) have been known to play vital roles in energy metabolism, anti-oxidation, and reductive biosynthesis. In recent years, these co-factors have been shown to be involved in other physiological functions as well, including aging, oxidative stress, intracellular calcium homeostasis, ROS production, cell death and gene expression (Ying, 2008), (Figure 43).

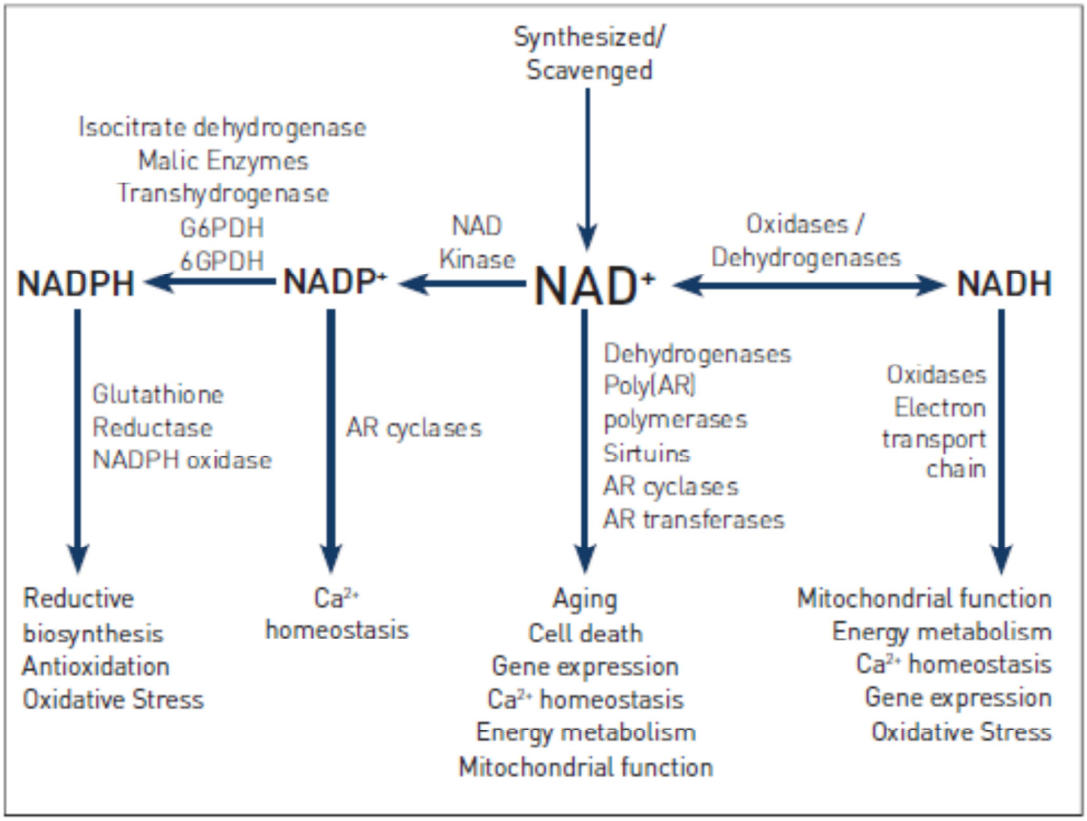

Figure 43 -Biological and cellular functions of NAD+/NADH and NADP+/NADPH, modified from (Ying, 2008) **(AR = ADP-ribose, G6PDH = glucose-6-phosphate dehydrogenase, 6GPDH = 6-glyconate phosphate dehydrogenase)**

In addition to NADPH, the coenzyme flavin in the form of $FADH_2$ can serve as the reducing agent in biochemical reactions. While the flavin coenzyme is a direct source of hydrides in these reductive reactions, the hydrides originally come from NADPH.

It is, therefore, reasonable to consider that the acquisition of data using MLNDS on the level of these metabolic compounds may be offer the prospect of discovering biomarkers of disease conditions.

Metabolic enzyme spectroscopy

NADH is probably the most well-known and highly researched spectroscopic marker of cellular metabolism and redox status (Koenig & Schneckenburger, 1994) (Dell & Ganske, 2008) (Mayevsky & Chance, 2007) (Kirkpatrick, Zou, Brewer, Brands, Drezek, & Utzinger, 2005) . It exhibits absorption at 350nm and fluorescence peak at 450nm. Increased relative levels of NADH, the reduced state of NAD+, are a known biomarker of reduced cellular respiration. Taken together with LDF and TRO the *in vivo* spectroscopic analysis of tissues provides data on important markers of tissue metabolic state and vitality (Mayevsky & Chance, 2007).

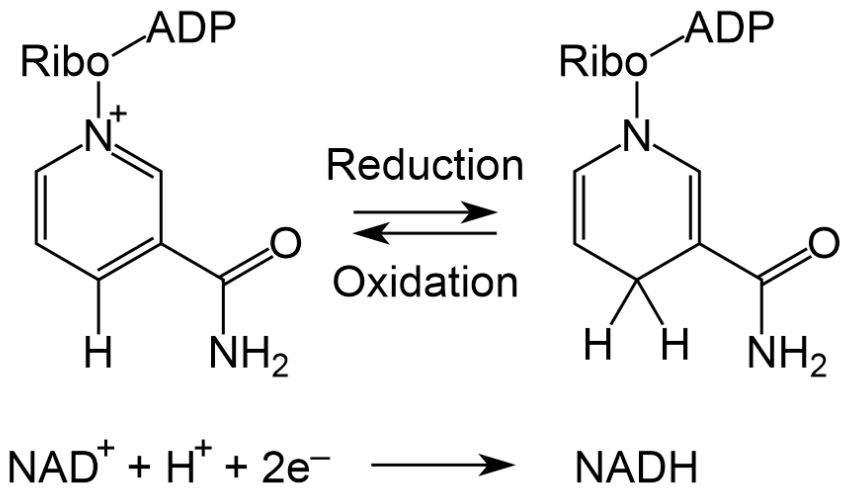

Figure 44- Reduction and oxidation of the coenzyme NAD

Above is the molecular structure of the pyridine coenzyme nicotinamide adenine dinucleotide, (NADH). This is the reduced form of NAD and it is formed by the hydrogen uptake at position 4 of the pyridine ring. NADH is re-oxidized by transfer of electrons to a second acceptor. Both these molecules exhibit an absorption band at 260nm is due to adenine. There is a second absorption band at 340nm, due to the reduced pyridine ring, clearly NAD will therefore not absorb at the 340nm band see Figure 45.

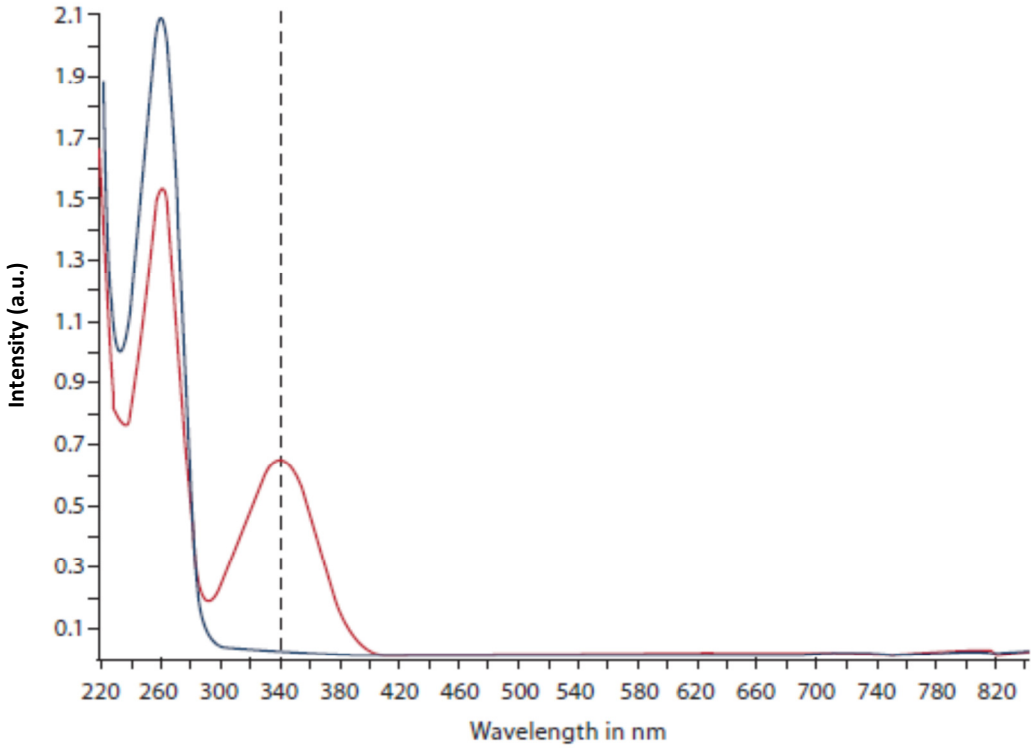

Figure 45 - Absorbance spectra of NAD+ (blue line) and NADH (red line), adapted from **(BMG Labtech, 2013)**

The coenzymes NAD(H) and NADP(H), located mainly in the mitochondria of cells, act as hydrogen transferring molecules in the respiratory chain (**Figure 44).** As discussed above the hydrogen uptake at position 4 of the pyridine ring results in significant absorption spectral changes. Excitation at >300nm produces a fluorescence emission with a peak at about 470 nm in aqueous solution. The oxidized forms NAD and NADP also fluoresce, at about 445 nm. However, the fluorescence yield of the oxidized forms is 1,000 times less than the reduced forms (for excitation > 300 nm). Therefore, in practice, UVA excited *in vivo* fluorescence can be attributed solely to the reduced states, NADH/ NADPH.

Flavin adenine dinucleotide (FAD) is another redox cofactor involved in several important reactions in metabolism. FAD can be reduced to $FADH_2$, whereby it accepts two hydrogen atoms (a net gain of two electrons) The primary biochemical role of $FADH_2$ in eukaryotes is

to carry high-energy electrons used for oxidative phosphorylation. The spectra of oxidized flavomononucleotide (FNM), flavodinucleotide (FAD), and riboflavin, unsurprisingly, are very similar. They have main electronic transitions at 260, 370, and 450 nm (Galland & Senger, 1988) and a wide fluorescence band with a peak at 550 nm. The FAD fluorescence quantum yield is a factor of 10 less than that of FMN and riboflavin (Galland & Senger, 1988) and most other flavoproteins are only weak fluorophores therefore they are not considered further for our purposes of MLNDS evaluation.

The fluorescent coenzymes act as sensitive bio-indicators of metabolic functions such as the degradation of glucose or respiration. In particular, NADH may serve as an indicator of the intracellular oxygen concentration (Mayevsky & Chance, 2007). Any change in the oxygen supply results in changes in the mechanisms of electron transport of the respiratory chain. In particular, a reduced oxygen concentration leads to a higher NADH concentration. The increase in NADH concentration can be explained by local hypoxia and also by enhanced NADH synthesis due to higher activation of mitochondrial enzymes as a result of the calcium increase during muscle contraction (Guezennec & al, 1991). However, skin fluorescence in the blue/green spectral region is based on various other endogenous fluorophores such as collagen, elastin, and the coenzymes mentioned above (**Figure 47**). As a result, the precise determination of NADH emission is difficult.

The absorption and fluorescence spectra of relevant tissue biomarkers are shown in **Figure 46** and **Figure 47** respectively.

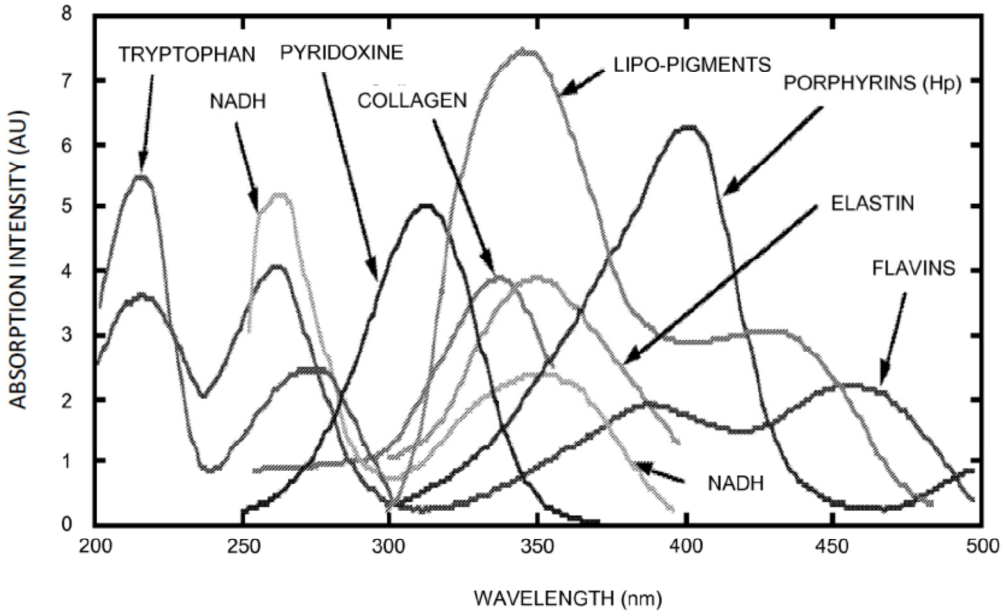

Figure 46 - Absorption spectra of tissue biomarkers, from US Pat US 20090137908 A1

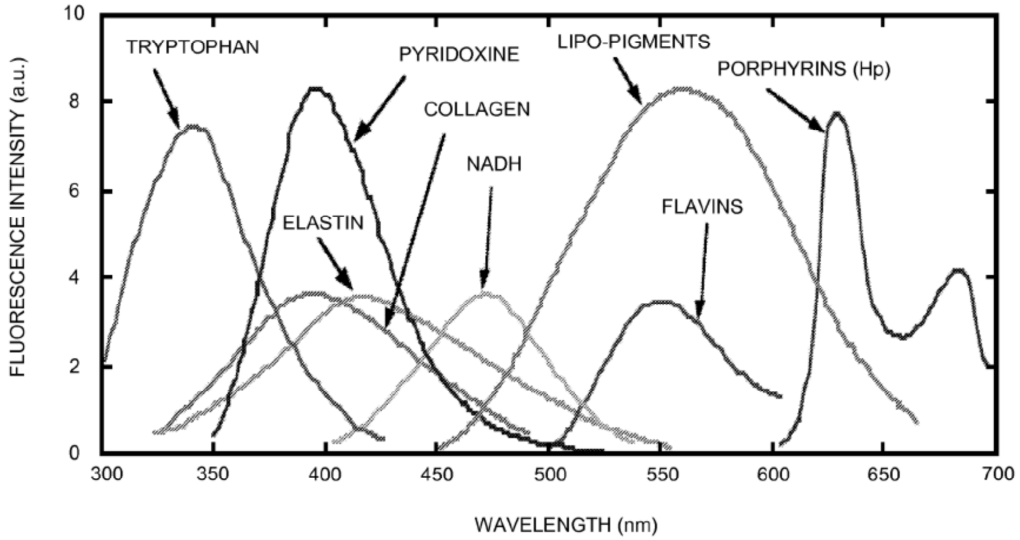

Figure 47 - Fluorescence spectra of tissue biomarkers, from US Pat US 20090137908 A1

If metabolic assessment by MLNDS of a patient is to find meaningful use in the diagnosis of disease then baseline data against which to calibrate any diagnostic conclusion is necessary. The absorption and fluorescence spectra for NADH and NAD+ are known and calibrated to

molar concentration (Figure 45). Nevertheless, there is an absence of published data to inform calibration of the NADH spectroscopic results for normal healthy patients. Numerous experiments have identified unacceptably high variations in LDF and TRO readings, up to 30% of standard deviation from the average value for each parameter reported (Makarov & Rogatkin, 2010). This presents a serious problem for the correct interpretation of data acquired by doctors and seriously limits the prospects for use of this approach in general medical practice. This work aims to overcome this high level of parameter variation by integrating the multiple data available from an integrated multifunctional analysis and the development and assessment of complex relative parameters with the aim of reducing variations and easing the analysis and interpretation of blood flow parameters, tissue oxygen utilisation and fluorescence biomarkers. This approach proposes to use all four of the LAKK-M channels to improve the possibilities to present readily interpretable and meaningful information.

4.2 Experimental methodology

Data collection using the LAKK-M was carried out on Caucasian apparently healthy volunteers (n=3) with low levels of skin pigmentation. The measurements were made from right hand middle finger pulp over a period of 2 weeks with measurements taken 3 times per day. The laser Doppler flowmetry and tissue reflectance oximetry data was collected simultaneously for duration of 3 minutes, followed by detection of the fluorescence spectra all at the same volume sampling point.

4.3 Results and Discussion

Different approaches have been proposed for the calculation if the fluorescence redox ration (FRR). The most straightforward approaches to the calculation of the FRR is to take the ratio of the fluorescence signal for NADH over the signal for flavins:

Equation 4-1

$$FRR = I_{NADH} / I_{flavins}$$

Where, I_{NADH} is amplitude of fluorescence of reduced coenzyme nicotinamide-adenine dinucleotide, $I_{flavins}$ is amplitude of fluorescence of flavoproteins (FAD). Another approach to the calculation FRR parameter is to divide the sum of NADH and flavins signals by the flavins signal amplitude by (Kirkpatrick, Zou, Brewer, Brands, Drezek, & Utzinger, 2005):

Equation 4-2

$$FRR = (I_{NADH} + I_{flavins}) / I_{flavins}$$

Clearly, use of Equation 4-2 will produce a higher FRR result than Equation 4-1 and also reduces, but does not eliminate, the impact of overall amplitude changes which will occur in the emission amplitude due to the fluorescence of lipo-pigments in the FAD range and collagen and elastin in the NADH range. Furthermore, the levels of skin pigmentation (melanin) will have a significant effect, by re-absorption, on any ratio measuring total fluorescence signal as the absorption of melanin is stronger at the NADH peak than the FAD peak meaning the produced ratio will appear lower corresponding to the level of skin pigmentation which is also subject to seasonal variation associated with sun exposure.

Table 9 – Calculation of FRR ratio according to different approaches.

№	Date	A(NADH)	A(flavins)	NADH/FLAV	(NADH+FLAV)/FLAV	FLAV/ NADH
1	23.03.2012	227	97	2.340	3.340	0.427
2	26.03.2012	216	86	2.512	3.512	0.398
3	27.03.2012	277	105	2.638	3.638	0.379
4	28.03.2012	173	68	2.544	3.544	0.393
5	29.03.2012	187	73	2.562	3.562	0.390
6	30.03.2012	222	87	2.552	3.552	0.392
7	31.03.2012	145	62	2.339	3.339	0.428
8	02.04.2012	215	93	2.312	3.312	0.433
9	03.04.2012	208	85	2.447	3.447	0.409
10	04.04.2012	321	134	2.396	3.396	0.417
STD.DEV		50.11	20.59	0.10	0.10	0.02
RSD %		23%	23%	0.013%	0.013%	0.000%

Table 9 shows the results of the calculation using different approaches, in this case the homogeneity of the sample group provided limited variation in the resultant FRR despite significant variance in the raw fluorescence data due to individual sample selection and unavoidable methodology variances. For use in evaluating the developed complex parameters the “classic” FRR with an average value of 2.464 was used. The selection and development of a preferred option for the calculation of FRR, in our opinion, requires further research and technology development to establish a reliable redox index baseline applicable to different cell and tissue types.

The primary data collected is presented in Table 10, below with the calculated standard deviation.

Table 10 - LDF, TRO and LFD primary data

	LDF Channel			TRO Channel						LFD Channel	
№	M, PU	S, PU	kv	M (SO2), %	S, %	kv	M (Vb), %	S, %	kv	A(NADH)	A(flavins)
1	29.1	1.5	5.1	57.5	1.7	3.0	8.7	0.3	3.9	227	97
2	19.8	1.9	9.7	59.7	1.3	2.2	7.2	0.2	2.6	216	86
3	27.1	2.1	7.8	56.3	5.2	9.2	7.2	0.6	8.8	277	105
4	23.4	2.4	10.1	73.0	1.8	2.5	10.0	0.3	3.4	173	68
5	30.3	1.9	6.4	61.4	1.9	3.0	8.7	0.3	3.0	187	73
6	24.7	3.1	12.6	46.8	3.0	6.5	7.6	0.3	4.4	222	87
7	33.7	2.7	8.0	71.2	2.9	4.0	11.2	0.6	5.1	145	62
8	26.3	1.0	4.0	75.7	2.2	3.0	7.5	0.4	5.6	215	93
9	23.7	1.5	6.5	85.4	2.0	2.3	8.3	0.5	6.1	208	85
10	24.1	2.6	10.9	53.1	3.6	6.8	8.0	0.4	5.6	321	134
STD.DEV	4.0	0.6	2.7	11.9	1.2	2.4	1.3	0.1	1.8	50.1	20.6
%RSD	15%	31%		19%	45%		15%	35%		23%	23%

From this data the index of tissue oxygen consumption rate (*U*), parameter which characterises the specific oxygen consumption per unit of blood volume in the tissue region under the optic probe as defined by (Krupatkin, Rogatkin, & Sidorov, 2007) is calculated as:

Equation 4-3

$$U_2=(S_aO_2-S_tO_2)/V_b$$

or can also be expressed in a simplified form;

Equation 4-4

$$U_1=S_aO_2/S_tO_2$$

Oxygen transport in microvasculature and its respiration in the tissue was estimated by another complex parameter: Oxygen Metabolism Efficiency (OME):

Equation 4-5

$$OME = M \cdot U \cdot FRR$$

Where, *M* is average of perfusion units (I_m);

FRR = fluorescence redox ratio.

Table 11 - Resulting Oxygen Metabolism Efficiency (OME)

№	U1	U2	FRR	OME1	OME2
1	1.7	2.4	2.3	116	161
2	1.6	3.9	2.5	81	194
3	1.8	2.7	2.6	125	187
4	1.3	3.2	2.6	80	189
5	1.6	4.3	2.6	125	335
6	2.0	6.3	2.6	128	399
7	1.4	2.4	2.3	108	187
8	1.3	3.1	2.3	80	189
9	1.1	1.5	2.4	67	88
10	1.8	5.6	2.4	107	324
STD.DEV	0.3	1.2	0.1	19.8	76.4
%RSD	18%	42%	5%	22%	42%

U_1 calculated by the formula (Equation 4-4);
U_2 calculated by the formula (Equation 4-3);
FRR calculated by the formula (Equation 4-1);
OME1 calculated using U1;
OME2 calculated using U2;

The calculated results of the parameter U_2 were in a range from 1.5 to 6.3, using the formula in Equation 4 3 with a variance of 42%. This simplified parameter, which does not include the blood volume V_b in its formulation produces a very high variance in the sample

and is therefore a poor complex parameter to use in calculation of the oxygen metabolism efficiency (OME2) which showed the same level of inconsistency and a range of 88 to 324.

The parameter U_1 which includes the factor V_b in its calculation was much stable leading to a reduction in the %RSD from 42% to 22% in OME1 compared to OME2 and a range of 67 to 128 (according to the embodiment to calculate the FRR and U). The cause of the improved stability can be seen for example in No7, where a high LDF arterial perfusion (M,PU) was matched by a high TRO based V_b, thus including the V_b value as a divisor in the calculation of tissue oxygen consumption U_2 (Equation 4-3) account is thereby made in the calculation of the complex parameter for variance in the blood volume of a specific sample volume as would be expected given the variability of vasculature in the dermis.

A multi-parametric indicator of tissue oxygen consumption, oxygen metabolism efficiency (OME) is potentially a generally informative complex parameter for laser based tissue investigation *in vivo* in comparison with primary parameters of blood microcirculation condition. I_m, V_r, S_aO_2, and S_tO_2 are much more variable and demonstrate individual/specific physiological condition of the tissue at in particular time moment.

The results suggest a defined relationship between NADH and FAD suggesting its use as a potentially very stable baseline parameter in the calculation of complex parameters. The complex approach to this allows physicians to receive complementary data about micro-haemodynamic, oxygen consumption and condition of metabolic processes for their interpretation and decision making concerning disease diagnosis. Patient data from different sex, age and health condition is required to establish and validate a baseline OME.

4.4 Analysis of Fluorescence Spectroscopy Parameters of Biological Tissue

Many diseases and other destructive inflammatory processes are accompanied by changes in the fluorescent activity of in the tissues cells as a result of the accumulation or depletion of natural fluorophores: flavin-containing enzyme, NADH, lipofuscin, porphyrins etc. However, to date the clinical use of laser fluorescence diagnostics (LFD) is limited by several unresolved issues.

Many fluorophores are characterised by similar or overlapping regions of absorption and fluorescence see Figure 46 and Figure 47. Consequently, the fluorescence spectrum of tissue is a highly complex. Therefore, it cannot simply be defined by the amplitude of the absorption or emission at the wavelength of the selected fluorophore of interest; we propose that this is one of the major challenges faced by LFD today.

Fluorescence spectroscopy of biological tissue is a complicated process which depends on the temperature, topological heterogeneity and other specific characteristics of each sample, etc. Therefore, the reliability of LFD is affected multiple factors including the availability of data concerning the scattering and absorbing properties of specific tissues in specific conditions, light pollution at optical fibre tip and instrument errors such as excitation source instability, photodetector limitations, light filter precision, grating precision, CCD performance, etc. To achieve clinically significant and reliable results issues of accuracy, convergence and dispersion measurement also need to be addressed.

A number of publications dealt with these issues. For example, in (Rogatkin, Prisnyakova, Moiseeva, & Cherkasov, 1998), the random error was 8-10% for healthy tissue and 30-35% on malignant tissue in a samples size of 30. In (Rogatkin & al, 2013) the reproducibility of

the parameters are reported based on simulated measurements. The relative random error in the measured amplitude of the backscattered radiation on a PTFE phantom was within ± 2-3%, and the in recorded amplitude error of the fluorescence for a specific phantom and selected wavelength was ± 7-8%. The coefficient of fluorescence variability was ± 2-3%. No data could be found on the long-term assessment of LFD parameter variability for healthy tissue. This study aims to fill this gap and to assess individual parameter variability in laser fluorescence diagnosis, and to analyse its potential sources.

Experimental methodology

The study was carried out with the participation of three conditionally healthy volunteers:

V1. a male	35 years of age	(for 9 months)
V2. a male	22 years of age	(for 5 months)
V3. a female	24 years of age	(for 3 months)

The measurements were performed at two points on the skin; skin pads (palmar surface) of the right middle finger, which is in an area rich in arteriolar-venular anastomoses (AVAs), and on the inside of the right forearm which is almost devoid of anastomoses and dominated by nutritional blood flow. All measurements were performed daily at 11:00 am to avoid any influence of circadian rhythms on the blood circulation. The measuring fibre was positioned in the same place, without applying any pressure. Local light pollution and other environmental factors that could possible cause errors were mitigated.

Different excitation wavelengths were used to generate the autofluorescence in the two physical areas of study.

Table 12 – Number of spectral recordings by wavelength and body zone

	Recordings			
	Fingertip			Forearm
Volunteer No.	UV (370nm)	Green (530nm)	Red (630nm)	UV (370nm)
V1	120	20	50	80
V2	40	-	50	-
V3	30	-	30	-

An LAKK-M multifunctional laser non-invasive diagnostic system was used in the research as described in section 2.10, LAKK-M MLNDS, page 67. Typical skin fluorescence spectra generated by the LAKK-M using the three laser wavelengths indicated are overlaid and shown in Figure 48.

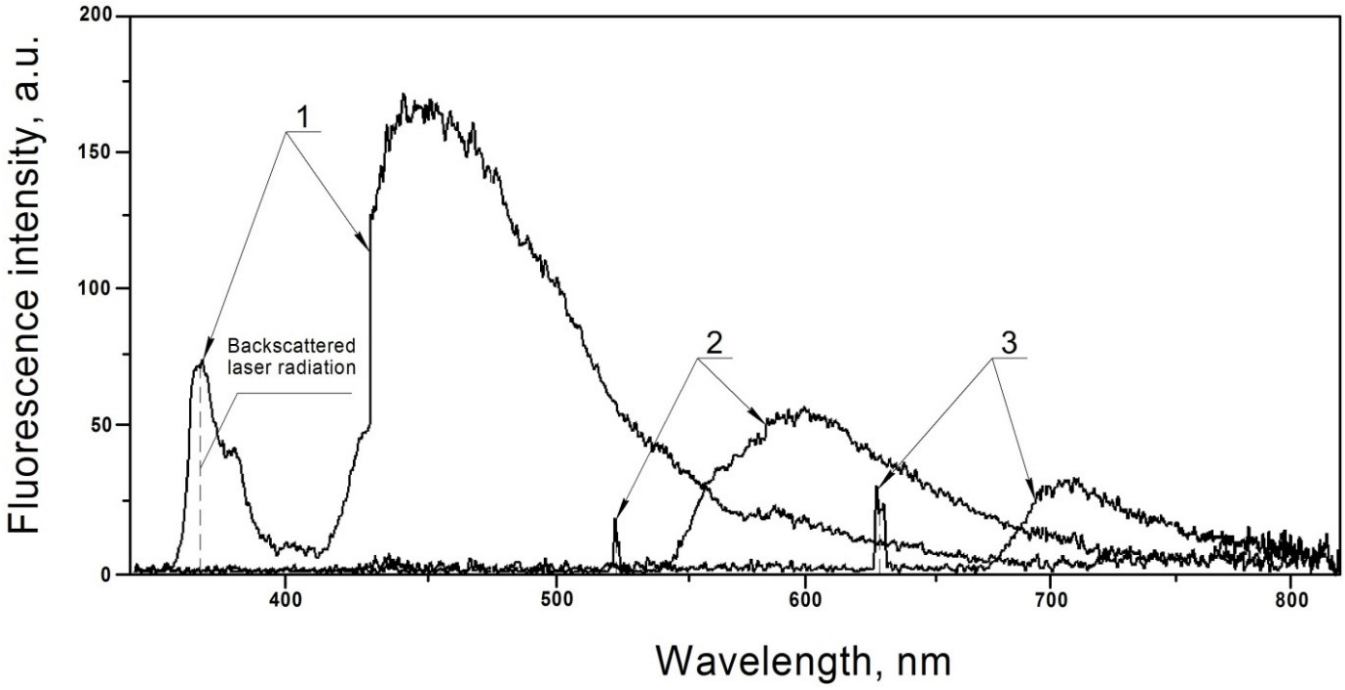

Figure 48 – Fluorescence spectra for endogenous fluorophores in the skin at 370 nm (1), 530 nm (2) and 630 nm (3).

By analysing the amplitude of the intensity at the maximum of the fluorescence spectrum $I(\lambda)$ for different wavelengths used and the intensity of the backscattered radiation $I_{bs}(\lambda)$ we can calculate the coefficient of the fluorescent contrast CFC and the fluorescence redox ratio (FRR).

The CFC was calculated using two different approaches for the UV wavelength which produces two difference coefficient ranges, 0-1 and 0-2. The fluorescent contrast ratio for red and green is calculated as:

Equation 4-6

$$CFC = k_f(\lambda) = 1 + \frac{I_f(\lambda) - I_{bs}(\lambda)}{I_f(\lambda) + I_{bs}(\lambda)}$$

Where, $I_f(\lambda)$ represents registered fluorescence intensity at wavelength λ and $I_{bs}(\lambda)$ represents the maximum intensity of the backscattered laser radiation.

Using Equation 4-6 the coefficient of the fluorescent contrast will be in the range of 0 to 2. The CFC was calculated using Equation 4-6 for the compounds reference peak at the wavelengths shown in Table 13 – Reference wavelengths used for tissue fluorophores Table 13. Two sets of reference wavelengths were examined and used in the algorithms for UV, from published fluorescence data, when applying Equation 4-7, below:

Equation 4-7

$$k_f{}^*(\lambda) = \frac{I_f(\lambda)}{I_f(\lambda) + I_{bs}(\lambda)}$$

As with Equation 4-6, the CFC according to this equation will be between 0 and 2.

Table 13 – Reference wavelengths used for tissue fluorophores

	Excitation beam		
Compound	UV_{b1} – Eqn. 4.6	UV_{b2} – Eqn. 4.7	Green
Collagen	420	422/433	
Elastin	450	422	
NADH	490	466/494	
Keratin		466	670
Pyridoxine	525		
FAD		555	
Lipofuscin	570	605	570
Carotene	608		608
Porphyrins		635/704	648/680/710

UV_{b1} =biomarker fluorescence lines b1; UV_{b2} = biomarker fluorescence lines b2

The fluorescence redox ration (FRR) was calculated according to Equation 4-2, page 128.

The arithmetic mean, Mn, of the parameters were calculated over the study period, and from the standard deviation, σ, of Mn the coefficient of variation or relative scatter of measurements δ taken as a percentage of the average, Mn.

4.5 Results and Discussion

Histograms showing the recorded fluorescence intensities (Figure 49 to Figure 52 and the calculated coefficients of fluorescence contrast using Equation 4-6 and Equation 4-7 for the panel of biomarkers defined by the fluorescence wavelengths in Table 13, for surface pad of the middle finger (high AVA zone) of the three volunteers. Results of calculating the coefficients of variation (scatter measurements) for fluorescence intensity and coefficient of the fluorescent contrast for this case are presented in the summary Table 14.

Reasonable homogeneity can be seen between the different individuals in terms of the relative differences between biomarkers using both sets of fluorescence lines in these high AVA zones.

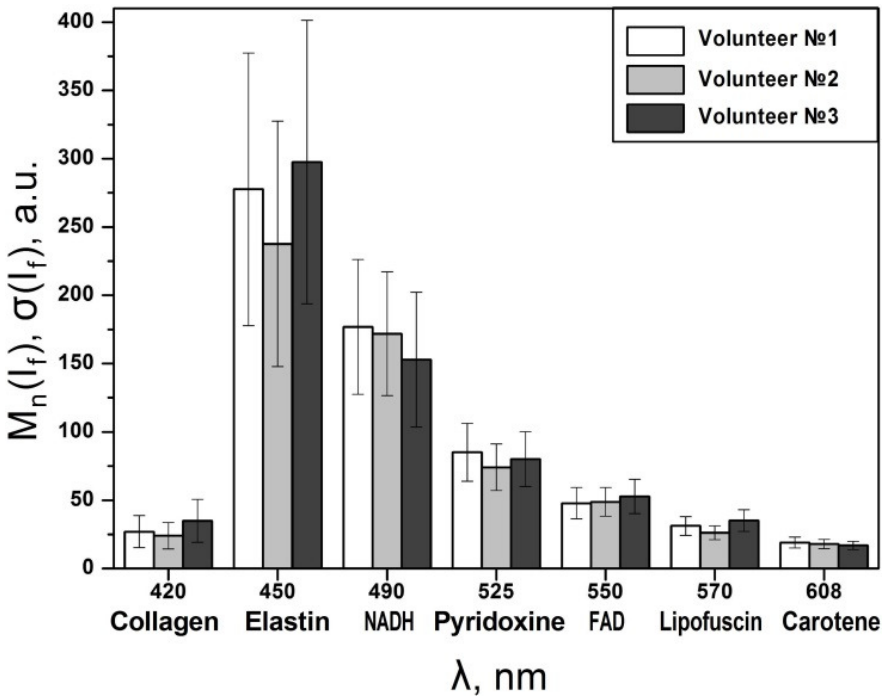

Figure 49 – Histogram plot of average UV stimulated fluorescence amplitude difference δI_f with error bars for selected biomarker wavelengths UV_{b1}

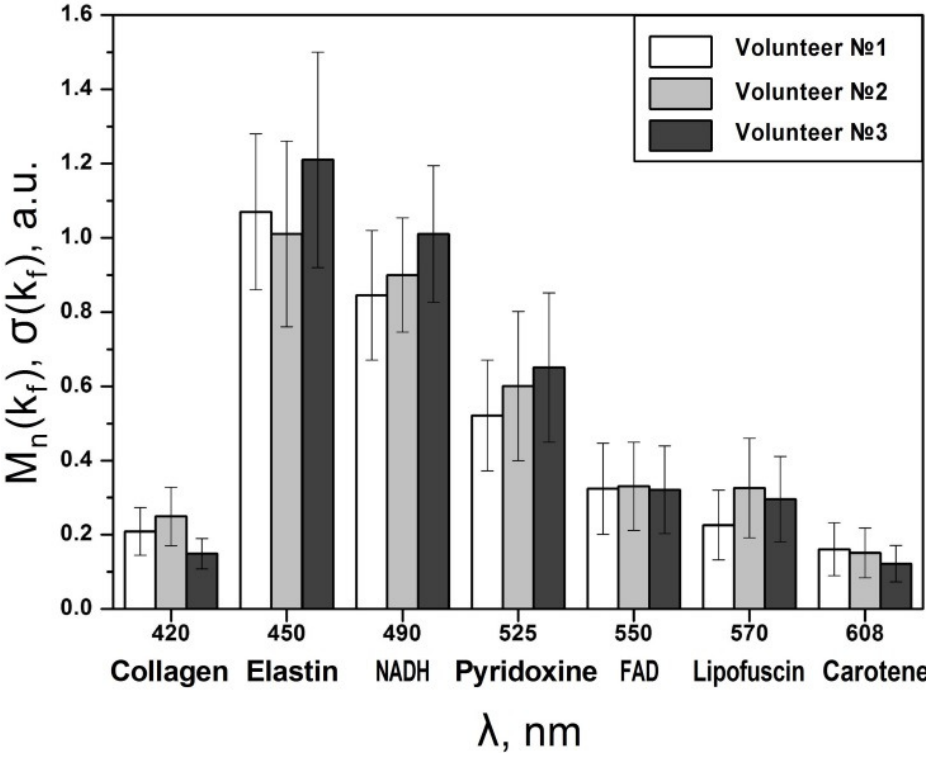

Figure 50 - Histogram plot of average coefficient of fluorescence contrast k_f with error bars for selected biomarker wavelengths UV_{b1}

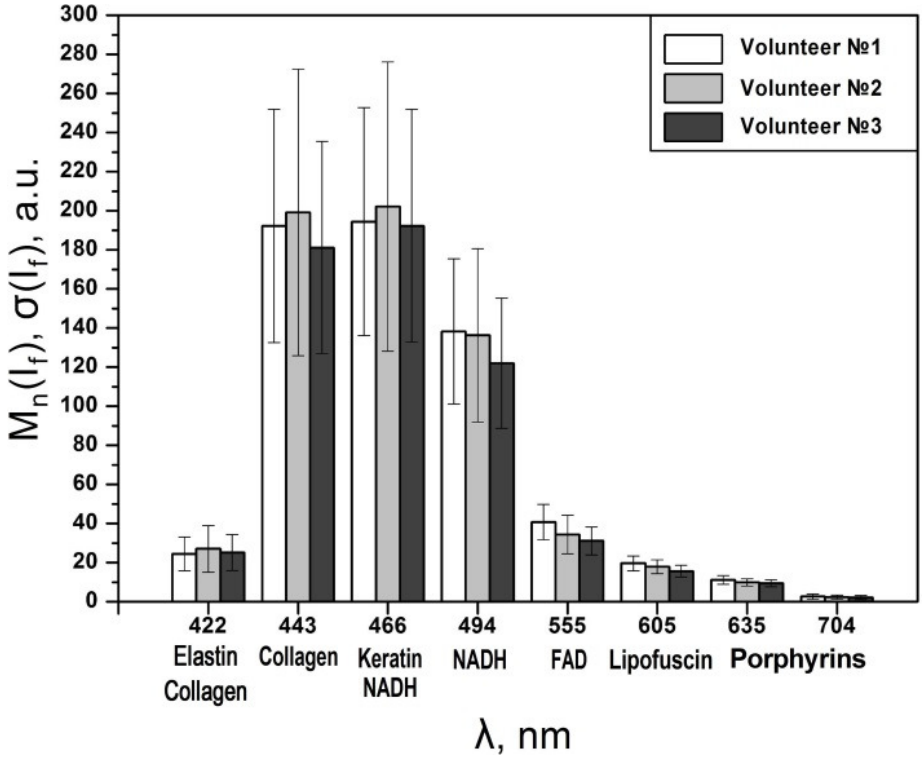

Figure 51 - Histogram plot of average UV stimulated fluorescence amplitude difference δI_f with error bars for selected biomarker wavelengths UV_{b2}

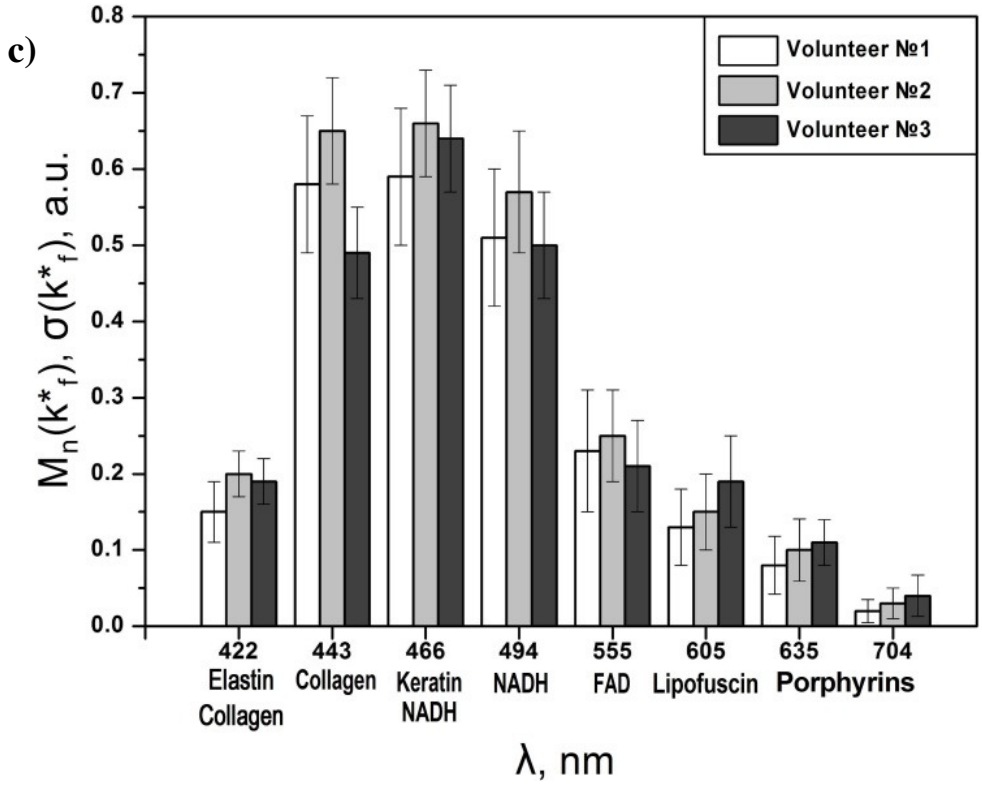

Figure 52 - Histogram plot of average coefficient of fluorescence contrast k^*_f with error bars for selected biomarker wavelengths UV_{b2}

Table 14 – The coefficients of variation for the fluorescence intensities If(λ)and coefficients of the fluorescent contrast kf(λ) and k*f(λ) for the area with the AVA

Type biomarker	λ, nm	Volunteer No					
		1	2	3	1	2	3
		δ (I_f), %			δ (k_f), %		
Collagen	420	43,42	40,51	44,93	30,62	31,73	27,52
Elastin	450	35,95	37,79	34,88	19,63	24,75	23,97
NADH	490	27,91	26,39	32,29	20,71	17,11	18,22
Pyridoxine, 525	525	24,84	23,11	25,14	28,60	33,44	30,88
FAD, 550	550	24,09	21,54	23,70	37,96	35,95	36,76
Lipofuscin	570	22,30	19,34	22,61	41,59	41,10	38,85
Carotene	608	21,15	18,99	17,75	44,10	44,37	40,16
		δ (I_f), %			δ (k_f*), %		
Elastin and Collagen	422	35,56	44,13	36,48	26,67	15,00	15,79
Collagen	443	31,02	36,80	29,95	15,52	10,77	12,24
Keratine/NADH	466	30,01	36,58	30,96	15,25	10,61	10,94
NADH	494	26,88	32,54	27,31	17,65	14,04	14,00
FAD	555	22,13	28,73	22,89	34,78	24,00	28,57
Lipofuscin	605	19,39	19,80	19,21	38,46	33,33	31,58
Porphyrins	635	19,17	18,72	18,88	47,50	41,00	27,27
Porphyrins	704	49,24	47,33	49,77	75,00	66,67	67,50

A comparison of the data presented in the analysis shows that the relative variation of measurements between the three individual volunteers are low. Depending on the biomarkers fluorescence line, the difference in recorded intensity varies mostly in the range from 20 to 40% and the coefficient of the fluorescent contrast from 10 to 45%.

Significant larger variances rates of 50% and 70% for I_f and k_f* respectively were calculated for the porphyrins emission wavelength of 704 nm, which has been used recently by some authors (Smirnova, Rogatkin, & Litvinova, 2012) and is also a factor used in the LAKK-M analysis algorithms. This could be due to spread of the SHG spectrum of the laser (about 730 nm), which is also an instrumental artifact of the LAKK-M. However, normally this SHG peak

does not spread as far as 704nm and it seems more likely that there is some other factor causing the large variance at this spectral line.

Histograms showing the recorded fluorescence intensities If and the calculated coefficients of fluorescence contrast kf using Equation 4-6 and Equation 4-7 for the panel of biomarkers defined by the fluorescence wavelengths in Table 13, for inner forearm skin (low AVA zone) of the three volunteers. Results of calculating the coefficients of variation (scatter measurements) for fluorescence intensity and coefficient of the fluorescent contrast for this case are presented in the summary Table 14.

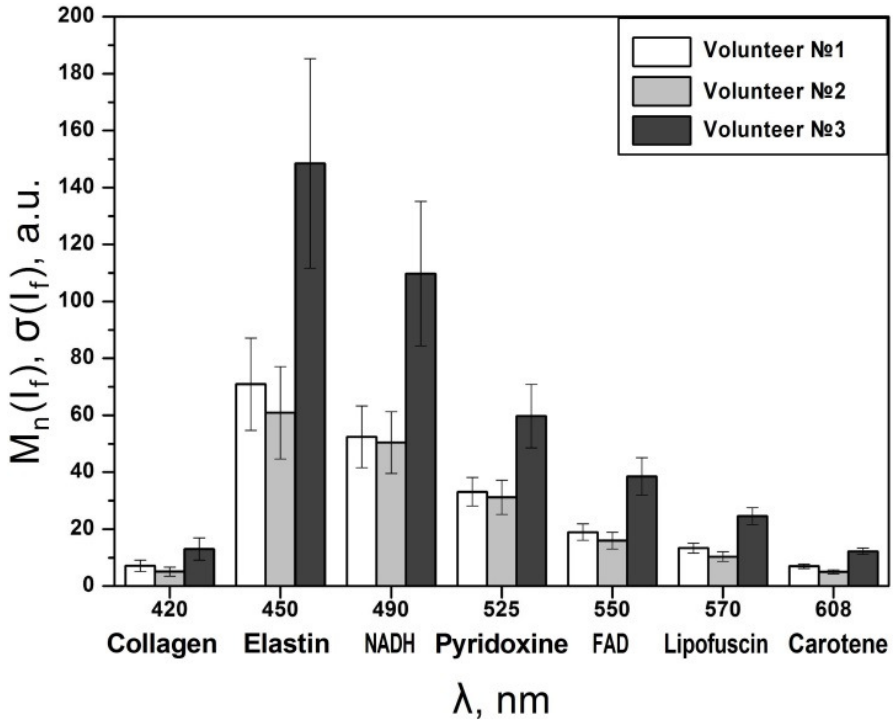

Figure 53 - Histogram plot of average UV stimulated fluorescence amplitude δ I_f difference with error bars in zone of low AVA for selected biomarker wavelengths UV_{b1}

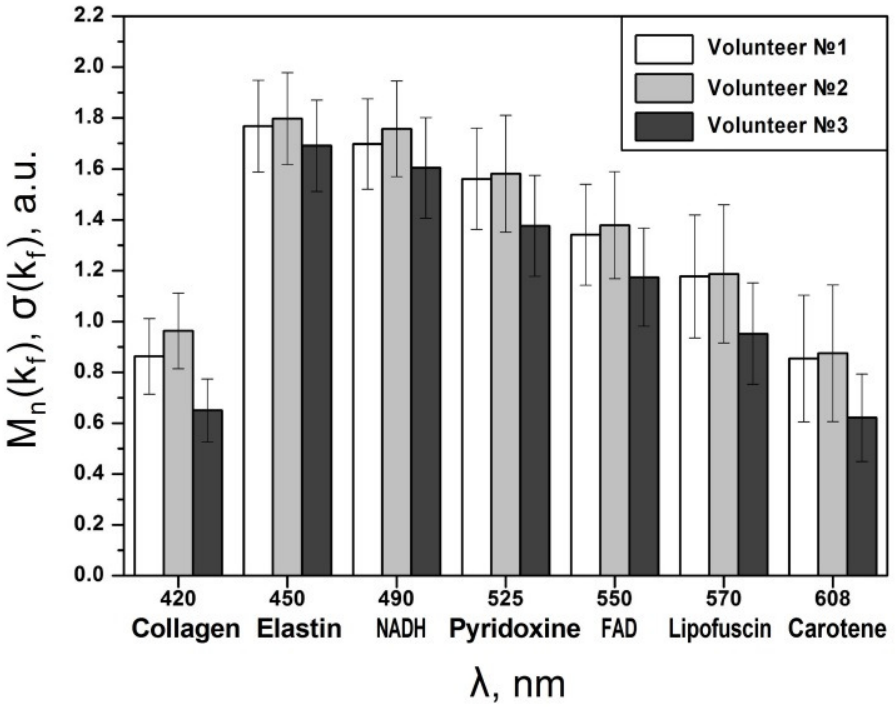

Figure 54 - Histogram plot of average coefficient of fluorescence contrast k_f with error bars in low AVA zone for selected biomarker wavelengths UV_{b1}

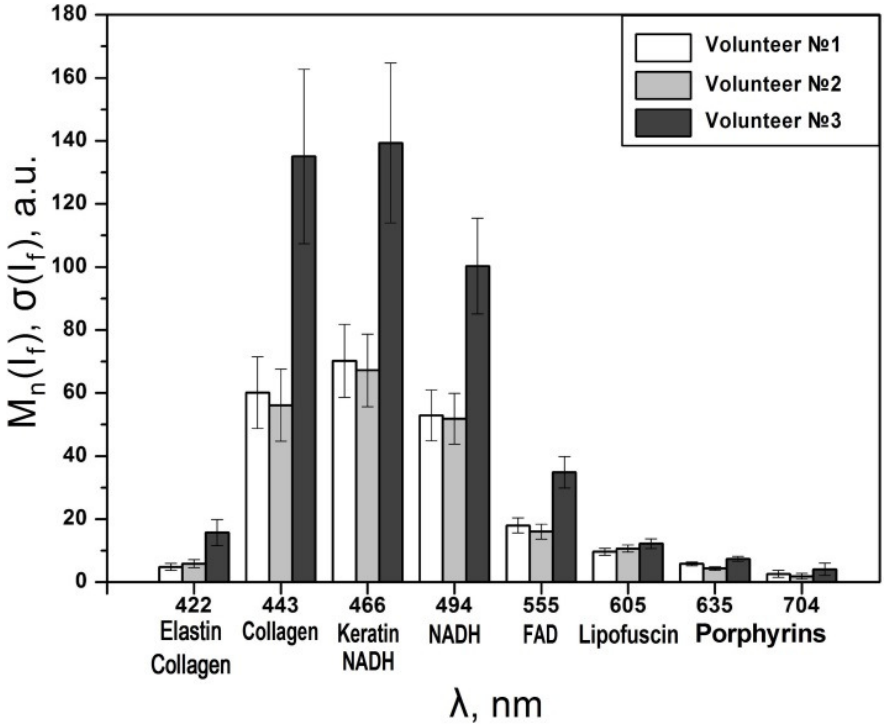

Figure 55 - Histogram plot of average UV stimulated fluorescence amplitude δ I_f with error bars in low AVA zone for selected biomarker wavelengths UV_{b2}

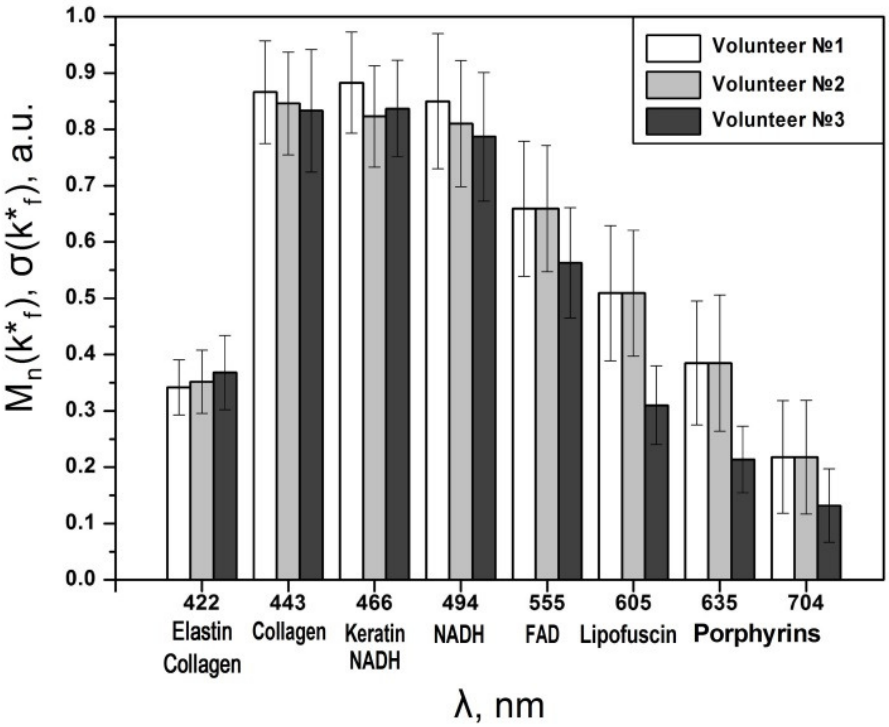

Figure 56 - Histogram plot of average coefficient of fluorescence contrast k^*_f with error bars in low AVA zone for selected biomarker wavelengths UV_{b2}

Table 15 - The coefficients of variation for the fluorescence intensities $I_f(\lambda)$and coefficients of the fluorescent contrast $k_f(\lambda)$ and $k^*_f(\lambda)$ for the area without the AVA

Type biomarker	λ, nm	№ volunteer					
		1	2	3	1	2	3
		δ (I_f), %			δ (k_f), %		
Collagen	420	28,07	31,25	29,94	17,27	15,47	19,08
Elastin	450	22,90	26,66	24,79	10,18	10,01	10,64
NADH	490	20,62	21,43	23,10	10,48	10,69	12,34
Pyridoxine, 525	525	15,14	19,32	18,67	12,75	14,55	14,46
FAD, 550	550	15,44	18,34	16,88	14,84	15,23	16,44
Lipofuscin	570	12,92	16,68	11,99	20,56	22,91	20,90
Carotene	608	10,24	14,39	9,037	29,16	30,74	27,65
		δ (I_f), %			δ (k_f*), %		
Elastin and Collagen	422	23,21	22,15	26,57	14,33	15,91	17,93
Collagen	443	18,96	20,31	20,47	10,51	10,76	13,09
Keratine/NADH	466	16,43	17,17	18,20	10,19	10,94	10,27
NADH	494	15,26	15,56	15,12	14,12	13,83	14,49
FAD	555	13,32	14,98	14,35	18,21	17,00	17,41
Lipofuscin	605	11,38	10,31	12,34	23,58	22,00	22,58
Porphyrins	635	9,94	13,38	10,95	28,57	31,43	27,57
Porphyrins	704	42,45	48,38	46,92	45,87	46,33	49,24

The relative spread of the measurement results for the forearm was 30% to 50% less than for surface pad of the finger. This confirms the strong influence of the volume of blood in the tissue volume and the significance of blood vessels in the individual variability in the properties of biological tissues. Clearly, the skin blood circulation is one of the main factors affecting the measurement results in the LFD.

Comparing the results for V3 in Figure 53 and Figure 54 clearly demonstrates the advantage of using data analysis to produce the coefficient of the fluorescent contrast which brings the level of variation in the result much lower in comparison to using the conventional difference in absolute values of the intensity of fluorescence. Furthermore, V3 also provides evidence of the normalisation of the differences in fluorescence intensities recorded with

high levels of backscattered radiation likely caused by the influence of increase blood supply in the tissues studied. This could be a route to allow comparison of the relative levels of the biomarkers in a variety of biological tissues and in different patients.

To further assess the potential utility of Equation 4-6 to reduce inconsistency a similar study was performed on V1 with green and red fluorescence excitation wavelengths. The results of statistical processing of the data obtained are shown in Table 16.

Table 16 - Statistical evaluation of the results of measurements of fluorescence for the green and red excitation wavelengths

Excitation wavelength, nm	Compound	Fluorescence λ, nm	The recorded fluorescence intensity I_f (λ)			The coefficient of fluorescent contrast k_f(λ)		
			M_n	σ	δ, %	M_n	σ	δ, %
530	Lipofuscin	570	35,21	13,45	38,20	1,87	0,54	28,89
	Carotene	608	55,76	16,18	29,02	1,92	0,44	22,92
	Porphyrins	640	38,85	9,12	23,48	1,89	0,36	19,05
	Porphyrins	680	18,66	4,73	25,35	1,78	0,39	21,91
630	Keratin	670	0,84	1,14	134,92	0,03	0,05	143,85
	Porphyrins	710	25,41	15,34	60,37	0,81	0,35	43,21

The results indicate that the relative variation is minimal at certain wavelengths. The high variability of the parameters at the 670nm keratin wavelength clearly makes its use problematic. These results should be considered when standardising the spectrometric algorithms used in MLNDS. It is notable that the intensity was very low at this wavelength which is likely the root cause of the high variability which is likely due to system noise.

Analysis of the distribution of the recorded results in the fluorescence spectra for all three volunteers showed that the distribution of the deviation in the fluorescence intensity and fluorescence contrast ratio for UV excitation is generally normal. The exception is the

fluorescence wavelength of 704 nm where the distribution is not consistent, and for which there was the greatest range of results.

Figure 57 shows an example of the resulting density values the fluorescence intensity and the coefficient of the fluorescent contrast of NADH fluorescence at a wavelength of 494 nm for V1. Distribution for NADH is truncated normal distribution, this may be due to the limited range of possible values.

Both criteria with a confidence level of 0.95 serve to confirm the normalizing effect on the selected distributions. More generally, we can conclude that the distribution of fluorescence parameter may also depend on parameters such as the individual characteristics of the studied tissues, the specific type of fluorophore and so on. Technical factors such as irregular photodetector sensitivity in the reception endogenous fluorescence spectra should also be considered.

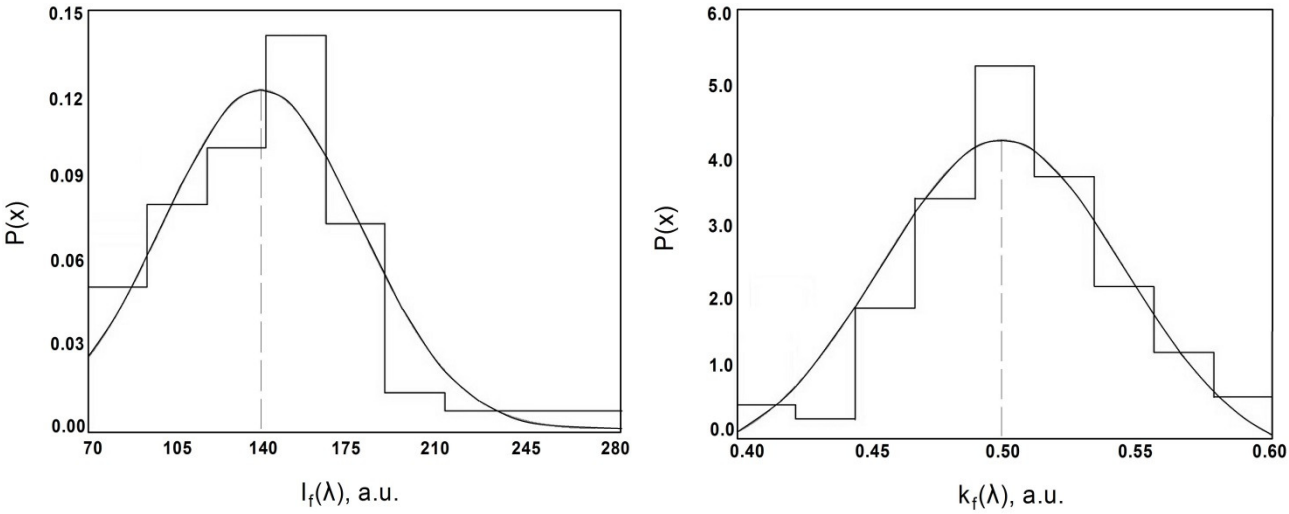

Figure 57 - The probability density distribution *P*(*x*) values of fluorescence intensity (a) and coefficient of the fluorescent contrast (б) to NADH

Clearly, the larger the coefficient of variation, the greater spread and lower the relative uniformity of the recorded values will be. If a coefficient of variation of less than 33% is considered indicative of data uniformity, then the individual data of variability measured by foregoing calculated fluorescence spectroscopy parameters can be considered acceptable for most biomarkers studied for diagnostic purposes.

The fluorescence redox ratio (FRR) for three volunteers was calculated using the classic FRR formula Equation 4-1.

V1 = 3,1 ± 0,75; V2 = 2,9 ± 0,71 V3 = 3,3 ± 0,74

The spread of the values obtained for all three volunteers did not exceed 25%.

Different sources suggest different formulae for redox-ratio calculations. In (Skala, et al., 2007) it is proposed to use the ratio of the fluorescence intensity of FAD over NADH, as used here. In (Quan-Liu & et.al., 2011) the redox ratio is defined as the ratio of the fluorescence intensity of FAD over the sum of the fluorescence intensities of FAD and NADH. Regardless

of these differences in redox ratio calculation the main issue remains the inconsistency of auto-fluorescence spectral amplitude at wavelengths of fluorophores of interest when using different excitation source wavelengths. Figure 58 illustrates the difference when using various excitation sources with the fluorescence excitation spectra when pumped with UV (370 nm) and blue (450nm) light. The FAD detection fluorescence wavelength is shown by the dotted lines moving from 550 nm with UV excitation to 510 nm when excited with blue light.

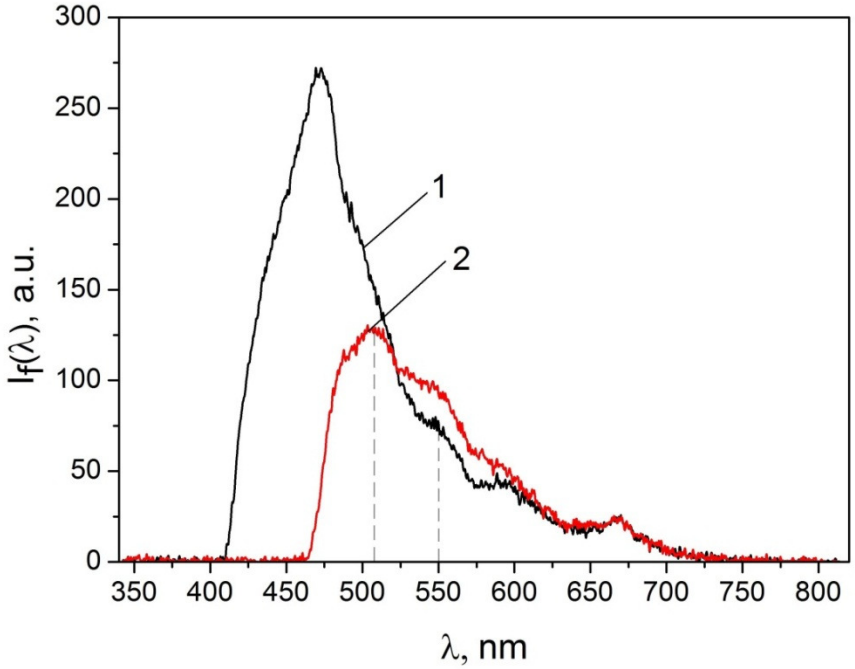

Figure 58 - Example of the fluorescence spectra excitation UV (1) and blue light (2)

It has been reported by (Bottiroli, et al., 1995) and (Tuchin, 2002) that the fluorescence of FAD is more accurately detected in the UV excitation wavelength.

4.6 Influence of blood on backscattering and LFD

The foregoing results have clearly suggested that the intensity of the backscattered radiation is highly dependent on the blood supply to the skin which is likely to change during pathological processes in tissues, and thus provide additional diagnostic information.

To assess the nature of this effect a sample of 30 daily measurements in V1 from the two study zones of the skin was collected to assess the intensity of backscattered radiation Ibs (Equation 4-6) relative to the volume of capillary blood supply to tissues Vb (TRO channel). The results are plotted in Figure 59.

As can be seen, the intensity of the backscattered radiation is inversely related to the blood supply to tissues for both zones of the skin. This is more clearly evident in the AVA region as would be expected.

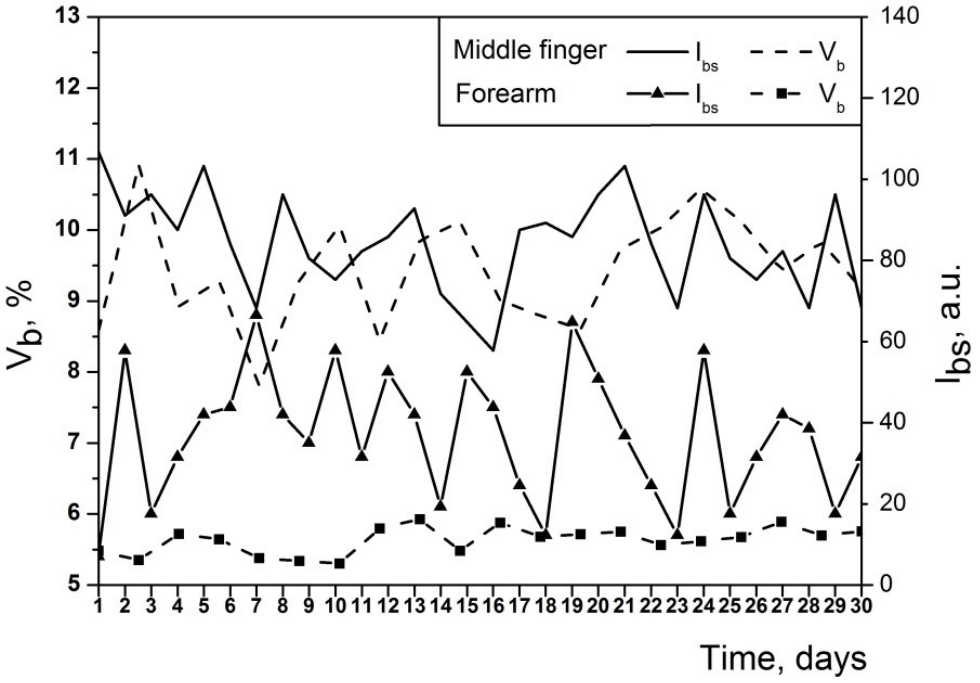

Figure 59 - Graphs parameter changes $I_{bs}(\lambda)$ and V_b for the two zones of the skin for V1

4.7 Melanin absorption

A further confounding factor in the calculation of FRR is the individual to individual variation in skin colour. It is generally known that the higher level of melanin in coloured skin has a significant impact on the ability of LFD to detect fluorophores of interest in LFD due to the increasing levels of absorbance by melanin across the visible spectrum. Nevertheless, MLNDS algorithms have not taken account of the fact that the absorbance varies significantly between for example the NAHD and FAD fluorescence lines.

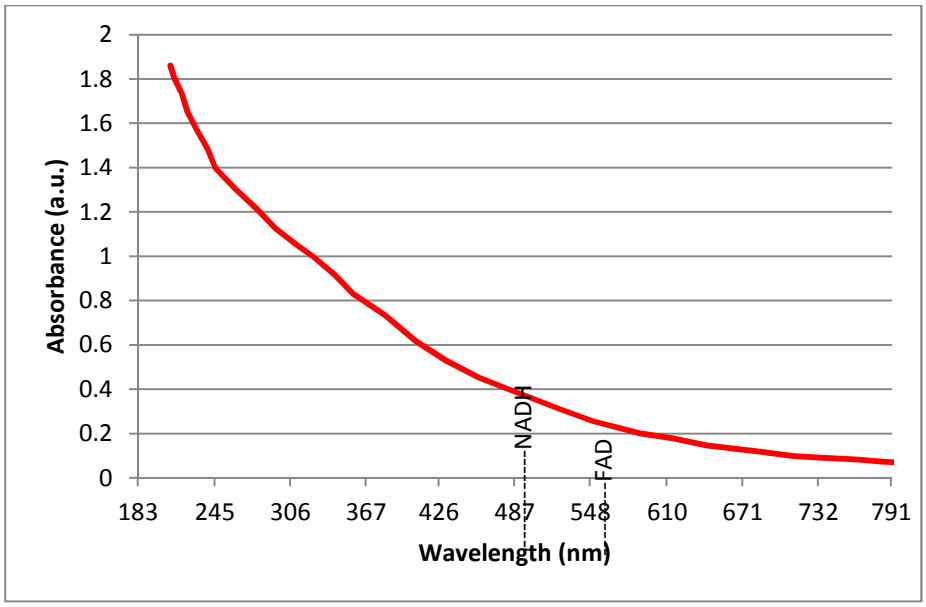

Figure 60 – Absorption spectra of melanin and fluorescence bands of NADH and FAD
(Adapted data from http://www.spectra.arizona.edu/)

It can be seen from Figure 60 that the absorption of the NADH auto-fluorescence by melanin is approximately 60% higher than at the FAD fluorescence band. To confirm this dependence of the fluorescence signal on the pigmentation of the skin, experimental results were gathered from a female 25 year old with dark skin. Measurements were carried out, as previously, in the two zones of the skin: a weakly pigmented finger pad and forearm area with a high content of melanin. The results are shown in Fig. 9.

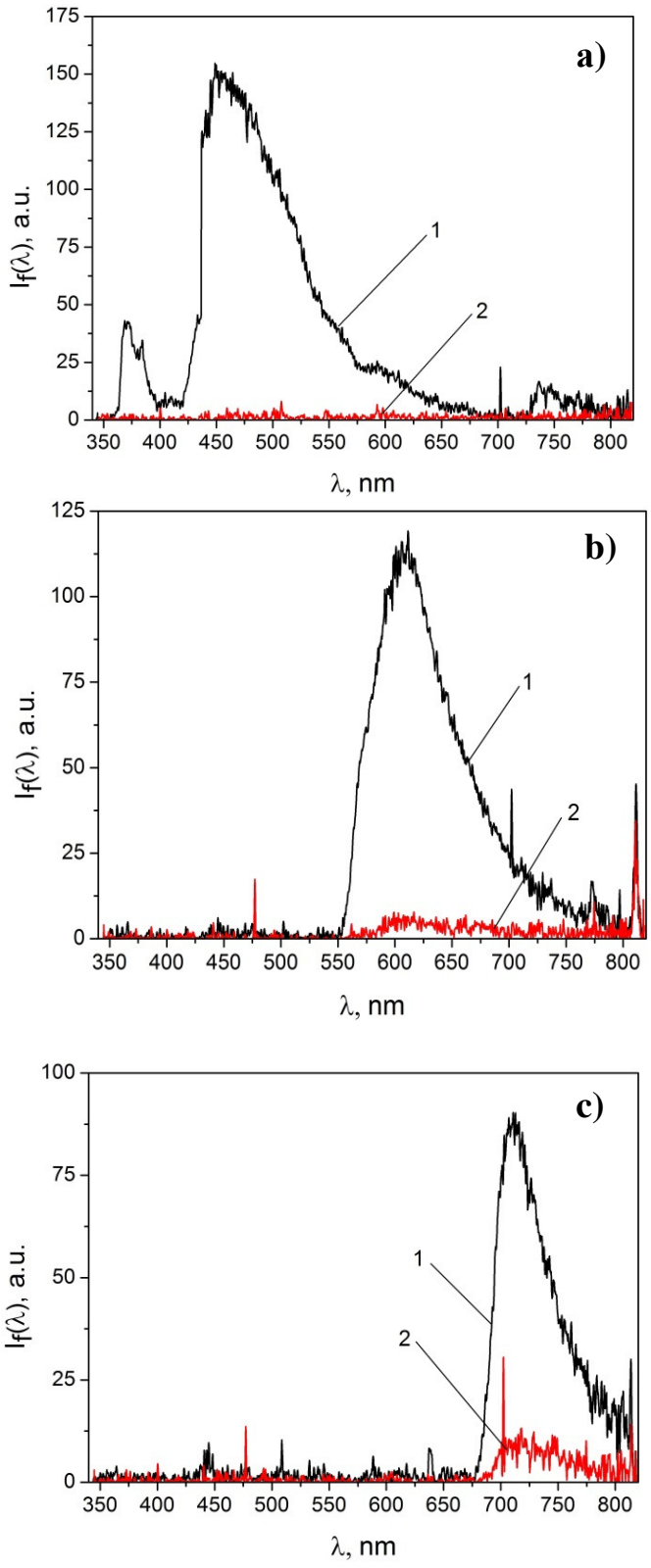

Figure 61- Examples of the fluorescence spectra: the UV light excitation (a), green (b) red and (c) wavelengths; 1 – the middle finger pad; 2 – forearm

The results clearly show the near 100% absorption of the visible spectrum in the pigmented skin area compared to the informative fluorescence spectra obtained in the un-pigmented zone. Nevertheless, a weakly informative fluorescence spectra was obtained in the pigmented zone using the red excitation laser as a result of the weaker melanin absorption in this region. Thus, it is possible to conclude that dermal spectroscopy can be potentially useful in the assessment of differences in melanin content of skin pigmentation changes in vivo and furthermore, that such data can potentially be of utility in calculating, using appropriate algorithms, the corrected relative amplitude of auto-fluorescence signals. Currently, the red spectral region is used in MLNDS for the detection of porphyrin fluorescence. The results above show that highly pigmented skin auto-fluorescence is highly dependent on the wavelength of excitation, which requires further detailed study.

Conclusions

These experimental studies have provided values collected over long-term periods for the individual variability (generally up to 30%) based on directly measured values of the endogenous fluorescence intensities and calculated the relative parameters: the coefficient of the fluorescent contrast and fluorescence redox ratio. One of the main factors affecting the variability distribution of the measurements has been shown as the level of blood in the analysed tissue volume. It is also shown that the probability density of the intensities of fluorescence and fluorescent contrast ratio for most investigated biomarkers are normal.

The results obtained should be considered when developing new integrated medical and biological parameters or measurement techniques and algorithms, as well as addressing

specific diagnostic problem in clinical practice. The presented results demonstrate the relevance of the MLNDS technology in general and in particular the importance of the instrument and its software.

4.8 KO Animal Metabolism Preliminary Study

The group of Glutathione S-transferases (GSTs) enzymes perform a catalytic role in cell detoxification acting as a catalyst for the reaction of compounds with glutathione reductase. Mitochondrial glutathione is critical to cell vitality, and is a crucial antioxidant defence system within the mitochondria. Defects in GSTs have been associated with mitochondrial dysfunction and oxidative stress. Glutathione S-transferase pi (GSTP) such a detoxifying enzyme displaying important defensive roles against the accumulation of reactive metabolites by regulating several processes including S-glutathionylation, modulation of glutathione levels and control of kinase-catalytic activities.

In work aimed at revealing the endogenous role(s) of GST pi a mouse strain completely deficient in the expression of this enzyme has been created by homologous recombination in embryonic stem (ES) cells to inactivate both murine GST Pi genes (Henderson, McLaren, Moffat, Bacon, & Wolf, 1998) which was made available for this MLNDS research. This provides a unique animal model with which to study *in vivo* and compare against wild-type mice the metabolic assessment capabilities of the LAKK-M MLNDS.

Research Methodology

In this study we used male C57BL/6 wild-type (n=4) and GSTP knockout mice (n=4). The models were scanned on the surface of the tail, at 1-2 cm from the body. The mice were not anaesthetised and were held by hand to minimise movement (Figure 62). The WT mice were monitored first followed by the GSTP- KO mice. An excitation wavelength of 370nm was used and spectroscopic autofluorescence data was collected for duration of 1 minute.

The methodology applied was relatively crude; however, anesthetising the mice was deliberately avoided as this could affect the metabolism and results. Future work should explore stability of the subject and means of minimising handling anxiety caused during the scan.

Figure 62 – Picture showing scan position on mouse tail and pigmentation level

Results and discussion

The results of this preliminary study are presented in the chart of the spectra of the WT and KO mice, Figure 63 below. A clear auto-fluorescence band is evident in both the regions expected for NADH and FAD. The peak width in both sets of samples at 450-490 nm confirms NADH is the main fluorophore contributing to the fluorescence. The flavin peak at 550 nm is less distinct; however the shoulder after the 550nm flavin peak is confirmation that flavins are a substantial component of the emission in this region. This encourages

future work as the high skin pigmentation and position of the scan has not completely attenuated the autofluorescence signal as may have been anticipated.

It should be noted that the fluorescence signal strength was generally weak. In the spectral region of interest there is an overall increase in signal amplitude from the KO mice in the region from 550nm through to 700nm associated with FAD, lipo-pigments and porphyrins compared to the WT. The increased fluorescence at the flavin 550 nm peak is clear. Table 17 shows the calculated increase was +24% higher in the FAD region compared to a nominal +5% increase in the NADH region. Interestingly, this led to a reduction in the FRR from 1.88 in the WT to 1.60 in the KO model. These results suggest there may be a difference in the metabolic state of the two different models; they suggest there is a higher relative level of the FAD metabolites and that the higher autofluorescence may be a result of a slightly different tissue composition, higher levels of collagen, elastin and lipo-pigment in the KO mice.

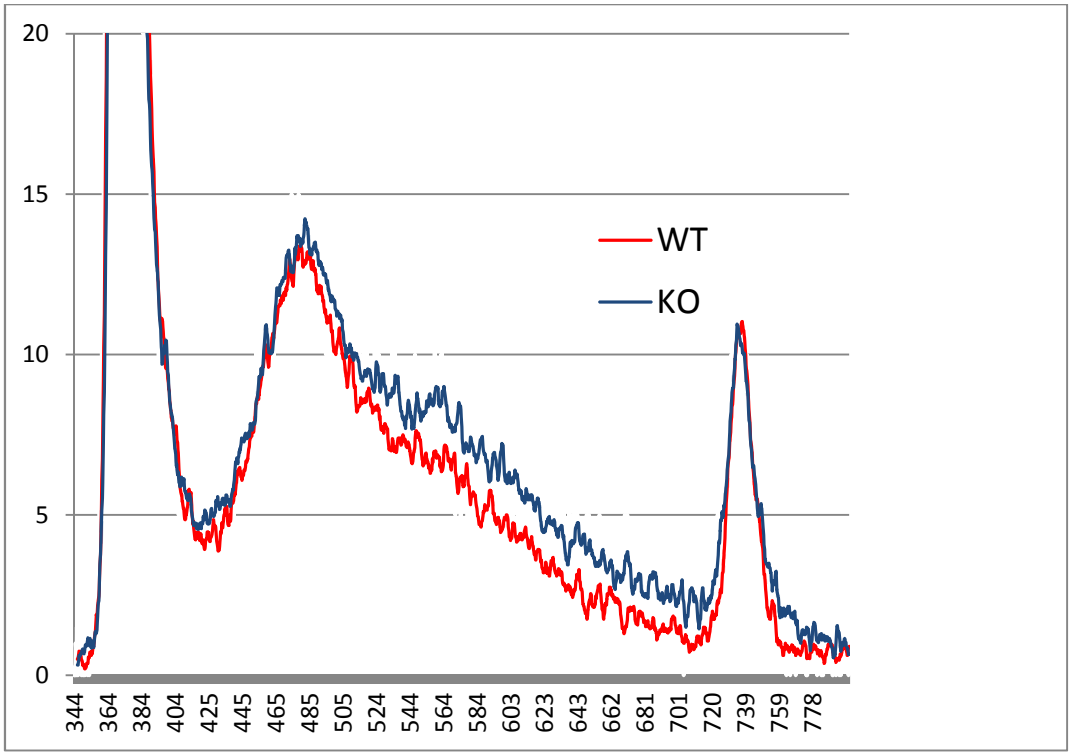

Figure 63 – Fluorescence spectra for WT and GSTP-KO models

The peak at 740 nm is unexpected. This wavelength corresponds to the autofluorescence of chlorophyll, however as this is not a likely source in this case a more likely explanation is second order diffraction from pump wavelength. Biological interactions with light will generally increase in efficiency when the pump wavelength is near to an electronic resonance. In this experiment the absorption peaks of collagen and elastin at 330 nm and 350 nm respectively will strongly absorb the 370 nm excitation wavelength used here.

The results of this preliminary work suggest that based on the small sample size (n=4), GSTP knockout mice may have a slightly altered metabolic status. Compared to the wild-type, GSTP knockout mice have a slightly reduced FRR indicating higher relative levels of FAD and suggesting the metabolic rate limiting process in the mitochondria is the respiratory chain not ADP or oxygen as would be marked by elevated NADH levels. The respiration rate in

these mice could be expected to be higher than in the WT (Mayevsky & Chance, 2007). This would lead us to conclude that while basal oxygen consumption is likely to be lower the mitochondria lacking GSTP1 are respiring at a higher rate in response to stress.

Table 17 – Autofluorescence amplitude and FRR comparison

		Signal amplitude (AU)		Δ A	% Δ A
Fluorescent marker	λ (nm)	WT	KO		
NADH	490	12.44	13.12	0.68	+5%
FAD	550	6.62	8.19	1.57	+24%
FRR		1.88	1.60	-0.28	-15%

Further work in this area might include a monitoring the growth patterns of the KO mice, where slower growth might add weight to the metabolic state changes suggested above. Tissue analysis may also be useful to determine if an increased level of lipo-pigments are present in the KO models corresponding to the modest increase in fluorescence in this region.

Similar conclusions based on the use of MLNDS were found (unpublished) by (Akbar, Sokolovski, Dunaev, Belch, Rafailov, & Khan, 2013) in a study of CVD biomarkers in an *in vivo* mouse model and diet induced CVD group where no differences were observed in structural proteins and a significant change in antioxidant defences suggested altered tissue homeostasis.

4.9 Summary of Chapter 4

This chapter has explored the potential of MLNDS to provide clinicians with useful information on the condition of patients rather than many individual analysis using different spectroscopic tools and technologies. It has shown that many factors need to be taken into account in the development of complex parameters and that an understanding of the limitations of the technology and the complexity of the biological materials and processes it seeks to report on is crucial. Furthermore, it has investigated and demonstrated the potential to assess metabolic function variances in models where such variances might be expected.

Chapter 5 – FUTURE OF MULTI-FUNCATIONAL LASER DIAGNOSTICS

5.1 Light based diagnostics

Light and laser based diagnostics are already well established and routinely used in condition assessment, monitoring and diagnostics throughout the global healthcare sector. Continued advances in photonics and computing in the form of low costs, compact and high speed offer new prospects for biophotonics in the field of research and health. Perhaps of most significance to the future prospects for MLNDS is the development of high performance compact low cost laser sources meaning laser sources previously necessitating expert set-up, operation, maintenance in a laboratory environment will be available in the form of semiconductor chips which at a low cost will individually or in hybrid format, cover virtually any spectral band required for laser diagnostics.

The ageing population and consequent challenges placed on the healthcare system to provide earlier more reliable diagnostics at lower cost and ideally outside of the hospital environment provides a strong social and economic driver for the development of improved diagnostics and higher efficacy therapeutics.

With the possibilities for miniaturisation of technology available today and in the future the possibility of the Star Trek Tricorder as used by Dr McCoy to quickly scan and diagnose patients becomes a serious prospect. Indeed, some devices are already claiming to provide this (Time Tech, 2013) and X Prize Foundation are offering $10M for the individual or team who most accurately diagnoses a set of diseases independent of a healthcare professional (X PRIZE Foundation, 2013).

Figure 64 - Dr. 'Bones' McCoy analyzes a patient's condition with his tricorder in Star Trek Season One, Episode Eight, "Miri." ©Paramount Home Entertainment

5.2 Poly-parametric diagnostics

The challenges in developing accurate and highly predictive diagnostics are not limited to the field of biophotonics. In life sciences research, the concept of "poly-omics" is developing whereby genetics, epigenetics, proteomics and metabolomics have failed individually to deliver the previously hailed solutions to diagnostics. The complexity of life makes the identification of single highly predictive biomarkers unlikely. In the future diagnostics will migrate from the clinic to the home and workplace where advanced technical solutions integrating multiple scientific advances will provide early warning of disease risk and onset.

Biophotonics and MLNDS can certainly play a part in progressing towards that goal. The work presented here suggests that despite the penetration depth limitations of light based technologies insights into the function and condition of biological processes deep inside the body can be gleaned simply from skin based analysis. With further research, it is easy to imagine major global diseases such as CVD, cancer and type II diabetes being detected and diagnosed much earlier, more conveniently and at a lower cost than is possible today.

The work presented here offers a contribution towards these developments, it provides a validated framework and systematic methodology for the theoretical design and potential standardisation of laser diagnostics devices. Moreover, it describes advances in the development of new important biological parameters calculated using complex algorithms to represent biological and physiological processes.

The work highlights opportunities for further work in developing algorithms which measure then represent in software the complexity of light interactions taking place in biological

tissue such as the absorption curves of common biological components and the rhythmic oscillations of microcirculation dynamics. A simple example would be to have a software feedback loop to control the laser power based on the level of melanin being spectroscopically detected. These developments would enable more reliable and less variable calculation of important parameters and potential identification of important biomarkers of human conditions.

To realise this vision combinations of biomarkers likely to demand multiple technology integrations will be essential. In tomorrow's even more connected digital world, real-time data-streaming from implanted diagnostics devices to high power computers running complex poly-parametric diagnostics algorithms informing patients of any significant findings via their mobile communication devices seems a more credible prospect than Dr McCoy's "tricorder".

7 REFERENCES

Aalkjaer, C., & Nilsson, H. (2005). Vasomotion: cellular background for the oscillator and for the synchronization of smooth muscle cells. *British Journal of Pharmacology*, 144: 605-616.

Ahutin, V. (1981). *Biotechnical systems: theory and projecting.* Leningrad: LGU-Press.

Akbar, N., Sokolovski, S., Dunaev, A., Belch, J., Rafailov, E., & Khan, F. (2013). In-vivo non-invasive measurement of skin auto-fluorescnce biomarkers relate to CVD in mice. *Unpublished*.

Allen, T., & Potten, C. (1974). Fine-structural identification and organization of the epidermal proliferative uni. *(1974). Journal of Cell Science*, 15 (2): 291–319.

Amzina, M., Micheev, A., Rogatkin, D., & Sidorov, V. (2005). Combined medical diagnostic system with separated laser-Doppler and reflectance oximeter channels. *Optical Technologies in Biophysics and Medicine* (p. 6163). Saratov: SPIE.

Andersen, P., & Bjerring, P. (1990). Spectral reflectance of human skin in vivo. *Photodermatol. Photoimmunol. Photomed 7*, 5–12.

Anderson, R. R., Parrish, J. A., & Jaenicke, K. F. (1982). Optical properties of human skin. In J. Rogan, & J. Parrish, *The Science Photomedicine* (pp. 147–194). New York: Plenum Press.

Anderson, R., & Parrish, B. (1981). The optics of human skin. *Journal of Investigative Dermatology*, 77(1), 13-19.

Andersson-Engels, S., & Wilson, B. (1992). In vivo fluorescence in clinical oncology: Fundamental and practical issues. *J. Cell Pharmacol. 3*, 48-61.

Arifler, D., Pavlova, I., Gillenwater, A., & Richards-Kortum, R. (2008). Light Scattering from Collagen Fiber Networks: Micro-Optical Properties of Normal and Neoplastic Stroma. *Biophys J. Vol. 92(9)*, 3260-3274.

Bacskai, B., & al, (2002). Alzheimer's disease: What multiphoton microscopy teaches us . *Neuroscientist*, 8(5): p. 386-390.

Barad, Y., Eisenberg, H., Horowitz, M., & Silberberg, Y. (1997). Nonlinear scanning laser microscopy by third harmonic generation. *Applied Physics Letters*, 70(8): p. 922-924.

Bernjak, A., Stefanovska, A., McClintock, P., Owen-Lynch, P., & Clarkson, P. (2012). Coherence between fluctuations in blood flow and oxygen saturation. *Fluctuation and Noise Letters*, 11.

Bernjak, A., Stefanovska, A., Urbancic-Rovan, V., & Azman-Juvan, K. (2005). Quantitative assessment of oscillatory components in blood circulation: classification of the effect of ageing, diabetes and acute myocardial infarction. *Advanced Biomedical and Clinical Diagnostic Systems* (p. 5692). San Jose: SPIE.

Bessonov, A., Kolbas, Y., & Rogatkin, D. (2007). Virtual diagnostic apparatus in medical noninvasive spectrophotometry. *Technology of living systems*, 4(1), 50-57.

BMG Labtech. (2013). *Application Note: Detection of NADH and NADPH with the Omega's High Speed, Full UV/Vis Absorbance Spectrometer.* Retrieved from BMG Labtech: http://www.bmglabtech.com/application-notes/absorbance/spectrometer-nadh-nadph-170.cfm

Bohren, C., & Huffman, D. (1986). Absorption and Scattering of Light by Small Particles. *Mir.* Moscow.

Bottiroli, G., Croce, A., Locatelli, D., Marchesini, R., Pignoli, E., Tomatis, S., et al. (1995). Natural fluorescence of normal and neoplastic human colon: a comprehensive ex vivo study. *Lasers in Surgical Medicine*, 16, 48-60.

Bouama, B., & Tearney, G. (2002). *Handbook of Optical Coherence Tomography.* New York: Dekker.

Bracic, M., & Stefanovska, A. (1998). Wavelet-based analysis of human blood-flow dynamics. *Bulletin of Mathematical Biology*, 60(5), 919-935 .

Bronzino, J. D. (2000). *The Biomedical Engineering Handbook.* Florida: CRC Press.

Cheong, W. F., & Prahl S.A., W. A. (1990). A review of the optical properties of biological tissue. *IEEE J. Quant. Electr.*, 26(12) 2166–2185.

Coca, D., Zheng, Y., Mayhew, J., & Billings, S. (1998). Non-linear analysis of vasomotion oscillations in reflected light measurements. In A. Hudetz, & D. Bruley, *Oxygen Transport to Tissue Xx.* New York: Plenum Press Div Plenum Publishing.

Coca, D., Zheng, Y., Mayhew, J., & Billings, S. (2000). Nonlinear system identification and analysis of complex dynamical behavior in reflected light measurements of vasomotion. *International Journal of Bifurcation and Chaos*, 10, 461-476.

Colquhoun, D., Tucker-Schwartz, J., Durieux, M., & Thiele, R. (2012). Non-invasive estimation of jugular venous oxygen saturation: a comparison between near infrared spectroscopy and transcutaneous venous oximetry. *Journal of Clinical Monitoring and Computing*, 91-98.

Cvijetic, M. (2004). *Optical Transmission Systems Engineering.* Artech House.

Cysewska-Sobusiak, A. (2000). Metrological problems with noninvasive transillumination of living tissues. *Light and Optics in Biomedicine* (pp. 15-24). Bellingham: SPIE.

Czichos, H., Saito, T., & Smith, L. (2011). *Springer Handbook of Metrology and Testing.* Berlin: Springer-Verlag.

de Boer, J., Milner, T., & Nelson, J. (1999). Determination of the depth-resolved Stokes parameters of light backscattered from turbid media by use of polarization-sensitive optical coherence tomography. *Optics Letters*, 24(5): p. 300-302.

de Boer, J., Milner, T., van Gemert, M., & Nelson, J. (1997). Two-dimensional birefringence imaging in biological tissue by polarization-sensitive optical coherence tomography. , *Optics Letters*, 22(12): p. 934-936.

Dell, E., & Ganske, F. (2008, May). *Detection of NADH and NADPH with the Omega's High Speed, Full UV/Vis Absorbance Spectrometer.* Retrieved from www.bmglabtech.com: www.bmglabtech.com

Denk, W., & al, e. (1990). 2-Photon Laser Scanning Fluorescence Microscopy. *Science*, 248(4951): p. 73-76.

Dunaev, A., Sidorov, V., Stewart, N., Sokolovski, S., & Rafailov, E. (2013). Laser reflectance oximetry and Doppler flowmetry in assessment of complex physiological parameters of cutaneous blood microcirculation," in Proc. SPIE 8572, . *Advanced Biomedical and Clinical Diagnostic Systems XI* (p. 857205). San Francisco: SPIE.

Dunaev, A., Zherebtsov, E., Rogatkin, D., Stewart, N., Sokolovski, S., & Rafailov, E. (2013). Substantiation of medical and technical requirements for noninvasive spectrophotometric diagnostic devices. *Journal of Biomedical Optics*, 18(10), 107009.

Fercher, A., Mengedoht, K., & Werner, W. (1988). Eye-Length Measurement by Interferometry with Partially Coherent-Light. *Optics Letters,* , 13(3): p.186-188.

Fredriksson, I., & Larsson, M. (2009). Measurement depth and volume in laser Doppler flowmetry. *Microvascular Research*, 78(1), 4-13.

Fredriksson, I., Fors, C., & Johansson, J. (2007). *Laser Doppler Flowmetry - a Theoretical Framework.* Retrieved from Department of Biomedical Engineering, Linköping University: www.imt.liu.se/bit/ldf/ldfmain.html

Galland, P., & Senger, H. (1988). The Role of Pterins in the Photoreception and Metabolism of Plants. In P. Galland, *Photochemistry and Photobiology* (pp. 811-820). Augusta: AMERICAN SOCIETY PHOTOBIOLOGY.

Georgakoudi, I. (2013). *Optical Monitoring of Cell-Matrix Interaction in Engineered Tissues*. Retrieved 2013, from Tufts University: http://ase.tufts.edu/biomedical/research/Georgakoudi/researchOpticalAssessment.asp

Goldsmith, L. A., & Odland, G. (1991). *Structure of the skin, in Physiology, Biochemistry, and Molecular Biology of the Skin.* New York: Oxford: University Press pp. 3–62.

Gorenkov, R., Rogatkin, D., & al, e. (2002). *Patent No. 2234242.* Russia.

Graff, R., Morales, F., Smit, A., De Jong, E., De Mul, F., & Rakhorst, G. (2007). Normalization of vasomotion in laser Doppler perfusion monitoring. *Annual International Conference of the IEEE Engineering in Medicine and Biology Society* (pp. 4076-9). Lyon, France: IEEE.

Guezennec, C., & al, e. (1991). EFFECTS OF INSITU NADH LASER FLUOROMETRY DURING MUSCLE-CONTRACTION IN HUMANS. *EUROPEAN JOURNAL OF APPLIED PHYSIOLOGY AND OCCUPATIONAL PHYSIOLOGY* , Vol 63,36-42.

Gurvich, A., & Frenkel, Y. (1943). The physico-chemical basis of mitogenetic radiation. *Transactions of the Farady Society*, 39, 201-204.

HAMAMATSU. (2013, August 28). *"HAMAMATSU"* . Retrieved from http://www.hamamatsu.com/us/en/product/category/3100/4001/4103/ index.html

Haus, J. (2010). Photodetectors. In J. Haus, *Optical Sensors* (pp. pp. 27-36). Berlin: Wiley-VCH Verlag GmbH.

Health_Advisors. (2013). *Health Picture Reference*. Retrieved 2013, from Health Advisers: http://health-advisors.org/wp-content/uploads/2013/04/human-skin-diagram.jpg

Henderson, C., McLaren, A., Moffat, G., Bacon, E., & Wolf, C. (1998). Pi-class glutathione S-transferase: regulation and function. *Chemico-Biological Interactions*, V111-112,69–82.

Heusmann, H., Koelzer, J., & Mitic, G. (1996). Characterization of female breasts in vivo by time-resolved and spectroscopic measurements in the near infrared spectroscopy. *Journal of Biomedical Optics*, 1, 425-434.

Hewett, J., Nadeau, V., Ferguson, J., Moseley, H., Ibbotson, S., Allen, W., et al. (2000). The application of a Compact Multispectral Imaging System with Integrated Excitation Source to in vivo monitoring of fluorescence during topical photodynamic therapy of superficial skin cancers. *Photochem. and Photobiology. Vol.73. No 3*, 278-282.

Houben, E., De Paepe, K., & Rogiers, V. (2007). (). "A keratinocyte's course of life". . *Skin pharmacology and physiology*, 20(3) 122-32.

Huang, D., Swanson, E., Lin, C., Schuman, J., Stinson, W., Chang, W., et al. (1991). Optical Coherence Tomography. *Science*, 254(5035): p. 1178-1181.

iData. (2012). *U.S. Market for Patient Monitoring Equipment.* i Data Research.

Ishimaru, A. (1981). *Wave propagation and scattering in random media.* New-York: Academic Press.

Jacques, S. (1991). *, The role of skin optics in diagnostic and therapeutic uses of lasers, in Lasers in Dermatology.* Berlin: Springer-Verlag, pp. 1–21.

Jacques, S. (1996). Origins of tissue optical properties in the UVA, visible and NIR regions. In R. Alfano, & J. Fujimoto, *Advances in Optical Imaging and Photon Migration* (pp. pp. 364–370). Washington, DC: OSA.

Jacques, S. (1998, 01). *Skin Optics*. Retrieved from Oregon Medical Laser Center News: http://omlc.ogi.edu/news/jan98/skinoptics.html

Jacques, S. (2013). Optical properties of biological tissues: a review. *Physics in Medicine and Biology*, 58(11), R37-R61.

KCL. (2013). *Kings College London Centre for Biophotonics*. Retrieved from Home: http://www.kcl.ac.uk/innovation/groups/biophotonics/index.aspx

Khalil, O. (2006). Metabolites, noninvasive optical measurements of. In M. Akay, *Wiley encyclopedia of biomedical engineering.* New Jersey: A John Wiley & Sons, Inc.

Kienle, A., Lilge, L., Patterson, M., Wilson, B., Hibst, R., & Steiner, R. (1995). Investigation of multilayered tissue with in vivo reflectance measurements. *SPIE 2326, Photon Transport in Highly Scattering Tissue* (pp. 212-221). Lille, France: SPIE.

Kirkpatrick, N., Zou, c., Brewer, M., Brands, W., Drezek, R., & Utzinger, U. (2005). Endogenous Fluorescence Spectroscopy of Cell Suspensions for Chemopreventive Drug Monitoring. *Photochemistry and Photobiology*, 125-134.

Kislukhin, V. (2004). Regulation of oxygen consumption by vasomotion. *Mathematical Biosciences*, 191, 101-108.

Koenig, K., & Schneckenburger, H. (1994). Laser-Induced Autofluorescence for Medical Diagnosis. *Journal of Fluorescence Vol. 4. No. 1*, 17-21.

Kollias, N. S. (1991). Photoprotection by melanin. *, . J. Photochem. Photobiology ()*, B. 9, 135–160.

Kraitl, J., Timm, U., & Ewald, H. (2010). Non-invasive measurement of blood and tissue parameters based on VIS-NIR spectroscopy. *SPIE 8591, Optical Diagnostics and Sensing XIII: Toward Point-of-Care Diagnostics* (p. 859105). San Francisco: SPIE.

Kramme, R., Hoffmann, K., & Pozos, R. (2011). *Springer Handbook of Medical Technology.* Springer.

Krasnikov, G., Matrusov, S., Piskunova, G., Sidorov, V., & Chemeris, N. (2000). Age characteristics of peripheral blood flow oscillations in the skin. *Proc. "Application of laser Doppler flowmetry in medical practice"*, (pp. 32-34).

Krupatkin A., Rogatkin, D., & Sidorov, V (2007). Haemorheology and microcirculation. *Abstr. Book of the VI-th Int. Conf* (p. 106). Yaroslavl, RF: YGSU.

Krupatkin, A. (2008). Cardiac and respiratory oscillations of the blood flow in microvessels of the human skin. *Human Physiology*, 34, 323-329.

Krupatkin, A. (2009). Blood flow oscillations at a frequency of about 0.1 Hz in skin microvessels do not reflect the sympathetic regulation of their tone. *Human Physiology*, 35, 183-191.

Krupatkin, A. (2011). The Problem of Information Value. *Microvascular Networks. Human Physiology*, 37, 312-317.

Krupatkin, A. (2012). Noninvasive estimation of human tissue respiration with wavelet-analysis of oxygen saturation and blood flow oscillations in skin microvessels. *Human Physiology*, 38, 396-401.

Krupatkin, A., & Sidorov, V. (2005). *Laser Doppler flowmetry of blood microcirculation.* Moscow, RF: Meditcina-Press.

Krupatkin, A., Rogatkin, D., & Sidorov, V. (2007). Clinical-diagnostic parameters for complex investigation of microhaemodynamics and oxygen transport in the system of microcirculation . *Abstr. book of the VIth. International Conference - Hemorheology and microcirculation* (p. 106). Yaroslavl, RF: VIth. International Conference.

Kulikov, K. (2014). *Laser Interaction with Biological Materials - Mathematical Modelling.* London, UK: Springer.

Kvandal, P., Landsverk, S., Bernjak, A., Stefanovska, A., Kvernmo, H. D., & Kirkeboen, K. (2006). Low-frequency oscillations of the laser Doppler perfusion signal in human skin. *Microvascular Research*, 72(3), 120-127.

Kvandal, P., Landsverk, S., Bernjak, A., Stefanovska, A., Kvernmo, H., & Kirkenboen, K. (2006). Low-frequency oscillations of the laser Doppler perfusion signal in human skin. *Microvascular Research*, 72, 120-127.

Kvernmo, H., Stefanovska, A., Kirkeboen, K., & Kvernebo, K. (1999). Oscillations in the human cutaneous blood perfusion signal modified by endothelium-dependent and endothelium-independent vasodilators. *Microvascular Research*, 57, 298-309.

Kyvelidou, C., & al, e. (2011). Following the course of pre-implantation embryo patterning by non-linear microscopy. *J. of Structural Biology*, 176 379-386.

LaVisionBiotech. (n.d.). *Trimscope*. Retrieved from http://www.lavisionbiotec.com/trim-scope-ii-overview.html

Leahy, M., & Nilsson, G. (2010). Laser Doppler flowmetry for assessment of tissue microcirculation: 30 years to clinical acceptance," in Proc. SPIE 7563, Dynamics and Fluctuations in Biomedical Photonics VII V. V. Tuchin, D. D. Duncan and K. V. Larin, Eds. *Dynamics and Fluctuations in Biomedical Photonics VII* (p. 75630E). San Francisco: SPIE.

Liebert, A., Leahy, M., & Maniewski, R. (1998). Multichannel laser-Doppler probe for blood perfusion measurements with depth discrimination. *Medical Biological Engnginering and Computing*, 36(6), 740-747.

Life Technologies. (n.d.). *Fluorescence fundamentals*. Retrieved from http://www.lifetechnologies.com/uk/en/home/references/molecular-probes-the-handbook/introduction-to-fluorescence-techniques.html

Linke, W., Bartoo, M., & Pollack, G. (1993). Spontaneous sarcomeric oscillations at intermediate activation levels in single isolated cardiac myofibrils. *Circulation research*, 73:724-734.

Lister, T., Wright, P., & Chappell, P. (2012). Optical properties of human skin. *Journal of Biomedical Optics*, 17(9), 0909011-09090115.

Liu, H., Kohl-Bareis, M., & Huang, X. (2011). Design of a tissue oxygenation monitor and verification on human skin. *Proc. SPIE 8087, Clinical and Biomedical Spectroscopy and Imaging II* (p. 80871Y). Munich, Germany: SPIE.

Lohmann, W., & Paul, E. (1989). NATIVE FLUORESCENCE OF UNSTAINED CRYO-SECTIONS OF THE SKIN WITH MELANOMAS AND NEVI . *NATURWISSENSCHAFTEN* , 424-426.

Loschenov, V., & al, e. (1998). Portable spectroscopic system for fluorescent diagnostics and photodinamic therapy. *Russian Chemical J.*, XLII(5), 50-53.

Makarov, D., & Rogatkin, D. (2010). Physiological deviation of individual blood microcirculation parameters as a source of errors in noninvasive medical spectrophotometry. *Proceedings the 9-th International conference - Physics and radioelectronics in medicine and ecology PREME* (pp. p.82-86). Vladimir RF: SPIE.

Makita, S., & al, e. (2006). Optical coherence angiography. *Optics Express*, 14(17): p. 7821-7840.

Matcher, S., Cope, M., & Delpy, D. (1997). In vivo measurements of the wavelength dependence of tissue-scattering coefficients between 760 and 900 nm measured with time-resolved spectroscopy. *Appl. Optics* , 36(1), 386-396.

Mayevsky, A., & Chance, B. (2007). Oxidation–reduction states of NADH in vivo: From animals to clinical use. *Mitochondrion*, 330-339.

Medical_Dictionary. (2013). *Fick Principle*. Retrieved 2013, from http://medical-dictionary.thefreedictionary.com/Fick+principle

Meglinski, I. (2001). Simulation of the reflectance spectra of optical radiation from a randomly inhomogeneous multilayer strongly scattering and absorbing light environments using the Monte Carlo. *Quantum Electronics*, 31(12), 1101–1107.

Meglinski, I., & Matcher, S. (2002). Quantitative assessment of skin layers absorption and skin reflectance spectra simulation in the visible and near-infrared spectral regions. *Physiological Measurement*, 23(4), 741-753.

Meglinski, I., & Matcher, S. (2003). Computer simulation of the skin reflectance spectra. *Computer Methods and Programs in Biomedicine*, 70(2), 179-186.

Monici, M. (2005). Cell and tissue autofluorescence research and diagnostic applications. *Biotechnol Annu Rev*, 11:227-56.

Moor_Inst. (2013). *Moor LD12 Laser Doppler Imager*. Retrieved 10 10, 2013, from moor.co.uk: http://www.moor.co.uk/product/moorldi2-laser-doppler-imager/8

Mosyagin, G., Nemtinov, V., & Lebedev, E. (1990). *General theory of optical-electronic systems.* Moscow: Engineering-Press.

Mueller, M., & Fusenig, N. E. (2002). Tumor-stroma interactions directing phenotype and progression of epithelial skin tumor cells. *Differentiation. Vol. 70*, 486-497.

Müller, M., & al., e. (2003). Spectroscopic detection and evaluation of morphologic and biochemical changes in early human oral carcinoma. *Cancer. Vol. 97*, 1681–1692.

National_Laser. (2013). *National Laser*. Retrieved from National Laser Company: http://www.national-laser.com/laser-history.htm

Newman, J., Dwyer, R., St-Pierre, P., Richards, S., Clark, M., & Rattigan, S. (2009). Decreased microvascular vasomotion and myogenic response in rat skeletal muscle in association with acute insulin resistance. *Journal of Physiology-London*, 587, 2579-2588.

Obeid, A. (1993). In vitro comparison of different signal-processing algorithms used in laser doppler flowmetry. *Medical & Biological Engineering & Computing*, 31, 43-52.

Oppenheim, A., & Schafer, W. (1975). *Digital Signal Processing.* New Jersey, USA: Prentice Hall ISBN: 9780132146357.

Oxford_Optronix. (2013, August 28). *Tissue Vitality Monitoring*. Retrieved from Oxford Optronix: http://www.oxford-optronix.com/cat10/page29/Tissue-Vitality-Monitoring.html

Papadakis, A., & al, e. (2010). A new optical-CT apparatus for three-dimensional radiotherapy dosimetry: Is free space scanning feasible? *IEEE Transactions of Medical Imaging*, 29, 1204 – 1212.

Petrov, G., Doronin, A., Whelan, H., Meglinski, I., & Yakovlev, V. (2012). Human tissue color as viewed in high dynamic range optical spectral transmission measurements. *Biomedical Optics Express*, 3(9), 2154-2161.

Popp, F. (1973). CORRELATION BETWEEN PORPERTIES OF EXCITED-STATES OF MOLECULES AND BIOLOGICAL-ACTIVITY, AS RADIOSENSIBILIZATION AND CARCINOGENIC ACTIVITY. *JOURNAL OF BIOSCIENCES*, C28:9-10: 517-522.

Quan-Liu, & et.al. (2011). Quan Liu and et.al. Compact point-detection fluorescence spectroscopy system for quantifying intrinsic fluorescence redox ratio in brain cancer diagnostics. *Journal of Biomedical Optics*, 16(3), 037004 .

Quaresima, V., Ferrari, M., & Fantini, S. (2013). Accurary of Oxygen Desaturation of Hemoglobin in Muscle by Near-Infrared Oximeters. , . *Medicine and Science in Sports and Exercise*, 45, 1217-1217.

Quizlet. (2013). *Haemoglobin and Myoglobin*. Retrieved 08 10, 2013, from Quizlet.com: http://quizlet.com/7051703/bc-ch-7-hemoglobin-and-myoglobin-flash-cards/

ResearchInChina. (2008). *Key"Portable Medical Device Vendors Worldwide". China Portable Medical Devices Report.* Beijing: ResearchInChina.

Rogatkin D. and L. Lapaeva. (2003). Prospects for development of non-invasive spectrophotometry medical diagnostics. *Biomed. Engineering, 37*(4), 217-222.

Rogatkin, D. (1998). The laser clinical diagnostics as one of the perspective branch of biomedical radio-electronics and medical physics of the next millennium. *Biomed. Radio-Electronics*, (3), 34-41.

Rogatkin, D. (2004). Basic principles of organization of system software for multifunctional noninvasive spectrophotometric diagnostic devices and systems. *Biomed. Engineering*, 38(2), 61-65.

Rogatkin, D. (2007). A specific feature of the procedure for determination of optical properties of turbid biological tissues and media in calculation for non-invasive medical spectrophotometry. *Biomedical Engineering*, 41(20), 59-65.

Rogatkin, D., & al, e. (2013). Principal sources of errors in noninvasive medical spectrophotometry. Part 1. Physicotechnical sources and factors of errors. *Measurement Technology*, 56(2), 201–210.

Rogatkin, D., & Lapaeva, L. (2003). Prospects for development of non-invasive spectrophotometry medical diagnostics. *Biomed. Engineering*, 2.37(4), 217-222.

Rogatkin, D., Dunaev, A., & Lapaeva, L. (2010). Metrological Support of Methods and Devices for Noninvasive Medical Spectrophotometry. *Biomedical Engineering*, 44(2), 66-70.

Rogatkin, D., Lapaeva, L., Bychenkov, O., Tereshchenko, S., & Shumskii, V. (2013). Principal Sources of Errors in Noninvasive Medical Spectrophotometry. Part 1. Physicotechnical Sources and Factors of Errors. *Measurement Technology*, 56(2), 201-210.

Rogatkin, D., Lapaeva, L., Petritskaya, E., & Sidorov, V. (2009). Multifunctional laser noninvasive spectroscopic system for medical diagnostics and metrological provisions. *ECBO* (p. pp. 7368Y). Munich: SPIE.

Rogatkin, D., Prisnyakova, O., Moiseeva, L., & Cherkasov, A. (1998). Analysis of the accuracy of clinical laser fluorescence diagnosis. *Measurement Techniques*, Vol. 41, No. 7, p. 670-674. http://medphyslab.com/images/publications/stat_it_01_e.pdf.

Rogatkin, D., Sidorov, V., & Schumsky, V. (2008). *Patent No. WO2008140355 (A1) — 2008-11-20* . Russia/EU.

Rogatkin, D., Sokolovski, S., Fedorova, K., Stewart, N., Sidorov, V., & Rafailov, E. (2011). Basic principles of design and functioning of multifunctional laser diagnostic system for non-invasive medical spectrophotometry, *Proceedings of SPIE Vol. 7890, art. no. 78901H, Photonics West* San-Francisco,2011.

Roggan, A., Friebel, M., Dorschel, K., Hahn, A., & Muller, G. (1999). Optical properties of circulating human blood in the wavelength range 400-2500 nm. *Journal of Biomedical Optics*, 4(1), 36-46.

Rossi, M., Matteucci, E., Pesce, M., Consani, C., Galetta, F., Giampietro, O., et al. (2013). Study of skin vasomotion in type 1 diabetic patients and of its possible relationship with clinical and laboratory variables. . *Clinical Hemorheology and Microcirculation*, 53, 357-367.

Salerud, E., Tenland, T., Nilsson, G., & Oberg, P. (1983). Rhythmical variations in human-skin blood-flow. *International Journal of Microcirculation-Clinical and Experimental*, 2(2), 91-102.

Salerud, E., Tenland, T., Nilsson, G., & Oberg, P. (1983). Rhythmical variations in human-skin blood-flow. *International Journal of Microcirculation-Clinical and Experimental*, 2(2), 91-102.

Saxer, C., de Boer, J., Park, B., Zhao, Y., Chen, Z., & Nelson, J. (2000). High-speed fiber-based polarization-sensitive optical coherence tomography of in vivo human skin. *Optics Letters, .*, 25(18): p. 1355-1357.

Schmidt-Lucke, C., Borgstrom, P., & Schmidt-Lucke, J. (2002). Low frequency flowmotion/(vasomotion) during patho-physiological conditions. *Life Sciences*, 71, 2713-2728.

Schmiedel, O., Schroeter, M., & Harvey, J. (2007). Microalbuminuria in Type 2 diabetes indicates impaired microvascular vasomotion and perfusion. *American Journal of Physiology - Heart and Circulatory Physiology*, 293, H3424-H3431.

Scott, M. A., & al, e. (2000). Fluorescence photodiagnostics and photobleaching studies of cancerous lesions using ratio imaging and spectroscopic techniques. *Lasers Medical Science. Vol.15.*, 63-72.

SensorInc. (2013). *Application: IR Sensors for High Resolution Imaging in Tissue*. Retrieved 2013, from UTC Aerospace Systems: http://www.sensorsinc.com/imaging-tissue.html

Shadzad, A., Edetsberger, M., & Koehler, G. (2010). Fluorescence Spectroscopy: An Emerging Excellent Diagnostic Tool in Medical Sciences. *Applied Spectroscopy Reviews*, 45:1, 1-11.

Shoulders, M. a. (2009). Collagen Structure and Stability. *Annual Review of Biochemistry*, Vol. 78: 929-958.

Sikorski, Z. E. (2001). *Chemical and Functional Properties of Food Proteins.* Boca Raton: CRC Press p. 242.

Skala, M., Riching, K., Gendron-Fitzpatrick, A., Eickhoff, J., Eliceiri, K., White, J., et al. (2007). In vivo multiphoton microscopy of NADH and FAD redox states, fluorescence lifetimes, and cellular morphology in precancerous epithelia. *Proc. Natl. Acad. Sci. USA*, 104(49), 19494–19499 .

Smirnova, O. D., Rogatkin, D., & Litvinova, K. (2012). Collagen as in vivo quantitative fluorescent biomarkers of abnormal tissue changes. *Journal of Innovative Optical Health Science*, Vol. 5, N 2. - 1250010.

SPE LAZMA. (n.d.). *Laser noninvasive diagnostic system LAKK* . Retrieved from http://www.lazma.ru/eng/catalog/prod.php?pid=12

Spectrum Medical. (n.d.). *System M*. Retrieved from http://www.spectrummedical.com/products/system-m/

Stefanovska, A. (2009). Dynamics of blood oxygenation gives better insight into tissue hypoxia than averaged values. *American Journal of Physiology - Heart and Circulatory Physiology*, 296, H1224-H1226.

Stefanovska, A., Bracic, M., & Kvernmo, H. (1999). Wavelet analysis of oscillations in the peripheral blood circulation measured by laser Doppler technique. *IEEE Transactions on Biomedical Engineering*, 46(10), 1230-1239.

Stern, M. (1985). LASER DOPPLER VELOCIMETRY IN BLOOD AND MULTIPLY SCATTERING FLUIDS - THEORY. *APPLIED OPTICS*, 24/13 1968-1986.

Stewart, N., Dunaev, A., Sokoliovski, S., Siderov, V., & Rafailov, E. (2012). MULTI-PARAMETER ANALYSIS IN BLOOD CIRCULATIONAND PERFUSION BASED DIAGNOSTICS. *15th International Conference on Laser Optics.* St.Petersburg, Russia: ICLO.

Stokes G.G. (1852). *On the Change of Refrangibility of Light.* Cambridge: University of Cambridge.

Takatani, S. (1989). Toward absolute reflectance oximetry: I. Theoretical consideration for noninvasive tissue reflectance oximetry. *Advances in experimental medicine and biology*, 248 91-102.

Tankanag, A., & Chemeris, N. (2008). Application of the adaptive wavelet transform for analysis of blood flow oscillations in the human skin. *Physics in Medicine and Biology*, 53, 5967-5976.

Tankanag, A., & Chemeris, N. (2009). A method of adaptive wavelet filtering of the peripheral blood flow oscillations under stationary and non-stationary conditions. *Physics in Medicine and Biology*, 54, 5935-5948.

Tchernyi, V., & al., e. (2006). Complex non-invasive spectrophotometry in examination of patients with vibration disease. *Photonic Therapeutics and Diagnostics II. SPIE Proc* (pp. 6078, 607828). Sanfrancisco: SPIE.

Tchernyi, V., Rogatkin, D., Bychenkov, O., & Polyakov, P. (2005). Some results of multiwave in situ autofluorescence diagnostics. *Photonics West* (pp. 336-343). San Jose: SPIE.

TeleAnatomy. (2013). *Chapter 8 - Skin*. Retrieved from TeleAnatomy: http://teleanatomy.com/introductiontoanatomy-Skin.html

Thorn, C., Kyte, H., Slaff, D., & Shore, A. (2011). An association between vasomotion and oxygen extraction. *American Journal of Physiology-Heart and Circulatory Physiology*, 301(2), H442-H449.

Thorn, C., Matcher, S., Meglinski, I., & Shore, A. (2009). Is mean blood saturation a useful marker of tissue oxygenation? . *American Journal of Physiology - Heart and Circulatory Physiology*, 296, H1289-H1295.

Tikhonova, I., Tankanag, A., & Chemeris, N. (2013). Age-related changes of skin blood flow during. *Skin Research and Technology;* , 19: e174–e181.

Time Tech. (2013, May 24). *A Star Trek Tricorder? 'Scanadu Scout' Health Monitor Surges Past Indiegogo Funding Goal*. Retrieved from Time Tech: http://techland.time.com/2013/05/24/a-star-trek-tricorder-scanadu-scout-health-monitor-surges-past-indiegogo-funding-goal/

Timm, U., Kraitl, J., Schnurstein, K., & Ewald, H. (2013). Photometric sensor system for a non-invasive real-time hemoglobin monitoring," . *in Proc. SPIE 8572, Advanced Biomedical and Clinical Diagnostic Systems XI* (p. 857204). San Franscisco: SPIE.

Tserevelakis, G., & al, e. (2011). Cell tracking in live Caenorhabditis elegans embryos via Third Harmonic Generation imaging microscopy measurements. *J. of Biomedical Optics* , 16, 046019.

Tuchin, V. (1997). Light scattering study of tissues. *Successes phys. sci.*, 167, 517–539.

Tuchin, V. (2000). Tissue Optics - Light Scattering Methods and Instruments for Medical Diagnosis. *Optical Engineering Vol. TT38*.

Tuchin, V. (2002). *Handbook of optical biomedical diagnostics.* Bellingham, Washington, USA: SPIE Press.

Tyrrell, J., Thorn, C., Shore, A., Campbell, S., & Curnow, A. (2011). Oxygen saturation and perfusion changes during dermatological methylaminolaevulinate photodynamic therapy. *British Journal of Dermatology*, 165, 1323-1331.

Utz, S., Barth, J., Knuschke, P., & Sinichkin, Y. (1993). Fluorescence spectroscopy of human skin. . *Proc. SPIE. 2081* (pp. 48–57). Sanfrancisco: SPIE.

Wagnieres, G., Star, W., & Wilson, B. (1998). In vivo fluorescence spectroscopy and imaging for oncological application. *Photochemestry and Photobiology. Vol. 68*, 603-632.

Wallace, D. (2012). Mitochondria and cancer. *Nature Reviews Cancer*, 3365.

Weinstein, G. a. (1960). Collagen and elastin of human dermis. *J. Investig. Dermatol. 35, 227–229*, 35, 227–229.

White, B., & al, e. (2003). In vivo dynamic human retinal blood flow imaging using ultra-high-speed spectral domain optical Doppler tomography. *Optics Express*, 11(25): p. 3490-3497.

Witte, S., Negrean, A., Lodder, J., de Kock, C., Silva, G., Mansvelder, H., et al. (2011). Label-free live brain imaging and targeted patching with third-harmonic generation microscopy. *Proceedings of the National Academy of Sciences of the United States of America*, 108(15): p. 5970-5975.

Woodley Lab Diagnostics. (n.d.). *QCB Paralens Advance*. Retrieved from http://www.woodleyequipment.com/laboratory-diagnostics/qbc-paralens-advance-226.html

X PRIZE Foundation. (2013, 01). *Qualcomm TricorderX - Prize*. Retrieved from X-Prize: http://www.qualcommtricorderxprize.org/

Ying, W. (2008). NAD+/NADH and NADP+/NADPH in cellular functions and cell death: regulation and biological consequences. *Antioxidants and Redox Signalling*, 10(2), 179-206.

Zacharakis, G., & al, e. (2011). Spectroscopic detection improves multi-color quantification in fluorescence tomography. *Biom. Optics Express*, 2, 431 – 439.

Zhao, Y. C., Shen, Q., Xiang, S., de Boer, J., & Nelson, J. (2000). Doppler standard deviation imaging for clinical monitoring of in vivo human skin blood flow. *Optics Letters*, 25(18): p. 1358-1360.

Zhao, Y., & al, e. (2000). Phase-resolved optical coherence tomography and optical Doppler tomography for imaging blood flow in human skin with fast scanning speed and high velocity sensitivity. *Optics Letters*, 25(2): p. 114-116.

Zipfel, W., & al, e. (2003). Live tissue intrinsic emission microscopy using multiphoton-excited native fluorescence and second harmonic generation. *Proceedings of the National Academy of Sciences of the USA*, 100(12): p. 7075-7080.

Annex 1 - Publications

Investigating tissue respiration and skin microhaemocirculation under adaptive changes and the synchronization of blood flow and oxygen saturation rhythms

Journal:	*Physiological Measurement*
Manuscript ID:	PMEA-100019.R1
Manuscript Type:	Paper
Date Submitted by the Author:	n/a
Complete List of Authors:	Dunaev, Andrey; University of Dundee, Photonics and Nanoscience Group, Division of Physics; State University – Education-Science-Production Complex, Scientific-Educational Center of "Biomedical Engineering" Sidorov, Victor; SPE-LAZMA Ltd, Krupatkin, Alexander; Priorov Central Research Institute of Traumatology and Orthopaedics, Rafailov, Ilya; University of Dundee, Department of Urology Palmer, Scott; University of Dundee, Photonics and Nanoscience Group, Division of Physics; University of Dundee, Department of Urology Stewart, Neil; University of Dundee, Photonics and Nanoscience Group, Division of Physics; University of Dundee, Department of Urology Sokolovski, Sergei; University of Dundee, Photonics and Nanoscience Group, Division of Physics Rafailov, Edik; University of Dundee, Photonics and Nanoscience Group, Division of Physics
Article Keywords:	laser Doppler flowmetry, tissue reflectance oximetry, vasomotion, oxygen consumption, adaptive changes
Abstract:	Multi-functional laser non-invasive diagnostic systems allow the study of a number of microcirculatory parameters, including index of blood microcirculation (Im) (by laser Doppler flowmetry, LDF) and oxygen saturation (StO2) of skin tissue (by tissue reflectance oximetry, TRO). This research aimed to use such a system to investigate the synchronization of microvascular blood flow and oxygen saturation rhythms under normal and adaptive change conditions. Studies were conducted on 8 healthy volunteers of 21-49 years. These volunteers were observed between 1 and 6 months , totalling 422 basic tests (3 minutes each). Measurements were performed on palmar surface of right middle finger and the lower forearm's medial surface. Rhythmic oscillations of LDF- and TRO were studied using wavelet analysis. Combined tissue oxygen consumption data for all volunteers during "adaptive changes" increased relative to normal conditions with and without arteriovenous anastomoses (AVAs). Data analysis revealed resonance and synchronized rhythms in microvascular blood flow and oxygen saturation as an adaptive change in myogenic oscillation (vasomotion) resulting from exercise and possibly psychoemotional stress. Synchronization of myogenic rhythms during adaptive changes may lead to increased oxygen consumption as a result of increased microvascular blood flow velocity.

Investigating tissue respiration and skin microhaemocirculation under adaptive changes and the synchronization of blood flow and oxygen saturation rhythms

Running head: Tissue respiration and vasomotion under adaptive changes

AV Dunaev[1,2,6], VV Sidorov[3], AI Krupatkin[4], IE Rafailov[5], SG Palmer[1,5], NA Stewart[1,5], SG Sokolovski[1] and EU Rafailov[1]

[1]Photonics and Nanoscience Group, Division of Physics, School of Engineering, Physics and Mathematics, University of Dundee, Dundee DD1 4HN, UK

[2]State University – Education-Science-Production Complex, Scientific-Educational Center of "Biomedical Engineering", Oryol 302020, Russia

[3]SPE "LAZMA" Ltd., Moscow 125252, Russia

[4]Priorov Central Research Institute of Traumatology and Orthopaedics, Moscow 127299, Russia

[5]Department of Urology, Ninewells Hospital, University of Dundee, Dundee, DD1 9SY, UK

[6]Corresponding author

Corresponding author email: a.v.dunaev@dundee.ac.uk

Abstract. Multi-functional laser non-invasive diagnostic systems allow the study of a number of microcirculatory parameters, including index of blood microcirculation (I_m) (by laser Doppler flowmetry, LDF) and oxygen saturation (S_tO_2) of skin tissue (by tissue reflectance oximetry, TRO). This research aimed to use such a system to investigate the synchronization of microvascular blood flow and oxygen saturation rhythms under normal and adaptive change conditions. Studies were conducted on 8 healthy volunteers of 21-49 years. These volunteers were observed between 1 and 6 months, totalling 422 basic tests (3 minutes each). Measurements were performed on palmar surface of right middle finger and the lower forearm's medial surface. Rhythmic oscillations of LDF- and TRO were studied using wavelet analysis. Combined tissue oxygen consumption data for all volunteers during "adaptive changes" increased relative to normal conditions with and without arteriovenous anastomoses

(AVAs). Data analysis revealed resonance and synchronized rhythms in microvascular blood flow and oxygen saturation as an adaptive change in myogenic oscillation (vasomotion) resulting from exercise and possibly psychoemotional stress. Synchronization of myogenic rhythms during adaptive changes may lead to increased oxygen consumption as a result of increased microvascular blood flow velocity.

Keywords: laser Doppler flowmetry, tissue reflectance oximetry, vasomotion, oxygen consumption, adaptive changes

1. Introduction

The evaluation of stress-induced adaptive changes in the tissue respiration and circulatory systems of individuals may provide important information for studies in physiology and clinical medicine. Optical techniques are one of the most promising non-invasive technologies for the diagnosis of medical conditions. The fields of photonics and biophotonics have witnessed real progress and accomplishments. This has led to the development and introduction of novel and compact noninvasive optical diagnostic devices into biomedicine. Especially, progress has been achieved in developing methods and devices for non-invasive studies of blood flow (Zakharov et al., 2009, Zakharov et al., 2011) as well as quantitative assessment and imaging associated with this (Kalchenko et al., 2011, Kalchenko et al., 2012, Fine et al., 2012, Daly et al., 2013). However, these methods and devices do not allow full analysis of the consumption and utilization of oxygen in tissue, as well as frequency modulation rhythms of blood flow and tissue oxygen saturation. Simultaneous use of several methods, such as the laser Doppler flowmetry (LDF) for the measurement of tissue perfusion and absorption spectroscopy for the analysis of tissue oxygenation, can provide additional information about the different types and features of oscillation hemodynamics in the same diagnostic tissue volume (Thorn et al., 2009). The recent development of multi-functional non-invasive laser based diagnostic systems, such as the “LAKK-M” (SPE "LAZMA" Ltd, Russia) (Rogatkin et al., 2010, Rogatkin et al., 2011), has made it possible to conduct simultaneous real-time studies on a number of tissue parameters, including microvascular blood flow (by LDF) and oxygen saturation of skin tissue (by tissue reflectance oximetry, TRO) (Rogatkin and Lapaeva, 2003, Stewart et al., 2012, Dunaev et al., 2013). This diagnostic system can be applied in angiology and physiology for studying the status of the microvascular tone and analysing the neurophysiological mechanisms of regulatory microhemodynamics, in oncology and radiology for identification of the oxygen status of the tumour and the prognosis of radiation treatment, and in transplantation for assessment of graft acceptance and tissue viability.

The results of LDF measurements, representing “index of blood microcirculation (I_m)” or “perfusion”, assessed in conventional (arbitrary) perfusion units (PU), reveal a complex, non-periodic process. This variable component contains information on the modulation of blood flow. Use of spectral signal processing algorithms on LDF-graphs for decoding and analysis provides information about the condition of vascular tone in terms of its contribution to the different mechanisms of micro-hemodynamic regulation (Bracic and Stefanovska, 1998, Krupatkin and Sidorov, 2005). Oscillatory processes play an important role in the functioning of the system of tissue microcirculation (Stefanovska et al., 1999, Bernjak et al., 2005, Krupatkin, 2007, Krupatkin, 2011). Several frequency ranges of blood flow oscillations in microvascular networks, each of a different regulatory origin, have been identified (endothelial, neurogenic, myogenic, etc.) (Kvernmo et al., 1999, Kvandal et al., 2006,

Krupatkin, 2011). Many medical publications are devoted to the study of myogenic oscillations, because they characterise the state of pre-capillary sphincters, which play an important role in the regulation of blood flow (Schmidt-Lucke et al., 2002, Graaff et al., 2007, Schmiedel et al., 2007, Rossi et al., 2008, Newman et al., 2009, Rossi et al., 2013).

Tissue reflectance oximetry is based on the principles of absorption spectroscopy and allows non-invasive (in vivo, transcutaneous) monitoring of microhemodynamics and oxygen transport and utilisation within the entire blood microcirculation system. Using and comparing this technique with the method of pulse oximetry, which only measures oxygen saturation in arterial blood (S_aO_2), provides much more information for clinical medicine (Amzina et al., 2006, Colquhoun et al., 2012, Quaresima et al., 2013). TRO determines the relative volume of all fractions of haemoglobin (total haemoglobin) in a tissue volume (average level of blood volume – V_b, in percent) and oxygen saturation of the microvasculature, generally containing arterioles with oxyhemoglobin and venules with deoxyhemoglobin (average level of tissue oxygen saturation – S_tO_2, in percent). It should be noted that the changes in tissue oxygen saturation are essentially the increases and decreases of tissue oxygen consumption. There are few studies of rhythms (for example, spectral processing algorithms) within these recorded TRO-signals (Coca et al., 1998, Coca et al., 2000, Stefanovska, 2009, Thorn et al., 2009), and literature reporting the relationships between I_m and S_tO_2-graphs are rare (Tyrrell et al., 2011, Bernjak et al., 2012). In isolated cases it has been used to assess vasomotion and myogenic rhythms for perfusion and tissue oxygen saturation, for example (Thorn et al., 2011). Here we propose that, similarly to the LDF plots, the analysis of oscillation signals recorded by TRO is of practical interest in studying the parameters of microcirculation of blood. This is particularly important as the relationships between LDF and TRO attract increasing attention from researchers in the field.

The aim of this research was to use LDF- and TRO-graphs to investigate tissue respiration during the synchronization of microvascular blood flow and oxygen saturation rhythms under normal conditions and during adaptive changes.

2. Methods and materials

In this study we used a "LAKK-M" system, which, besides LDF and TRO, contains pulse oximetry and laser fluorescence diagnostic channels (Dunaev et al., 2013) (Fig. 1). This system includes near-infrared (1064 nm), red (640 nm) and green (532 nm) lasers for LDF- and TRO-channels and allows simultaneous recording of the I_m, S_tO_2 and V_b parameters in a tissue volume about 3-5 mm^3 (with the separation distance between the source and detector fibers at around 1 mm).

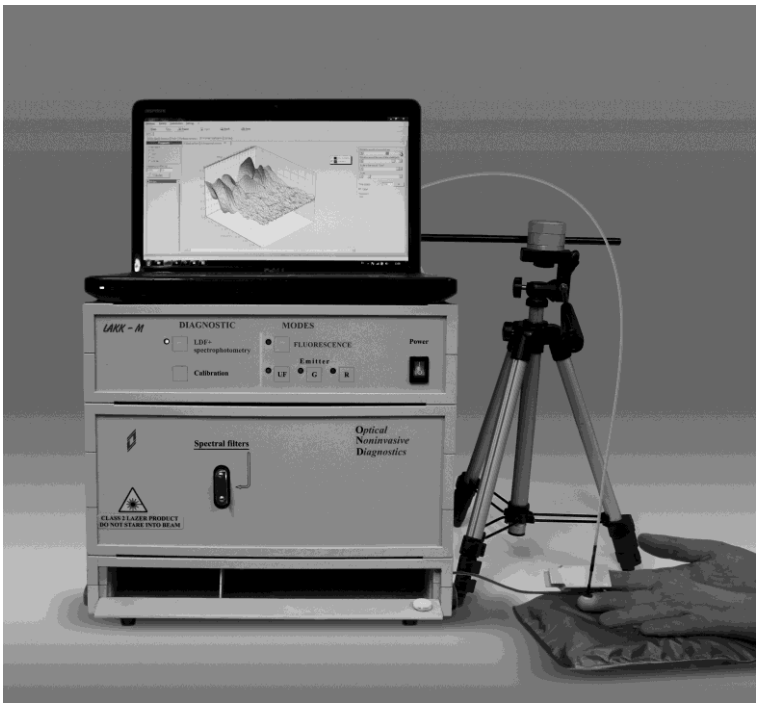

Figure 1. The multi-functional laser non-invasive diagnostic system "LAKK-M".

The LDF channel used traditional methodology, with the results of perfusion in accordance with the following well known equation (Obeid, 1993, Leahy and Nilsson, 2010):

$$I_m = \frac{k\int f \cdot V(f)df}{\int V(f)df}, \tag{1}$$

where k is the coefficient of the device (calibration factor), f is the value of the Doppler frequency and the $V(f)$ is the Doppler signal amplitude.

The TRO channel of the "LAKK-M" system calculates the parameters S_tO_2 and V_b according to the following methodology. Tissue oxygen saturation is defined as the percentage composition of oxyhaemoglobin in the sum of only two haemoglobin fractions – oxyhaemoglobin and deoxyhaemoglobin (Krupatkin et al., 2007):

$$S_tO_2 = \frac{C_{HbO_2}}{C_{HbO_2} + C_{Hb}} \cdot 100\%, \tag{2}$$

where, if the molar concentration of HbO_2 in the blood is designated as C_{HbO2} and the overall molar concentration of all the fractions of haemoglobin in the blood, including HbO_2, is designated as the sum of C_{HbO2} and C_{Hb}, then the parameter V_b can be calculated as follows:

$$V_b = \frac{C_{Hb} + C_{HbO_2}}{C_{Hb} + C_{HbO_2} + C_{other}} \cdot 100\%, \quad (3)$$

where C_{other} is the molar concentration of all secondary cellular structures in the examined volume of tissue.

The value of the molar concentration is determined by the absorption by biological tissue of radiation at different wavelengths. On the basis of the well-known Beer-Lambert law and taking into account multicomponent biotissue, the absorption coefficient can be calculated using the following formula:

$$\mu_a(\lambda) = \sum_i \varepsilon_i(\lambda) \cdot C_i. \quad (4)$$

where $\varepsilon_i(\lambda)$ is the molar extinction coefficient for the biochemical medium component *i*, while C_i is the molar concentration of component *i* in the tested region.

During the implementation of the TRO function of this device, two wavelengths (640 nm and 532 nm) are used. Taking into account certain restrictions, the molar concentrations of haemoglobin fractions vital for the calculation of S_tO_2 and V_b can be calculated using the following equations (Khalil, 2006, Heusmann et al., 1996):

$$\mu_a(\lambda_1) = \varepsilon_{Hb}(\lambda_1) \cdot C_{Hb} + \varepsilon_{HbO_2}(\lambda_1) \cdot C_{HbO_2} + \varepsilon_{other}(\lambda_1) \cdot C_{other}, \quad (5)$$
$$\mu_a(\lambda_2) = \varepsilon_{Hb}(\lambda_2) \cdot C_{Hb} + \varepsilon_{HbO_2}(\lambda_2) \cdot C_{HbO_2} + \varepsilon_{other}(\lambda_2) \cdot C_{other},$$

where $\varepsilon_{other}(\lambda_j)$ is the sum molar extinction coefficient of light at different wavelengths by all other skin structures.

Studies of different durations were conducted with 8 volunteers with no history of cardiovascular disease and without chronic diseases and medication, aged 21-49 years, comprising 3 females and 5 males (Table 1). These studies involved simultaneously recording the parameters of LDF (I_m), TRO (S_tO_2) and pulse oximetry (S_aO_2). In order to assess the I_m and the S_tO_2 oscillatory component, spectral wavelet analysis of oscillations was used (software 3.0.2.384, LAZMA, Russia). This program uses a continuous wavelet transform, with the Morle complex valued wavelet being used as the analysing wavelet (Tankanag and Chemeris, 2008, Tankanag and Chemeris, 2009). The study was performed approximately at the same time of day (around 12:00) to avoid circadian rhythms influence on the blood circulation, at ambient room temperature (21–22°C) in a sitting position after a 30 min rest period (allowed for acclimatization). The temperature of the volunteers was measured on

the tested regions of skin by an infrared clinical thermometer "Medisana" 76120 (FTN). All temperatures recorded were within the range of 34-36°C. The measurements were performed on the inner (palmar) surface of the right middle finger. This area was chosen because it is rich in arteriovenous anastomoses (AVAs) and variability of the LDF signal is less than in tissue with fewer shunts (Salerud et al., 1983). It should be emphasized that this area is regulated almost exclusively by the autonomic nervous system and is very responsive to adaptive changes. In addition, studies were conducted in an area almost completely devoid of AVAs - the lower forearm's medial surface (the skin without AVAs), characterized by greater nutritive blood flow. The necessary calibration of the "LAKK-M" system was carried out prior to each study. Immobility of the optical probe on the surface of the skin was ensured according to the user manual.

Table 1. Volunteer and study data.

№ volunteer	Age, years	Sex	Duration of studies, months	Number of basic tests		Number of occlusion tests	Number of studies after sport
				With AVAs	Without AVAs		
1	36	male	6	80	41	-	20
2	29	female	1	19	-	20	-
3	49	male	2	23	5	-	-
4	20	male	1	18	14	-	-
5	23	male	2	27	25	-	-
6	29	female	4	34	31	-	-
7	24	female	2	22	21	-	-
8	23	male	3	25	17	-	-
Total:	29±9.5	-	-	248	154	20	20
							422

It should be noted that for a versatile study of adaptive changes of microcirculation under stressful conditions, a part of the volunteers were studied for a longer duration of time and at different physical activities. Moreover, even with a short period of research of some volunteers (1-2 months) taking measurements in two areas of the skin and using physiological tests, has provided a sufficient number of measurements (no less 28 for each volunteer) for the proposed research.

Thus, the male participant of 36 years (volunteer №1) was studied over the course of 6 months, totalling 100 records in the skin with AVAs (n=100): 60 basic tests for 3 min, plus 20 "before and after" records to monitor the effects of exercise, in this case swimming (500 m) with the water temperature in the pool about 24-28 °C, which can be considered a form of stress for the study of the adaptive changes. Readings were taken after a rest period of 20-30 minutes after the exercise, with the temperatures being recorded prior to each one falling in the range of 34-35°C. It should be noted that the use of LDF and TRO to investigate the blood microcirculation system was done over a duration of

51 days. In addition to basic test controls recorded prior to swimming, further basic test (BT) recordings were produced for an hour after each session (with short 1-2 minute breaks). This led to the experiments based on sports load having 183 basic tests. However, as the adaptive changes under sports load were recorded on a volunteer without prior athletic training, only data from 20 basic tests (n=20) recorded in the first two weeks of training were used for analysis and calculation of oxygen consumption. This volunteer's studies were also conducted in the skin without AVAs (n=41).

The female participant (volunteer №2) was studied over the course of 1 month, totalling 39 studies only in the skin with AVAs: 19 basic tests for 3 minutes plus 20 tests with an occlusion for 1 min followed by a 3 min post occlusion period. The occlusion was used to induce adaptive changes in the volunteer. These occlusion tests were carried out on the same day as the basic tests, after a period of 20-30 minutes rest.

For the remaining volunteers (№3-8), only basic tests were performed on both points of interest (skin with and without AVAs) and they were not subjected to additional stress. Studies of these volunteers were carried out five times a week (when possible) at around the same time of day, and always followed the methodology described above. Measurements were carried out under conditions of physiological dormancy and non-physiological rest (physical or emotional and psychological stress). It is important to note that all volunteers prior to testing were questioned about their psychoemotional state and were recorded as either normal or under emotional stress.

Wavelet analysis was performed on 5 rhythmic components (oscillations) of I_m- and S_tO_2-records, namely endothelial (0.0095-0.02 Hz); neurogenic (0.02-0.06 Hz); myogenic (0.06-0.16 Hz); breathing (0.16-0.4 Hz) and pulse (0.4-1.6 Hz) (Stefanovska et al., 1999, Kvandal et al., 2006, Krupatkin, 2008, Krupatkin, 2009). For the purposes of this investigation, however, the endothelial component was not required. The typical forms of perfusion and tissue oxygen saturation are shown in Fig 2a and the results of the wavelet analysis for them during the basic test are presented in Fig. 2b.

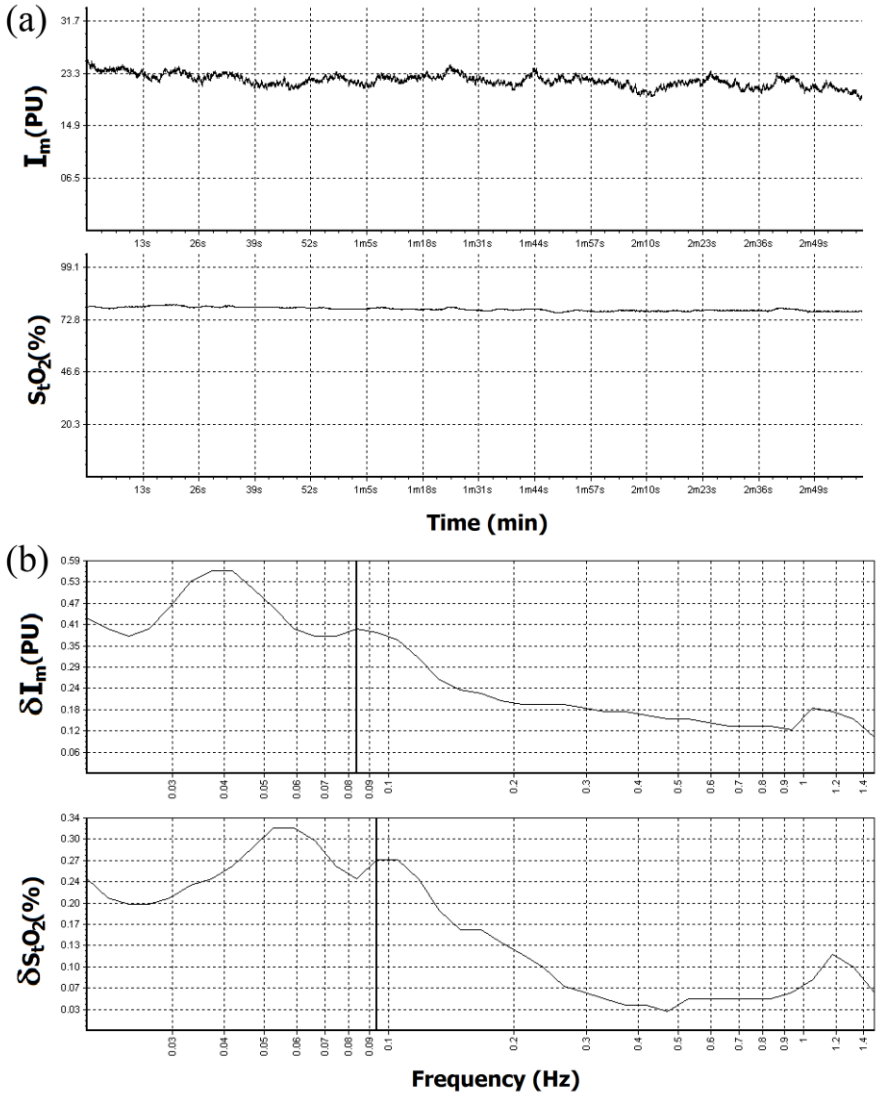

Figure 2. (a) The typical form of perfusion and tissue oxygen saturation graphs, measured using LDF and TRO, respectively and (b) wavelet analysis results following such basic tests, where δI_m – amplitude of perfusion oscillations, δS_tO_2 - amplitude of oxygen saturation oscillations. Furthermore, in (B), a line is used to represent the amplitude oscillation of microvascular blood flow $(\delta I_m)_m$=0.40 PU at a frequency of f_m=0.084 Hz and tissue oxygen saturation $(\delta S_tO_2)_m$=0.27% at a frequency of f_m=0.094 Hz for myogenic rhythms.

Of particular interest is the analysis and comparison of oxygen consumption in tissue under normal conditions and during adaptive changes, accompanied by sympathetic vasomotor reflex (synchronization and resonance of the myogenic oscillation in perfusion and tissue oxygen saturation). This is especially interesting as a relationship between the activation of vasomotion and oxygen consumption has been previously identified (Kislukhin, 2004). According to the methodology thoroughly explained in the article (Krupatkin, 2012) and using data from the spectral wavelet analysis

of I_m- and S_tO_2-graphs, we have calculated the extraction and consumption of oxygen in tissue for all 8 volunteers. It should be noted that what we understand of general oxygen saturation oscillations and particularly of myogenic rhythms is as follows. Myogenic oscillations of oxygen saturation we consider primarily as oxygen saturation changes in light of the changes in tissue oxygen consumption. These changes correspond to the oscillations of blood flow in the myogenic range. As stated above the tissue oxygen saturation is determined by a spectrophotometric method. In fact, this value undergoes changes primarily during the modulation of blood flow as a result of the oscillations of perfusion due to the myogenic regulation of microvascular tone. Thus, the oxygen saturation value oscillations primarily depend on the blood flow oscillations resulting from changes in the microvascular tone.

Oxygen extraction (*OE*), assessed in arbitrary units (AU), was calculated as follows:

$$OE = \frac{S_aO_2 - S_vO_2}{S_aO_2}, \tag{6}$$

where S_vO_2 - venous blood oxygen saturation, calculated using spectral wavelet analysis of tissue oxygen saturation changes. We also analysed the amplitude of tissue oxygen saturation changes $(\delta S_tO_2)_c$, topographically linked to the influent blood of the microvasculature (predominantly cardiac rhythms), and the amplitude of tissue oxygen saturation changes $(\delta S_tO_2)_r$, topographically linked to the effluent blood of the microvasculature (predominantly respiratory rhythms) . If the $(\delta S_tO_2)_c/(\delta S_tO_2)_r$ ratio ≤ 1, then S_vO_2 is taken to be equal to S_tO_2. This variant predominates in most cases of recordings from the skin without AVAs. If the $(\delta S_tO_2)_c/(\delta S_tO_2)_r$ ratio > 1, then:

$$S_vO_2 = \frac{S_tO_2}{(\delta S_tO_2)_c/(\delta S_tO_2)_r}. \tag{7}$$

This variant predominates in most cases of recordings from the skin with AVAs. In the cases of resonance in oxygen saturation changes in the active frequency bands (for example, in the myogenic range during adaptive changes), the value $(\delta S_tO_2)_c$ and $(\delta S_tO_2)_r$ may not be expressed in the spectrum, and the S_vO_2 calculation has some specific features. In the cases of resonance in oxygen saturation changes in the total myogenic and respiratory bands, $S_vO_2 = S_tO_2$. In the skin zones with AVAs, an additional factor, the bypass index (*BI*) for S_tO_2, is necessary:

$$S_vO_2 = \frac{S_tO_2}{BI(S_tO_2)}, \tag{8}$$

where:

$$BI(S_tO_2) = 1 + \frac{(\delta S_tO_2)_n}{(\delta S_tO_2)_m}, \quad (9)$$

where $(\delta S_tO_2)_n$ and $(\delta S_tO_2)_m$ are amplitudes of oxygen saturation changes in neurogenic and myogenic rhythms respectively.

Oxygen consumption (*OC*), assessed in arbitrary units (AU), was calculated as follows:

$$OC = I_{mn} \cdot (S_aO_2 - S_vO_2), \quad (10)$$

where I_{mn} is the nutritive blood flow value was calculated according to the equation:

$$I_{mn} = \frac{I_m}{BI(I_m)}, \quad (11)$$

where $BI(I_m)$ is the bypass index is calculated for skin with AVAs similarly to formula (9), but only using perfusion data. For skin zones without AVAs:

$$BI(I_m) = \frac{(\delta I_m)_{\max}}{(\delta I_m)_m}, \quad (12)$$

where $(\delta I_m)_{max}$ is the maximum amplitude of the dominant oscillations in the active range of frequencies up to 0.15 Hz and $(\delta I_m)_m$ is amplitude of oscillations of myogenic rhythms.

Features involved in the calculation of oxygen consumption in cases with adaptive changes (for synchronization and resonance of myogenic oscillations in perfusion and oxygen saturation changes) were processed separately. It should be noted that the OC equation includes the perfusion rate value, due to which the OC value (calculated according to Fick's principle) reflects the oxygen consumption rate.

Furthermore, the normalized amplitude of myogenic rhythms was calculated using the standard deviation of perfusion and of tissue oxygen saturation, respectively:

$$(\delta I_m)'_m = \frac{(\delta I_m)_m}{\sigma_{per}}; \qquad (\delta S_tO_2)'_m = \frac{(\delta S_tO_2)_m}{\sigma_{sat}}, \quad (13)$$

where σ_{per} and σ_{sat} - standard deviation of perfusion and tissue oxygen saturation during a basic test, respectively.

Data presented in the text are means ± SD. Statistical analysis was performed using OriginPro 8 SRO version v.8.0724 with data sets tested for normality by the Kolmogorov-Smirnov and Shapiro-

Wilk tests. For normally distributed data, group comparisons were made by carrying out a parametric unpaired *t*-test. For the non-normally distributed data, the Mann-Whitney test of nonparametric statistics was used to compare the two groups (normal and with conditions of adaptive changes).

3. Results and discussion

Analysis of the data has demonstrated the emergence of synchronization and resonance of vasomotion in microvascular blood flow and oxygen saturation only in the range of myogenic oscillation during adaptive changes – for example, stressful situations or reaction to sports load. The typical form of perfusion and tissue oxygen saturation, along with the results of wavelet analysis of these parameters during adaptive changes, are presented in Fig. 3.

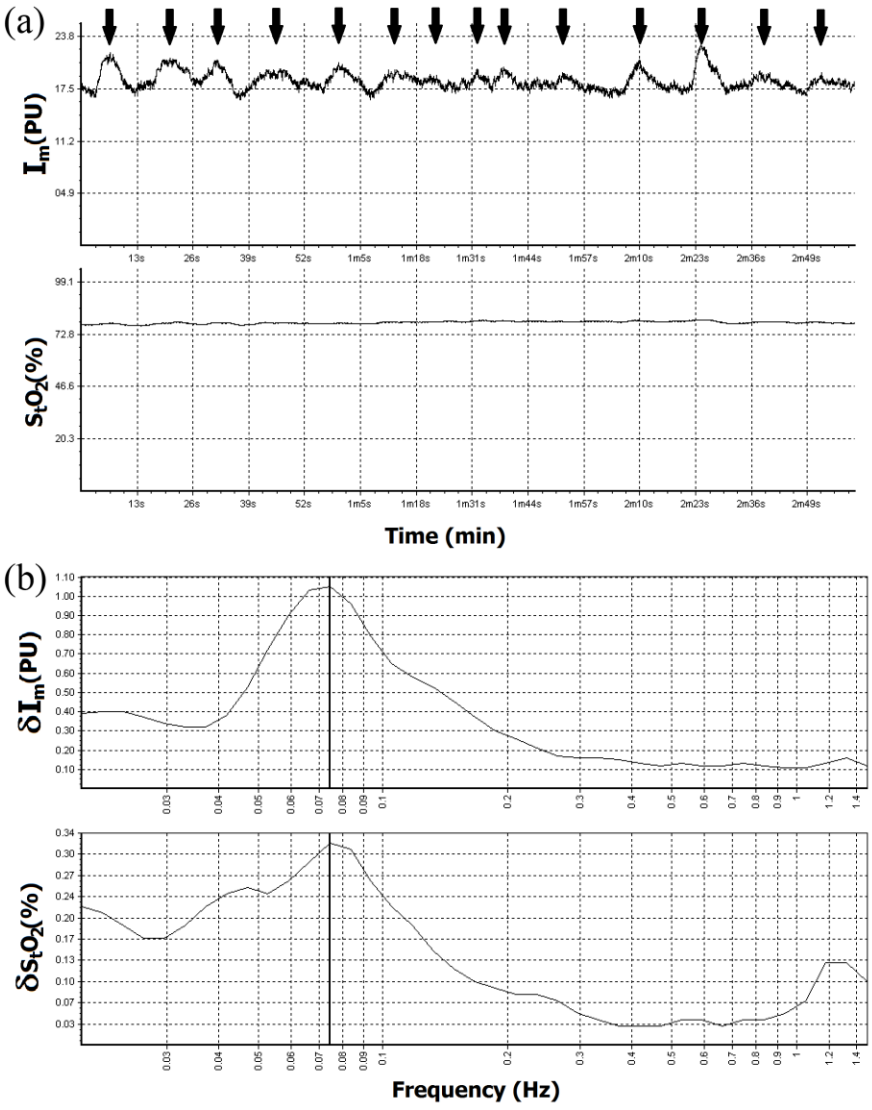

Figure 3. (a) Perfusion and oxygen saturation graphs in cases of myogenic oscillation, represented on the I_m-graph by a ↓ and (b) typical example of resonance and synchronized

rhythms (f_m=0.074 Hz) of microvascular blood flow $(\delta I_m)_m$=1.05 PU and oxygen saturation $(\delta S_tO_2)_m$=0.32% within the range of only myogenic oscillation (vasomotion) during adaptive changes.

The parameters for calculating oxygen extraction and consumption for all volunteers were obtained using the approaches detailed in the methods section above. The results of measurements in the skin with AVAs and calculations of the parameters of tissue respiration (oxygen extraction and consumption) for volunteer №1 with the single largest sample of recorded data are shown in Table 2. The results of measurements and calculations for both areas studied (skin with and without AVAs) for all the 8 volunteers are shown in Table 3.

Table 2. The results of measurements in the skin with AVAs and calculation of oxygen extraction and consumption for volunteer №1.

№	Parameters	State		
		Norm (n=58)	With adaptive changes - stress (n=21)	With adaptive changes - sport (n=20)
1	I_m(total), PU	20.8±2.7	20.3±3.1	20.3±2.4
2	I_{mn}(nutritive), PU	8.4±1.6	10.6±1.9[a]	11.5±1.3[a]
3	S_aO_2, %	98.1±0.5	97.9±0.5	97.7±0.5
4	S_tO_2, %	76.1±2.9	75.2±2.8	76.3±4.2
5	S_vO_2, %	39.8±10.3	41.2±5.5	41.7±5.5
6	V_b, %	9.9±0.9	10.0±0.9	10.4±0.8
7	$(\delta I_m)'_m$, AU	0.44±0.14	0.54±0.15[b]	0.61±0.14[b]
8	$(\delta S_tO_2)'_m$, AU	0.39±0.15	0.44±0.15	0.54±0.21[b]
9	$f_m(\delta I_m)$, Hz	0.071±0.012	0.077±0.019[b]	0.092±0.015[b]
10	$f_m(\delta S_tO_2)$, Hz	0.081±0.026	0.092±0.035	0.092±0.014[b]
11	$BI(I_m)$, AU	2.5±0.4	1.9±0.2[b]	1.8±0.2[b]
12	$BI(S_tO_2)$, AU	2.4±0.7	1.8±0.2[b]	1.9±0.2[b]
13	*OE*, AU	0.59±0.11	0.58±0.06	0.57±0.06
14	*OC*, AU	488.6±131	597±109[b]	641±91[b]

[a] significant difference ($p < 0.05$) observed from normal state, calculated by a *t*-test.

[b] significant difference ($p < 0.05$) observed from normal state, calculated by the Mann-Whitney test.

Table 3. The results of measurements and calculations for all 8 volunteers

№	Parameters	Skin with AVAs		Skin without AVAs	
		Norm (n=187)	With adaptive changes (n=60)	Norm (n=128)	With adaptive changes (n=26)
1	I_m(total), PU	21.0±3.1	21.4±3.4	2.5±0.8	2.8±0.9
2	I_{mn}(nutritive), PU	8.6±0.5	11.1±2.2[a]	1.7±0.8	2.8±0.8[b]
3	S_aO_2, %	98.1±0.4	97.9±0.4	97.9±0.4	97.8±0.6
4	S_tO_2, %	78.3±4.7	77.7±5.7	66.2±9.3	61.9±7.3

5	S_vO_2, %	41.6±13.7	41.9±6.1	58.2±12.7	61.3±7.3
6	V_b, %	10.2±1.8	9.9±1.5	6.3±1.7	6.0±1.4
7	$(\delta I_m)'_m$, AU	0.44±0.13	0.52±0.13[b]	0.46±0.13	0.67±0.11[b]
8	$(\delta S_tO_2)'_m$, AU	0.33±0.15	0.41±0.17[b]	0.25±0.13	0.77±0.19[b]
9	$f_m(\delta I_m)$, Hz	0.086±0.023	0.084±0.025	0.089±0.018	0.086±0.021
10	$f_m(\delta S_tO_2)$, Hz	0.091±0.029	0.093±0.035	0.090±0.019	0.084±0.021[b]
11	$BI(I_m)$, AU	2.5±0.5	1.9±0.2[b]	1.6±0.6	1.0±0.06[b]
12	$BI(S_tO_2)$, AU	2.7±0.7	1.9±0.2[b]	2.4±1.6	1.0±0.2[b]
13	*OE*, AU	0.58±0.14	0.57±0.06	0.41±0.13	0.37±0.07
14	*OC*, AU	495±170	617±123[b]	69±40	102±38[b]

[a] significant difference ($p < 0.05$) observed from normal state, calculated by a *t*-test.

[b] significant difference ($p < 0.05$) observed from normal state, calculated by the Mann-Whitney test.

The data received for volunteer №1 (Table 2) presented 41 cases (20 cases of which were after exercise) of synchronization and resonance of vasomotion in microvascular blood flow and oxygen saturation out of a total of 99 recorded measurements of skin containing AVAs. For the total population (Table 3), 60 out of 247 measurements of AVA containing skin and 26 out of 154 measurement in AVA free skin were observed to have synchronization.

The human skin contains functionally distinct zones, differing in morphological properties and the regulation of microvascular blood flow. These can be classified as with and without the presence of AVAs. The zones with AVAs are functionally tied to the implementation of thermoregulatory homeostasis and are almost exclusively regulated by the sympathetic adrenergic nervous system. Additionally, the values of perfusion and intravascular pressure of the skin microvessels is generally higher in regions containing AVAs. The zones of skin without AVAs are characterised by lower blood flow in microvessels and a higher contribution of the venous component. As the data of Tables 2-3 shows, during adaptive changes, a significant increase in the nutritive perfusion (I_{mn}) is observed in the zones with AVAs: for example, for volunteer №1 – 8.4±1.6 PU vs. 10.6±1.9 PU, $p < 0.05$ (for stress) and 8.4±1.6 PU vs. 11.5±1.3 PU, $p < 0.05$ (for sport) and for all volunteers – 8.6±0.5 PU vs. 11.1±2.2 PU $p < 0.05$ (for stress). Oxygen extraction did not change in the zones with and without AVAs. Increasing oxygen consumption was therefore due to an increase in perfusion rather than an increase in OE, thus adaptive changes naturally lead to the intensification of oxygen consumption in zones with AVAs: for example, for volunteer №1 – 488.6±131 AU vs. 597±109, $p < 0.05$ (for stress) and 488.6±131 AU vs. 641±91 AU, $p < 0.05$ (for sport); for all volunteers - 495±170 AU vs. 617±123 AU, $p < 0.05$ (for stress). More cases of synchronization of myogenic rhythms of microvascular blood flow and oxygen saturation were observed in zones with AVAs, this is most likely due to the larger numbers of autonomic nerves, which are very responsive to adaptive changes. Additionally, adaptive changes caused by sport were manifested more clearly during the early stages of physical training (first 2-3 weeks). This may be due to an adaptation of the microcirculatory system to the physical loads upon the organism.

The results from our studies on adaptive changes (stress- or exercise-induced) support our hypothesis that during resonance and synchronization of blood flow oscillations and oxygen saturation changes via myogenic oscillation there is increased tissue oxygen consumption compared with normal conditions. Thus, extraction of oxygen remains unchanged. In all cases the bypass index reduced under conditions of stress and exercise, therby confirming reduced circulatory AVAs as one healthy physiological response to stress.

Therefore, we suggest that the bypass index may be used as a marker of adaptive changes (indicating stress conditions), calculated based on perfusion and tissue oxygen saturation.

The increase in amplitude of myogenic rhythm reflects a modulation of the hydrostatic pressure in the capillaries, resulting in an increase in diffusion of oxygen into the tissues, hence the changes in tissue oxygen saturation. Time shifts and frequency characteristics are obviously specific to particular individuals. For example, the number of recorded cases of adaptive changes for each volunteer is presented in Table 4.

Table 4. Individual cases of adaptive changes per volunteer.

№ Volunteer	With AVAs		Without AVAs	
	Adaptive chages	Total	Adaptive changes	Total
1	41	99	7	41
2	5	39	-	-
3	4	23	1	5
4	4	18	4	14
5	11	27	0	25
6	9	34	9	31
7	2	22	3	21
8	3	25	2	17

Analysis of recorded time fragments under normal conditions, during stress and following exercise presented distinct differences in the frequency of myogenic oscillations in perfusion and tissue oxygen saturation changes. As the data on Tables 2-3 shows, the frequency of oxygen saturation changes corresponding to the oscillations of blood flow in the myogenic range and the vasomotion in perfusion both increase under adaptive changes (heading towards the so-called central frequency of myogenic oscillations – 0.1 Hz). This is particularly expressed in the case of the reaction to sports load for volunteer №1 with perfusion 0.071±0.012 Hz vs. 0.092±0.015 Hz, $p < 0.05$ and tissue oxygen saturation 0.081±0.026 Hz vs. 0.092±0.014 Hz, $p < 0.05$. This is likely the result of higher levels of adaptive change causing more intense and clear synchronisation of vasomotion. Occasionally, complete synchronization will be achieved when the frequency of both myogenic oscillations coincide. For example, this case is presented in Fig.4.

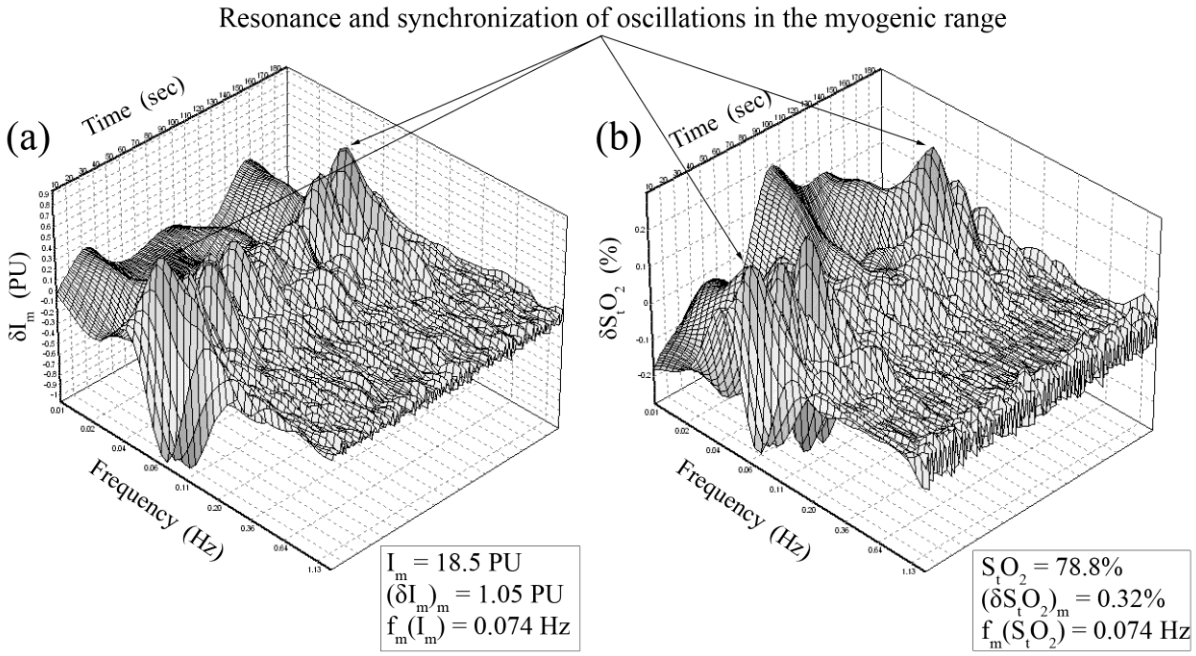

Figure 4. Typical example of the 3D wavelet analysis of resonating and synchronized myogenic rhythms of microvascular blood flow (a) and oxygen saturation changes (b) during adaptive changes.

The analysis of data presented in tables 2-3 also shows that normalized perfusion vasomotion amplitudes (for example in the regions with AVA for all volunteers – 0.44±0.13 AU vs. 0.52±0.13, $p < 0.05$) and tissue oxygen saturation (0.33±0.15 AU vs. 0.41±0.17, $p < 0.05$) increase under adaptive changes. This is the result of these amplitudes shifting towards synchronisation at the microcirculatory level to maintain homeostasis in the oxygen delivery and consumption system. These cases demonstrate increased blood flow and oxygen into the nutritive flux, which is reflected in the spectrum as a rise in myogenic oscillations amplitude. The oxygen delivered to the nutritive flux can move into tissues and be consumed in the process of metabolism. This results in an increasing OC and/or OE. If the tissue exchange is not active, the oxygen may be shunted. This is particularly visible in areas without AVAs, where the shunting happens via major vessels. In this circumstance, however, OC and/or OE do not rise or fall despite an increase in myogenic amplitudes to a resonance within the spectrum (for example, for the perfusion of all volunteers 0.46±0.13 AU vs. 0.67±0.11 AU, $p < 0.05$ and for the tissue oxygen saturation 0.25±0.13 AU vs. 0.77±0.19 AU, $p < 0.05$).

Data analysis has demonstrated an increase in resonance and synchronization of microvascular blood flow and oxygen saturation rhythms as an adaptive change in myogenic oscillation (vasomotion) resulting from exercise and potentially from psychoemotional stress. An explanation for this observed

response may be that the synchronization of myogenic rhythms facilitates maximum oxygen delivery to tissue following or during periods of physical or emotional stress. The data obtained show differences in myogenic oscillations in both the ordinary state of the body (normality) and during episodes of sympathoadrenal activation (e.g. emotional stress). Normally, all systems of the body (including blood circulation, respiration, metabolism, etc.) work in different phases and frequencies, exhibiting non-linearity and independence. Synchronization of myogenic rhythms during adaptive changes may promote increased oxygen consumption resulting from increased microvascular blood flow velocity. The data above indicates that adaptive changes lead to the intensification of oxygen consumption in zones with AVAs due to an increased perfusion. Furthermore, as these zones have rich autonomic innervation, they are very sensitive to adaptive change leading to them having a higher incidence of myogenic rhythm synchronization of microvascular blood flow and oxygen saturation. During adaptive changes (under particular emotional stress, etc.), synchronization increases, reducing the freedom of microvascular blood flow regulation.

Ultimately, our suggested approaches for the use of the laser technology in investigating tissue respiration and skin microhaemocirculation under adaptive changes, through the use of the synchronization of blood flow and oxygen saturation rhythms observed within the data, have shown themselves to be highly informative of the response of the microcirculation system and offers interesting prospects for further investigation as a potential diagnostic methodology relevant to vascular function.

Acknowledgements

We would like to thank all of our volunteers for their contribution to this research project.

Grants

This work was supported by the European Community's Seventh Framework Programme (FP7-People-2009-IAPP) under Grant Agreement no. 251531 MEDILASE.

References

AMZINA, M. V., MICHEEV, A. A., ROGATKIN, D. A. & SIDOROV, V. V. 2006. Combined medical diagnostic system with separated laser-Doppler and reflectance oximeter channels. *Proc. SPIE 6163, Saratov Fall Meeting 2005: Optical Technologies in Biophysics and Medicine VII***,** 616317.

BERNJAK, A., STEFANOVSKA, A., MCCLINTOCK, P. V. E., OWEN-LYNCH, P. J. & CLARKSON, P. B. M. 2012. Coherence between fluctuations in blood flow and oxygen saturation. *Fluctuation and Noise Letters,* 11.

BERNJAK, A., STEFANOVSKA, A., URBANCIC-ROVAN, V. & AZMAN-JUVAN, K. 2005. Quantitative assessment of oscillatory components in blood circulation: classification of the effect of ageing, diabetes and acute myocardial infarction. *In:* VODINH, T., GRUNDFEST, W. S., BENARON, D. A. & COHN, G. E. (eds.) *Advanced Biomedical and Clinical Diagnostic Systems III.*

BRACIC, M. & STEFANOVSKA, A. 1998. Wavelet-based analysis of human blood-flow dynamics. *Bulletin of Mathematical Biology,* 60**,** 919-935.

COCA, D., ZHENG, Y., MAYHEW, J. E. W. & BILLINGS, S. A. 1998. Non-linear analysis of vasomotion oscillations in reflected light measurements. *In:* HUDETZ, A. G. & BRULEY, D. F. (eds.) *Oxygen Transport to Tissue Xx.* New York: Plenum Press Div Plenum Publishing Corp.

COCA, D., ZHENG, Y., MAYHEW, J. E. W. & BILLINGS, S. A. 2000. Nonlinear system identification and analysis of complex dynamical behavior in reflected light measurements of vasomotion. *International Journal of Bifurcation and Chaos,* 10**,** 461-476.

COLQUHOUN, D., TUCKER-SCHWARTZ, J., DURIEUX, M. & THIELE, R. 2012. Non-invasive estimation of jugular venous oxygen saturation: a comparison between near infrared spectroscopy and transcutaneous venous oximetry. *Journal of Clinical Monitoring and Computing,* 26**,** 91-98.

DALY, S. M., SILIEN, C. & LEAHY, M. J. 2013. Optimization and extraction of functional information from in vitro flow models using dual-beam spectral-domain optical coherence tomography cross-correlation analysis. *Journal of Biomedical Optics,* 18.

DUNAEV, A. V., SIDOROV, V. V., STEWART, N. A., SOKOLOVSKI, S. G. & RAFAILOV, E. U. 2013. Laser reflectance oximetry and Doppler flowmetry in assessment of complex physiological parameters of cutaneous blood microcirculation. *In:* MAHADEVAN-JANSEN, A., VO-DINH, T. & GRUNDFEST, W. S. (eds.) *Proc. SPIE 8572, Advanced Biomedical and Clinical Diagnostic Systems XI.* San Francisco, California, USA: SPIE.

FINE, I., KAMINSKY, A., KUZNIK, B. & SHENKMAN, L. 2012. A non-invasive method for the assessment of hemostasis in vivo by using dynamic light scattering. *Laser Physics,* 22**,** 469-475.

GRAAFF, R., MORALES, F., SMIT, A. J., DE JONG, E. D., DE MUL, F. F. M. & RAKHORST, G. 2007. Normalization of vasomotion in laser Doppler perfusion monitoring. *Conference proceedings : ... Annual International Conference of the IEEE Engineering in Medicine and Biology Society. IEEE Engineering in Medicine and Biology Society. Conference,* 2007**,** 4076-9.

HEUSMANN, H., KOELZER, J. G. & MITIC, G. 1996. Characterization of female breasts in vivo by time-resolved and spectroscopic measurements in the near infrared spectroscopy. *Journal of Biomedical Optics,* 1**,** 425-434.

KALCHENKO, V., KUZNETSOV, Y., MEGLINSKI, I. & HARMELIN, A. 2012. Label free in vivo laser speckle imaging of blood and lymph vessels. *Journal of Biomedical Optics,* 17.

KALCHENKO, V., MADAR-BALAKIRSKI, N., MEGLINSKI, I. & HARMELIN, A. 2011. In vivo characterization of tumor and tumor vascular network using multi-modal imaging approach. *Journal of Biophotonics,* 4**,** 645-649.

KHALIL, O. S. 2006. Metabolites, noninvasive optical measurements of. *In:* AKAY, M. (ed.) *Wiley encyclopedia of biomedical engineering.* New Jersey: A John Wiley & Sons, Inc.

KISLUKHIN, V. V. 2004. Regulation of oxygen consumption by vasomotion. *Mathematical Biosciences,* 191**,** 101-108.

KRUPATKIN, A. I. 2007. Dynamic oscillatory circuit of regulation of capillary hemodynamics. *Human Physiology,* 33**,** 595-602.

KRUPATKIN, A. I. 2008. Cardiac and respiratory oscillations of the blood flow in microvessels of the human skin. *Human Physiology,* 34**,** 323-329.

KRUPATKIN, A. I. 2009. Blood flow oscillations at a frequency of about 0.1 Hz in skin microvessels do not reflect the sympathetic regulation of their tone. *Human Physiology,* 35**,** 183-191.

KRUPATKIN, A. I. 2011. The Problem of Information Value in Microvascular Networks. *Human Physiology,* 37**,** 312-317.

KRUPATKIN, A. I. 2012. Noninvasive estimation of human tissue respiration with wavelet-analysis of oxygen saturation and blood flow oscillations in skin microvessels. *Human Physiology,* 38**,** 396-401.

KRUPATKIN, A. I., ROGATKIN, D. A. & SIDOROV, V. V. 2007. Clinical-diagnostic parameters for complex investigation of microhaemodynamics and oxygen transport in the system of microcirculation Hemorheology and microcirculation, 2007 Yaroslavl, Russia. 106.

KRUPATKIN, A. I. & SIDOROV, V. V. (eds.) 2005. *Laser Doppler flowmetry of blood,* Moscow: Meditcina-Press.

KVANDAL, P., LANDSVERK, S. A., BERNJAK, A., STEFANOVSKA, A., KVERNMO, H. D. & KIRKEBOEN, K. A. 2006. Low-frequency oscillations of the laser Doppler perfusion signal in human skin. *Microvascular Research,* 72**,** 120-127.

KVERNMO, H. D., STEFANOVSKA, A., KIRKEBOEN, K. A. & KVERNEBO, K. 1999. Oscillations in the human cutaneous blood perfusion signal modified by endothelium-dependent and endothelium-independent vasodilators. *Microvascular Research,* 57**,** 298-309.

LEAHY, M. J. & NILSSON, G. E. Laser Doppler flowmetry for assessment of tissue microcirculation: 30 years to clinical acceptance. 2010. 75630E-75630E-5.

NEWMAN, J. M. B., DWYER, R. M., ST-PIERRE, P., RICHARDS, S. M., CLARK, M. G. & RATTIGAN, S. 2009. Decreased microvascular vasomotion and myogenic response in rat skeletal muscle in association with acute insulin resistance. *Journal of Physiology-London,* 587**,** 2579-2588.

OBEID, A. N. 1993. *In vitro* comparison of different signal-processing algorithms used in laser doppler flowmetry. *Medical & Biological Engineering & Computing,* 31**,** 43-52.

QUARESIMA, V., FERRARI, M. & FANTINI, S. 2013. Accurary of Oxygen Desaturation of Hemoglobin in Muscle by Near-Infrared Oximeters. *Medicine and Science in Sports and Exercise,* 45**,** 1217-1217.

ROGATKIN, D. A., DUNAEV, A. V. & LAPAEVA, L. G. 2010. Metrological Support of Methods and Devices for Noninvasive Medical Spectrophotometry. *Biomedical Engineering,* 44**,** 66-70.

ROGATKIN, D. A. & LAPAEVA, L. G. 2003. Prospects for development of non-invasive spectrophotometry medical diagnostics. *Biomedical Engineering,* 37**,** 217-222.

ROGATKIN, D. A., SOKOLOVSKI, S. G., FEDOROVA, K. A., SIDOROV, V. V., STEWART, N. Z. & RAFAILOV, E. U. 2011. Basic principles of design and functioning of multifunctional laser diagnostic system for non-invasive medical spectrophotometry. Photonics West, 2011 San-Francisco. SPIE Proceedings 78901H1.

ROSSI, M., CARPI, A., GALETTA, F., FRANZONI, F. & SANTORO, G. 2008. Skin vasomotion investigation: A useful tool for clinical evaluation of microvascular endothelial function? *Biomedicine & Pharmacotherapy,* 62**,** 541-545.

ROSSI, M., MATTEUCCI, E., PESCE, M., CONSANI, C., GALETTA, F., GIAMPIETRO, O. & SANTORO, G. 2013. Study of skin vasomotion in type 1 diabetic patients and of its possible relationship with clinical and laboratory variables. *Clinical Hemorheology and Microcirculation,* 53**,** 357-367.

SALERUD, E. G., TENLAND, T., NILSSON, G. E. & OBERG, P. A. 1983. Rhythmical variations in human-skin blood-flow. *International Journal of Microcirculation-Clinical and Experimental,* 2**,** 91-102.

SCHMIDT-LUCKE, C., BORGSTROM, P. & SCHMIDT-LUCKE, J. A. 2002. Low frequency flowmotion/(vasomotion) during patho-physiological conditions. *Life Sciences,* 71**,** 2713-2728.

SCHMIEDEL, O., SCHROETER, M. L. & HARVEY, J. N. 2007. Microalbuminuria in Type 2 diabetes indicates impaired microvascular vasomotion and perfusion. *American Journal of Physiology - Heart and Circulatory Physiology,* 293**,** H3424-H3431.

STEFANOVSKA, A. 2009. Dynamics of blood oxygenation gives better insight into tissue hypoxia than averaged values. *American Journal of Physiology - Heart and Circulatory Physiology,* 296**,** H1224-H1226.

STEFANOVSKA, A., BRACIC, M. & KVERNMO, H. D. 1999. Wavelet analysis of oscillations in the peripheral blood circulation measured by laser Doppler technique. *IEEE Transactions on Biomedical Engineering,* 46**,** 1230-1239.

STEWART, N. A., DUNAEV, A. V., SOKOLOVSKI, S. G., SIDOROV, V. V. & RAFAILOV, E. U. 2012. Multi-parameter analysis in blood circulation and and perfusion based diagnostics. Laser Optics 2012, 25-29 June 2012 2012 St.Petersburg, Russia.

TANKANAG, A. & CHEMERIS, N. 2008. Application of the adaptive wavelet transform for analysis of blood flow oscillations in the human skin. *Physics in Medicine and Biology,* 53**,** 5967-5976.

TANKANAG, A. V. & CHEMERIS, N. K. 2009. A method of adaptive wavelet filtering of the peripheral blood flow oscillations under stationary and non-stationary conditions. *Physics in Medicine and Biology,* 54**,** 5935-5948.

THORN, C. E., KYTE, H., SLAFF, D. W. & SHORE, A. C. 2011. An association between vasomotion and oxygen extraction. *American Journal of Physiology-Heart and Circulatory Physiology,* 301**,** H442-H449.

THORN, C. E., MATCHER, S. J., MEGLINSKI, I. V. & SHORE, A. C. 2009. Is mean blood saturation a useful marker of tissue oxygenation? *American Journal of Physiology - Heart and Circulatory Physiology,* 296**,** H1289-H1295.

TYRRELL, J., THORN, C., SHORE, A., CAMPBELL, S. & CURNOW, A. 2011. Oxygen saturation and perfusion changes during dermatological methylaminolaevulinate photodynamic therapy. *British Journal of Dermatology,* 165**,** 1323-1331.

ZAKHAROV, P., DEWARRAT, F., CADUFF, A. & TALARY, M. S. 2011. The effect of blood content on the optical and dielectric skin properties. *Physiological Measurement,* 32**,** 131.

ZAKHAROV, P., TALARY, M. S. & CADUFF, A. 2009. A wearable diffuse reflectance sensor for continuous monitoring of cutaneous blood content. *Physics in Medicine and Biology,* 54**,** 5301.

Journal of Biomedical Optics

SPIEDigitalLibrary.org/jbo

Substantiation of medical and technical requirements for noninvasive spectrophotometric diagnostic devices

Andrey V. Dunaev
Evgeny A. Zherebtsov
Dmitrii A. Rogatkin
Neil A. Stewart
Sergei G. Sokolovski
Edik U. Rafailov

SPIE

Substantiation of medical and technical requirements for noninvasive spectrophotometric diagnostic devices

Andrey V. Dunaev,[a,b] Evgeny A. Zherebtsov,[b] Dmitrii A. Rogatkin,[c] Neil A. Stewart,[a] Sergei G. Sokolovski,[a] and Edik U. Rafailov[a]

[a]University of Dundee, Photonics and Nanoscience Group, School of Engineering, Physics and Mathematics, Dundee DD1 4HN, United Kingdom
[b]State University—Education-Science-Production Complex, Scientific-Educational Center of Biomedical Engineering, Oryol 302020, Russian Federation
[c]Moscow Regional Research and Clinical Institute "MONIKI," Laboratory of Medical & Physics Research, Moscow 12911, Russian Federation

Abstract. A scientific approach to the formulation of medical and technical requirements (MTRs) for noninvasive spectrophotometric diagnostic devices using optical technologies such as laser Doppler flowmetry and absorption spectroscopy is proposed. The theoretical modeling framework, metrological certification, and testing of these devices are still in the early stages of development. The theoretical estimation of the received signal levels for wavelengths between 514 and 940 nm is highly dependent on the blood volume level in the subject tissue. The proposed approach allows, in particular, the calculation of technical and metrological performance constraints of the instruments, such as the ranges of the sensitivity and power-related signal-to-noise ratios for different spectral channels and different biomedical (biochemical and physiological) parameters. Substantiation of specialized MTRs for the noninvasive spectrophotometric diagnostic devices can enable them to develop to the level of standardized measurement techniques. [DOI: 10.1117/1.JBO.18.10.107009]

Keywords: noninvasive medical spectrophotometry; laser Doppler flowmetry; tissue reflectance oximetry; medical devices; medical and technical requirements; tissue blood volume.

Paper 130344RRR received May 13, 2013; revised manuscript received Sep. 13, 2013; accepted for publication Oct. 1, 2013; published online Oct. 28, 2013.

1 Introduction

Recent years have seen great progress and accomplishments in photonics and biophotonics bringing the development of novel and compact noninvasive optical diagnostic devices in biomedicine.[1–6] Though there are a great variety of devices in this class, the largest group of equipment implements the principle of noninvasive medical spectrophotometry (NMS).[7] These optical systems can report the levels of various biochemical components, such as de/oxyhemoglobins, collagen/elastin, porphyrins, lipofuscin, NADH, flavins, etc., in tissues. They can, thus, measure the dynamics of metabolism and examine the major regulatory processes of blood flow without the need to take biopsies (skin, oral mucosa, etc.). A promising direction in the development of NMS devices is the creation of multifunctional noninvasive diagnostic systems, which combine in a single-hardware different methods of NMS: fluorescence spectroscopy (laser fluorescence diagnostics), absorption spectroscopy (UV/VIS or near IR spectral region)—tissue reflectance oximetry (TRO) and/or near infrared spectroscopy (NIRS), laser Doppler flowmetry (LDF), pulse oximetry, etc.[8] Such devices allow acquisition of comprehensive real-time biomedical information from the site examined.

Until recently, such diagnostic systems were generally empirically designed in the absence of any well-developed and systematized theory. The theoretical modeling framework, metrological certification, and testing of these devices are still in the earliest stages of development. There are virtually no evidence-based approaches and techniques to intelligently formulate specialized medical and technical requirements (MTRs) for diagnostic device parameters. For example, there are few recommendations and rationales in the literature for selecting the accuracy class required for NMS devices.[9] Recently, the theoretical issues of formalizing diagnostic tasks for NMS have been examined, with structural and functional model circuits developed and physical–mathematical theory generalized for NMS.[2,10,11] These apply to the general phases of the ideological and technical design and realization of such devices. These authors considered some key features of metrology of the NMS for *in vivo* measurements.[9] For instance, they proposed an investigation into the diagnostic volume in NMS, alongside a theoretical and experimental study of the impact of diagnostic volume on the metrological parameters of such devices. In addition, there have been propositions to develop reproducible and standard methods of tuning, calibration, and verification of NMS devices without the use of human subjects by using optical phantoms as test objects.

In this article, we report further developments in the scientific approaches to substantiate meeting of MTRs for noninvasive spectrophotometric diagnostic devices. This is primarily based on study of the influence of tissue blood volume on registered signal levels and the sensitivity of such devices.

2 Methods and Functional Scheme of Measurements by the NMS

In NMS, the most sensitive method for recording the dynamic processes in the blood microcirculatory system is LDF. This is based on the assessment of Doppler frequency shifts, which occur after the backscattering of radiation from red blood cells moving at different speeds in small vessels—arterioles,

Address all correspondence to: A. V. Dunaev, University of Dundee, Photonics and Nanoscience Group, School of Engineering, Physics and Mathematics, Dundee DD1 4HN, United Kingdom. Tel: +441382386571; Fax: +441382388313; E-mail: a.v.dunaev@dundee.ac.uk

0091-3286/2013/$25.00 © 2013 SPIE

capillaries, and venules.[4] This is represented as a microcirculation index I_m in arbitrary perfusion units. Perfusion fluctuations are recorded as a complex nonperiodic process. The variable component provides valuable information on the modulation of blood flow. Spectral signal processing algorithms used for decoding and analysis provide information about the vascular tone in terms of contribution of the different regulatory mechanisms of microhemodynamics (endothelial, neurogenic, myogenic, breath, pulse, etc.).[12]

Tissue reflectance oximetry is based on the principles of absorption spectroscopy and allows noninvasive (*in vivo*, transcutaneous) monitoring of microhemodynamics and oxygen transport and utilization within the entire blood microcirculation system.[13,14] TRO determines the relative volume of all fractions of hemoglobin (total hemoglobin) in a tissue volume (average level of blood volume—V_b) and oxygen saturation of the microvasculature, generally containing arterioles with oxyhemoglobin and venules with deoxyhemoglobin (average level of tissue oxygen saturation—S_tO_2).[2]

Following an integrated biotechnical approach, we can formulate the measurement tasks for the methods incorporated into the NMS and consider the general functional scheme of the measurements made in NMS (Fig. 1). In the diagnostic device, light with a wavelength λ and with a power $P_s(\lambda)$ from the radiation source 1 is delivered by optical lighting system 2 to the examined biological object (BO) 3. Depending on the diagnostic method, the light source may be either a monochromatic (laser) or a set of variable light sources with different emission spectra.

In tissue, radiation is extensively scattered at the boundaries of morphological irregularities and is partially absorbed by substances like water, melanin, hemoglobin, etc., before the reemergence of the attenuated radiation. Due to multiple scattering events, part of the radiation exiting the BO forms a flux of backscattered light. This irradiation with power $P_r(\lambda) < P_s(\lambda)$ is delivered to the device by the irradiation transporting system 4 to the recording unit of the diagnostic device. In a simplified case, it is sent to the photodetector 5 that performs a linear transformation of the optical power $P_r(\lambda)$ to the photocurrent $I_c(\lambda)$. The produced electrical signal is processed in analogue mode (photocurrent $I_c(\lambda)$ to voltage $U(\lambda)$ conversion, amplification, filtering, etc.) in the electronics block 6, digitized and transmitted to the computer 7 for further computation. As a result, biomedical parameters, such as I_m, S_tO_2, and V_b, are calculated. Thus, the NMS implements an indirect measurement method.[15,16]

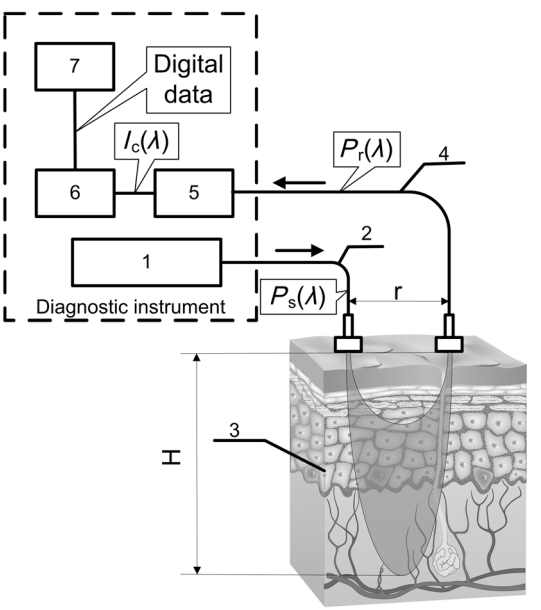

Fig. 1 The generalized functional scheme of the optical measurements by the NMS: 1—radiation source, 2—optical lighting system, 3—biological object, 4—irradiation transporting system, 5—photodetector, 6—electronics block, 7—computer. $P_s(\lambda)$—power from the radiation source, $P_r(\lambda)$—received power (backscattered radiation), I_c (λ)—photocurrent on photodetector, H—measurement depth, r—separation distance between the source and detector fibers.

Changes in blood microcirculation can be registered by the diagnostic NMS following changes in the optical properties of biotissue. Thus, changes in the optical properties of biological tissues have a major impact on signal levels recorded by the NMS and can be used in developing the MTRs of optical diagnostic devices.

3 Theoretical Estimation of the Levels of the Received Signals

Theoretical estimation of the signal variability measured by NMS devices operating in a backscattering mode using different spectral channels leads to the challenge of quantitative metrology using such measurements. It should be noted that attempts have been made to estimate the measurement depth (parameter H in the schematic Fig. 1) and the diagnostic volume for some methods of NMS [for example, LDF (Ref. 17)]. However, they use numerical simulation methods which do not deal with the relationship of estimated signal levels or MTRs for optical diagnostic devices. Depending on the types of tissues studied (with different absorption, scattering, and others properties), the measurement depth can range from 1 to 8 mm.[9]

A BO considered in the functional schematic (Fig. 1) can be represented as a nonlinear spectral-optical filter, which converts the power of initial $P_s(\lambda)$ to the power of secondary radiation $P_r(\lambda)$. Such representation is mathematically equivalent to the multiplication of the original optical signal by a dimensionless coding function $B(\lambda)$, which is dependent on the optical and physical, and medical and biological parameters of the object as well as the lighting conditions and delivered irradiation. The well-known expression obtained for the diffusion approximation of a semi-infinite medium can be cited as an example of the $B(\lambda)$ function:[18]

$$B(\lambda) = \frac{z_0 A}{2\pi} \cdot \left[\frac{\mu_d}{r^2 + z_0^2} + \frac{1}{(r^2 + z_0^2)^{3/2}}\right] \cdot \exp[-\mu_d (r^2 + z_0^2)^{1/2}], \quad (1)$$

where $z_0 = 1/\mu_s'$ represents the effective path length of the light; A is the detector area; r is the separation distance between the source and detector fibers in Fig. 1; $\mu_d = [3\mu_a(\mu_a + \mu_s')]^{1/2}$ and $\mu_s' = (1 - g)\mu_s$ are the reduced scattering coefficient; $g = g(\lambda)$, the anisotropy factor; $\mu_s = \mu_s(\lambda)$, the scattering coefficient; and $\mu_a = \mu_a(\lambda)$, the absorption coefficient.

For most of the nontransparent biological tissues, the anisotropy factor value is in the range of 0.7 to 0.95, and the $g(\lambda)$ for skin (both the dermis and epidermis) can be determined by the following empirical equation:[19]

$$g(\lambda) = 0.7645 + 0.2355 \cdot \left[1 - \exp\left(-\frac{\lambda - 500\ \text{nm}}{729.1\ \text{nm}}\right)\right]. \quad (2)$$

For the theoretical estimates of the parameters for the received signals, it is possible to calculate values of the $B(\lambda)$ function according to Eq. (1) for commonly used wavelengths at different levels of blood volume:

$$\mu_s(V_b) = V_b \cdot \mu_{sb}(\lambda) + (1 - V_b) \cdot \mu_{st}(\lambda), \quad (3)$$

$$\mu_a(V_b) = V_b \cdot \mu_{ab}(\lambda) + (1 - V_b) \cdot \mu_{at}(\lambda), \quad (4)$$

where V_b is the blood volume in tissue, μ_{sb} and μ_{ab} are scattering and absorption coefficients of blood, and μ_{st} and μ_{at} are scattering and absorption coefficients of the bloodless tissue (bloodless dermis/papillary dermis).

Absorption spectroscopy (TRO/NIRS) commonly uses wavelengths in the visible (more often—green, yellow, red) and/or infrared ranges, whereas in LDF, red/infrared ranges are used.[1,2,4,7] Considering, e.g., the "multifunctional laser analyzer of capillary blood flow" system[2] or other NMS devices using LDF and absorption spectroscopy technology,[1,5,20] for calculations in this article we will use the 514- to 940-nm wavelength range (namely for green—514 nm, for yellow—584 nm, for red—633 nm, and for infrared—800 and 940 nm).

There are a number of articles in existing literature which offer data regarding the impact of blood volume on tissue optical characteristics.[19,21–23] From these publications, it is possible to assess the approximate range of blood volume of different skin surfaces. Thus, Meglinski and Matcher[24,25] provide data on the blood volume of skin layers, for example, papillary dermis—4% and upper blood net dermis—30%. Lister et al.[23] report the range of 0.2% to 2% for epidermal and dermal blood volume fractions. The reported data on the blood volume in the skin of the forearm is 5.03%,[26] and at a tissue depth of 100 to 300 μm, the blood volume is 2 to 5%,[19] and from our experience, blood volume of the palmar surface of middle finger is 10 to 20%.[27] Taking all of these into account, our study uses 0 to 20% as the range of the tissue blood volume and in some cases up to 50% to assess the changes in functions.

Taking the value of the spacing $r = 1$ mm[17,28] (which can be up to 3 mm[29]), the area of the detector (an optical multimode fiber with about NA = 0.22) $A = 0.003$ mm^2 and using the appropriate scattering and absorption coefficients[30–35] (Table 1), $B(\lambda)$ can be plotted against tissue blood volume V_b (Fig. 2). Figure 3 shows $B(\lambda)$ with $V_b = 1\%$, 5%, 10%, and 15% for the 514 to 940 nm range of wavelengths, respectively. It should be noted that these graphs are constructed using five points, as it is difficult to find the values of the necessary scattering and absorption coefficients for blood and bloodless dermis for the same wavelengths. It is shown in Fig. 4 that $B(\lambda)$ is dependent on the value of the source–detector spacing $r = 0.5$ to 2 mm when $V_b = 10\%$.

Thus, as shown in Fig. 2, the signal attenuation is 4 to 5 orders of magnitude. Probe power in such devices generally ranges up to 10 mW,[7] with 3 to 4 mW being used in the LAKK-M system. At a probe power of 3 mW and sensor sensitivity of 0.5 A/W (e.g., silicon photodiode literature values are 0.72 A/W[36] and 0.3 to 0.7 A/W[37]), the registered photocurrents will be in the order of several microamperes.

The dependence of the photocurrent I_c and its derivative with respect to the blood volume of tissue dI/dV_b (the differential

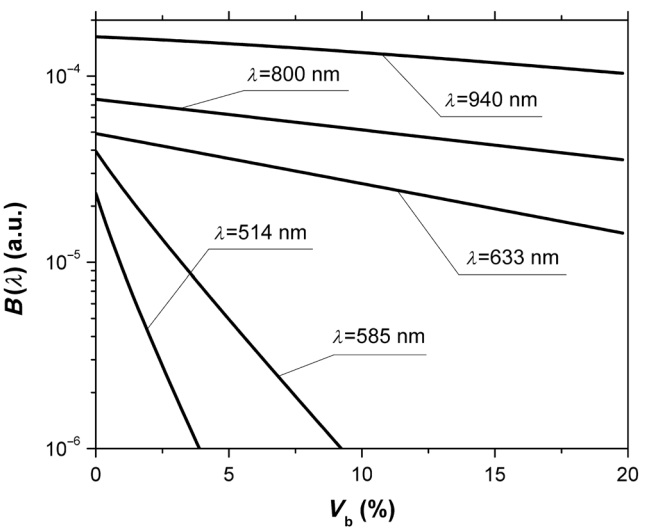

Fig. 2 The dependence of $B(\lambda)$ on the level of the tissue blood volume V_b. Here and in the following graphs, calculations for the 514- and 800-nm curves used the optical properties of blood for a wavelength of 517 and 810 nm, respectively (from Table 1).

Table 1 Optical properties for blood and tissue (bloodless dermis).

	Blood				Tissue			
λ (nm)	μ_{sb} (cm^{-1})	μ_{ab} (cm^{-1})	g	Notes	μ_{st} (cm^{-1})	μ_{at} (cm^{-1})	g	Notes
514	—	—	—	Ref. 30	250	3	0.77	Ref. 35
517	468	354	0.995		—	—	—	
585	467	191	0.995		196	3	0.79	
633	644.7	15.5	0.982	Ref. 31 (oxygenation >98%, Hct = 0.45 to 0.46)	187.5	2.7	0.80	
800	—	—	—		175	2.3	0.85	
810	690	6.5	0.989		—	—	—	
940	458.58	6.79	0.990	Refs. 32–34 (Hct = 0.45)	105.57	0.24	0.91	Ref. 33

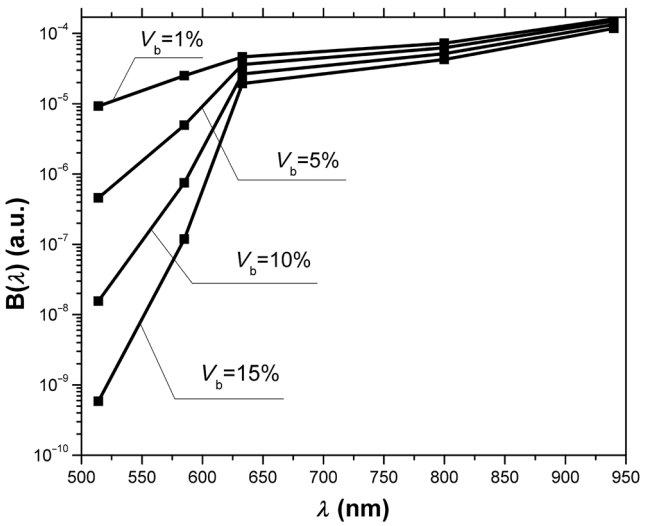

Fig. 3 The dependence of $B(\lambda)$ on the range of the wavelengths from 514 to 940 nm for different levels of the tissue blood volume (V_b = 1%, 5%, 10%, 15%).

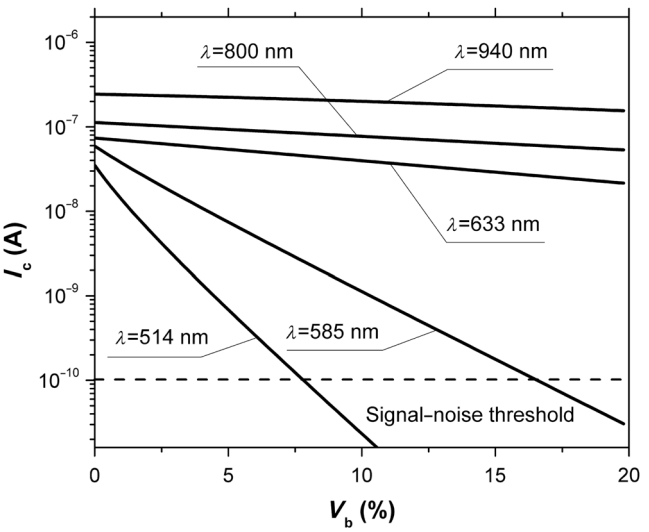

Fig. 5 The dependence of the photocurrent I_c upon the level of the tissue blood volume V_b.

sensitivity) relative to the level of the blood volume V_b are shown in Figs. 5 and 6, respectively. To account for signal noise, instrument errors, etc., a signal ambiguity threshold was set to respect the MTRs for noninvasive spectrophotometric diagnostic devices. A magnitude of 0.1 nA was selected for this threshold as dark photocurrent is in the range of 1 pA[37] to 10 nA.[38] The minimum registered change in blood volume ΔV_b must be greater than or equal to the volume corresponding to the selected threshold photodetector current change. Figure 7 shows the change in blood volume ΔV_b corresponding to the change of the photocurrent by 0.1 nA against the tissue blood volume V_b.

The ratio $V_b/\Delta V_b$ (Fig. 8) can be interpreted as the signal-to-noise ratio (SNR) during blood volume registration by the NMS devices. Hence, the relation in Fig. 8 is the dependence of SNR upon the level of blood volume at a given wavelength. Figure 8 shows that in the cases of 633 and 800 nm (red and infrared) light, the maximum SNR for NMS devices is in the higher tissue blood volume ranges near 15% to 20%, and for the 940-nm wavelength, the maximum SNR corresponds to 25% to 30% tissue blood volume.

4 Discussion

Theoretical data gained in this work shows that the use of NMS devices for functional diagnostics has specialized MTRs. The development of a common basis for the engineering design of such systems is necessary. With NMS, it is also necessary to create a complete system of metrological support as for instruments and measurement techniques, in general.[9] However, there are a number of specific features of the technology that add complexity in solving such problems. One of these features is a nonlinear dependence on the physical properties of the BO (such as light transmission) from its physiological state (e.g., blood volume level) and the wavelength of the probe radiation. A second feature is a wide range of variation of the physiological parameters, e.g., blood volume, which strongly affects the absorption of the radiation in the tissue. All of these problems can be solved by deriving the appropriate relationships which will improve the accuracy of diagnostics of the corresponding methods.

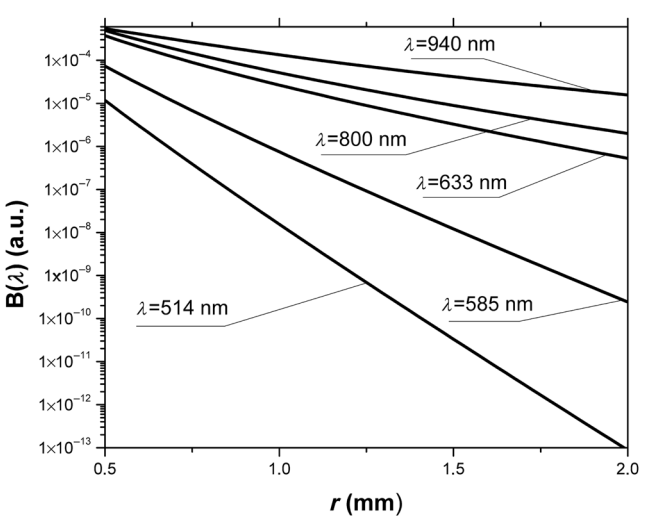

Fig. 4 The dependence of $B(\lambda)$ on the value of the source–detector spacing r = 0.5 to 2 mm for the tissue blood volume V_b = 10%.

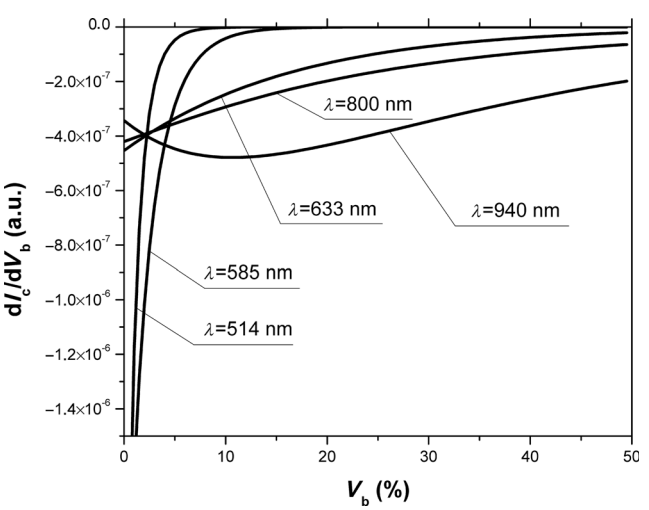

Fig. 6 The dependence of the derivative of photocurrent I_c with respect to blood volume upon the level of the tissue blood volume V_b.

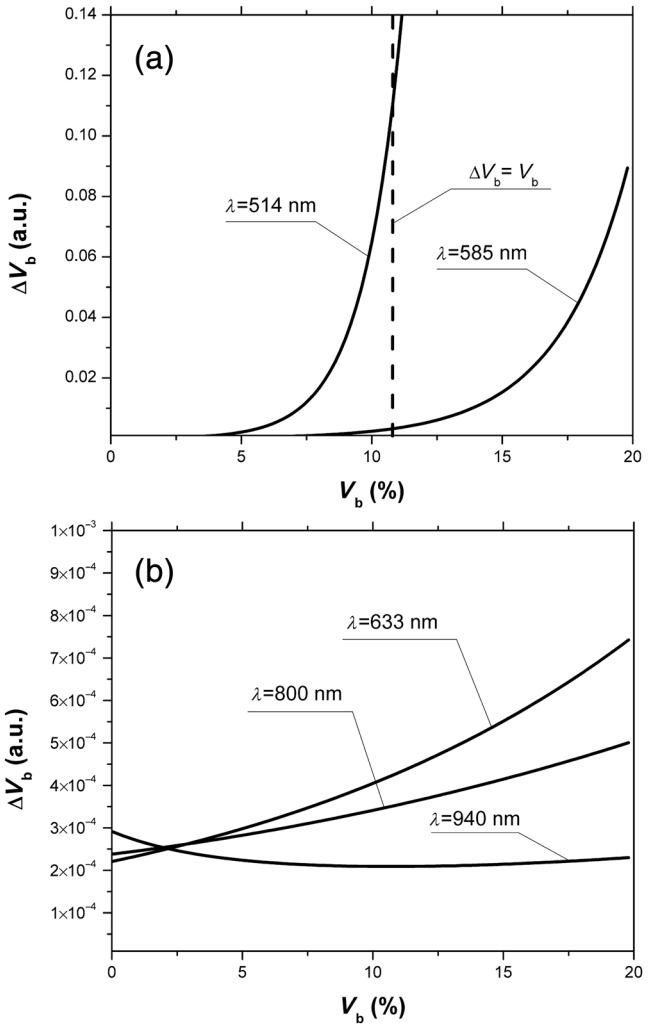

Fig. 7 The dependence of the change of the blood/tissue ratio ΔV_b, which corresponds to the change of the photocurrent in 0.1 nA, on the tissue blood volume V_b: for $\lambda = 514$ and 585 nm (a) and for $\lambda = 633$, 800, and 940 nm (b).

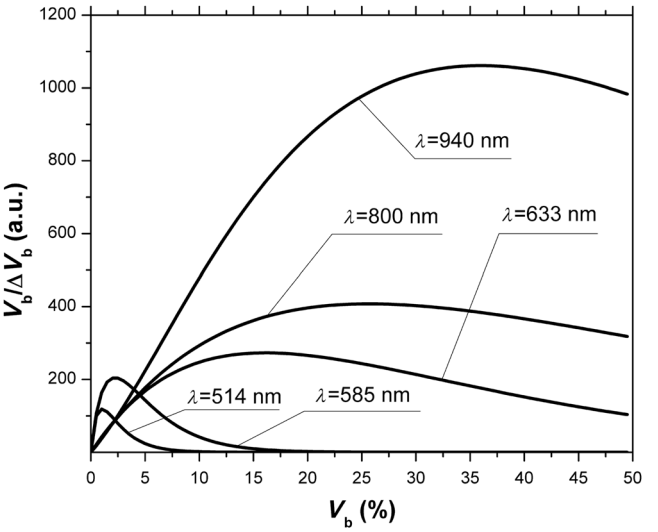

Fig. 8 The dependence of the signal-to-noise ratio of the signal on the level of the tissue blood volume V_b.

As shown in Figs. 2 to 8, the analysis of the dimensionless coding function graphs $B(\lambda)$ and the derivative characteristics based on this function (I , dI $/dV_b$, ΔV_b, $V_b/\Delta V_b$) highlights three spectral range–dependent groups. These groups are related to the changes in optical absorption and scattering coefficients of blood and tissue (see Table 1). The first group, at 514 and 585 nm, is defined by the blood's similar and strong absorption curves for green and yellow light. In the second group, the absorption coefficient of blood decreases by an order of magnitude for red and IR wavelengths. In the third group at IR (940 nm), the absorption coefficient of blood remains at a similar level, but the absorption coefficient of tissue decreases by an order of magnitude.

For example, Figs. 2 to 5 show that with linear variation of the blood volume, the light transmission through the tissue will vary nonlinearly, but the logarithm of photocurrent can make the characteristics of MTRs linear. Figure 3 demonstrates that increasing the wavelength of tissue irradiation in the range of 314 to 940 nm increases the dimensionless coding function $B(\lambda)$ at any fixed tissue blood volume. It is evident that in the spectral range of 633 to 940 nm, $B(\lambda)$ has an almost linear inverse relationship to tissue blood volume. However, between 514 and 633 nm, this function exhibits a significant nonlinear decrease with increased tissue blood volume. These dependences are probably due to absorption by blood at 500 to 585 nm being an order of magnitude higher than at 630 to 700 nm.[21,23,39] Figures 2 and 3 demonstrate that optical properties of blood (primarily the absorption coefficient) in the observed spectral range, and consequently, the tissue blood volume, have a major impact on $B(\lambda)$.

Figure 4 confirms the need to consider the parameter r using different wavelengths in the NMS devices depending on the tissue of study (absorption and scattering coefficients and the level of tissue blood volume).

It is apparent from the computed data (Fig. 5) that the green (when $V_b \approx 8\%$) and yellow (when $V_b \approx 16\%$) irradiation power used in the present case must be increased in order to exceed the signal-to-noise threshold due to the stronger absorption of these wavelengths by biological tissue.

The analysis of data from Figs. 6 and 7 shows that at higher blood volume, the discrimination of the changes in the blood volume by NMS devices is reduced and the relationship can be described by a nonlinear function. In turn, the sensitivity of the NMS devices to the blood volume is also a nonlinear function. Thus, in formulation of MTRs for NMS devices, this nonlinearity must be considered. The differential sensitivity (dI $/dV_b$) depicted in Fig. 6 clearly demonstrates that the detection of lower blood volumes in tissue (under 10%) should preferably be probed with green (514 nm), yellow (585 nm), red (633 nm), and infrared (800 nm) wavelengths. However, to detect tissue blood volumes of greater than 10% to 20% with a high differential resolution and sensitivity, a wavelength of 940 nm is preferred.

Figure 7 shows the minimum discernible ΔV_b signal and the consequent rapid reduction in SNR with an increase in blood volume for green and yellow lights [Fig. 7(a)]. For example, the useful signal becomes indistinguishable against background noise ($\Delta V_b = V_b$) when $V_b \approx 11\%$ at a wavelength of 514 nm. The dependence of ΔV_b upon V_b is much less pronounced for the red and infrared spectra [Fig. 7(b)] compared to the green and yellow lights, although these relationships are also nonlinear.

Data from Fig. 8 justifies the use of different wavelengths for measuring different ranges of tissue blood volumes. Green and yellow lights provide a greater sensitivity for a lower blood volume (up to 5%), whereas the infrared irradiation is more efficient in terms of sensitivity and SNR even at higher blood volumes. Delivering the necessary light power for each wavelength for a given blood volume is essential, particularly for measurement of the upper levels of blood volume by TRO. In addition, at levels >5% of tissue blood volume, the blood perfusion and consequently S_tO_2 measurements become unreliable due to SNRs of <10 for the green wavelength. In general, the theoretical limit of the measurement scale for TRO is an average tissue blood volume level of 0% to 30% with the selected input data and geometry of the receiving radiation.

Similar reasoning can be extended to laser Doppler flowmetry (800 to 940 nm), which is the most sensitive technique for monitoring microvascular rhythms. According to the data presented, this approach is not near to its limit of sensitivity and should have good resolution over a broad range of V_b. According to Fig. 8, for examination of tissue with blood volume level around 10% to 15% with an acceptable SNR, a wavelength of 800 nm should be applied. In the case of 20% to 30% (for example, when measuring the internal organs with an endoscopic probe) of tissue blood volume, however, the 940-nm wavelength is preferable. Moreover, our data (Fig. 6) defines the lowest detection limits of the blood volume for each wavelength.

It should be noted that the function $B(\lambda)$, based on a homogeneous model, has a number of limitations. It does not account for a number of optical characteristics and properties of biological tissues, for example, the refractive index as well as layer structures of skin and the so called vessel packaging effect.[40] Moreover, it is reported that differing levels of melanin and water alter the optical properties of the tissue relevant to the $B(\lambda)$ function.[25,41] These factors affect the NMS measurement result and must be taken into account in formulating the MTRs for devices of this type. It must be emphasized that the measurement accuracy (systematic error) of NMS is significantly affected by the algorithms used for calculation of biomedical parameters.[9] Thus, the computational algorithms currently used for calculating S_tO_2 and V_b by TRO have a complex and multistep character; the scatter of the measured results is two to three times greater than the measurement errors of the initial physical signals.[42]

It should also be underlined that in addition to the thermal noise in NMS systems, there are other limitations (electrical noise, instability of the radiation source, etc.), which should also be taken into account and normalized in formulating MTRs.

5 Conclusion

The application of new noninvasive medical spectrophotometric techniques and instruments for the functional diagnosis and evaluation of therapeutic interventions requires the specification of the MTRs for the specific type of medical devices. Considering different levels of the tissue blood volume, the approach proposed here allows the calculation of important technical and metrological restrictions of the instruments such as the sensitivity ranges and power-related SNRs for different spectral channels and biomedical parameters. It is clear that the nonlinearity of the measurements carried out with NMS systems depends directly on the characteristics of the examined object. In general, the further successful development of NMS technology will be heavily dependent on the metrological support of these devices and their methods of use. This support will enable noninvasive spectrophotometric diagnostics to be raised from research level technology to a standardized level satisfying the requirements of medical end users.

Acknowledgments

This work partially was supported by the European Community's Seventh Framework Programme (FP7-People-2009-IAPP) under Grant Agreement no. 251531 MEDILASE.

References

1. H. Liu, M. Kohl-Bareis, and X. Huang, "Design of a tissue oxygenation monitor and verification on human skin," *Proc. SPIE* **8087**, 80871Y (2011).
2. D. A. Rogatkin et al., "Basic principles of design and functioning of multifunctional laser diagnostic system for non-invasive medical spectrophotometry," *Proc. SPIE* **7890**, 78901H (2011).
3. "Oxford Optronix," http://www.oxford-optronix.com/cat10/page29/Tissue-Vitality-Monitoring.html (28 August 2013).
4. M. J. Leahy and G. E. Nilsson, "Laser Doppler flowmetry for assessment of tissue microcirculation: 30 years to clinical acceptance," *Proc. SPIE* **7563**, 75630E (2010).
5. R. Kramme, K.-P. Hoffmann, and R. S. Pozos, *Springer Handbook of Medical Technology*, Springer, Berlin, Heidelberg (2011).
6. J. Kraitl, U. Timm, and H. Ewald, "Non-invasive measurement of blood and tissue parameters based on VIS-NIR spectroscopy," *Proc. SPIE* **8591**, 859105 (2013).
7. D. A. Rogatkin and L. G. Lapaeva, "Prospects for development of non-invasive spectrophotometry medical diagnostics," *Biomed. Eng.* **37**(4), 217–222 (2003).
8. D. A. Rogatkin et al., "Multifunctional laser noninvasive spectroscopic system for medical diagnostics and metrological provisions for that," *Proc. SPIE* **7368**, 73681Y (2009).
9. D. A. Rogatkin, A. V. Dunaev, and L. G. Lapaeva, "Metrological support of methods and devices for noninvasive medical spectrophotometry," *Biomed. Eng.* **44**(2), 66–70 (2010).
10. A. Cysewska-Sobusiak, "Metrological problems with noninvasive transillumination of living tissues," *Proc. SPIE* **4515**, 15–24 (2000).
11. V. Tchernyi et al., "Some results of multiwave in situ autofluorescence diagnostics," *Proc. SPIE* **5693**, 336–343 (2005).
12. A. I. Krupatkin and V. V. Sidorov, Eds., *Laser Doppler Flowmetry of Blood Microcirculation*, Meditcina-Press, Moscow (2005).
13. D. Colquhoun et al., "Non-invasive estimation of jugular venous oxygen saturation: a comparison between near infrared spectroscopy and transcutaneous venous oximetry," *J. Clin. Monit. Comput.* **26**(2), 91–98 (2012).
14. M. V. Amzina et al., "Combined medical diagnostic system with separated laser-Doppler and reflectance oximeter channels," *Proc. SPIE* **6163**, 616317 (2006).
15. J. D. Bronzino, Ed., *The Biomedical Engineering Handbook*, CRC Press, LLC, Boca Raton, Florida (2000).
16. H. Czichos, T. Saito, and L. E. Smith, *Springer Handbook of Metrology and Testing*, Springer-Verlag, Berlin, Heidelberg (2011).
17. I. Fredriksson, M. Larsson, and T. Strömberg, "Measurement depth and volume in laser Doppler flowmetry," *Microvasc. Res.* **78**(1), 4–13 (2009).
18. V. V. Tuchin, Ed., *Handbook of Optical Biomedical Diagnostics*, SPIE Press, Bellingham, Washington (2002).
19. S. L. Jacques, "Origins of tissue optical properties in the UVA, visible and NIR regions," in *Advances in Optical Imaging and Photon Migration*, R. R. Alfano and J. G. Fujimoto, Eds., pp. 364–370, OSA, Washington, DC (1996).
20. U. Timm et al., "Photometric sensor system for a non-invasive real-time hemoglobin monitoring," *Proc. SPIE* **8572**, 857204 (2013).
21. S. L. Jacques, "Optical properties of biological tissues: a review," *Phys. Med. Biol.* **58**(11), R37–R61 (2013).

22. G. Zonios and A. Dimou, "Modeling diffuse reflectance from semi-infinite turbid media: application to the study of skin optical properties," *Opt. Express* **14**(19), 8661–8674 (2006).
23. T. Lister, P. A. Wright, and P. H. Chappell, "Optical properties of human skin," *J. Biomed. Opt.* **17**(9), 090901 (2012).
24. I. V. Meglinski and S. J. Matcher, "Quantitative assessment of skin layers absorption and skin reflectance spectra simulation in the visible and near-infrared spectral regions," *Physiol. Meas.* **23**(4), 741–753 (2002).
25. I. V. Meglinski and S. J. Matcher, "Computer simulation of the skin reflectance spectra," *Comput. Methods Programs Biomed.* **70**(2), 179–186 (2003).
26. S. J. Matcher, M. Cope, and D. T. Delpy, "In vivo measurements of the wavelength dependence of tissue-scattering coefficients between 760 and 900 nm measured with time-resolved spectroscopy," *Appl. Opt.* **36**(1), 386–396 (1997).
27. A. V. Dunaev et al., "Laser reflectance oximetry and Doppler flowmetry in assessment of complex physiological parameters of cutaneous blood microcirculation," *Proc. SPIE* **8572**, 857205 (2013).
28. A. Liebert, M. Leahy, and R. Maniewski, "Multichannel laser-Doppler probe for blood perfusion measurements with depth discrimination," *Med. Biol. Eng. Comput.* **36**(6), 740–747 (1998).
29. S. Takatani, "Toward absolute reflectance oximetry: I. Theoretical consideration for noninvasive tissue reflectance oximetry," *Adv. Exp. Med. Biol.* **248**, 91–102 (1989).
30. A. Kienle et al., "Investigation of multilayered tissue with in vivo reflectance measurements," *Proc. SPIE* **2326**, 212–221 (1995).
31. A. N. Yaroslavsky et al., "Optical properties of blood in the near-infrared spectral range," *Proc. SPIE* **2678**, 314–324 (1996).
32. T. H. Dai et al., "Comparison of human skin opto-thermal response to near-infrared and visible laser irradiations: a theoretical investigation," *Phys. Med. Biol.* **49**(21), 4861–4877 (2004).
33. S. L. Jacques, "Skin Optics," 1998, http://omlc.ogi.edu/news/jan98/skinoptics.html (28 August 2013).
34. R. Graaff et al., "Optical properties of human dermis in vitro and in vivo," *Appl. Opt.* **32**(4), 435–447 (1993).
35. V. V. Tuchin, *Tissue Optics—Light Scattering Methods and Instruments for Medical Diagnosis, Tutorial Texts in Optical Engineering*, Vol. TT38, SPIE, Bellingham, WA (2000).
36. J. Haus, "Photodetectors," in *Optical Sensors*, pp. 27–36, Wiley-VCH Verlag GmbH & Co. KGaA, Weinheim, Germany (2010).
37. "HAMAMATSU," http://www.hamamatsu.com/us/en/product/category/3100/4001/4103/ index.html (accessed 28 August 2013).
38. M. Cvijetic, *Optical Transmission Systems Engineering*, Artech House, Norwood, MA (2004).
39. A. Roggan et al., "Optical properties of circulating human blood in the wavelength range 400–2500 nm," *J. Biomed. Opt.* **4**(1), 36–46 (1999).
40. I. Fredriksson, M. Larsson, and T. Strömberg, "Accuracy of vessel diameter estimated from a vessel packaging compensation in diffuse reflectance spectroscopy," *Proc. SPIE* **8087**, 80871M (2011).
41. G. I. Petrov et al., "Human tissue color as viewed in high dynamic range optical spectral transmission measurements," *Biomed. Opt. Express* **3**(9), 2154–2161 (2012).
42. D. A. Rogatkin et al., "Principal sources of errors in noninvasive medical spectrophotometry. Part 1. Physicotechnical sources and factors of errors," *Meas. Tech.* **56**(2), 201–210 (2013).

Anaerobic digestion of municipal solid wastes containing variable proportions of waste types

J.C. Akunna, Y.A. Abdullahi and N.A. Stewart

Urban Water Technology Centre, School of Contemporary Sciences, University of Abertay, Bell Street, Dundee DD1 1HG, United Kingdom (E-mail: *j.akunna@abertay.ac.uk*)

Abstract In many parts of the world there are significant seasonal variations in the production of the main organic wastes, food and green wastes. These waste types display significant differences in their biodegradation rates. This study investigated the options for ensuring process stability during the start up and operation of thermophilic high-solids anaerobic digestion of feedstock composed of varying proportions of food and green wastes. The results show that high seed sludge to feedstock ratio (or low waste loading rate) is necessary for ensuring process pH stability without chemical addition. It was also found that the proportion of green wastes in the feedstock can be used to regulate process pH, particularly when operating at high waste loading rates (or low seed sludge to feedstock ratios). The need for chemical pH correction during start-up and digestion operation decreased with increase in green wastes content of the feedstock. Food wastes were found to be more readily biodegradable leading to higher solids reduction while green wastes brought about pH stability and higher digestate solid content. Combining both waste types in various proportions brought about feedstock with varying buffering capacity and digestion performance. Thus, careful selection of feedstock composition can minimise the need for chemical pH regulation as well as reducing the cost for digestate dewatering for final disposal.

Keywords Anaerobic digestion; food waste; green waste; pH regulation; seed sludge to feedstock ratio; solid reduction

Water Science & Technology Vol 56 No 8 pp 143–149 © IWA Publishing 2007

Introduction

The organic fraction of municipal solid waste (OFMSW) is a rich source of organic carbon, which can potentially be recycled for energy recovery and for the production of soil conditioners. The economic performance of biogas is thus dependent on the nature and type of wastes digested. As high biogas yield and fertiliser of high quality is only obtainable from source-separated OFMSW, more information is required on the role of waste composition on the digestion process. This is particularly important in areas that undergo significant seasonal variations relating to population, agricultural and outdoor activities, such as mountainous and isolated tourist areas.

The economic viability and sustainability of any anaerobic system depends on process stability. Extreme pH fluctuations during the digestion process (including start-up) may lead to process failure. To ensure process stability in anaerobic treatment systems treating highly putrescible wastes, pH is usually regulated by the addition of lime or other chemical buffers. These chemicals are expensive and their addition may sometimes present technical difficulties to plant operators. Alternatively, pH regulation can be carried out by operating at low loading rate, which may lead to poor biogas production and hence, uneconomical operation.

For quick start-up and high loading rates to be achieved in any solid waste digestion system, the process stability will depend mainly on pH stability of the digesting feedstock. Variations in the nature of available raw feedstock can bring about changes in the requirement for, or amount of, chemical buffer needed to ensure process stability.

doi: 10.2166/wst.2007.725

Thus, understanding the effect of feedstock composition on digester pH variation will assist in informing the appropriate proportion of the different waste stocks required in order to minimise the complexities of chemical pH correction.

Food wastes from kitchens and restaurants, livestock wastes and green wastes from gardens, parks, forests and agricultural activities as well as wood chips are some of the organic matter suitable for anaerobic digestion in these isolated rural areas. In small rural tourist regions, there will be significant seasonal variations in the production of these waste types. Food and livestock wastes are relatively wet and decompose rapidly (Mata-Alvarez, 2003). Their digestion may lead to high initial acid accumulation resulting in acid pH, thus necessitating the need for pH correction to prevent process failure. In comparison green wastes and wood chips are relatively dry and decompose slowly. With these wastes as the main feedstock in any digestion process, there will be less likelihood of high initial acid accumulation, and thus little need for pH regulation.

Apart from the nature of waste, the rate of digestion will also depend on the type of digestion process (low solid or high solids) and the digestion temperature (mesophilic or thermophilic). In comparison to low solids digestion, high solids anaerobic digestion has been reported as being more effective in biogas production (McDougall *et al.*, 2001). An additional benefit of high solids digestion is that the resulting digestate does not require dewatering before land application (Cecchi *et al.*, 2002). Thermophilic high solids anaerobic digestion systems have been found to be faster and produce three times more biogas compared to those operated at mesophilic temperatures (Cecchi *et al.*, 2002) with less offensive solids (Di-Stephano *et al.*, 2004) and can accommodate higher organic loadings at shorter retention times (Mata-Alvarez *et al.*, 2000).

The study reported in this paper investigated options for ensuring process stability during the start up and operation of thermophilic high-solids anaerobic digestion of different types of solid wastes that are usually produced in highly variable proportions in small and mobile communities. The study aimed to evaluate:

- the effect of seed sludge to feedstock ratio during the digestion process
- the effect of varying proportions of waste types on the natural pH regulation during digestion.

Material and methods

Waste composition

Green waste. Model green waste was prepared by mixing freshly mown grass clippings with dried fine wood chips and water at a w/w ratio of 3:2:1, respectively. The mixture had a total solids (TS) level of 35%; total volatile solids (TVS) 34% and carbon to nitrogen (C/N) ratio of 34.8.

Food waste. Model food waste was composed of a mixture of the foods, comprising cooked pasta (22%), cooked meat (9%), lettuce (11%), carrots (3%), potato (44%) and milk (11%). It was cooked from fresh by boiling in water for 20 minutes, drained and mixed in a food processor for 30 seconds to a smooth paste. The mixture had TS 20.8%, TVS 20.4% and C/N ratio of 13.0.

Seed sludge. The seed sludge consisted of digestate biomass taken from a continuous flow thermophilic anaerobic reactor treating a solid waste mixture of green and food wastes. The feed substrate had TS 29.9%; VS 29.1% and C/N ratio of 19.5. The seed sludge had TS 23.6%, VS 13.1% and C/N ratio 23.7.

Experimental methodology

Determination of the biodegradability potential of food and green wastes

These experiments were carried out with relatively high seed sludge to feedstock ratio of 9 in order to prevent volatile acids build-up which might lead to low pH during digestion. Triplicate samples of 10 g each of 50:50 (w/w) mixed food and green wastes, mixed food wastes only and green wastes only were each mixed with 90 g of seed sludge and placed in 500 ml plastic gastight vessels, with a port attached to a 4 litre gas-bag. Three blanks, containing only 90 g of seed sludge, were run in parallel with the samples. The headspaces of all the assays were flushed with nitrogen gas for 2 minutes before sealing. The vessels were incubated at 55 °C and the weight loss and biogas production was measured daily over a period of seven days. The digestate samples were collected from each vessel at the end of digestion for physical and chemical analysis.

Determination of the effect of feed composition on natural pH buffer

This experiment was carried out with lower seed sludge to feedstock ratio of 0.25 (or high waste loading), to encourage organic acid build-up during digestion. About 500 g each of five duplicate cultures of food waste (FW), green waste (GW) and seed sludge (AS) in various proportions, viz: FW 80%, GW 0%, AS 20%; FW 40%, GW 40%, AS 20%; FW 60%, GW 20%, AS 20%; GW 60%, FW 20%, AS 20%; and FW 0%, GW 80%, AS 20% were prepared in three-litre capacity digesters. The cultures were named A_1, B_1, C_1, D_1 and E_1 respectively and to each was added 0.06% (of their respective total solids content) of $NaHCO_3$ as a chemical pH buffer, as recommended by Brummeler *et al.* (1991). Duplicates cultures A_2, B_2, C_2, D_2, and E_2 were made without adding the $NaHCO_3$ buffer. The headspaces of all the assays were flushed with nitrogen gas for 2minutes before sealing. The vessels were incubated at 55 °C and the digestate physical and chemical characteristics were measured after 15 days of digestion.

Method of analysis

The moisture content was measured gravimetrically by drying the samples at 103 °C for 24 hours. Volatile solids were measured gravimetrically following incineration at 430 °C for 8 hours according to *Standard Methods* (APHA, 1992). Gas volume was measured by water displacement. Methane content of the produced biogas was calculated from the volume reduction by bubbling the collected biogas twice through a solution of 1M NaOH at a rate of 1 litre/min to remove CO_2. Carbon and nitrogen ratios were analysed using a mass spectrophotometer. For this test, samples were finely ground in a ball mill and approximately 1 mg samples were weighed into 6 × 4 mm tin cups for analysis by continuous flow Dumas combustion using a Europa Scientific (Crewe, UK) sample converter. Nitrogen and carbon were selectively detected (as N_2 and CO_2) using a Europa Scientific ANCASL mass spectrophotometer 2,020 (Scrimgeour and Robinson (2003)).

Results and discussion

Digestion performance at high seed sludge to feedstock ratio (or low waste loading)

Figure 1 shows the results obtained for biogas production (net of the effect of the blank experiment containing only the seed sludge). This graph shows that the 7-day biogas productions (BGP7) were 492 and 174 cc/g$TVS_{initial}$ for fresh food and green wastes respectively. The methane content of the biogas produced was measured consistently at 62%.

Figure 2 shows the rate and degree of VS reduction. Volatile solids reduction of 78%, 22% and 49% (net of blank experiment results) were achieved for food, green and 50:50 mixture wastes respectively. These observations were consistent with the biogas production shown in Figure 1.

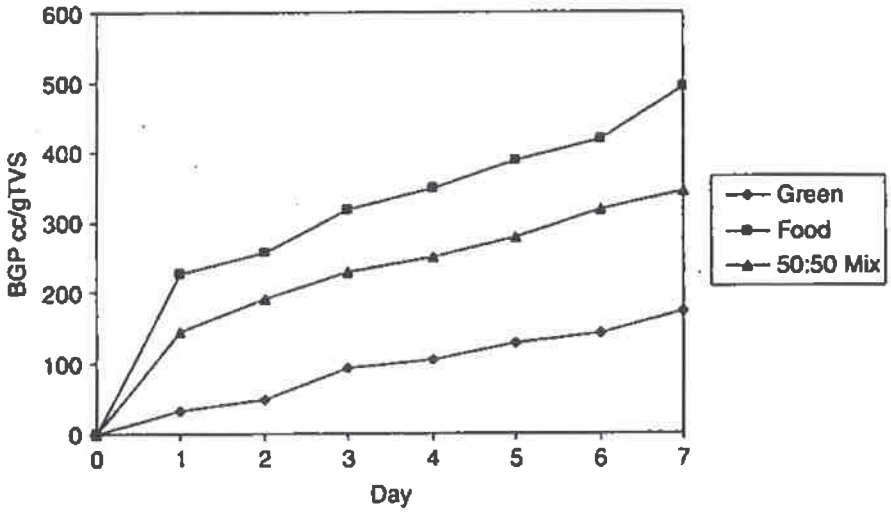

Figure 1 Biogas production from fresh organic wastes

These results clearly reflect the highly biodegradable nature of the food waste in comparison to the green waste. Throughout the digestion period, the digestate pH values for all the cultures were between 6.0 and 7.5.It was believed that the high proportion of the seed sludge relative to the feedstock contributed in maintaining the pH in the optimum range of anaerobic digestion process, particularly for the cultures containing only the food wastes.

Taking account of the biogas production and VS reduction achieved, the mean average biogas production rates per gram volatile solids removed (VSr) for each of the substrates were 635, 737 and 751 cc/gVS_r for food, green and mixed waste respectively.

Digestion performance at low seed sludge to feedstock ratio (or high waste loading)

The pH values of the cultures measured at the end of the 15-day digestion period show that generally buffered cultures showed greater pH stability compared to non-buffered ones. Amongst the sampled cultures, pH resilience was greater in cultures composed mainly of GW as shown in Figure 3. Where FW dominated the feedstock as in culture A, low pH was observed indicating excessive accumulation of fatty acids. Chemical addition

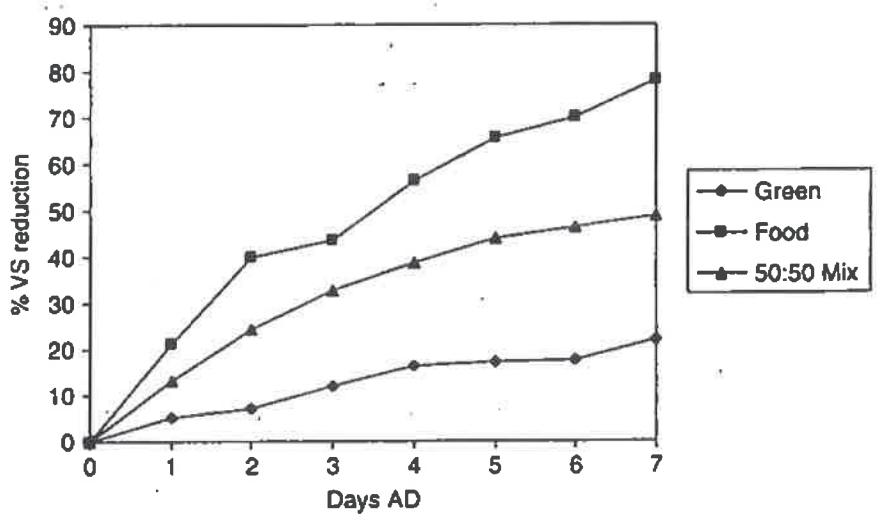

Figure 2 Volatile solids reduction during digestion

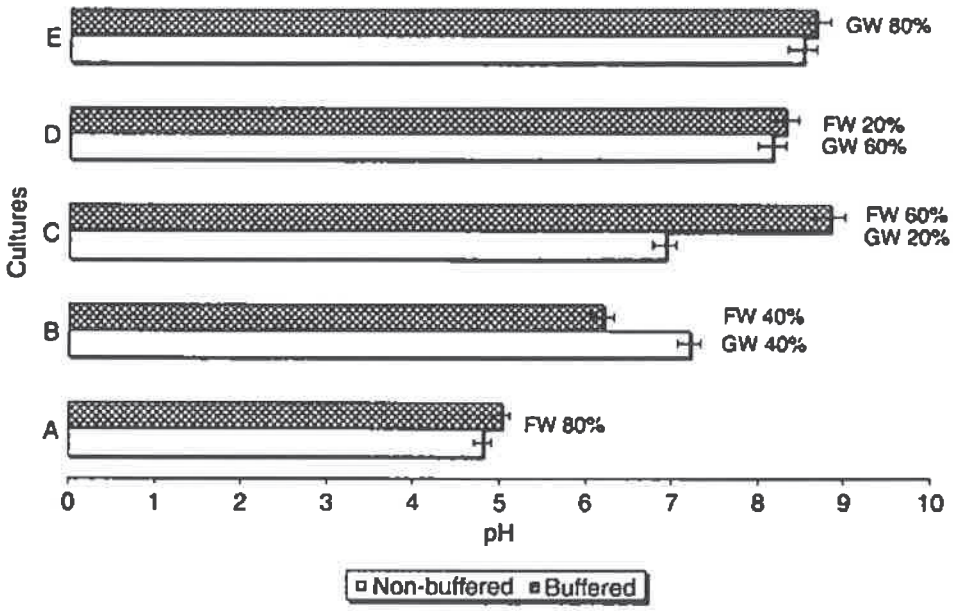

Figure 3 pH comparison in buffered and non-buffered cultures. Bars represent standard deviation

did not seem to have a significant impact on these cultures (A). On the other hand, cultures with higher GW content recorded high pH values at the end of digestion indicating that these cultures underwent a slower rate of acidification than those containing predominantly food wastes. For these cultures with higher GW content, the addition of buffer did not seem to be of any benefit to the digestion process. Thus, for relatively low seed sludge to feedstock ratio, the need for chemical pH correction during start-up and digestion operation decreases with increase in GW proportion of waste feedstock.

These results also show that literature estimations of the quantity of buffer chemicals needed to ensure optimum pH buffer may not necessarily achieve the desired results when digesting readily biodegradable wastes. It may be necessary to carry out bench-scale studies to determine the correct dose for a given waste type and combination.

Figure 4 confirms that GW is less readily biodegradable than FW, and hence its ability to act as a pH regulator. The relatively low solid reduction recorded for cultures

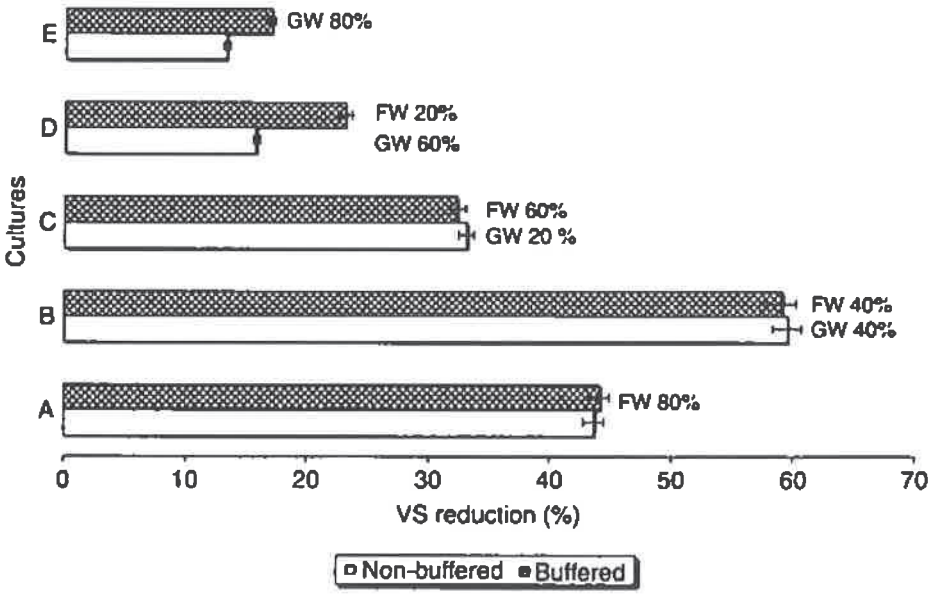

Figure 4 Volatile solids reduction in buffered and non-buffered cultures. Bars represent standard deviation

A (when compared with the near 80% shown in Figure 2) was believed to be caused by the low pH values observed in these cultures.

In general, the moisture content of the digestates increased with increase in the amount of VS reduction, i.e. decreasing with increase in GW content of the raw feedstock. For cultures containing mainly FW, the digestate contained less that 2% dry solids at the end of digestion period. Where there are restrictions in the application of liquid sludge to land, the addition of GW can reduce the need for post digestion dewatering which may be necessary for the final disposal of the digestates, thus bringing about a significant reduction in overall waste management costs.

Conclusions

These results reflect the highly biodegradable nature of the food waste in comparison to the green waste and the importance of the seed sludge to feedstock ratio in process stability during digestion. A high ratio is necessary to ensure process pH stability without chemical addition. This study also shows that the proportion of green wastes in the feedstock can be used to ensure process pH stability, particularly when operating at high waste loading rates (or low seed sludge to feedstock ratios). Under these conditions, the need for chemical pH correction during start-up and digestion operation will decrease with increase in the GW proportion of the feedstock. Food wastes were found to have a greater impact on feedstock biodegradability (and solid reduction) while green wastes enhances pH stability. Combining FW and GW in various proportions brought about a feedstock with a natural buffering capacity and varying performance in solids reduction during digestion.

For the thermophilic high solids digestions carried out in this study, the mean average biogas production rates per gram volatile solids removed (VS_r) for each of the substrates were found to be 635, 737 and 751 cc/gVS_r for food only, green only and mixed (i.e. 50% food and 50% green wastes) waste respectively.

The solid content of digestates was found to increase with an increase in green wastes content of the feedstock. Post digestion digestate dewatering required for some final disposal routes (e.g. land application, agricultural use, landfill sites) may be reduced by combining FW and GW in various proportions.

In conclusion, this study has shown that careful selection of the feedstock composition can minimise the need for artificial pH regulation as well as reducing the cost for digestate dewatering for final disposal.

Acknowledgements

The authors wish to thank University of Abertay, Dundee for funding and supporting this study.

References

APHA (1992). *Standard Method for the Examination of Water and Wastewater*, 18th Edition, Greenberg, A.E., Clesceri, L.S. and Eaton, A.D. (eds), American Public Health Association, Washington.

Brummeler, T.E., Horbach, H.C.J.M. and Koster, I.W. (1991). Dry anaerobic batch digestion of organic fraction of municipal solid waste. *J. Chem. Tech. Biotechnol.*, 50, 191–209.

Cecchi, F., Traverso, P., Pavan, P., Bolzonella, D. and Innocenti, L. (2002). Characteristics of OFMSW and behaviour of anaerobic digestion process. In: *Biomethanization of the Organic Fraction of Municipal Solid Wastes*, Mata-Alvarez, J. (ed.), IWA Publishing, London, pp. 141–178.

Di-Stephano, T.D., Speece, R.E. and Hnatin, M. (2004). Evaluation of anaerobic process configuration on food waste and municipal solid waste. In: *Proceedings of 10th World Congress 2004*, Montreal.

Mata-Alvarez, J., Macé, S. and Llabrés, P. (2000). Anaerobic digestion of organic solid waste: an overview of research achievements and perspectives. *Bioresour. Technol.*, 74, 3–16.

McDougall, F., White, P., Frank, M. and Handle, P. (2001). *Integrated Solid Waste Management: a Life Cycle Inventory*, 2nd Edition, Blackwell Publishing, Cornwall.

Mata-Alvarez, J. (2002). Fundamentals of anaerobic digestion. In: *Biomethanization of Organic Fraction of Municipal Solid Wastes*, Mata-Alvarez, J. (ed.), IWA Publishing, London, pp. 1–20.

Scrimgeour, C.M. and Robinsons, D. (2003). Stable isotope analysis and applications. In: *Soil Environmental Analysis: Modern Instrumental Techniques*, Smith, K.A. and Cresser, M.S. (eds), Marcel Dekker Inc, pp. 381–431.

Basic principles of design and functioning of multifunctional laser diagnostic system for non-invasive medical spectrophotometry

D.A. Rogatkin[1], S.G. Sokolovski[2], K.A. Fedorova[2], N.A. Stewart[2], V.V. Sidorov[3], E.U. Rafailov[2]

[1]Laboratory of Medical & Physics research, MONIKI by Vladimirsky, Moscow 12911, RF; [2]Carnegie Laboratory of Physics, School of Engineering, Physics and Mathematics, University of Dundee, Dundee DD1 4HN, UK; [3]SPE "LAZMA" Ltd., Moscow 125252, RF

Keywords: non-invasive medical spectrophotometry, multifunctional diagnostic systems, laser Doppler flowmetry, optical pulse oximetry, fluorescence diagnostics, unit-module algorithm, generalised task description.

1. Abstract

The devising of a general engineering theory of multifunctional diagnostic systems for non-invasive medical spectrophotometry is an important and promising problem in modern biomedical engineering. We aim in this study to formalize in scientific engineering terms the detailed objectives for the problem multifunctional laser non-invasive diagnostic system (MLNDS). The structure-functional model as well as the united aim-function of generalized MLNDS was formulated and developed. The key role of the system software for MLNDS general architecture at steps of ideological-technical designing has been proved. The basic principles of block-modules composition of MLNDS hardware are suggested as well.

2. Introduction

Last decades all over the world optical properties of biological tissues at normality and pathology (*in vivo*, *in situ)* became mainstream of intensive studies which allow us to confidently talk about the formation of a new multifunctional diagnostics as well as development of optical non-invasive diagnostic devices and systems [1-3]. In fact, it became common on medical technology market to have instruments of the optical pulse oximetry [4] and laser Doppler flowmetry [5] as well as devices for fluorescence diagnostics [6], optical coherence and diffusion tomography [3, 7], tissue fat detectors, blood glucose, haemoglobin, and oxyhemoglobin analysers [1-3, 8]. Of the variety of devices of this type the most numerous group of equipment is systems implementing ideology of non-invasive medical spectrophotometry (**NMS**) [3], when without any bio-samples taken in accessible areas of patient body (skin, oral mucosa, blood, etc.) levels and accumulation dynamics of various biochemical markers: oxyhemoglobin, flavin respiratory enzymes, porphyrins, lipofuscin, NADH, etc. can be estimated. Moreover the most promising direction in developing such NMS devices is the creation of multifunctional (universal) laser non-invasive diagnostic systems (**MLNDS**) which in a single hardware implementing various methods of NMS combines fluorescence and absorption spectroscopy, laser Doppler flowmetry, etc. [9]. This allows therapist and clinicians not only receive the arithmetic sum of the diagnostic information that could be collected by each of individual method but conduct multifunctional patient examination measurements aimed for identifying subtle individual characteristics of blood flow and tissue metabolism using simultaneous and comprehensive data from different diagnostic techniques [10].

Until recently such mono- and at the best double-functional diagnostic instruments have been designing mostly empirically at lack of any serious consideration and systemic theory. It is clear that the most common theoretical basis for the creation and operation of any medical and optical-electronic devices are applicable in general and in the case of MLNDS. However it is also well known that any new class of devices especially diagnostic one has its own specificities which in varying degrees affect the entire process of developing and further exploitation starting from most common stages of the ideological and technical design and integration of the entire system. First of all it concerns to the formalised features of substantive representation of the problem, development of generalized structural and functional design, physical and mathematical model of the device. Specificity of such devices appears at formulation of general function of the device, as well as in architectural layout, informational, software, methodological and metrological support.

Unfortunately until recent time all these issues are poorly developed regarding to MLNDS and this article aims to at least partly fill this gap. This article uncovers main systemic and methodological principles underlying the design of MLNDS. Here we are going to give formal description of objectives for this task, structural and functional model of the generalized MLNDS and formulate its main function. According to these principles of module construction of MLNDS hardware is developed and the key role of programme-algorism maintenance of MLNDS in all matters of the overall design and synthesis of the system as a whole is established.

3. Formal description of detailed task representation

Following the latest trends in the development of methods and instruments for NMS [2] we consider certain MLNDS meaning by this term any particular implementation of any diagnostic device of this class regardless of inherited individual techniques of optical and laser (if using lasers as a source of radiation) NMS. According to the classical canons of Medical Instrumentation [11], any medical diagnostic device is an open medical biotechnology system (MBS), so it is a combination of biological and technical elements jointed into a uniform functional system where all elements are linked into control loop (open-loop in this case). There are two biological objects in this open-loop system: a patient and an operator-physician controlling the system analysing out-coming information from the device and deciding what medical treatments shall be prescribed to the patient.

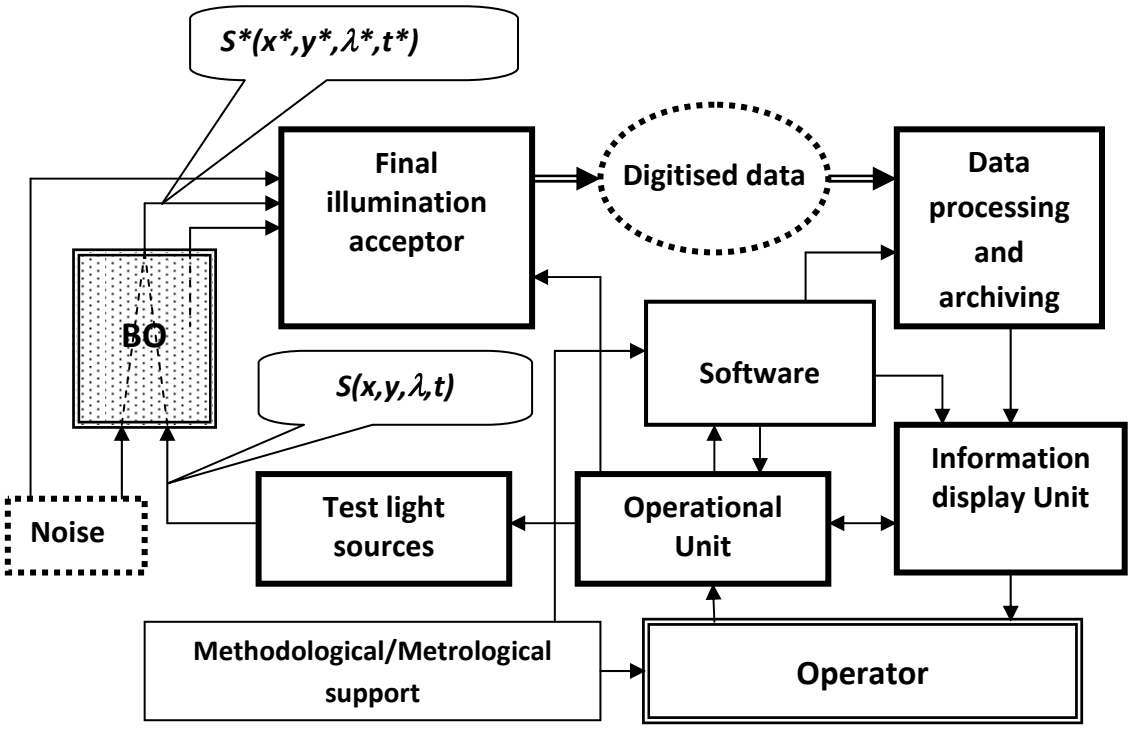

Figure 1. The formal representation of detailed task in design MLNDS (explanation in text)

Therefore the main goal of this study is to create multi-functional diagnostic BPS-M (MLNDS) for obtaining comprehensive information from BO by optic spectral sensing. Developed MLNDS contains light irradiation sources illuminating BO that gives output analogue information called initial analogue optical signal $S(x, y, \lambda, t)$, where x and y, the spatial coordinates on the surface of the BO, λ - wavelength, t - time. BOs due to their individual optical properties associated with anatomical morphological and biochemical properties of tissue, encode initial optical signal $S(x, y, \lambda, t)$ changing its basic parameters: spectral power density, shape, repetition rate and pulse duration, depth, and the law of the amplitude-frequency modulation into final optical signal $S^*(x^*, y^*, \lambda^*, t^*)$. Main task of MLNDS is to collect as full as possible final encoded signal $S^*(x^*, y^*, \lambda^*, t^*)$ filter it off external interference signals and noises and bearing information of the initial signal $S(x, y, \lambda, t)$ to calculate all the essential optical and physical BO parameters. At the final

stage of data processing these optical and physical data should be converted by MLNDS into meaningful medical and biological parameters and interpreted in terms adopted in medicine [14].

Since the final optical signal coming from BO is also an analogue signal MLNDS should process discretise and digitise $S^*(x^*, y^*, \lambda^*, t^*)$ signal sampling all basic parameters: amplitude, wavelength, time intervals (the basic principle of extracting information from any analogue signals [13]). The final optical-physical and biomedical information of inspected BO should be processed in MLNDS on the base of high level of computing, processing and/or interpretive algorithms and procedures implemented in the programme [14, 15]. MLNDS operator (doctor) should be able to adopt this information in familiar form and backup it for database and documentation.

In general this formal description of task representation is well illustrated at figure 1. That MLNDS appears to be a complex parameter-measuring BPS-M which functional characteristics and efficacy more than on two-thirds are determined by the capacity of its computing resources and user methodical software [14]. Consequently, the most important step in creating any MLNDS is the development of information, algorithmic and software support, especially at the phase of creation of general ideology of computational process in terms of diagnostic data processing and analysis.

Till now there are no uniform data processing algorithms for MLNDS. Moreover there are no even general mathematical models for calculation of the irradiation field distributed in randomly inhomogeneous medium like biological tissues which (models) are based on the

algorithms that allow in any case to obtain potentially precise analytical solutions of task for irradiation fluxes emerging from the bio-tissue alike by parameters dense, light scattering and absorbing medium. Therefore, a large amount of theoretical research in NMS is related today to development of approximate models and algorithms that are suitable in a particular case [1, 3, 16] including the creation of virtual physical and mathematical models of BO in terms of the theory of light propagation and scattering in turbid media [17]. Since these models are the basis of modern methods of analysis and data processing in NMS [14] their successful choice in designing phase will mainly influent on the overall clinical efficacy and diagnostic potential of MLNDS. Since all these models and algorithms could be solved so far only in particular cases of specific wavelengths, implementations of particular BO irradiation schemes and in each case defined geometry of the perception of the final optical signal $S^*(x^*, y^*, \lambda^*, t^*)$ then so far we can reasonably say that chosen methods and data processing algorithms "dictate" to the developer all architecture of the transmitter-receiver unit of MLNDS. MLNDS hardware, as displayed in Figure 1 and the above arguments are secondary to the System Software MLNDS and act only as physical elements of the formation, registration and translation of optical and electronic signals that are necessary for the close-looped work of computing, processing and interpreting algorithms of MLNDS software.

4. Structural and functional model of MLNDS and its main function

One of the first and fundamental task of designing any new optic-electronic equipment including medical is the creation of adequate structural-functional model (**SFM**) of a new device and determining its general objective function [12, 13]. We will consider one of possible SFM (Fig.2) of generalized MLNDS based on our earlier published results [9].

In developing of SFM referring to previous section of the paper the ideology of unit-modular system with a discrete set of irradiation sources (**IS**) and correspondently with a discrete set of detecting wavelengths shall be used. This means that IS unit in MLNDS creates a discrete set of optical probing signals (the first level of signal discretisation by spectrum and exposure time)

$$W_i = W_i(\Delta\lambda_i, \Delta t_i)$$

where: W_i - the irradiation power of i-th source; $\Delta\lambda_i$ - spectral range of W_i; Δt_i - time interval of i-th source. Irradiation formation optical scheme (**IFOS**) creates focused light beam with surface power density (illumination) at BO tested:

$$P = f(x, y, \lambda, t, W_i)$$

Analyzed BO being in fact spectral nonlinear optical filter and IS on its own (fluorescence) converts power density P applied into power density P^* of final irradiation from BO that is equivalent to coding of the initial optical signal by some encoding function:

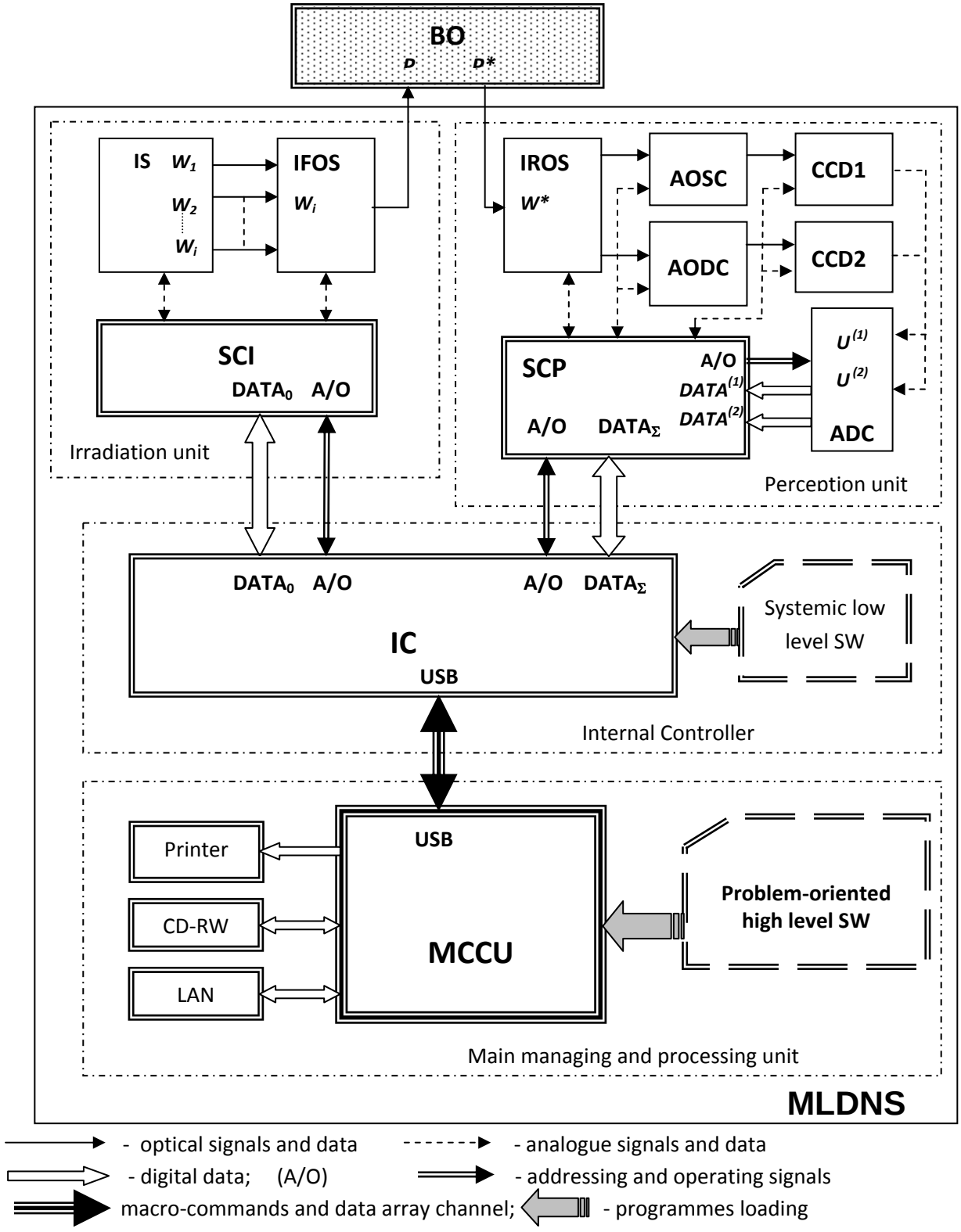

Figure 2. Structural-functional model of generalised MLNDS (refer to text for explanations).

$$P^* = f^*(x^*, y^*, \lambda^*, t, W_i, W_{f1}) = B(x \to x^*, y \to y^*, \lambda \to \lambda^*, t, \{m_j(t)\}) \cdot (P + P_{f1})$$

where: B - encoding dimensionless function of irradiation by BO; $\{m_j(t)\}$ - an array of biomedical, optical-physical parameters of the BO that affects the coding function; W_{f1} and P_{f1} - power and power density of the background irradiation (noise) that when passes through the BO is encoded by it.

Irradiation registration optical scheme (**IROS**) of MLNDS collects at some aperture angle ω^* final irradiation P^* coming from BO distributed over its surface and delivers it to MLNDS. Along with this IROS collects some of the initial background irradiation (W_{f2}) not of BO origin. Thus, MLNDS gets total radiation power of W^*:

$$W^*(\lambda^*, t, \{m_j(t)\}, ...) = \int_0^{\omega^*} P^*(x^*, y^*, \lambda^*, t, \{m_j(t)\}, ...) d\omega + W_{f2}(\lambda^*, t)$$

Now general objective function of MLNDS can be formulated as determining the array $\{mj\ (t)\}$ of measured W^* values as a function of signal amplitude, wavelength range and the BO investigation time at known function:

$$P = f(x, y, \lambda, t, W_i).$$

In general to determine the unknown elements in j $\{mj\ (t)\}$ array as a function of time it is necessary to have $k \geq j$ measurements as function of time. For this purpose as shown in [9] for MLNDS perception unit would be enough to realise main functions in detecting and separating two diverse BO signals weak in amplitude but static during short time intervals (seconds) of fluorescence (fluorescent diagnostics channel) and dynamic signal of the main spectrum range $\Delta\lambda i$ (scattering and absorption spectroscopy and Doppler flowmetry channel). In the present SFM it is taken into account by introducing two analogue optical channels - static one (**AOSC**) and dynamic one (**AODC**). Discretisation of the signals by registered optical spectrum (λ^*) in AOSC (second level of discretisation) is carried out by designing the channel as a polychromator with simultaneous recording of full spectrum by range of sensitive detectors like CCD. Signal discretisation in AODC is performed on the base of initial discretisation by spectrum ($\Delta\lambda i$) of emitting sources by choosing suitable set of lasers, and general discretisation by signal time in AOSC and AODC is performed by chosen sampling time and different sampling frequency of CCD for each channel: CCD1 and CCD2.

The amplitude signal discretisation can be carried out using a standard analogue-digital conversion (ADC) of electrical signals from CCD of perception unit and transmits data arrays for temporary storage, sorting and further processing into the memory of internal controller (**IC**). The same controller provides MLNDS with low-level distribution of control commands and data between perception unit and illumination unit. Low-level electronic control of units and modules perception and illumination units is covered by specialized control units (**SCI** and **SCP**). The final high-level data processing and communication of MLNDS with operator is made by the main control and computing system (**MCCU**) on the basis of modern high-speed computer. Thus the system signal processing W^* in MLNDS leads to creation of two main sets of stresses $\{U(n)\}$ from CCD and two full digital data sets {DATA (n)} storing information about amplitude, optical spectrum, and dynamic parameters of the signals:

$$W^* \to \begin{Bmatrix} \{U^{(1)}_{\Delta\lambda_i, \lambda^*}\} \to \{DATA^{(1)}_{\Delta\lambda_i, \lambda^*, t_1}\} \\ \{U^{(2)}_{\Delta\lambda_i, t_2}\} \to \{DATA^{(2)}_{\Delta\lambda_i, t_2, t_1}\} \end{Bmatrix}$$

where: $t2 << t1$ and $t1$ is the time scales of signal discretisation at short time intervals (≤ seconds) and a relatively long time intervals (minutes, hours, days), correspondently. High-level computational algorithms tasks of MCCU are mainly reduced to two main functions: the restoration on the base of actual measurements of optical-physical, medical, and biological properties of BO:

$$\{m_j(t)\} = CA\begin{Bmatrix} \{DATA^{(1)}_{\Delta\lambda_i, \lambda^*, t_1}\} \\ \{DATA^{(2)}_{\Delta\lambda_i, t_2, t_1}\} \end{Bmatrix}$$

where, conventionally, *CA* is a computational algorithm and the interpretation of the computed data array {*mj (t)*} in terms of biology and medicine with the probabilistic classification of the situation:

$$\{CS\} = IA[\{m_j(t)\}]$$

Where: *IA* is interpretive algorithm and {*CS*} is an informational text array of clinical situation observed for that particular survey.

Such a representation of the SFM of MLNDS allows at following stages of design to isolate reasonably and explicitly basic subtasks to be solved: computational algorithms, parametric synthesis of units and blocks of MLNDS, etc. as well as to create already at the step of the ideological and technical design virtual simulative mathematical MLNDS models.

5. Principles of design of unit-module MLNDS

MLNDS SFM presented tells a developer the most logical simple and optimal way of further design-structural elaboration of the MLNDS. The way to create an integrated unit-modular system that individual structural-functional elements are quite typical for many optic-electronic devices.

The opportunity of such an approach was considered in analyzing recent publication containing description and technical specification of various existing optic-electronic units and their scheme-technical, technological etc. solutions. Also the general trends in global instrument development have been investigated reviewing the advertising publications (magazines "Opto & Laser Europe", "Photonics Spectra", "Europhotonics" etc.). Finally this analysis suggests that along with a traditional manufacturers of individual components (chips, lenses, etc.) and final products (full scale equipment) a new class of the producers appears which was not evident in mid-1970-1980's, manufacturers of individual universal optic-electronic subunits and functional blocks. For example, "Point Source Ltd." and "Photonics Products" (USA) offers the finalised different wavelengths laser modules with electronic drivers, perceiving computer macro commands for direct embedding these modules into an integral automated system. "Piezosystem Jena GmbH" also produces a system for positioning and alignment of optical elements for be imbedded into integral complex systems. "Andor Technology Co." offers CCD detectors and sensors for "OEM" technology for direct coupling of signals to every computer through typical USB connection. "Acton Research Corp." produces spectrophotometry modules with various sensitivity and spectral resolution from tiny, located on the board with "PCI" connector, to install on PC to highly sensitive mono-and polychromator with built-in electronic alignment, CCD, analogue amplifier, and ADC modules are capable to work with any PC.

Thus for the manufacturer of final medical diagnostic equipment such as MLNDS, today there is no need to develop from scratch all the basic components and units of the device. It is enough to choose the module (unit) with most suitable technical characteristics on the market and adapt it to the input and output parameters required for developing a new system. This allows to reduce the design of individual MLNDS elements to engineering of classical optic-electronic and laser elements. Using wide world experience in this area as well as databases produced to the date units and modules of optic-electronic, laser and medical devices, all of these tasks can mainly be reduced (on 85-90%) to adaptation and interfacing of well known scheme-technical approaches into combined MLNDS.

So scientifically-based concept of MLNDS design has got basic principles of:

a) maximal standardization of individual units and modules of the MLNDS;
b) maximal functional specialization of units and modules of the MLNDS;
c) structural-functional hierarchy of the units and modules within MLNDS;
d) optimal sharing of hardware and software functions between MLNDS units and modules
e) obedience of all these modules and systems to higher in hierarchy controller (PCs);
f) up-grating of the system with more efficient elements.

6. Conclusion

As it can be seen from all described above, the main peculiarity of the MLNDS design is an existence of a large number of problem-oriented computing and interpretive algorithms that at very strong extent determine the appearance and functionality of the system as a whole. The proposed structural-functional model and objective function of the generalized MLNDS consider these features and at the early stages of MLNDS design allow fully formalizing and

explicitly highlighting the basic subtasks of the subsequent integration of the system, and also creating mathematical simulation model of the MLNDS. Another feature of the diagnostic systems of this class is the method of optical spectroscopy of biological tissues requiring discretisation of signals by spectrum, amplitude, and characteristic time. This imposes certain restrictions on the total number of the channels in MLNDS and their performance rate. On the other hand, MLNDS hardware itself is not very much specific regarding to the current level of development of optics, electronics and laser technology. Therefore these days the design of certain units of the MLNDS can be reduced to the classical optic-electronic and laser engineering.

This work was supported by RFBR (grant № 05-08-33354a) and FASI (contract № 02.442.11.7269) and FP7 EU IAPP project (MEDILASE, #806026).

References

1. Rogatkin, D.A. “The laser clinical diagnostics as one of the perspective branch of biomedical radio-electronics and medical physics of the next millennium”. Biomed. Radio-Electronics, (3), 34-41. (1998).
2. Rogatkin, D.A., Lapaeva, L.G., “Prospects for development of non-invasive spectrophotometry medical diagnostics”, Biomed. Engineering, 37(4), 217-222. (2003).
3. Tuchin, V.V., [Handbook of optical biomedical diagnostics], SPIE Press, Bellingham, Washington, USA, (2002).
4. Russian State Standard ISO 9919-99, “Medical Puls-Oximeters. Technical requerements and methods of examination”, Moscow, State Standard Press, (2000).
5. Krupatkin, A.I. and Sidorov, V.V., [Laser Doppler flowmetry of blood], Meditcina-Press, Moscow, (2005).
6. Loschenov, V.B., et al. “Portable spectroscopic system for fluorescent diagnostics and photodinamic therapy”, Russian Chemical J, XLII(5), 50-53. (1998).
7. Gladkova, N.D., Shakhova, N.M., Sergeev A.M. [Handbook on optical coherent tomography], PhysMath Literature Press, Moscow. (2007).
8. Anderson R.R., Parrish B.B. “The optics of human skin”, J. of Inv. Dermatology, 77(1), 13-19. (1981).
9. Gorenkov R.V., RogatkinD.A. et al. “A method of determination of functional condition of biological tissues and a diagnostic system to realize that.” Russian patent No. 2234242. (2002).
10. Tchernyi, V.V., et al., “Complex non-invasive spectrophotometry in examination of patients with vibration disease,” Photonic Therapeutics and Diagnostics II. SPIE Proc., 6078, 607828, (2006).
11. Ahutin V.M., [Biotechnical systems: theory and projecting], LGU-Press, Leningrad. (1981).
12. Ahutin V.M., Lurie O.B. et al. [Theory and projecting of electronic medical diagnostic apparatus], LGU-Press, Leningrad. (1980).
13. Mosyagin, G.M., Nemtinov, V.B., Lebedev, E.N. [General theory of optical-electronic systems] Engineering-Press. Moscow. (1990).
14. Rogatkin D.A. “Basic principles of organization of system software for multifunctional noninvasive spectrophotometric diagnostic devices and systems.” Biomed. Engineering, 38(2), 61-65. (2004).
15. Bessonov A.S., Kolbas Yu. Yu., Rogatkin D.A. “Virtual diagnostic apparatus in medical noninvasive spectrophotometry.” Technology of living systems, 4(1), 50-57. (2007)
16. Rogatkin, D.A. “A specific feature of the procedure for determination of optical properties of turbid biological tissues and media in calculation for non-invasive medical spectrophotometry.” Biomed. Engineering, 41(20), 59-65. (2007).
17. Ishimaru, A. [Wave propagation and scattering in random media], Academic Press, New-York. (1981).

MULTI-PARAMETER ANALYSIS IN BLOOD CIRCULATION AND PERFUSION BASED DIAGNOSTICS

Stewart* N.A. [1], Dunaev A.V. [1], Sokolovski S.G. [1], Sidorov V.V. [2], Rafailov E.U. [1]

[1] *University of Dundee, Dundee, UK*
[2] *SPE “LAZMA” Ltd, Moscow, Russia*
[*] *Corresponding author's email: N.Z.Stewart@dundee.ac.uk*

Development of multifunctional non-invasive laser-based diagnostic systems where a single device integrating various optical diagnostics techniques is a promising and progressing area in biomedical spectrophotometry. These systems usually combine a number of approaches: laser fluorescence diagnostics (LFD), absorption spectroscopy (tissue reflectance oximetry – TRO), laser Doppler flowmetry (LDF) and pulse oximetry. This allows medics and clinicians not only receive the collective results of the biochemical and physiological parameters which would normally be collected by each individual technique but also to perform multi-parameter patient examination to identify more subtle individual characteristics of blood flow and tissue metabolism based on the simultaneous use of different diagnostic techniques[1] and comprehensive data analysis. This possibility is realized in the LAKK-M system which allows the following blood microcirculation parameters to be obtained: index of blood microcirculation (I_m), tissue oxygen saturation (S_tO_2), relative blood volume (V_b), arterial blood saturation (S_aO_2). Together with collection and analysis of fluorescence spectra of tissue endogenous biomarkers this device is a unique and comprehensive system for research and diagnostics in various fields of biomedicine (cardiovascular diseases, diabetes, cancer, cosmetic surgery, etc.).
However, numerous experiments have identified unacceptably high variations in LDF and TRO readings (up to 30% of standard deviation from the average value for each parameter)[2]. This presents a serious problem for the correct interpretation of data acquired by doctors and seriously limits the prospects for use of this approach in general medical practice. This work aims to overcome this high level of parameter variation and via the use of complex relative parameters which reduce to variations and ease the analysis and interpretation of blood flow parameters, tissue oxygen utilization and biomarkers fluorescence. Furthermore, improved interpretation at a quantitative level of flow velocity based on LDF is targeted by correlation with representative cardiovascular flow phantoms. It is important that this approach can be used for all four LAKK-M channels resulting in increased and readily interpretable information content.
One of these parameters is index of oxygen rate of use in tissue, defined as[3]:

$$U = (S_aO_2 - S_tO_2)/V_b.$$

This parameter characterizes the specific oxygen consumption per unit of blood volume in the selected region of biological tissue.
Oxygen transport in microvasculature and its respiration in the tissue is estimated by characteristics – oxygen metabolism efficiency (OME):

$$OME = M \cdot U \cdot FOC,$$

where M – average of perfusion unit (I_m); FOC – index of fluorescence oxygen consumption, calculated as inversely to redox reaction (ratio). One of the approaches to the calculation of the FOC is the following: $FOC = I_{NADH} / I_{flavins}$, where I_{NADH} – amplitude of fluorescence radiation of reduced coenzyme nicotinamide-adenine dinucleotide, $I_{flavins}$ – amplitude of fluorescence radiation of flavoprotein. Another approach to the calculation of the parameter according to the FOC for the calculation of redox reaction is following:

$$FOC = (I_{NADH} + I_{flavins}) / I_{flavins}$$

Selection of the preferred option for the calculation of FOC, in our opinion, requires further research. To estimate the ranges of change represented by the parameters of the test, experiments were carried out on 3 apparently healthy volunteers: the measurements were made on the crumb right middle finger for 2 weeks, 3 times a day, recording LDF and TRO channel carried out for 3 min, then detected by fluorescence spectra. The parameter U was in a range from 1.5 to 6.3, the parameter OME – 78.7 to 147.4 (according to the first embodiment to calculate the FOC). In addition, each volunteer is clearly peculiar to a more narrow range of values. Typically, for a healthy volunteer (measurement taken in middle finger) the typical values of the complex parameter OME are in the range 70-120.
Thus, the parameter OME is a more informative characteristic of blood microcirculation condition in comparison with individual diagnostics measurements, i.e. microcirculation is much more variable and adapts for specific physiological needs of the tissue. The complex approach to the tissue investigation *in vivo* allows physicians to receive complementary data about microhemodynamics, oxygen consumption and condition of metabolic processes for their interpretation and decision making concerning disease diagnosis.
This work was supported by FP7 EU IAPP project (MEDILASE, #806026).

References:

1. Rogatkin D.A., Sokolovski S.G., Fedorova K.A., Stewart N.A., Sidorov V.V., Rafailov E.U. Basic principles of design and functioning of multifunctional laser diagnostic system for non-invasive medical spectrophotometry // SPIE Proc., Vol. 7890, 2011. – 78901H.
2. Makarov D.S., Rogatkin D.A. Physiological deviation of individual blood microcirculation parameters as a source of errors in noninvasive medical spectrophotometry // Proceedings the 9-th International conference «Physics and radioelectronics in medicine and ecology PREME’2010». – RF: Vladimir, 2010. – p.82-86.

3. Krupatkin A.I., Rogatkin D.A., Sidorov V.V. Clinical-diagnostic parameters for complex investigation of microhaemodynamics and oxygen transport in the system of microcirculation / Abstr. book of the VI-th. International Conference "Hemorheology and microcirculation" – RF, Yaroslavl, 2007. – p.106.

Laser reflectance oximetry and Doppler flowmetry in assessment of complex physiological parameters of cutaneous blood microcirculation

Andrey V. Dunaev*[a], Victor V. Sidorov[b], Neil A. Stewart[a], Sergei G. Sokolovski[a], Edik U. Rafailov[a]
[a]Photonics and Nanoscience Group, Division of Physics, School of Engineering, Physics and Mathematics, University of Dundee, Dundee DD1 4HN, UK; [b]SPE "LAZMA" Ltd., Moscow 125252, RF

ABSTRACT

The integration of multiple optical techniques within a single diagnostic device is used to address the difficulties in standardising measurement of cutaneous blood micro-dynamics caused by high variability. We demonstrate the benefits of simultaneous assessment of blood relative volume (V_b), microcirculation index (I_m) and tissue oxygen saturation (S_tO_2), during long-term examination of healthy volunteers. Consequently, five rhythmic components: endothelial, neurogenic, myogenic, breath and heart pulses were established showing high variability up to 30 – 50% as well as in initial parameters around 16%. All rhythmic components were synchronous with some latency between I_m and S_tO_2 in the myogenic component supports the hypothesis of strong correlation between peripheral hemodynamics and oxygen utilisation in tissues.

Keywords: laser Doppler flowmetry, tissue reflectance oximetry, microcirculation, bloodflow oscillations, variability

1. INTRODUCTION

Optical techniques are one of the promising non-invasive technologies for diagnosis of medical conditions. The integration of various techniques in an instrument and methodological framework that combines them in a single device using integrating algorithms for multi-modal diagnostics is particularly promising. Multi-functional laser non-invasive diagnostic systems (MLNDS), with up to 4 active channels are emerging, for example: laser Doppler flowmetry (LDF), tissue reflectance oximetry (TRO), laser fluorescence diagnostics (LFD), pulse oximetry and other. The most promising methods of optical non-invasive diagnostic methods are LDF and TRO. These methods are widely used in studying the dynamics of processes of blood microcirculation and oxygen transport and utilisation in biological tissues.

The results of LDF measurements, index of blood microcirculation (I_m) or perfusion, assessed in conventional perfusion units (PU), reveal a complex, non-periodic process. This variable component contains information on the modulation of blood flow. Use of spectral signal processing algorithms (LDF-graphs) for decoding and analysis provides information about the condition of vascular tone in terms of its contribution to the different mechanisms of micro-hemodynamic regulation (myogenic, endothelial, etc.) [1].

The TRO method determines relative blood volume (V_b) microcirculation in the surface layers of the soft tissues (skin, mucous membranes of the organs) and tissue oxygen saturation (S_tO_2) of the microvasculature in the inspected area of biological tissue. There are isolated cases of spectral processing algorithms recorded signals (S_tO_2- and V_b-graphs), being used to assess vasomotion and myogenic rhythms, for example[2]. We propose that analysis of oscillation signals recorded by TRO according to the frequency ranges, similar to LDF-graphs, is of practical interest in studying the parameters of microcirculation of blood, as the relationships between LDF and TRO attract the increasing attention of researchers in this field.

*a.v.dunaev@dundee.ac.uk; phone 44 1382 386571; dundee.ac.uk/elecengphysics/research/photonics/photonicsnanoscience

dvanced Biomedical and Clinical Diagnostic Systems I, edited by nita ahadevan- ansen, Tuan Vo-Dinh, arren S. rundfest, Proc. of SPIE Vol. 8572, 857205 · © 2013 SPIE
CCC code: 1605-7422/13/$18 · doi: 10.1117/12.2001797

It is well known that *in vivo* LDF and TRO measurements have high variability, at least in the range of ± 30% in terms of σ (standard deviation, *SD*) of the average measured values for each parameter (I_m, S_tO_2, V_b) [3]. Moreover, these results were obtained during long-term studies in two apparently healthy volunteers to estimate the individual momentary variability in the oscillation of the oxygenation in peripheral tissue blood microflow and also over a long period of observation. It should be emphasised that this work did not set out to evaluate the variability of the oscillations in a statistically defined group (age, sex, pathology, etc.). The aim was to assess long-term individual variability of the oscillations in a subject (a healthy volunteer) over one month, as such data does not exist in the literature.

2. CLASSIFICATION OF THE BLOOD FLOW OSCILLATIONS AND ITS VARIABILITY

Currently, for diagnostic purposes five rhythmic components (oscillations) were isolated from LDF recordings with help of the wavelet analysis in accordance with the modern interpretation of their genesis [4-7]:

- endothelial rhythms (frequency interval 0.0095-0.02 Hz);
- neurogenic rhythms (0.02-0.06 Hz);
- myogenic rhythms (0.06-0.16 Hz);
- breathing rhythms (0.16-0.4 Hz);
- pulse rhythms (0.4-1.6 Hz).

Possible physiological processes causing fluctuations in blood microflow in the frequency range of endothelial rhythms still are currently under discussion. However one of the possible explanation is a release of vasodilator nitric oxide into the endothelium [6]. It is believed that fluctuations in neurogenic rhythms (about 0.04 Hz) are irrelevant to vasomotion of arterioles. The increase in the amplitude of the oscillations is an indicator of lower neurogenic resistance and the possible increase in blood flow in the arterioles, venular shunt with an increase in myogenic tone [1]. It is believed that the source of myogenic oscillations (approximately 0.1 Hz) is the spontaneous activity of smooth muscle cells in resistance vessels and pre-capillary sphincters, also called vasomotion associated with regulation of blood pressure. Periodic oscillations with a frequency of about 0.3 Hz are synchronized with the breath. The activity of respiratory function poorly represented in the LDF-signal. Periodic oscillations with a frequency of about 1 Hz in the skin are synchronized with the heart rate and represent the variations that reflect changes in the diameter of blood vessels induced by the pulsation of the flow due to cardiac cycle.

It is known that the amplitude of the oscillations in these ranges varies considerably for individuals as well as the high lability of blood flow in the capillaries and other vessels of the microvasculature are a prerequisite for tissue homeostasis. Displaying the average amplitude distribution of blood flow to the rhythms of two healthy age groups 18-20 years (62 subjects) and more than 40 years (40 subjects). As it can be seen from the distribution of the amplitude of the oscillations in the neurogenic range for both age groups predominate. Deviation of the oscillation amplitude at a test area for a homogeneous group of subjects can be up to 15% [8]. However, data on the physiological variation in one individual assessed for a long period of time was impossible to find in the literature.

3. THE METHOD OF RESEARCH

In this study we used a MLNDS "LAKK-M" (SPE "LAZMA", Russia), which besides of LDF and TRO had pulse oximetry and LFD channels (Fig. 1). This system allows simultaneous recording of the I_m, S_tO_2, V_b parameters in a tissue volume [9]. The study was conducted on an adult male, age 35, with no cardiovascular disease history. The measurements were performed on a skin pad (palmar surface) right middle finger. This area was chosen because it is rich in arteriolar-venular anastomoses (AVA) and variability of the LDF signal is less than in tissue with fewer shunts [4]. Consequently, it is ideal for this research aimed at evaluating the proportion of nutritive blood flow (*NB*) from the known formula, and hence the parameters such as myogenic (*MT*), neurogenic (*NT*) and endothelial-dependent component (*ET*) tone [1].

All measurements were performed daily during the month (except holidays) at the same time (around 11:00 am) to avoid circadian rhythms influence on the blood circulation. Length measurements was 3 min, total of 22 measurements (days). An example of screenshot of the registered parameters is presented in Fig. 2a. At the end of the observation time the oscillation rhythms of each measurement were analysed using the built-in module "wavelet analysis" (example screenshot is shown in Fig.2b). The wavelet analysis determined the maximum amplitude (δI_m, δS_tO_2, δV_b) and the corresponding frequency for each of the 5 oscillation types for each of the 3 parameters of I_m, S_tO_2 and V_b.

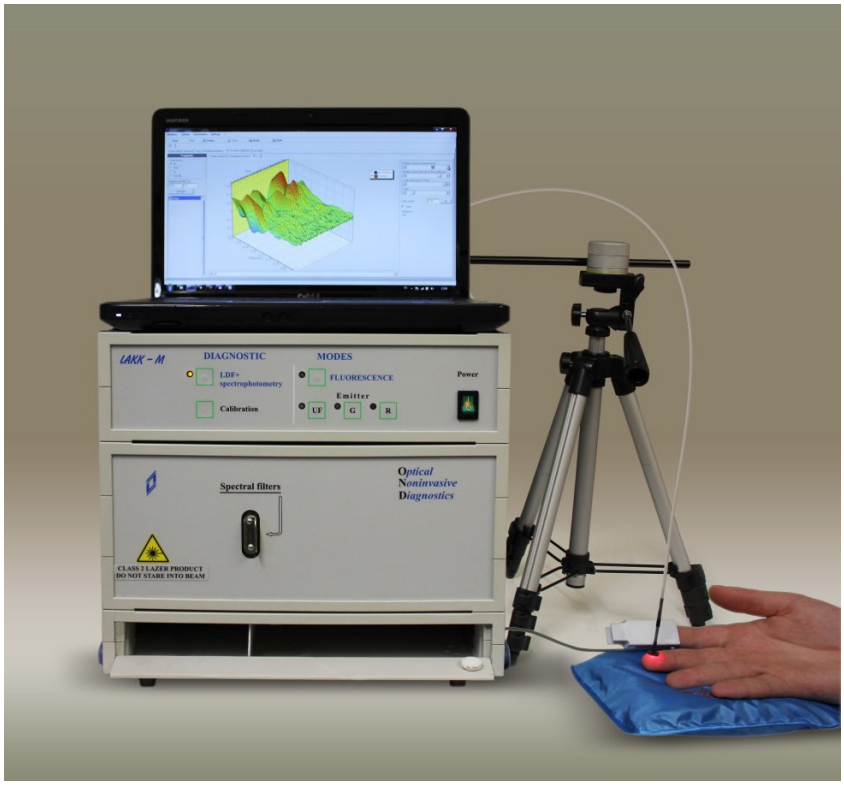

Figure 1. MLNDS "LAKK-M".

In addition to variability, the data was assessed for parameters such as: bypass index (*BI*), index of tissue oxygen use (taking into account nutritional blood flow) (*I*), index of perfusion oxygen saturation in microvascular blood (S_m), index of oxygen consumption rate in tissue (U_1 and U_2), calculated according to [10] and [11] respectively.

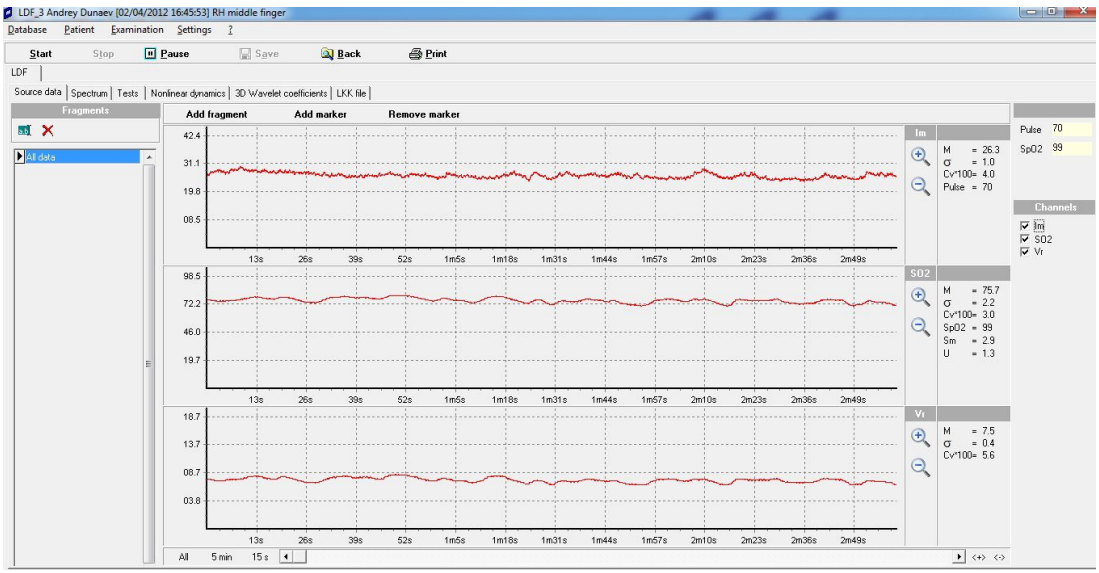

a)

b)

Figure 2. Screenshots of LDF- and TRO-recordings (a) and wavelet analysis (b).

4. RESULTS AND DISCUSSION

These results have been presented in Table 1 and Fig. 3-6.

Table 1 shows the statistical evaluation (*M*, is mean value, *SD is* standard deviation, k_v is a coefficient of variation) of the measured LDF and TRO methods for parameters of I_m, S_tO_2, V_b and calculated on the basis of their indicators. Fig. 3 show a diagram of changes in the parameters of I_m, S_tO_2 and V_b for a month in one subject.

Table 1. The statistical evaluation of the LDF and TRO parameters.

№	Statistic parameters	Measured parameters			Calculated parameters								
		I_m, PU	S_tO_2, %	V_b, %	*NT*	*MT*	*ET*	*BI*	*NB*, PU	*I*	S_m	U_1	U_2
1	*M*	25.6	62.5	8.7	1.76	2.06	2.00	1.23	11.90	19.36	2.5	1.6	3.9
2	*SD*	3.5	10.2	1.4	0.49	0.54	0.54	0.40	3.10	6.01	0.5	0.3	1.5
3	k_v, %	13.5	16.4	16.3	27.59	26.47	27.17	32.57	25.80	31.02	20.5	16.8	37.7

Analysis of the data shows the greatest variability in the parameters obtained by the TRO (16%), whereas the variability of the microcirculation index (I_m) in our study turned out not more than 14%, more than 2 times less than previously reported data [3], obtained for 10 days. Perhaps this is due to the specific devices used by these authors with different diagnostic volumes (due to different measurement bases) and the design of the optical probes. We conducted longer-term studies in order to contrast with the published short-term study data previously used to study variation.

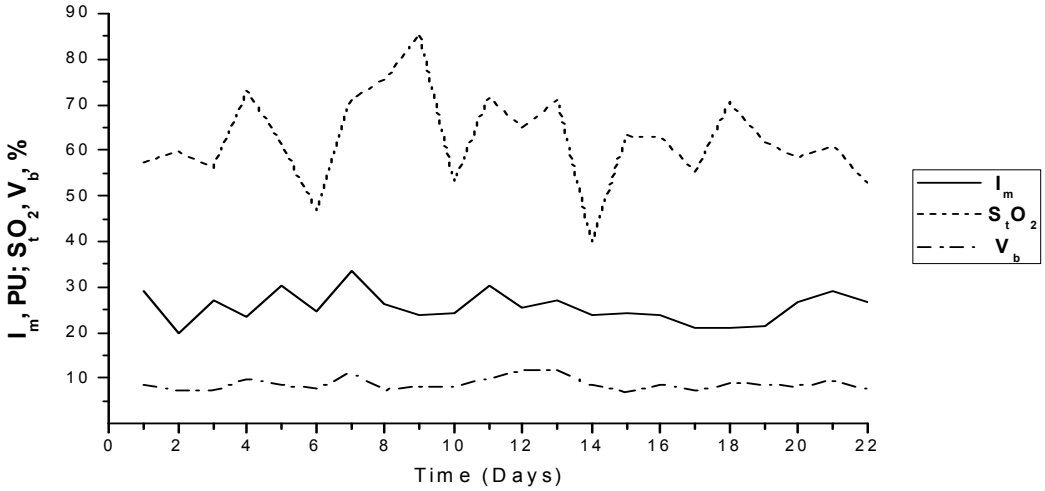

Figure 3.Representitive I_m, S_tO_2 and V_b parameters from one individual.

The calculated values of *MT*, *NT* and *ET*, as well as *BI* have a high variability (up to30%) due to use in their calculations, as it will be shown below, the oscillation amplitudes with high variability. The nutritional bloodflow (*NB*) component was 11.9±3.1 PU, which is about two times lower than the mean value of the index of blood microcirculation 25.6±3.5 PU. The S_m index has a variability of about 20%, while the index of oxygen rate of use in tissue (U_2) has a variability factor twice that of (U_1), since its calculation is based on two parameters at once with variability of 16%. In aiming to reducing the influence of the variation in the measured parameters it is preferable to use the integrated index calculation U_1.

Fig. 4 shows the changes in the study of oscillations during the month for the LDF-, S_tO_2- and V_b-graphs respectively (Fig. 4a, 4b, 4c). In Fig. 5 shows corresponding histogram showing the distributions of mean value and *SD* for these oscillations.

Analysis of the data in general shows a high variability of the investigated oscillations in all 3 graphs. The smallest variation is the V_b in endothelial (30%), neurogenic (35%) and myogenic components (40%). While pulse rhythms variability turned out about 33%, which is greater than 23% of data variability rhythms in blood perfusion. The greatest variable component in all the 5 rhythms was S_tO_2-parameter (50%) while the greatest variation is observed in endothelial (44%) and myogenic rhythms (40%) LDF-graphs, in myogenic (54%) and breathing rhythms (55%) S_tO_2-graphs and in myogenic (38%) and pulse rhythms (33%) V_b-graphs.

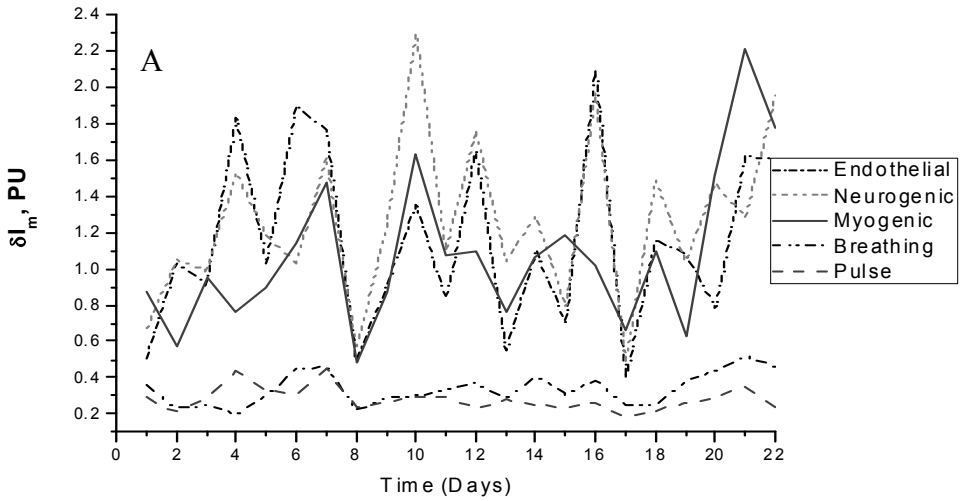

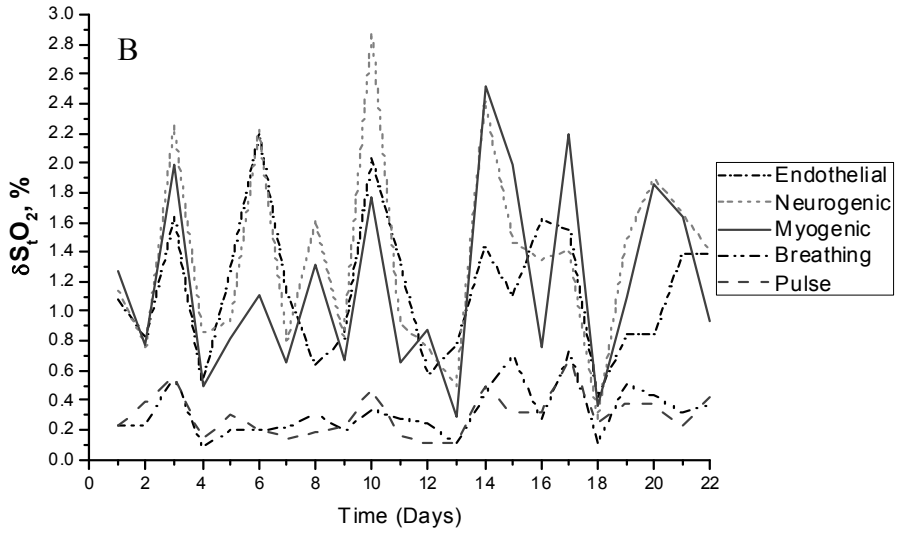

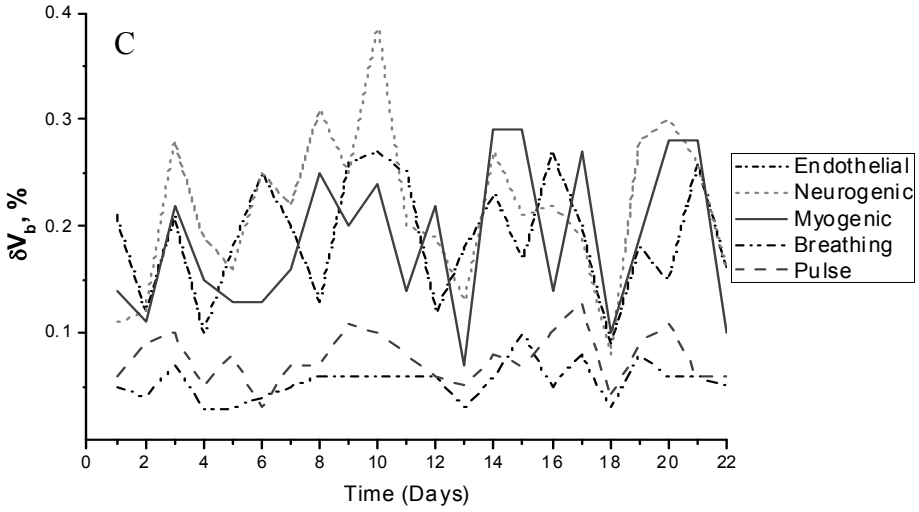

Figure 4. Representative changes in blood perfusion (A), S_tO_2 (B) and V_b (C) oscillations recorded from one individual.

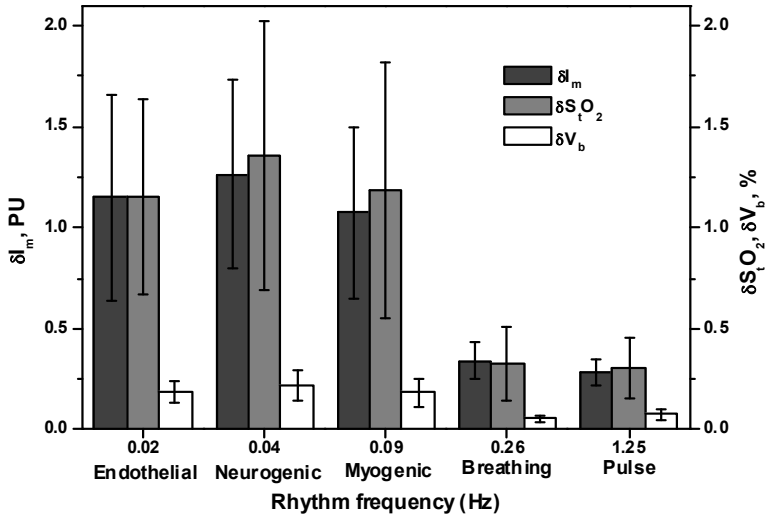

Figure 5. Blood perfusion, S_tO_2, and V_b parameters regularly taken from one individual form a month.

The synchronicity of all 5 components of the fluctuations during the whole period of studies can be seen in the Fig. 4 For example, analysis of Fig. 3 and Fig. 4 shows rising neurogenic rhythm of oscillations with a periodicity of about 8 days (3-, 10-, 16- and 22- days), which corresponds precisely to an increase in perfusion (I_m) on the same days. This may be considered quite natural due to the more intense work of myocytes of arterioles. At this time a subject indicated an increase in tissue oxygen saturation (S_tO_2).

It is interesting to note the ability the results provide to assess the relationships between blood perfusion and S_tO_2. For example, one can trace a pattern manifested three times during the time trials (7-, 16- and 18- days) where we observe a decrease in tissue oxygen saturation with increasing amplitude of myogenic oscillations. Thus, the increase in hydrostatic pressure is accompanied by an increase in the diffusion of oxygen in tissues and, consequently, a decrease in tissue oxygen saturation, which corresponds to the data given in [2].

Fig. 5, presents the histograms of oscillations in the LDF-, S_tO_2-and V_b-data of the amplitudes of repeated known data [8] for the LDF-graphs, except for the amplitudes of pulse rhythms to V_b-graphs, in which the pulse oscillations predominate over breathing. This is most likely due to the physiological meaning of the parameter V_b being more dependent on the pulse fluctuations. In addition, these data allow us to estimate the long-term variability of 5 rhythms for all 3 parameters.

Fig. 6 shows the related oscillations of myogenic vasomotion for the blood perfusion, S_tO_2 and V_b. This approach extends the assessment of the contribution of a particular component in each of the 3 graphs.

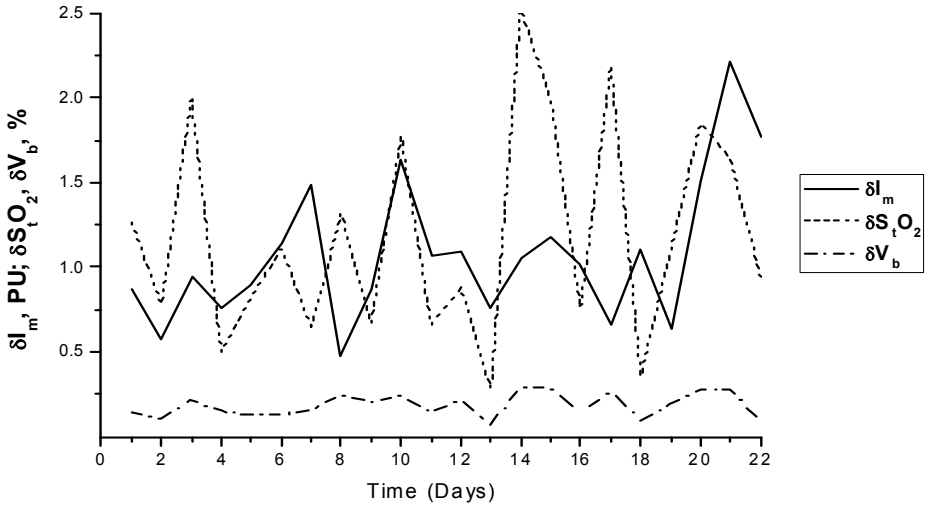

Figure 6.Representitive myogenic vasomotion oscillations of blood perfusion, S_tO_2 and V_b. recorded from one individual.

5. CONCLUSION

The obtained results confirm that peripheral blood flow and tissue oxygenation is characterised by high variability (lability), which is essential for adaptation of the organism to stresses. The observed high variability of the oscillations (about 30-50%) also may be partially explained by the peculiarities of non-invasive optical diagnostic techniques, primarily associated with low diagnostic volume (in this case about 1 mm^3). Obviously, the blood flow and oxygenation in a small volume will vary significant due to spatial heterogeneity in biological tissues.

However, the long-term observation of subject(s) and analysis of the individual variability of her/his blood rhythm (LDF- and S_tO_2-parameters) identified a new correlation between the peripheral hemodynamics and oxygen utilisation in tissues. This confirmed increase in the information content of the data also confirms the requirement to factor these variables into any models or algorithms used for non-invasive optical diagnostic techniques.

This work was supported by FP7 EU IAPP project (MEDILASE, #806026).

REFERENCES

[1] Krupatkin, A. I. and Sidorov, V. V., [Laser Doppler flowmetry of blood], Meditcina-Press, Moscow(2005).
[2] Thorn, C. E., Kyte, H., Slaff, D. W. and Shore, A. C., "An association between vasomotion and oxygen extraction," American Journal of Physiology-Heart and Circulatory Physiology, 301(2), H442-H449 (2011).
[3] Makarov, D. S. and Rogatkin, D. A., "Physiological deviation of individual blood microcirculation parameters as a source of errors in noninvasive medical spectrophotometry," Proc. "Physics and radioelectronics in medicine and ecology PREME'2010". 82-86 (2010).
[4] Salerud, E. G., Tenland, T., Nilsson, G. E. and Oberg, P. A., "Rhythmical variations in human-skin blood-flow," International Journal of Microcirculation-Clinical and Experimental, 2(2), 91-102 (1983).

[5] Bracic, M. and Stefanovska, A., “Wavelet-based analysis of human blood-flow dynamics,” Bulletin of Mathematical Biology, 60(5), 919-935 (1998).
[6] Stefanovska, A., Bracic, M. and Kvernmo, H. D., “Wavelet analysis of oscillations in the peripheral blood circulation measured by laser Doppler technique,” IEEE Transactions on Biomedical Engineering, 46(10), 1230-1239 (1999).
[7] Kvandal, P., Landsverk, S. A., Bernjak, A., Stefanovska, A., Kvernmo, H. D. and Kirkeboen, K. A., “Low-frequency oscillations of the laser Doppler perfusion signal in human skin,” Microvascular Research, 72(3), 120-127 (2006).
[8] Krasnikov, G. V., Matrusov, S. G., Piskunova, G. M., Sidorov, V. V. and Chemeris, N. K., "Age characteristics of peripheral blood flow oscillations in the skin," Proc. "Application of laser Doppler flowmetry in medical practice". 32-34 (2000).
[9] Rogatkin, D. A., Sokolovski, S. G., Fedorova, K. A., Sidorov, V. V., Stewart, N. Z. and Rafailov, E. U., "Basic principles of design and functioning of multifunctional laser diagnostic system for non-invasive medical spectrophotometry," Proc. SPIE. 7890, 78901H1 (2011).
[10] Stewart, N. A., Dunaev, A. V., Sokolovski, S. G., Sidorov, V. V. and Rafailov, E. U., "Multi-parameter analysis in blood circulation and and perfusion based diagnostics," Proc. "Laser Optics 2012". (2012).
[11] Krupatkin, A. I., Rogatkin, D. A. and Sidorov, V. V., "Clinical-diagnostic parameters for complex investigation of microhaemodynamics and oxygen transport in the system of microcirculation," Proc. "Hemorheology and microcirculation". 106 (2007).

The study of synchronization of rhythms of microvascular blood flow and oxygen saturation during adaptive changes

Andrey V. Dunaev*[a,b], Victor V. Sidorov[c], Alexander I. Krupatkin[d], Ilya E. Rafailov[e], Scott G. Palmer[a,e], Sergei G. Sokolovski[a], Neil A. Stewart[a,e], Edik U. Rafailov[a]

[a]Photonics and Nanoscience Group, Division of Physics, School of Engineering, Physics and Mathematics, University of Dundee, Dundee DD1 4HN, UK; [b]State University – Education-Science-Production Complex, Scientific-Educational Center of Biomedical Engineering, Oryol 302020, Russia; [c]SPE "LAZMA" Ltd., Moscow 125252, Russia; [d]Priorov Central Research Institute of Traumatology and Orthopaedics, Moscow 127299, Russia; [e]Department of Imaging and Technology, Ninewells Hospital, University of Dundee, Dundee DD1 9SY, UK

ABSTRACT

Multi-functional laser non-invasive diagnostic systems, such as "LAKK-M", allow the study of a number of microcirculatory parameters, including blood microcirculatory index (I_m) (by laser Doppler flowmetry, LDF) and oxygen saturation (S_tO_2) of skin tissue (by tissue reflectance oximetry, TRO). Such systems may provide significant information relevant to physiology and clinical medicine. The aim of this research was to use such a system to study the synchronization of microvascular blood flow and oxygen saturation rhythms under normal and adaptive change conditions. Studies were conducted with 8 healthy volunteers – 3 females and 5 males of 21-49 years. Each volunteer was subjected to basic 3 minute tests. The volunteers were observed for between 1-4 months each, totalling 422 basic tests. Measurements were performed on the palmar surface of the right middle finger and the forearm medial surface. Wavelet analysis was used to study rhythmic oscillations in LDF- and TRO-data. Tissue oxygen consumption (from arterial and venal blood oxygen saturation and nutritive flux volume) was calculated for all volunteers during "adaptive changes" as (617±123 AU) and (102±38 AU) with and without arteriovenous anastomoses (AVAs) respectively. This demonstrates increased consumption compared to normal (495±170 AU) and (69±40 AU) with and without AVAs respectively. Data analysis demonstrated the emergence of resonance and synchronization of rhythms of microvascular blood flow and oxygen saturation as an adaptive change in myogenic oscillation (vasomotion) resulting from exercise and potentially from psychoemotional stress. Synchronization of myogenic rhythms during adaptive changes suggest increased oxygen consumption resulting from increased microvascular blood flow velocity.

Keywords: laser Doppler flowmetry, tissue reflectance oximetry, vasomotion, oxygen consumption, adaptive changes

1. INTRODUCTION

The evaluation of stress-induced adaptive changes in the respiratory and circulatory systems of individuals could provide relevant information for studies in physiology and clinical medicine. In recent years, with the advent of multi-functional laser non-invasive diagnostic systems, such as the "LAKK-M" system (SPE "LAZMA" Ltd, Russia) [1], it has become possible to conduct studies on a number of tissue parameters, including microvascular blood flow (by laser Doppler flowmetry, LDF) and oxygen saturation of skin tissue (by tissue reflectance oximetry, TRO) [2].

The results of LDF measurements, representing "index of blood microcirculation (I_m)" or "perfusion", assessed in conventional perfusion units (PU), reveal a complex, non-periodic process. This variable component contains information on the modulation of blood flow. Use of spectral signal processing algorithms on LDF-graphs for decoding and analysis provides information about the condition of vascular tone in terms of its contribution to the different mechanisms of micro-hemodynamic regulation [3, 4].

*a.v.dunaev@dundee.ac.uk; phone 44 1382 386571; dundee.ac.uk/elecengphysics/research/photonics/photonicsnanoscience

dvanced Biomedical and Clinical Diagnostic and Surgical uidance Systems II, edited by Tuan Vo-Dinh, nita ahadevan- ansen, arren S. rundfest, Proc. of SPIE Vol. 8935, 89350 © 2014 SPIE · CCC code: 1605-7422/14/$18 · doi: 10.1117/12.2035748

Oscillatory processes play an important role in the function of the tissue microcirculation system. Several frequency ranges of blood flow oscillations in microvascular networks, each of a different regulatory origin, have been identified (endothelial, neurogenic, myogenic, etc.) [5-7]. Many medical publications are devoted to the study of myogenic oscillations, because they characterize the state of pre-capillary sphincters, which play an important role in the regulation of blood flow [8-10].

The TRO method determines relative blood volume (V_b, in percent) in microcirculation in the surface layers of the soft tissues (skin, mucous membranes of the organs) and tissue oxygen saturation (S_tO_2, in percent) in the microvasculature in the inspected area of biological tissue. There are few spectral processing algorithms for these recorded signals (S_tO_2- and V_b-graphs) [11, 12], and there are limited publications studying the relationships between LDF- and S_tO_2-graphs [13, 14]. In isolated cases this has been used to assess vasomotion and myogenic rhythms for perfusion and tissue oxygen saturation, for example [15]. We propose that analysis of oscillation signals recorded by TRO according to the frequency ranges, similar to LDF-graphs, is of practical interest in studying the microcirculation of blood, as the relationships between LDF and TRO attract increasing attention from researchers in this field.

The aim of this research was to use LDF- and TRO-graphs to investigate tissue respiration and the synchronization of microvascular blood flow and oxygen saturation rhythms under normal conditions and during adaptive changes.

2. THE METHOD OF RESEARCH

In this study we used a "LAKK-M" system, which, besides LDF and TRO, contains pulse oximetry and laser fluorescence diagnostic channels[1]. This system utilizes near-infrared (1064 nm), red (640 nm) and green (532 nm) lasers for LDF- and TRO-channels and performs simultaneous recording of the I_m, S_tO_2 and V_b parameters in a tissue volume of approximately 3-5 mm^3. Studies, of different durations, were conducted with 8 healthy volunteers (no history of cardiovascular disease) aged 21-49 years, comprising 3 females and 5 males. These studies were conducted by simultaneously recording parameters of LDF (I_m), TRO (S_tO_2) and pulse oximetry (S_aO_2 - arterial blood saturation with oxygen). In order to assess the I_m and the S_tO_2 oscillatory component, spectral wavelet analysis of oscillations was used (software LDF 3.0.2.384, LAZMA, Russia). This program uses a continuous wavelet transform, with the Morle complex valued wavelet being used as the analyzing wavelet [16]. The study was performed at an ambient temperature of 21–22°C in a sitting position after a 30 min rest. The measurements were performed on skin pad (palmar surface) of right middle finger (Fig. 1a). This area was chosen because it is rich in arteriovenous anastomoses (AVAs) and variability of the LDF signal is less than in tissue with fewer shunts [17]. It should be emphasized that this area is regulated almost exclusively by the autonomic nervous system and is very sensitive to adaptive changes. In addition, studies were conducted in an area almost completely devoid of AVAs - the lower arm's medial surface (the skin without AVAs), characterized by greater nutritive blood flow (Fig. 1b).

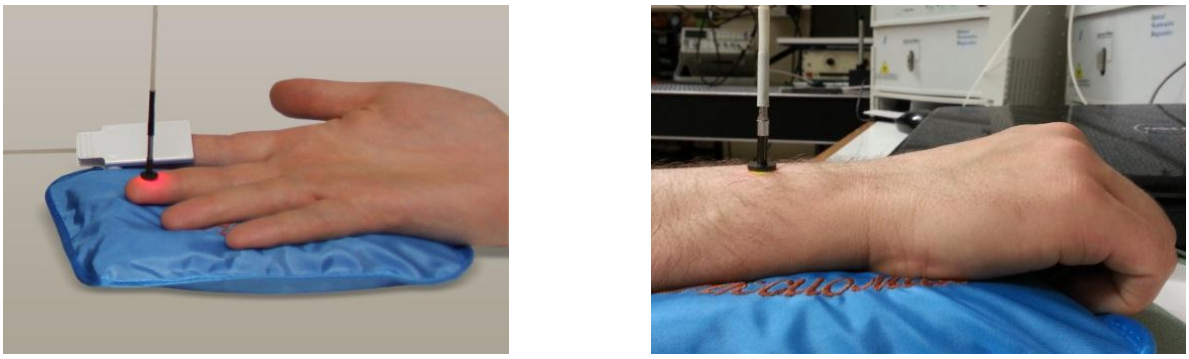

a) b)

Figure 1. Skin areas of study: with AVAs (a) and without AVAs (b).

The male participant of 36 years (volunteer №1) was studied over the course of 6 months, totaling 100 records in the skin with AVAs: 60 basic tests for 3 min, plus 20 "before and after" records to monitor the effects of exercise, in this case swimming (500 m). This volunteer's studies have also been conducted in the skin without AVAs. The female

participant (volunteer №2) was studied over the course of 1 month, totaling 40 studies only in the skin with AVAs: 20 basic tests for 3 minutes plus 20 tests with occlusion for 1 min followed by a 3 min post occlusion period. For the remaining volunteers, only basic tests were performed on both points of interest (skin with and without AVAs) and they were not subjected to additional stress. Wavelet analysis was performed on 5 rhythmic components (oscillations) of I_m- and S_tO_2-records, namely: endothelial (0.0095-0.02 Hz); neurogenic (0.02-0.06 Hz); myogenic (0.06-0.16 Hz); breathing (0.16-0.4 Hz) and pulse (0.4-1.6 Hz) [5, 18, 19]. The typical form of perfusion and tissue oxygen saturation are shown in Fig 2a and the results of the wavelet analysis for them during the basic test are presented in Fig. 2b.

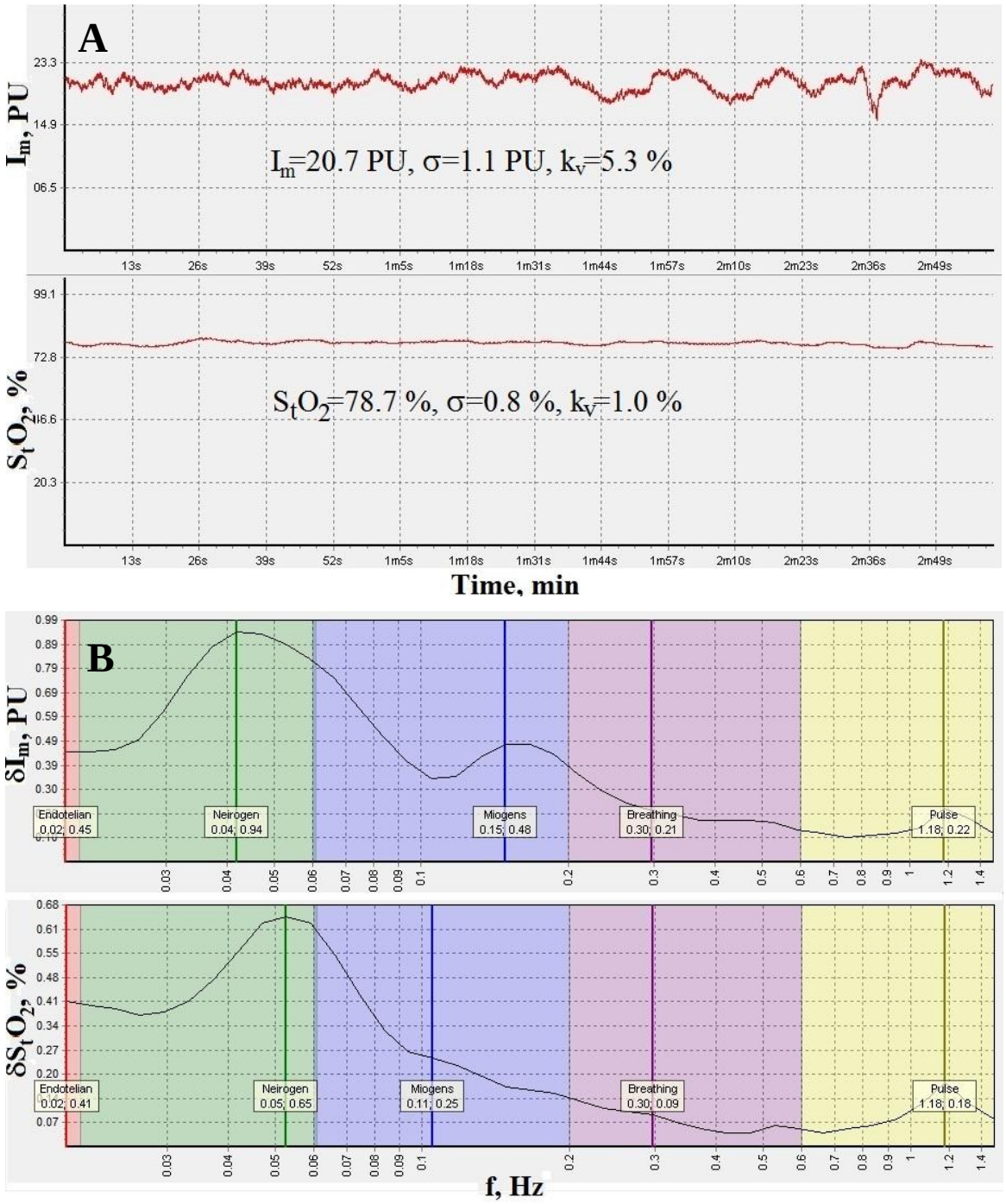

Figure 2. The typical form of perfusion and tissue oxygen saturation graphs of the skin area with AVAs for volunteer №1 (a), where σ – standard deviation, k_v – coefficient of variation, and wavelet analysis results following such basic tests (b), where δI_m – amplitude of perfusion oscillations, δS_tO_2 – amplitude of oxygen saturation oscillations. Furthermore, in (b), a line is used to represent the amplitude oscillation of microvascular blood flow (δI_m=0.48 PU) at a frequency of f_m=0.149 Hz and tissue oxygen saturation (δS_tO_2=0.25%) at a frequency of f_m=0.105 Hz for myogenic rhythms.

During every test, the psychoemotional state of the volunteer was recorded as either normal or under emotional stress. In the case of volunteer №2, physiological stress was induced through occlusion tests, while for volunteer №1 this was achieved by exercise (swimming), which can be considered as stress simulation.

Of particular interest is the analysis and comparison of oxygen consumption in tissue under normal conditions and during adaptive changes, associated with a sympathetic vasomotor reflex (synchronization and resonance of myogenic oscillation in perfusion and tissue oxygen saturation). This is especially noteworthy as a relationship between the activation of vasomotion and oxygen consumption has been previously reported [20]. Following the methodology explained in the article [21] and from spectral wavelet analysis of I_m- and S_tO_2-graphs, we calculated the extraction and consumption of oxygen in tissue for all 8 volunteers.

Oxygen extraction (*OE*), assessed in arbitrary units (AU), was calculated as follows:

$$OE = \left(S_aO_2 - S_vO_2\right) / S_aO_2, \tag{1}$$

where S_vO_2 – venous blood oxygen saturation, calculated using spectral wavelet analysis of S_tO_2 oscillations. We also analyzed the amplitude of oscillations of cardiac $(\delta S_tO_2)_c$ and respiratory rhythms $(\delta S_tO_2)_r$. If the $(\delta S_tO_2)_c/(\delta S_tO_2)_r$ ratio ≤ 1, then S_vO_2 is taken to be equal to S_tO_2. This variant predominates in most cases of recordings from the skin without AVAs [22]. If the $(\delta S_tO_2)_c/(\delta S_tO_2)_r$ ratio > 1, then:

$$S_vO_2 = S_tO_2 / ((\delta S_tO_2)_c / (\delta S_tO_2)_r. \tag{2}$$

This variant predominates in most cases of recordings from the skin with AVAs. In the cases of resonance oscillations in the active frequency bands (for example, in the myogenic range during adaptive changes), the cardiac and/or respiratory rhythm amplitudes may not be expressed in the spectrum, and the S_vO_2 calculation has some specific features. In the cases of resonance of oscillations in the total myogenic and respiratory bands, $S_vO_2 = S_tO_2$. In the skin zones with AVAs, an additional confirmation using the bypass index (*BI*) for S_tO_2 is necessary [21]:

$$S_vO_2 = S_tO_2 / BI(S_tO_2), \tag{3}$$

where:

$$BI(S_tO_2) = 1 + (\delta S_tO_2)_n / (\delta S_tO_2)_m, \tag{4}$$

where $(\delta S_tO_2)_n$ and $(\delta S_tO_2)_m$ - amplitudes of oscillations of neurogenic and myogenic rhythms respectively.

Oxygen consumption (*OC*), assessed in arbitrary units (AU), was calculated as follows:

$$OC = I_{mn} \cdot \left(S_aO_2 - S_vO_2\right), \tag{5}$$

where I_{mn} - the nutritive blood flow value was calculated according to the equation:

$$I_{mn} = I_m / BI(I_m), \tag{6}$$

where $BI(I_m)$ - bypass index calculated for skin with AVAs similarly to formula (4), but only using perfusion data. For skin zones without AVAs:

$$BI(I_m) = (\delta I_m)_{\max} / (\delta I_m)_m, \tag{7}$$

where $(\delta I_m)_{max}$ is the maximum amplitude of the dominant oscillations in the active range of frequencies up to 0.15 Hz and $(\delta I_m)_m$ - amplitude of oscillations of myogenic rhythms.

Accordingly, the calculation of oxygen consumption in cases with and without adaptive changes (for synchronization and resonance of myogenic oscillations in perfusion and oxygen saturation) were processed separately. It should be

noted that the *OC* equation includes the perfusion rate value, thus the *OC* value (calculated according to Fick's principle) reflects the oxygen consumption rate.

The following parameter has also been calculated and analyzed:

$$\Delta f_m = f_m(S_tO_2) - f_m(I_m), \tag{8}$$

where f_m - myogenic oscillation frequency of perfusion and tissue oxygen saturation, respectively.

Data presented in the text are means ± SD. Statistical analysis was performed by OriginPro 8 SRO version v.8.0724 with data sets tested for normality by the Kolmogorov-Smirnov and Shapiro-Wilk tests. For normally distributed data, group comparisons were made by carrying out a parametric unpaired *t*-test. For the obtained non-normal data distribution of data, Mann-Whitney test nonparametric statistics was used to compare the two groups (normal and with conditions of adaptive changes).

3. RESULTS AND DISCUSSION

Analysis of the data shows the emergence of synchronized rhythms in microvascular blood flow and oxygen saturation within the myogenic oscillation range (vasomotion) during adaptive changes – for example, stressful situations or response to physical exercise. The typical perfusion and tissue oxygen saturation data, along with the results of wavelet analysis of these parameters during adaptive changes for volunteer 1 are presented in Fig. 3.

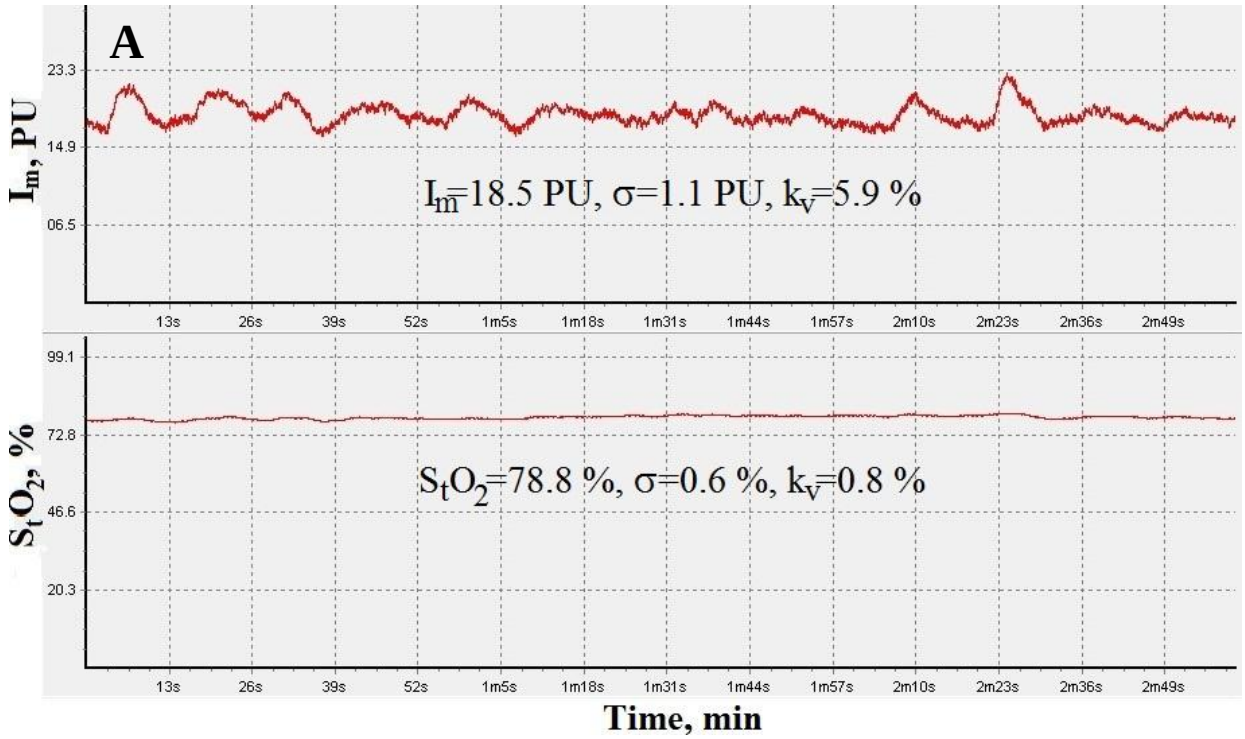

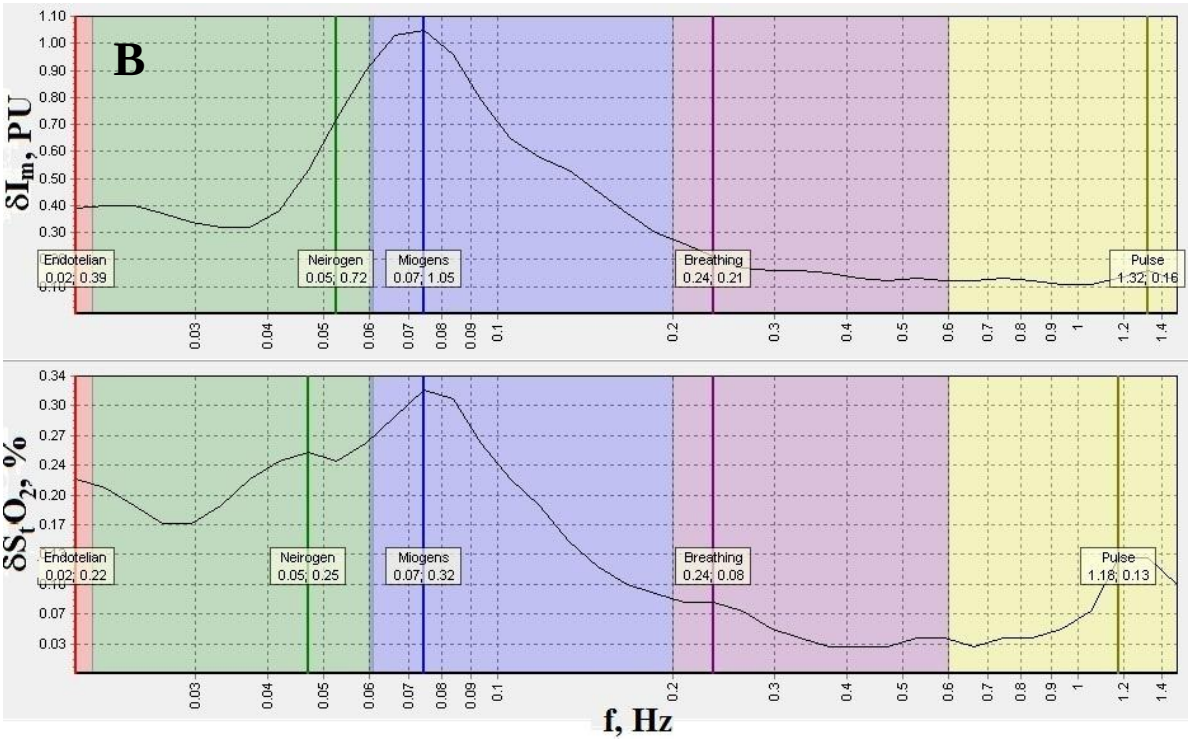

Figure 3. Perfusion and oxygen saturation graphs in cases of myogenic oscillation of the skin area with AVAs for volunteer №1 (A) and typical example of resonance and synchronized rhythms (f_m=0.074 Hz) of microvascular blood flow (δI_m=1.05 PU) and oxygen saturation (δS_tO_2=0.32%) within the range of only myogenic oscillation (vasomotion) during adaptive changes (B).

The parameters for calculating oxygen extraction and consumption for all volunteers were obtained using the approaches detailed in the methods section above. The results of measurements and calculations for both areas studied (skin with and without AVAs) for all the 8 volunteers are shown in Table 1.

Table 1. The results of measurements and calculations for all 8 volunteers.

№	Parameters	Skin with AVAs		Skin without AVAs	
		Norm (n=187)	With adaptive changes (n=60)	Norm (n=128)	With adaptive changes (n=26)
1	I_m(total), PU	21.0±3.1	21.4±3.4	2.5±0.8	2.8±0.9
2	I_{mn}(nutritive), PU	8.6±0.5	11.1±2.2*	1.7±0.8	2.8±0.8**
3	S_aO_2, %	98.1±0.4	97.9±0.4	97.9±0.4	97.8±0.6
4	S_tO_2, %	78.3±4.7	77.7±5.7	66.2±9.3	61.9±7.3
5	S_vO_2, %	41.6±13.7	41.9±6.1	58.2±12.7	61.3±7.3
6	V_b, %	10.2±1.8	9.9±1.5	6.3±1.7	6.0±1.4
7	$BI(I_m)$, AU	2.5±0.5	1.9±0.2**	1.6±0.6	1.0±0.06**
8	$BI(S_tO_2)$, AU	2.7±0.7	1.9±0.2**	2.4±1.6	1.0±0.2**
9	*OE*, AU	0.58±0.14	0.57±0.06	0.41±0.13	0.37±0.07
10	*OC*, AU	495±170	617±123**	69±40	102±38**

Note: There is significant difference (p > 0.05) observed from normal state, calculated by a *t*-test (*) and by the Mann-Whitney test (**).

The human skin contains functionally distinct zones, differing in morphological properties and the regulation of microvascular blood flow. These can be classified as with and without the presence of AVAs. The zones with AVAs are

functionally tied to implementation of the thermoregulatory homeostasis and are almost exclusively regulated by the sympathetic adrenergic nervous system. Additionally, the values of perfusion and intravascular pressure of the skin microvessels is generally higher in regions containing AVAs. The zones of skin without AVAs are characterized by lower blood flow in microvessels and a higher contribution of the venous component. During adaptive changes, a significant increase in the nutritive perfusion (I_{mn}) is observed in the zones with AVAs (from 8.6±0.5 PU to 11.1±2.2 PU, $p > 0.05$). Oxygen extraction did not change in the zones with and without AVAs. Increasing oxygen consumption was therefore due to an increase in perfusion rather than an increase in OE, thus adaptive changes naturally lead to the intensification of oxygen consumption in zones with AVAs (from 495±170 AU to 617±123 AU, $p > 0.05$). More cases of synchronization of myogenic rhythms in microvascular blood flow and oxygen saturation were registered in zones with AVAs, this is most likely because of the large numbers of autonomic nerves, which are very sensitive to adaptive changes.

The results from our studies on adaptive changes (stress- or exercise-induced) support our hypothesis that during resonance and synchronization of blood flow and oxygen saturation rhythms via myogenic oscillation there is increased tissue oxygen consumption compared with normal conditions. Thus the level of extraction of oxygen from blood remains unchanged. Therefore, we suggest that the bypass index may be used as a marker of adaptive changes (during stress conditions), calculated based on perfusion and tissue oxygen saturation.

The increase in amplitude of myogenic rhythm reflects a modulation of the hydrostatic pressure in the capillaries, resulting in an increase in diffusion of oxygen into the tissues, hence the changes in tissue oxygen saturation. Time shifts and frequency characteristics are obviously specific to particular individuals. For example, volunteer №1 registered 41 cases of synchronization (21 cases under emotional stress and 20 cases induced by exercise), volunteer №2 only registered 5 cases of synchronization of vasomotion (including cases obtained as a result of occlusion tests) and volunteer №3 registered 4 cases of adaptive changes. Analysis of recorded time fragments under normal conditions, during stress and following exercise presented distinct differences in the frequency of myogenic oscillations in perfusion and tissue oxygen saturation (Δf_m). In the normal state for all volunteers, this difference is almost always negative, because myogenic oscillations in perfusion typically display greater frequency than those for oxygen saturation. For example, the mean value for volunteer №1: 0.006 Hz; for volunteer №2: 0.022 Hz; for volunteer №3: 0.019 Hz. But during adaptive changes (in stressful situations – physical or emotional stress) when there is synchronization of myogenic oscillations, oxygen saturation is more intensive, giving Δf_m results which are generally positive. Occasionally, complete synchronization will be achieved when the frequency of both myogenic oscillations coincide. For example, this case is presented in Fig.4.

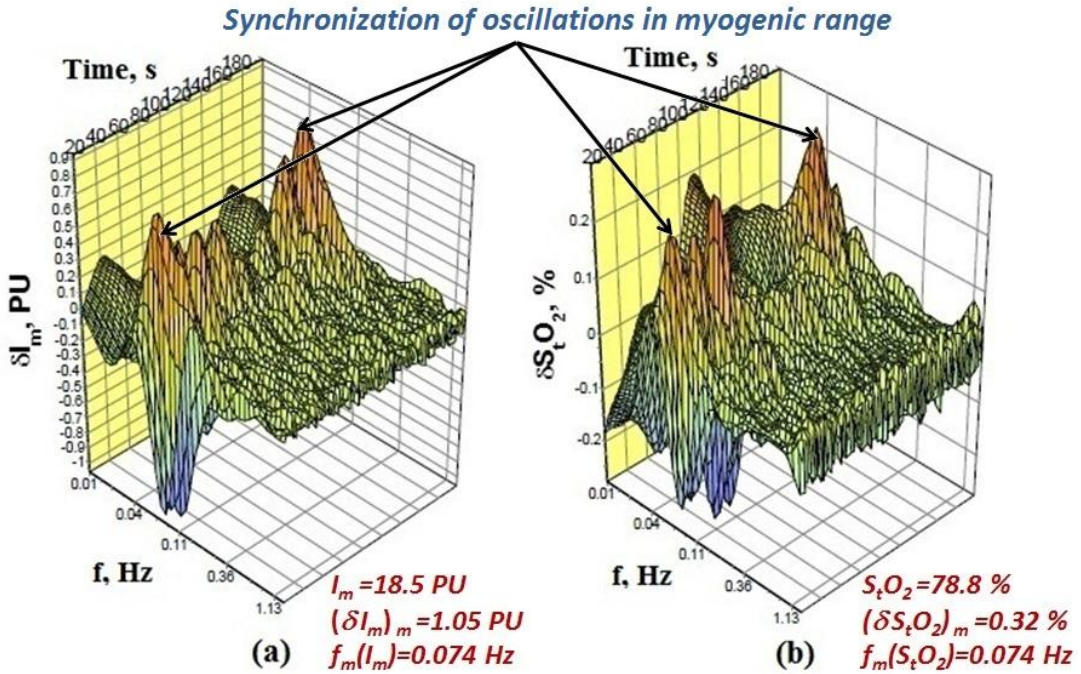

Figure 4. Typical example of the 3D wavelet analysis of resonating and synchronized myogenic rhythms of microvascular blood flow (a) and oxygen saturation (b) during adaptive changes.

The values of Δf_m during adaptive changes registered for the volunteers 1-3 were 0.027 Hz, 0.015 Hz and 0.040 Hz, respectively. It is worth noting that in studies of the effect of exercise (swimming) on blood flow and tissue oxygen saturation (especially at the initial stage of training) full synchronization of myogenic oscillations was achieved (Δf_m=0).

Data analysis has demonstrated the emergence of resonance and synchronized rhythms of microvascular blood flow and oxygen saturation as an adaptive change in myogenic oscillation (vasomotion) resulting from exercise and potentially from psychoemotional stress. Perhaps one explanation for the origin of this phenomenon is that the synchronization of myogenic rhythms facilitates maximum oxygen delivery to tissue following physical or emotional stress.

4. CONCLUSION

The data obtained show behavioral differences in myogenic oscillations in the ordinary state of the body (normality) and during episodes of sympathoadrenal activation (e.g. emotional stress). Normally, all systems of the body (including blood circulation, respiration, metabolism, etc.) work in different phases and frequencies, exhibiting non-linearity and independence. Synchronization of myogenic rhythms during adaptive changes may lead to increased oxygen consumption resulting from increased microvascular blood flow velocity. The data above suggests that adaptive changes naturally lead to the intensification of oxygen consumption in zones with AVAs due to an increased perfusion. Furthermore, as these zones have rich autonomic innervation, they are very sensitive to adaptive change leading to them having the highest incidence of myogenic rhythm synchronization of microvascular blood flow and oxygen saturation. During adaptive changes (under particular emotional stress, etc.), synchronization increases, reducing the freedom of microvascular blood flow regulation.

Ultimately, our suggested approaches for the use of the laser technology in investigating tissue respiration and skin microhaemocirculation under adaptive changes, through the monitoring of synchronization of blood flow and oxygen saturation rhythms observed within the data, have shown themselves to be highly informative and present interesting prospects for further investigation as a potential diagnostic methodology relevant to vascular function.

ACKNOWLEDGMENTS

This work was supported by the European Community's Seventh Framework Programme (FP7-People-2009-IAPP) under Grant Agreement no. 251531 MEDILASE.

REFERENCES

[1] Rogatkin, D. A., Sokolovski, S. G., Fedorova, K. A., Sidorov, V. V., Stewart, N. Z. and Rafailov, E. U., "Basic principles of design and functioning of multifunctional laser diagnostic system for non-invasive medical spectrophotometry," Proc. SPIE. 7890, 78901H1 (2011).

[2] Dunaev, A. V., Sidorov, V. V., Stewart, N. A., Sokolovski, S. G. and Rafailov, E. U., "Laser reflectance oximetry and Doppler flowmetry in assessment of complex physiological parameters of cutaneous blood microcirculation," Proc. SPIE. 8572, 857205 (2013).

[3] Bracic, M. and Stefanovska, A., "Wavelet-based analysis of human blood-flow dynamics," Bulletin of Mathematical Biology, 60(5), 919-935 (1998).

[4] Krupatkin, A. I. and Sidorov, V. V., [Laser Doppler flowmetry of blood microcirculation], Meditcina-Press, Moscow (2005).

[5] Kvandal, P., Landsverk, S. A., Bernjak, A., Stefanovska, A., Kvernmo, H. D. and Kirkeboen, K. A., "Low-frequency oscillations of the laser Doppler perfusion signal in human skin," Microvascular Research, 72(3), 120-127 (2006).

[6] Krupatkin, A. I., "The Problem of Information Value in Microvascular Networks," Human Physiology, 37(3), 312-317 (2011).

[7] Kvernmo, H. D., Stefanovska, A., Kirkeboen, K. A. and Kvernebo, K., "Oscillations in the human cutaneous blood perfusion signal modified by endothelium-dependent and endothelium-independent vasodilators," Microvascular Research, 57(3), 298-309 (1999).
[8] Schmidt-Lucke, C., Borgstrom, P. and Schmidt-Lucke, J. A., "Low frequency flowmotion/(vasomotion) during patho-physiological conditions," Life Sciences, 71(23), 2713-2728 (2002).
[9] Rossi, M., Carpi, A., Galetta, F., Franzoni, F. and Santoro, G., "Skin vasomotion investigation: A useful tool for clinical evaluation of microvascular endothelial function?," Biomedicine & Pharmacotherapy, 62(8), 541-545 (2008).
[10] Schmiedel, O., Schroeter, M. L. and Harvey, J. N., "Microalbuminuria in Type 2 diabetes indicates impaired microvascular vasomotion and perfusion," American Journal of Physiology - Heart and Circulatory Physiology, 293(6), H3424-H3431 (2007).
[11] Stefanovska, A., "Dynamics of blood oxygenation gives better insight into tissue hypoxia than averaged values," American Journal of Physiology - Heart and Circulatory Physiology, 296(5), H1224-H1226 (2009).
[12] Thorn, C. E., Matcher, S. J., Meglinski, I. V. and Shore, A. C., "Is mean blood saturation a useful marker of tissue oxygenation?," American Journal of Physiology - Heart and Circulatory Physiology, 296(5), H1289-H1295 (2009).
[13] Bernjak, A., Stefanovska, A., McClintock, P. V. E., Owen-Lynch, P. J. and Clarkson, P. B. M., "Coherence between fluctuations in blood flow and oxygen saturation," Fluctuation and Noise Letters, 11(1), (2012).
[14] Tyrrell, J., Thorn, C., Shore, A., Campbell, S. and Curnow, A., "Oxygen saturation and perfusion changes during dermatological methylaminolaevulinate photodynamic therapy," British Journal of Dermatology, 165(6), 1323-1331 (2011).
[15] Thorn, C. E., Kyte, H., Slaff, D. W. and Shore, A. C., "An association between vasomotion and oxygen extraction," American Journal of Physiology-Heart and Circulatory Physiology, 301(2), H442-H449 (2011).
[16] Tankanag, A. V. and Chemeris, N. K., "A method of adaptive wavelet filtering of the peripheral blood flow oscillations under stationary and non-stationary conditions," Physics in Medicine and Biology, 54(19), 5935-5948 (2009).
[17] Salerud, E. G., Tenland, T., Nilsson, G. E. and Oberg, P. A., "Rhythmical variations in human-skin blood-flow," International Journal of Microcirculation-Clinical and Experimental, 2(2), 91-102 (1983).
[18] Stefanovska, A., Bracic, M. and Kvernmo, H. D., "Wavelet analysis of oscillations in the peripheral blood circulation measured by laser Doppler technique," IEEE Transactions on Biomedical Engineering, 46(10), 1230-1239 (1999).
[19] Krupatkin, A. I., "Blood flow oscillations at a frequency of about 0.1 Hz in skin microvessels do not reflect the sympathetic regulation of their tone," Human Physiology, 35(2), 183-191 (2009).
[20] Kislukhin, V. V., "Regulation of oxygen consumption by vasomotion," Mathematical Biosciences, 191(1), 101-108 (2004).
[21] Krupatkin, A. I., "Noninvasive estimation of human tissue respiration with wavelet-analysis of oxygen saturation and blood flow oscillations in skin microvessels," Human Physiology, 38(4), 396-401 (2012).
[22] Krupatkin, A. I., "Cardiac and respiratory oscillations of the blood flow in microvessels of the human skin," Human Physiology, 34(3), 323-329 (2008).

Novel measure for the calibration of laser Doppler flowmetry devices

Andrey V. Dunaev*[a,b], Evgeny A. Zherebtsov[b], Dmitrii A. Rogatkin[c], Neil A. Stewart[a,d], Sergei G. Sokolovski[a], Edik U. Rafailov[a]

[a]Photonics and Nanoscience Group, Division of Physics, School of Engineering, Physics and Mathematics, University of Dundee, Dundee DD1 4HN, UK; [b]State University – Education-Science-Production Complex, Scientific-Educational Center of Biomedical Engineering, Oryol 302020, Russia; [c]Moscow Regional Research and Clinical Institute "MONIKI", Laboratory of Medical & Physics Research, Moscow 12911, Russia; [d]Department of Imaging and Technology, Ninewells Hospital, University of Dundee, Dundee DD1 9SY, UK

ABSTRACT

The metrological basis for optical non-invasive diagnostic devices is an unresolved issue. A major challenge for laser Doppler flowmetry (LDF) is the need to compare the outputs from individual devices and various manufacturers to identify variations useful in clinical diagnostics. The most common methods for instrument calibration are simulants or phantoms composed of colloids of light-scattering particles which simulate the motion of red blood cells based on Brownian motion. However, such systems have limited accuracy or stability and cannot calibrate for the known rhythmic components of perfusion (0.0095-1.6 Hz).

To solve this problem, we propose the design of a novel technique based on the simulation of moving particles using an electromechanical transducer, in which a precision piezoelectric actuator is used (e.g., P-602.8SL with maximum movement less than 1 mm). In this system, Doppler shift is generated in the layered structure of different solid materials with different optical light diffusing properties. This comprises a fixed, light transparent upper plane-parallel plate and an oscillating fluoroplastic (PTFE) disk. Preliminary studies on this experimental setup using the LDF-channel of a "LAKK-M" system demonstrated the detection of the linear portion (0-10 Hz with a maximum signal corresponding to Doppler shift of about 20 kHz) of the LDF-signal from the oscillating frequency of the moving layer. The results suggest the possibility of applying this technique for the calibration of LDF devices.

Keywords: laser Doppler flowmetry, metrological support, calibration, measure, biotissue phantom

1. INTRODUCTION

Metrological calibration of optical non-invasive diagnostic devices has not been sufficiently addressed [1]. Laser Doppler flowmetry (LDF) is widely used to measure the "index of blood microcirculation (I_m)" (or perfusion) in patients. These are conventionally reported in arbitrary perfusion units (PU), by detecting Doppler frequency shifts (20-24000 Hz) arising from the reflection of radiation from red blood cells (RBC) moving at speeds of 0.1-5 mm/s in small vessels [2, 3]. A major opportunity for this technology lies in the potential to utilise the data from individual devices from one manufacturer – as well as various manufacturers – to detect currently undetected blood flow defects and variances relevant for clinical diagnostics. LDF technology therefore requires standardization and metrological certification. LDF devices could be tested for accuracy and quantitative diagnostic information traceable back to international standards. Usually, in measuring techniques, these problems can be solved through the creation and standardization of special devices such as optical phantoms [4] or working standards (measures, test objects) [5].

*a.v.dunaev@dundee.ac.uk; phone 44 1382 386571; dundee.ac.uk/elecengphysics/research/photonics/photonicsnanoscience

Design and Quality for Biomedical Technologies VII, edited by Ramesh Raghavachari, Rongguang Liang,
Proc. of SPIE Vol. 8936, 89360D · © 2014 SPIE · CCC code: 1605-7422/14/$18 · doi: 10.1117/12.2035651

Currently, the most commonly used instrument calibration techniques use phantoms (for example, "Motility standard" ("Perimed AB", Sweden)) comprising colloids of light-scattering particles which simulate the motion of RBC based on the Brownian motion of particles in solution [6-8]. However, such systems have low accuracy and stability, designed to reproduce only one level of perfusion, exhibiting high sensitivity to vibration artefacts and offer limited validity for use simply as relative RBC motion sensors. Current devices cannot check the operational registration of various rhythmic components of blood flow perfusion (0.0095-1.6 Hz). The registration accuracy of these rhythms is an important aspect of the LDF method reliability in medical practice [9, 10]. The analysis showed that the development of the LDF method is constrained by its underdeveloped metrological basis.

The aim of this work was to develop a new principle of calibration measurement, devoid of the presented disadvantages and to study the experimental setup based on it.

2. MEASUREMENT PRINCIPLES FOR CALIBRATION OF LASER DOPPLER FLOWMETRY DEVICES

Today, the most common differential scheme for constructing LDF devices contains one probing and two receiving optical fibers, the difference in signal from which is used for further processing. A generalized formula for calculating perfusion (I_m) in these LDF devices is written as an expression [11]:

$$I_m = k_c \frac{\int_{f_{\min}}^{f_{\max}} S_{i_{ac}}(f)|f|\mathrm{d}f}{i_{dc}^2}, \quad (1)$$

where $S_{iac}(f)$ – the power spectral density function of the variable component of the photocurrent signal $i_{ac}(t)$, $i_{dc}(t)$ – a constant component of the photocurrent, k_c – instrument (calibration) coefficient.

From this formula it follows that to obtain accurate, quantitative and comparable data from different devices, the LDF method requires standardization, metrological certification and checking of individual LDF devices for correct selection of instrument calibration coefficients (k_c). For these purposes, except the most common approach, using colloidal solutions with light-scattering Brownian particles, there is also another research approach for metrological support of LDF devices. This approach uses alternating layers of different moving and solid materials with different known optical properties, providing a value of the light scattering, close to the values of the scattering in living biological tissues [12-14]. However, disadvantages of this approach include the following:

- the need to create a mechanical system motion from the drive motor layers, which reduces the potential accuracy due to inherent design limitations such as backlash and unwanted vibration;
- the inability to quickly and easily change the speed and range of oscillation amplitude of the motion layers to simulate the changing values of perfusion $I_m(t)$ according to known physiological events (reproducible complex modulated signal to simulate frequency rhythms of microcirculation);
- potential risk of abrasion over time of surfaces mechanically moving and rubbing of layers against each other changing optical properties leading to unstable values of perfusion $I_m(t)$ over time.

Analysis of existing approaches showed prospects for the reproduction of LDF signals by means of a moving diffusely scattering surface. Thus, it is possible to develop a reusable measure for calibration of LDF devices devoid of the drawbacks of the optical phantoms (test objects) based on light scattering on a solid surface using an electromechanical transducer (e.g. piezoelectric actuator) and managed by electrical signals (Fig. 1a).

We propose the design of a novel measure for the calibration of LDF devices, based on the principle of simulation of moving particles, in which an electromechanical transducer *3* converts electrical signal into mechanical vibrations in the moving diffuse reflector *2*. In order to create a constant component of the signal, laser radiation from the probe fiber (aperture of source S_{in}) passes first through a fixed light transparent plane-parallel plate *1*.

Basic principles of the proposed novel measure for calibration of LDF devices:

- laser radiation is scattered by the oscillating diffusing Lambertian surface and receives the component of the Doppler shift;
- when probing a fixed light transparent plane-parallel plate by laser radiation, reflected back radiation does not undergo Doppler shift;
- the physical properties of the materials used and the geometry of the problem being solved allow for the

quantification of the power of both components as well as the frequency of the reproduced Doppler components undergoing Doppler shift;

– the slope angle β (Fig. 1b) of the optical fiber probe to allow the formation of a specific quantitative difference between the input channels and registration signals of LDF devices.

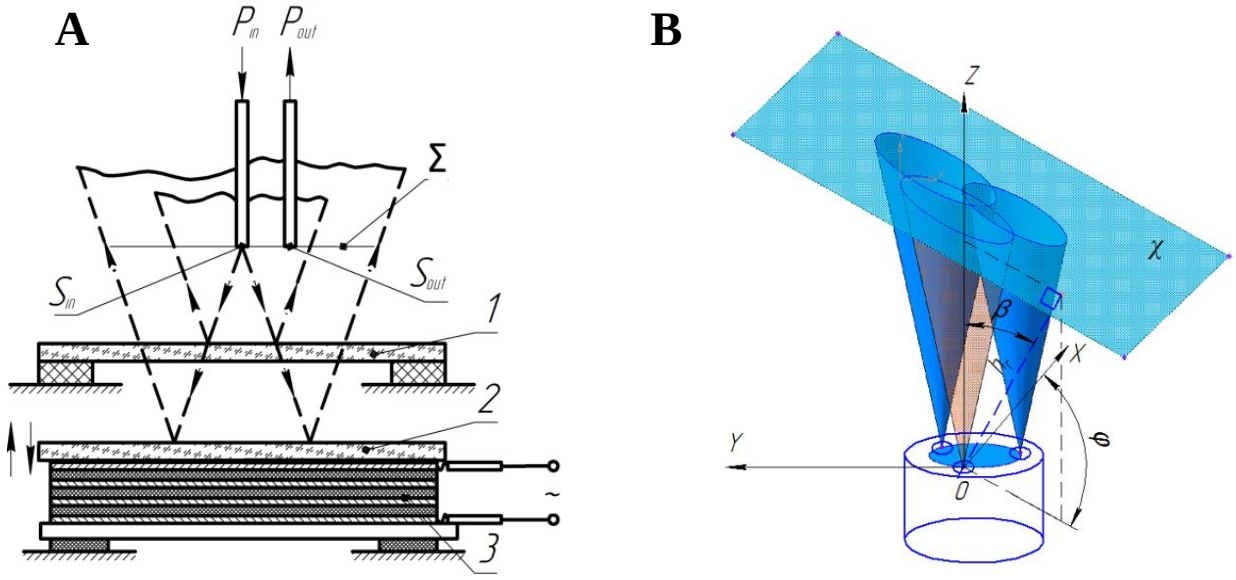

Figure 1. Principles of operation for calibration of LDF devices (a): *1* – light transparent plane-parallel plate, *2* – moving diffuse reflector, *3* – electromechanical transducer (batch piezoelectric actuator), S_{in} – aperture of source, S_{out} – aperture of the receiver, Σ – plane coincidence of aperture of receiver and source; and sectional view of the probe and receivers cones by the light scattering surfaces (b): h_r – distance from the core center of the probe fiber to the light scattering surface, β – angle of fiber-optic probe relative to the normal, carried to the plane of the light transparent plane-parallel plate, φ – angle between the projection of the height h_r on the plane of fiber-optic probe end and the x-axis (angle of rotation of the optical probe), χ – plane of the diffusely scattering surface.

3. EXPERIMENTAL RESULTS AND DISCUSSION

Pictures of the experimental setups are shown in Fig. 2. The technique uses a precision batch piezoelectric actuator P-602.8SL ("Physik Instrumente GmbH & Co", Germany) with maximum movement of less than 1 mm. In the proposed experimental setups Doppler shift is generated in the layered structure of various solid materials with different light diffusing properties. This comprises a fixed upper layer either in the form (Fig. 2a) of a mounted continuously variable neutral density filter NDC-100C-4M ("Thorlabs", USA) or in the form (Fig. 2b) of thin polymer film ("Rosco", USA), plus a fluoroplastic PTFE disk ("Ocean Optics", USA) moved by a piezoelectric actuator. In this study, we used the LDF-channel (with λ=1064 nm) of the multifunctional laser non-invasive diagnostic system "LAKK-M" (SPE "LAZMA", Russia) [15, 16] for calibration. A typical example of a reproducible constant level of perfusion using the proposed measure is shown on the Fig. 3.

Basic findings from the theoretical and experimental studies of the proposed setup for calibration of LDF devices:

– reproducible perfusion directly proportional to the amplitude and frequency of the oscillation light scattering surface of moving diffuse reflector was achieved (Fig. 4):

$$I_m = k_p A_o f_{osc}, \quad (2)$$

where A_0 and f_{osc} – amplitude and frequency of oscillation of the moving diffuse reflector respectively, k_p – proportionality coefficient;

– coefficient k_p does not depend on modes of oscillation – amplitude (A_0) and frequency (f_{osc}), and may be calculated based on knowledge of specific design parameters;

– slope angle of the fiber probe has a range of acceptable values $0 < \beta < \beta_{max}$ (Fig. 1b), such that when exceeded causes that the reflected radiation not to be used by the receiving fiber;
– reproducible level dependence on the angle β of the perfusion (I_m) has a local maximum in the range of valid values $0 < \beta < \beta_{max}$ that can be calculated for specific values of the design parameters.

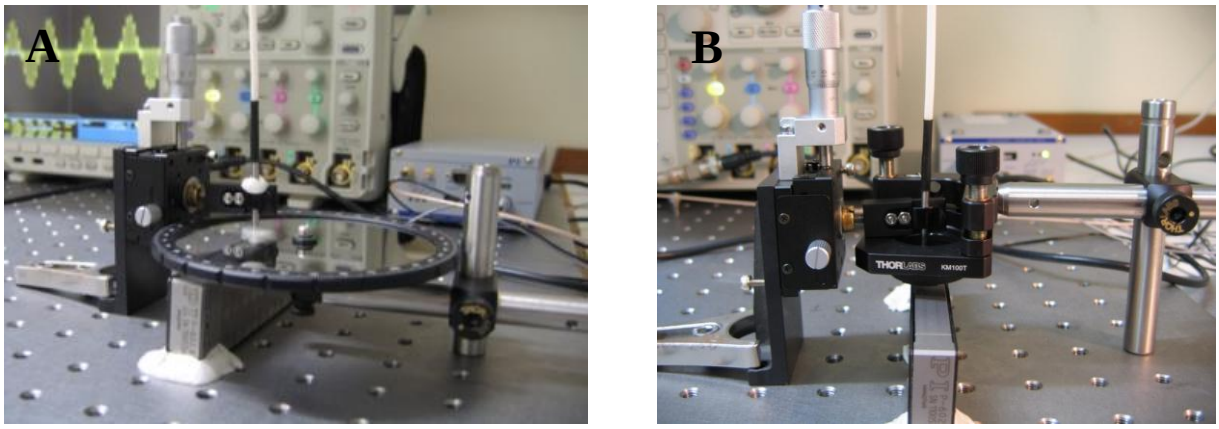

Figure 2. Experimental setups of measure for calibration of LDF devices.

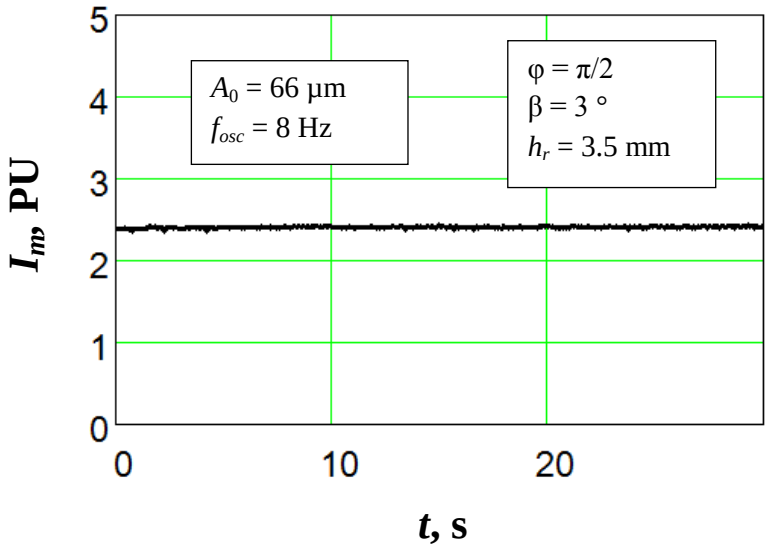

Figure 3. Example of reproducible constant level of perfusion using the proposed measure.

It should be emphasized that the proposed experimental setup is virtually insensitive to environmental vibration artefacts (Fig. 3), while use of colloidal phantoms for calibration requires an optical table with vibration damping (elimination of footsteps, closing doors, etc.).

Fig. 4 shows the graphs of the reproducible perfusion level on the amplitude (Fig. 4a) and frequency (Fig. 4b) of oscillation light scattering surface (on the experimental points with pending standard deviations added theoretical curve). Experimental and theoretical research has shown a linear portion for LDF-signal dependence on the amplitude of the oscillating layer (0-70 μm) and also a linear portion (0-10 Hz) for LDF-signal from the oscillating frequency of the light scattering surface of the moving diffuse reflector. It should be emphasized that the experimental measure setups used in both cases (the range of changes in the amplitude and the frequency of oscillations) are consistent with the range of RBC

velocity (0-4.5 mm/s). A linear dependence of this function of the reproducible perfusion level allows the application of the proposed principle for calibration and adjustment of LDF devices.

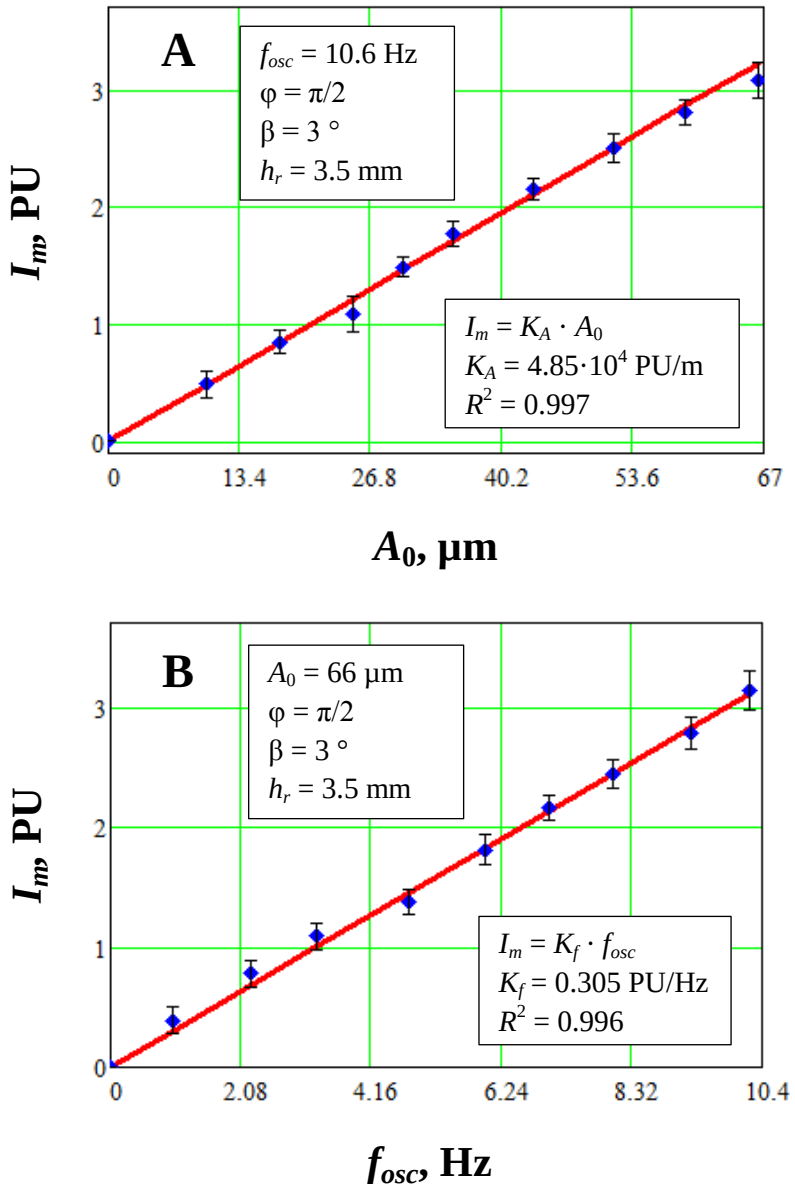

Figure 4. Experimental and theoretical dependencies reproducible levels of perfusion from the amplitude (a) and frequencies (b) oscillation of the light scattering surface of moving diffuse reflector.

For experimental verification of the type of function of reproducible perfusion level from the design parameters (h_r – distance from the plane of the fiber probe to the light scattering surface), a series of experiments was performed and the graph shown in Fig. 5 was constructed. The obtained graph dependence shows an inverse relationship of the reproducible perfusion levels on the distance from the light scattering surface. This result can be explained by the reduction of the solid angle subtended by the intersection area of the probe and reception areas of the center point of the core of the receiving fiber. The results suggest the possibility of applying the considered structure as a measure for calibration of LDF devices.

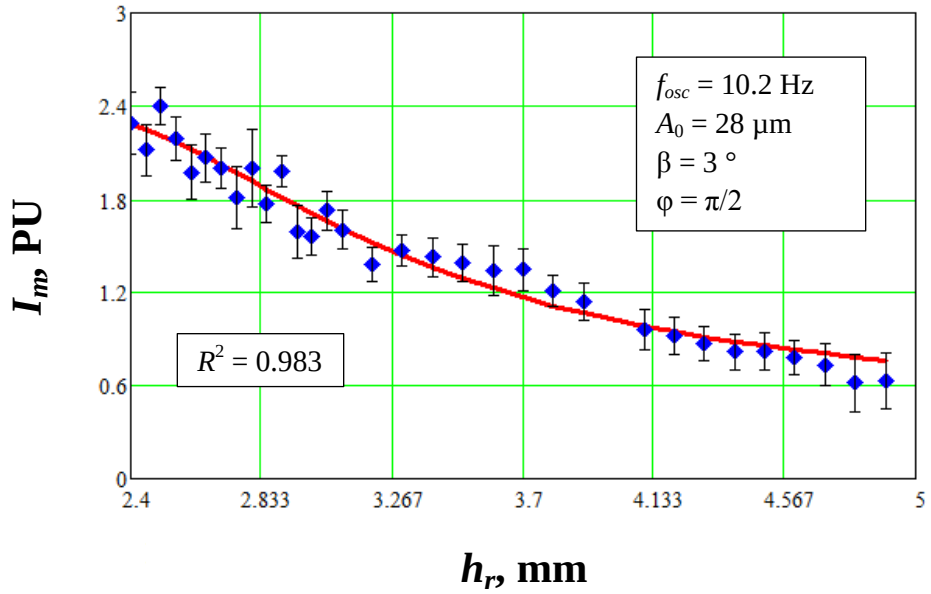

Figure 5. Experimental and theoretical dependencies reproducible levels of perfusion from the distance from the plane of the fiber probe to the light scattering surface of moving diffuse reflector.

4. CONCLUSION

Analysis of the experimental data shows the convenience and ease of operation of the proposed technique for the calibration of LDF devices, operational manageability of its modes and operability evaluation in devices systems of analysis of frequency rhythms of blood flow, which allows comparing them with each other. Proposed novel measure may be used to determine both static and dynamic errors of LDF devices. This allows evaluation of the suitability of LDF devices during production and specific diagnostic use in medical institutions. Developed algorithms for checking the metrological characteristics of LDF devices offer the possibility to improve the quality and reliability of the resulting diagnostic information.

ACKNOWLEDGMENTS

This work was supported by the European Community's Seventh Framework Programme (FP7-People-2009-IAPP) under Grant Agreement no. 251531 MEDILASE and partially by the grant of State University ESPC no. VK-3-2013.

REFERENCES

[1] Rogatkin, D. A., Dunaev, A. V. and Lapaeva, L. G., "Metrological Support of Methods and Devices for Noninvasive Medical Spectrophotometry," Biomedical Engineering, 44(2), 66-70 (2010).
[2] Obeid, A. N., Barnett, N. J., Dougherty, G. and Ward, G., "A critical-review of laser doppler flowmetry," Journal of Medical Engineering & Technology, 14(5), 178-181 (1990).
[3] Leahy, M. J. and Nilsson, G. E., "Laser Doppler flowmetry for assessment of tissue microcirculation: 30 years to clinical acceptance," Proc. SPIE. 7563, 75630E (2010).
[4] Tuchin, V. V., [Handbook of optical biomedical diagnostics], SPIE Press, Bellingham, Washington(2002).
[5] Dunaev, A. V., Zherebtsov, E. A., Rogatkin, D. A., Stewart, N. A., Sokolovski, S. G. and Rafailov, E. U., "Substantiation of medical and technical requirements for noninvasive spectrophotometric diagnostic devices," Journal of Biomedical Optics, 18(10), 107009 (2013).

[6] Binzoni, T., Leung, T. S., Seghier, M. L. and Delpy, D. T., “Translational and Brownian motion in laser-Doppler flowmetry of large tissue volumes,” Physics in Medicine and Biology, 49(24), 5445-5458 (2004).
[7] Fredriksson, I., Larsson, M., Salomonsson, F. and Strömberg, T., "Improved calibration procedure for laser Doppler perfusion monitors," Proc. SPIE. 7906, 790602 (2011).
[8] Liebert, A., Leahy, M. and Maniewski, R., “A calibration standard for laser-Doppler perfusion measurements,” Review of Scientific Instruments, 66, 5169 (1995).
[9] Bracic, M. and Stefanovska, A., “Wavelet-based analysis of human blood-flow dynamics,” Bulletin of Mathematical Biology, 60(5), 919-935 (1998).
[10] Tankanag, A. and Chemeris, N., “Application of the adaptive wavelet transform for analysis of blood flow oscillations in the human skin,” Physics in Medicine and Biology, 53(21), 5967-5976 (2008).
[11] Liebert, A., Leahy, M. and Maniewski, R., “Multichannel laser-Doppler probe for blood perfusion measurements with depth discrimination,” Medical & Biological Engineering & Computing, 36(6), 740-747 (1998).
[12] Soelkner, G., Mitic, G. and Lohwasser, R., “Monte Carlo simulations and laser Doppler flow measurements with high penetration depth in biological tissuelike head phantoms,” Applied Optics, 36(22), 5647-5654 (1997).
[13] Larsson, M., Steenbergen, W. and Stromberg, T., “Influence of optical properties and fiber separation on laser Doppler flowmetry,” Journal of Biomedical Optics, 7(2), 236-243 (2002).
[14] Steenbergen, W. and de Mul, F. F. M., "Application of a novel laser Doppler tester including a sustainable tissue phantom," Proc. SPIE. 3252, 14-25 (1998).
[15] Rogatkin, D. A., Sokolovski, S. G., Fedorova, K. A., Sidorov, V. V., Stewart, N. A. and Rafailov, E. U., "Basic principles of design and functioning of multifunctional laser diagnostic system for non-invasive medical spectrophotometry," Proc. SPIE. 7890, 78901H1 (2011).
[16] Dunaev, A. V., Sidorov, V. V., Stewart, N. A., Sokolovski, S. G. and Rafailov, E. U., "Laser reflectance oximetry and Doppler flowmetry in assessment of complex physiological parameters of cutaneous blood microcirculation," Proc. SPIE. 8572, 857205 (2013).